UNIVERSITY OF CALIFORNIA SAN DIEGO

Control and State Estimation for Materials Phase Change: Design, Analysis, Applications, and Experiments

A dissertation submitted in partial satisfaction of the
requirements for the degree
Doctor of Philosophy

in

Engineering Science (Mechanical Engineering)

by

Shumon Koga

Committee in charge:

Professor Miroslav Krstic, Chair
Professor Robert Bitmead
Professor Jorge Cortés
Professor Ian Eisenman
Professor Ping Liu

2020

The dissertation of Shumon Koga is approved, and it is acceptable in quality and form for publication on microfilm and electronically:

_____

_____

_____

_____

Chair

University of California San Diego

2020

DEDICATION

To Naoki, Yuko, Shintaro, and Juna.

TABLE OF CONTENTS

LIST OF FIGURES

LIST OF TABLES

ACKNOWLEDGEMENTS

I would like to express my deepest gratitude to my advisor, Professor Miroslav Krstic, for his enormous mentoring for me. Absolutely his guidance and advice have been essential to tackle numerous challenges I have faced with throughout my doctoral program. I would like to thank all members of the committee, Professor Robert Bitmead, Professor Jorge Cortés, Professor Ping Liu, and Professor Ian Eisenman, for their valuable feedback for the dissertation.

Many people have helped and collaborated with me on my doctoral research. I would like to especially thank Professor Mamadou Diagne for opening a door towards a path of my doctoral research through many discussions to achieve the first result on the Stefan problem. I am grateful for Professor Rafael Vazquez, Professor Delphine Bresch-Pietri, and Professor Iasson Karafyllis for their contributions to several extensions presented in Chapter 4. Their technical expertise (e.g. PDE control, delay systems, sampled-data system) and helpful guidance are essential for the dissertation. I would like to thank Professor Ian Eisenman for giving his suggestion on the physical model of the sea ice and giving several discussions. I would like to thank my nice colleague Leobardo Camacho-Solorio for his contributions to the battery management systems. I would also like to thank Professor Scott Moura for his feedback and comments on our results and motivations of battery managements. I am grateful for Professor Joseph Beaman for his contributions to the metal 3D-printing control system as a pioneer of the selective laser sintering technology. I would like to extend our gratitude to Mitutoshi Makihata, Professor Renkun Chen, and Professor Albert Pisano for their contribution to establishing the experimental setup for the thermal control system with phase change materials. This interdisciplinary collaboration in UCSD/MAE on the experiment project was extremely exciting for me.

I am grateful for Tiago Roux de Oliveira, Huan Yu, Ji Wang, Jan Feiling, David Straub, and Mona Buisson-Fenet for welcoming me as a collaborator or mentor of their projects. I would like to appreciate Ian Fenty, Ichiro Fukumori, Yoshihiro Nakayama, and Dimitris Menemenlis for mentoring and supporting me during my internship at NASA Jet Propulsion Laboratory. I am also

grateful for Mouhacine Benosman for serving a mentor of my internship at Mitsubishi Electric Research Laboratories (MERL) and genuinely providing consultation for my future career. I would also like to thank Claus Danielson, Yebin Wang, and Rui Ma at MERL for communicating with me.

I would like to thank great colleagues and friends at UC San Diego, in particular, Stephen Chen, Leobardo Camacho-Solorio, Huan Yu, Mostafa Bagheri, Imoleayo Abel, Nicholas Willems, Drew Steeves, Alan Williams, Cenk Damir, Mohammad Al Suwaidan, Ulf Jakob Aarsnes, Ji Wang, Lingling Su, Dylan Drotman, Yifu Zhang, Pio Ong, Dan Li, Priyank Srivastava, and Sven Brüggemann. The time I have spend with them at UCSD and some conference is highly precious. I would like to extend my gratitude to Professor Shuxia Tang, Gregory Matthew Mills, Paul Frihauf, Halil Ibrahim Basturk, Nikolaos Bekiaris-Liberis, Alexander Scheinker, Azad Ghaffari, Huazhen Fang, Anatoly Zlotnik, Jorge Poveda, Cameron Nowzari, Daniele Cavaglieri, Martin Sehr, Amit Pandey, Eduardo Jose Ramirez, Ashish Cherukuri, and Robert Moroto, for their sincere advice on graduate study and providing consultation for career path.

I am grateful for Masahiro Ono, Professor Shuichi Adachi, Professor Yohei Fujitani, Professor Kohei Ito, Professor Yutaka Hori for their invaluable support for me to pursue a PhD program when I was an undergraduate student at Keio University. I would like to thank Professor Shinji Hara and Professor Koji Tsumura for their mentoring and support when I was a research assistant at the University of Tokyo. I would like to thank Professor Amar G. Bose for inspiring me to have an interest in control engineering in the U.S., through his influential career as a professor at MIT and a founder of Bose Inc, though I have no met him in person.

I would like to thank the National Science Foundation for a partial financial support of this project.

Finally, I would like to express my great appreciation to may father Naoki, my mother Yuko, and my brother Shintaro, for always giving an invaluable support for me.

The dissertation includes reprints and adaptations of published papers that are product

of the research carried-out with the collaboration of several co-authors; to whom I acknowledge their contributions.

Chapters 2 and 3, in part, are a reprint of the material as it appears in:

- S. Koga, M. Diagne, S. Tang, and M. Krstic, "Backstepping Control of the One-Phase Stefan Problem", *American Control Conference*, 2016,
- S. Koga, M. Diagne, and M. Krstic, "Output Feedback Control of the One-Phase Stefan Problem", *IEEE Conference on Decision and Control*, 2016,
- S. Koga, M. Diagne, and M. Krstic, "Control and State Estimation of the One-Phase Stefan Problem via Backstepping Design", *IEEE Transactions on Automatic Control*, vol. 64, no. 2, pp. 510-525, 2019.

The dissertation author was the primary investigators and author of this paper.

Chapter 4, in part, is a reprint of the material as it appears in:

- S. Koga, R. Vazquez, and M. Krstic, "Backstepping Control of the Stefan Problem with Flowing Liquid", *American Control Conference*, 2017,
- S. Koga and M. Krstic, "Delay-Compensated Control of the Stefan Problem", *IEEE Conference on Decision and Control*, 2017,
- S. Koga, D. Bresch-Pietri, and M. Krstic, "Delay-Compensated Control of the Stefan Problem and Robustness to Delay Mismatch", *International Journal of Robust and Nonlinear Control*, vol. 30, no. 6, pp. 2304-2334, 2020,
- S. Koga, I. Karafyllis, and M. Krstic, "Input-to-State Stability for the Control of Stefan Problem with Respect to Heat Loss", *American Control Conference*, 2018,
- S. Koga, I. Karafyllis, and M. Krstic, "Towards Implementation of PDE Control for Stefan System: Input-to-State Stability and Sampled-Data Design", *Automatica*, under review.

The dissertation author was the primary investigators and author of this paper.

Chapter 5, in part, is a reprint of the material as it appears in:

- S. Koga and M. Krstic, "Control of the Two-Phase Stefan Problem via Single-Boundary Heat Input", *IEEE Conference on Decision and Control*, 2018,
- S. Koga and M. Krstic, "Single-Boundary Control of the Two-Phase Stefan System", *Systems & Control Letters*, vol. 135, p. 104573, 2020.

The dissertation author was the primary investigators and author of this paper.

Chapter 6, in part, is a reprint of the material as it appears in:

- S. Koga and M. Krstic, "Arctic Sea Ice Temperature Profile Estimation via Backstepping Observer Design", *IEEE Conference on Control Technology and Applications*, 2017,
- S. Koga and M. Krstic, "Arctic Sea Ice State Estimation from Thermodynamic PDE Model", *Automatica*, vol. 112, p. 108713, 2020.

The dissertation author was the primary investigators and author of this paper.

Chapter 7, in part, is a reprint of the material as it appears in:

- S. Koga, L. Camacho-Solorio, and M. Krstic, "State Estimation for Lithium Ion Batteries with Phase Transition Materials", *ASME Dynamic Systems and Control Conference*, 2017,
- S. Koga, L. Camacho-Solorio, and M. Krstic, "State Estimation for Lithium Ion Batteries with Phase Transition Materials via Boundary Observers", *ASME Journal of Dynamic Systems, Measurement, and Control*, under review.

The dissertation author was the primary investigators and author of this paper.

Chapter 8, in part, is a reprint of the material as it appears in:

- S. Koga, D. Straub, M. Diagne, and M. Krstic, "Thermodynamic Modeling and Control of Screw Extruder for 3D Printing", *American Control Conference*, 2018,

- S. Koga, D. Straub, M. Diagne, and M. Krstic, "Stabilization of Filament Production Rate for Screw Extrusion-Based Polymer 3D-Printing", *ASME Journal of Dynamic Systems, Measurement, and Control*, vol. 142, no. 3, p. 031005, 2020.

The dissertation author was the primary investigators and author of this paper.

Chapter 9, in part, is a reprint of the material as it appears in:

- S. Koga, M. Krstic, and J. Beaman, "Laser Sintering Control for Metal Additive Manufacturing by PDE Backstepping", *IEEE Conference on Decision and Control*, 2019,

- S. Koga, M. Krstic, and J. Beaman, "Laser Sintering Control for Metal Additive Manufacturing by PDE Backstepping", *IEEE Transactions on Control Systems Technology*, under review.

The dissertation author was the primary investigators and author of this paper.

Chapter 10, in part, is a reprint of the material as it appears in:

- S. Koga, M. Makihata, R. Chen, M. Krstic, and A.P. Pisano, "Energy Storage in Paraffin: a PDE Backstepping Experiment", *IEEE Transactions on Control Systems Technology*, under review. (Chapter 10)

The dissertation author was the primary investigators and author of this paper.

VITA

2014	Bachelor of Science in Applied Physics and Physico-Informatics, Keio University
2015	Master of Science in Engineering Sciences (Mechanical Engineering), University of California San Diego
2017	Visiting Student Researcher, Rensselaer Polytechnic Institute
2017	Visiting Student Researcher, NASA Jet Propulsion Laboratory/California Institute of Technology
2018	Outstanding Graduate Student Award, Department of Mechanical and Aerospace Engineering, University of California San Diego,
2018	Intern, Mitsubishi Electric Research Laboratories
2019	O. Hugo Schuck Best Paper Award, American Automatic Control Council
2020	Doctor of Philosophy in Engineering Sciences (Mechanical Engineering), University of California San Diego

PUBLICATIONS

Journal Articles

1. S. Koga, M. Makihata, R. Chen, M. Krstic, and A.P. Pisano, "Energy Storage in Paraffin: a PDE Backstepping Experiment", *IEEE Transactions on Control Systems Technology*, under review.
2. S. Koga, L. Camacho-Solorio, and M. Krstic, "State Estimation for Lithium Ion Batteries with Phase Transition Materials via Boundary Observers", *ASME Journal of Dynamic Systems, Measurement, and Control*, under review.
3. S. Koga, M. Krstic, and J. Beaman, "Laser Sintering Control for Metal Additive Manufacturing by PDE Backstepping", *IEEE Transactions on Control Systems Technology*, under review.
4. S. Koga, I. Karafyllis, and M. Krstic, "Towards Implementation of PDE Control for Stefan System: Input-to-State Stability and Sampled-Data Design", *Automatica*, under review.
5. J. Feiling, S. Koga, M. Krstic, T. R. Oliveira, "Gradient Extremum Seeking for Unknown Scalar Maps in Cascade with Reaction-Advection-Diffusion PDEs", *International Journal of Adaptive Control and Signal Processing*, under review.
6. T. R. Oliveira, J. Feiling, S. Koga, M. Krstic, "Multivariable Extremum Seeking for PDE Dynamic Systems", *IEEE Transactions on Automatic Control*, to appear.

7. S. Koga, D. Bresch-Pietri, and M. Krstic, "Delay-Compensated Control of the Stefan Problem and Robustness to Delay Mismatch", *International Journal of Robust and Nonlinear Control*, vol. 30, no. 6, pp. 2304-2334, 2020.
8. S. Koga, D. Straub, M. Diagne, and M. Krstic, "Stabilization of Filament Production Rate for Screw Extrusion-Based Polymer 3D-Printing", *ASME Journal of Dynamic Systems, Measurement, and Control*, vol. 142, no. 3, p. 031005, 2020.
9. S. Koga and M. Krstic, "Arctic Sea Ice State Estimation from Thermodynamic PDE Model", *Automatica*, vol. 112, p. 108713, 2020.
10. S. Koga and M. Krstic, "Single-Boundary Control of the Two-Phase Stefan System", *Systems & Control Letters*, vol. 135, p. 104573, 2020.
11. S. Koga, M. Diagne, and M. Krstic, "Control and State Estimation of the One-Phase Stefan Problem via Backstepping Design", *IEEE Transactions on Automatic Control*, vol. 64, no. 2, pp. 510-525, 2019.
12. J. Feiling, S. Koga, M. Krstic, T. R. Oliveira, "Gradient Extremum Seeking for Static Maps with Actuation Dynamics Governed by Diffusion PDEs", *Automatica*, vol. 95, pp. 197-206, 2018.
13. J. Wang, S. Koga, Y. Pi, and M. Krstic, "Axial Vibration Suppression in a PDE Model of Ascending Mining Cable Elevator", *ASME Journal of Dynamic Systems, Measurement, and Control*, vol. 140 , no. 11, pp. 111003, 2018.

Conference Proceedings

1. S. Koga, M. Krstic, and J. Beaman, "Laser Sintering Control for Metal Additive Manufacturing by PDE Backstepping", *IEEE Conference on Decision and Control*, 2019.
2. S. Koga, M. Benosman, and J. Borggaard, "Learning-Based Robust Observer Design for Coupled Thermal and Fluid Systems", *American Control Conference*, 2019.
3. S. Koga and M. Krstic, "Control of the Two-Phase Stefan Problem via Single-Boundary Heat Input", *IEEE Conference on Decision and Control*, 2018.
4. T. R. Oliveira, J. Feiling, S. Koga, M. Krstic, "Scalar Newton-based Extremum Seeking for a Class of Diffusion PDEs", *IEEE Conference on Decision and Control*, 2018.
5. M. Buisson-Fenet, S. Koga, and M. Krstic, "Control of Piston Position in Inviscid Gas by Bilateral Boundary Actuation", *IEEE Conference on Decision and Control*, 2018.
6. H. Yu, S. Koga, and M. Krstic, "Stabilization of Traffic Flow with a Leading Autonomous Vehicle", *ASME Dynamic Systems and Control Conference*, 2018.
7. S. Koga, I. Karafyllis, and M. Krstic, "Input-to-State Stability for the Control of Stefan Problem with Respect to Heat Loss", *American Control Conference*, 2018.
8. S. Koga, D. Straub, M. Diagne, and M. Krstic, "Thermodynamic Modeling and Control of Screw Extruder for 3D Printing", *American Control Conference*, 2018
9. S. Koga and M. Krstic, "Delay-Compensated Control of the Stefan Problem", *IEEE Conference on Decision and Control*, 2017

10. S. Koga and M. Krstic, "Arctic Sea Ice Temperature Profile Estimation via Backstepping Observer Design", *IEEE Conference on Control Technology and Applications*, 2017.
11. S. Koga, L. Camacho-Solorio, and M. Krstic, "State Estimation for Lithium Ion Batteries with Phase Transition Materials", *ASME Dynamic Systems and Control Conference*, 2017.
12. S. Koga, R. Vazquez, and M. Krstic, "Backstepping Control of the Stefan Problem with Flowing Liquid", *American Control Conference*, 2017.
13. S. Koga, M. Diagne, and M. Krstic, "Output Feedback Control of the One-Phase Stefan Problem", *IEEE Conference on Decision and Control*, 2016.
14. S. Koga, M. Diagne, S. Tang, and M. Krstic, "Backstepping Control of the One-Phase Stefan Problem", *American Control Conference*, 2016.

ABSTRACT OF THE DISSERTATION

Control and State Estimation for Materials Phase Change: Design, Analysis, Applications, and Experiments

by

Shumon Koga

Doctor of Philosophy in Engineering Science (Mechanical Engineering)

University of California San Diego, 2020

Professor Miroslav Krstic, Chair

The dissertation presents results on control and state estimation for a physics-based "Stefan" model of phase change. Design procedures, theoretical analysis, applications to industrial processes, and experimental validation are addressed. The Stefan model describes a time-evolution of a material's temperature profile during melting/solidification phenomena along with the dynamics of the liquid-solid interface position. The mathematical description comprises a parabolic Partial Differential Equation (PDE), defined on a time-varying spatial domain, whose boundary position dynamics are governed by an Ordinary Differential Equation (ODE) driven by the PDE's state. None of the existing systematic and theoretical control are applicable to this

problem due to the system's geometric nonlinearity as well as the infinite dimensionality. We design a boundary heat control to promote the melting so that the liquid-solid interface position is driven to a desired setpoint position. Our design is an extension of the "PDE backstepping" method to the Stefan system. The closed-loop stability is proven by Lyapunov analysis. The constraints of the temperature state and the heat input are guaranteed by virtue of the maximum principle. Analogous results for the state estimation are also developed to estimate the entire temperature profile from available measurements of the surface temperature and the liquid-solid interface position.

The latter half of the dissertation is devoted to the application of the designed method to several practical problems. First, we introduce a Stefan model of "sea ice", which has been studied intensively due to the recent rapid melting of sea ice. We verify the desired robust performance of the designed estimator in a numerical simulation, which incorporates further complexity in the model and uncertainties. Second, we focus on "lithium-ion batteries", which have become ubiquitous in electronic devices, such as laptops and smartphones, and in electric vehicles. The model is described by a Stefan system of the lithium-ion concentration due to a solid-solid phase change in the electrodes during the charging and discharging cycles. Our estimator achieves accurate State-of-Charge estimation in simulation. Third, we apply the designed control method to "polymer 3D-printing" via screw extrusion for the sake of stabilizing the filament production under a fast printing, by extending the design to deal with the convection and heat loss. Fourth, we focus on "metal 3D-printing" which has a high impact on products and supply chains in industries. The proposed control method is applied for generating the desired shape of the melt pool, which shows the robust performance with respect to a radiation effect and sensor noise in numerical study. Finally, we conduct experiments of melting paraffin wax as an energy storage material, which shows the successful performance of our PDE-based control algorithm.

Chapter 1

Phase Change Model–Stefan Problem

1.1 Introduction and Brief History

The Stefan problem is a well-known moving boundary problem modelling the thermodynamic liquid-solid phase change phenomena. It is named after an Austrian physicist Josef Stefan, who is one of the most distinguished and influential physicist in 19th century for his numerous contributions to thermodynamics and heat transfer from the experimental perspective. Perhaps the name is more recognized for Stefan-Bolzman's law, which revealed that the materials with its temperature T in absolute unit emits a radiative heat transfer which is proportional to T^4, through Stefan's experimental work and his student Ludwig Boltzman's work on the theoretical foundation.

After the publication of the thermal radiations law, Stefan started to focus on the thickness evolution of polar ice caps motivated by observed data of ice growth and air temperature acquired by British and German explorers during their expeditions. A long time before that, the phase change model by moving boundaries has been studied by Joseph Black in 1762, and Franz Neumann developed the solution in his lectures around 1860. However, Neumann's result has not been published until Weber's paper in 1901. Stefan developed his analysis on the solution of ice

growth and studied the correspondence with the empirical data, which was published in 1891. Since then, the model has been known as "Stefan problem", and has been studied widely by later researchers from middle of 1900s [33].

While there are several extended models on the phase change by incorporating additional factors, throughout this chapter we introduce the one-dimensional one-phase Stefan problem by assuming

- the temperature profile is uniformly distributed along a cross-sectional area
- the solid phase temperature is uniformly distributed at the melting temperature
- there is no material's convection
- the pressure field around the material is static and uniform
- the focused material is completely pure

In later chapters, we start to relax the first three assumptions one by one.

1.2 Physical Modelling

Consider a pure one-component material of length L in one dimension as depicted in Fig. 1.1. The dynamics of the process depends strongly on the evolution in time of the moving interface (here reduced to a point) at which phase transition from liquid to solid (or equivalently, in the reverse direction) occurs. Therefore, the melting or solidification mechanism that takes place in the physical domain $[0,L]$ induces the existence of two complementary time-varying sub-domains, namely, $[0,s(t)]$ occupied by the liquid phase, and $[s(t),L]$ by the solid phase. Assuming a temperature profile uniformly equivalent to the melting temperature in the solid phase, a dynamical model associated with the melting phenomenon (see Fig. 1.1) involves only

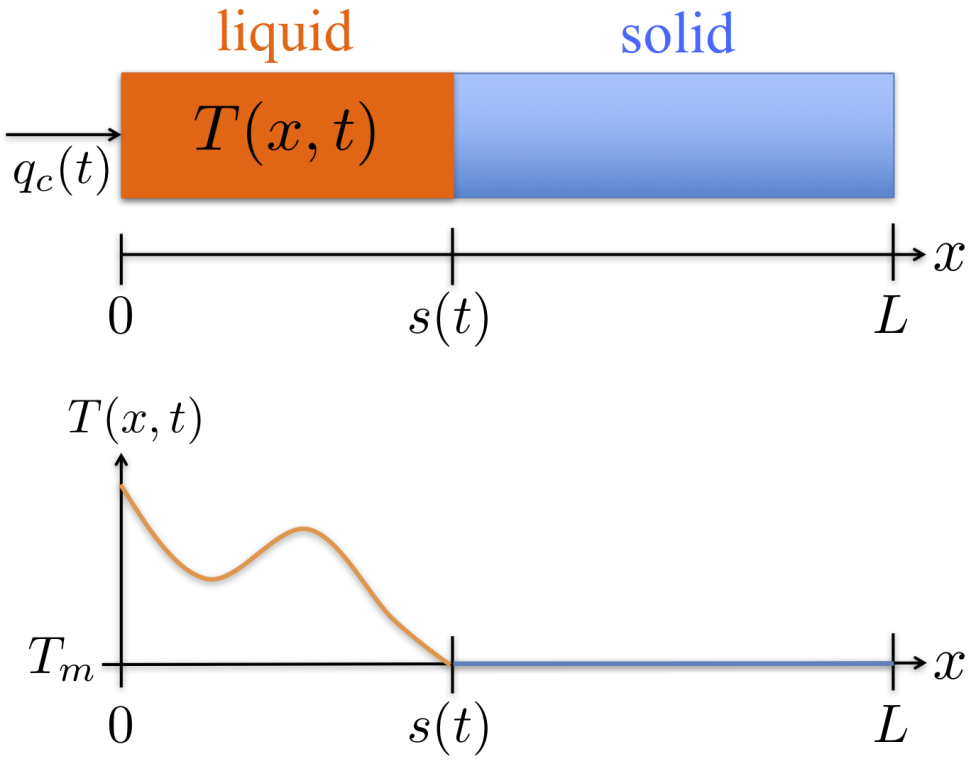

Figure 1.1: Schematic of one-dimensional one-phase Stefan problem. The temperature profile in the solid phase is assumed to be a uniform melting temperature.

the thermal behavior of the liquid phase. Considering a melting material with a density ρ and heat capacity C_p, the local energy conservation law is given by

$$\rho C_\mathrm{p} T_t(x,t) = -q_x(x,t), \quad x \in (0, s(t)) \tag{1.1}$$

where $q(x,t)$ is a heat flux profile and $T(x,t)$ is a temperature profile. Moreover, the local energy balance at the position of the liquid-solid interface $x = s(t)$ involved with the latent heat leads to the dynamics of the moving boundary

$$\rho \Delta H^* \dot{s}(t) = q(s(t),t). \tag{1.2}$$

At a fundamental level, the thermal conduction for a melting component obeys the well known Fourier's Law

$$q(x,t) = -kT_x(x,t), \quad x \in [0, s(t)] \tag{1.3}$$

where k is the thermal conductivity. Therefore, the time evolution of the temperature profile in the material's domain can be obtained by combining the energy conservation (1.1) and the thermal condition (1.3), which leads to the following heat equation of the liquid phase

$$T_t(x,t) = \alpha T_{xx}(x,t), \quad x \in (0, s(t)), \tag{1.4}$$

where $\alpha := \frac{k}{\rho C_p}$. At the boundary $x = 0$, there are two cases of how to impose the boundary condition. One is that a heat flux enters as an external source which can be manipulated as a controlled variable, denoted as $q_c(t)$ and the boundary condition is derived using the thermal conduction law (1.3). The other case is that the boundary temperature can be directly controlled as $T_c(t)$. Hence, the boundary condition at $x = 0$ is either

$$-kT_x(0,t) = q_c(t), \tag{1.5}$$

or

$$T(0,t) = T_c(t). \tag{1.6}$$

The boundary condition prescribed at $x = s(t)$ is involved with the melting temperature which is the constant threshold level to cause the phase change from the solid to liquid under a static

pressure, i.e.,

$$T(s(t),t) = T_{\mathrm{m}}. \tag{1.7}$$

Other than the spacial boundary conditions, the time initial conditions needs to be defined as an arbitral spatial function for the temperature profile and a positive valued interface position as

$$T(x,0) = T_0(x), \quad s(0) = s_0. \tag{1.8}$$

If we don't care about the dynamics of the moving boundary $s(t)$, PDE model (1.4)–(1.8) are somewhat simple linear system. However, the tricky property of the Stefan problem lies in the dynamics of the moving boundary $s(t)$. By combining the latent heat energy balance (1.2) and the thermal conduction (1.3), one can derive the so called "Stefan condition" defined as the following nonlinear ODE

$$\dot{s}(t) = -\beta T_x(s(t),t), \tag{1.9}$$

where $\beta := \frac{k}{\rho \Delta H^*}$ and ΔH^* denotes the latent heat of fusion. Equation (1.9) expresses the velocity of the liquid-solid moving interface.

As we have presented, there are two problems to describe the one phase Stefan problem as a nonlinearly coupled PDE-ODE system depending on how to impose the boundary condition at $x = 0$. Hereafter, we name each problem as PI (Problem I) and PII (Problem II) as follows.

PI : Neumann Boundary Actuation

$$T_t(x,t) = \alpha T_{xx}(x,t), \quad x \in (0, s(t)), \tag{1.10}$$

$$-kT_x(0,t) = q_c(t), \tag{1.11}$$

$$T(s(t),t) = T_m, \tag{1.12}$$

$$\dot{s}(t) = -\beta T_x(s(t),t), \tag{1.13}$$

PII : Dirichlet Boundary Actuation

$$T_t = \alpha T_{xx}(x,t), \quad x \in (0, s(t)), \tag{1.14}$$

$$T(0,t) = T_c(t), \tag{1.15}$$

$$T(s(t),t) = T_m, \tag{1.16}$$

$$\dot{s}(t) = -\beta T_x(s(t),t) \tag{1.17}$$

In addition, for each problem setup, there are two types of mathematical problem of how to obtain the pair of solution as follows.

Direct Stefan Problem : Given $q_c(t)$ in PI (or $T_c(t)$ in PII) as a prescribed function in time, solve $(T(x,t), s(t))$.

Inverse Stefan Problem : Given $s(t)$ as a prescribed function in time, solve $T(x,t)$ and $q_c(t)$ in PI (or $T_c(t)$ in PII).

Since we have established the model (1.10)–(1.13) in PI (or (1.14)–(1.17) in PII) based on the situation that the domain $x \in [0, s(t)]$ is occupied by the liquid phase, to maintain a physical validity of the homogeneous melting material, the Stefan problem exhibits a important property

that is discussed in the following remark.

Remark 1 *The formulation of the Stefan problem is a reasonable model only if the following condition holds:*

$$T(x,t) \geq T_{\mathrm{m}}, \quad \forall x \in [0, s(t)], \quad \forall t \geq 0, \tag{1.18}$$

$$0 < s(t) < L, \quad \forall t \geq 0. \tag{1.19}$$

Hence, the model is valid if and only if the liquid temperature is greater than the melting temperature, and the liquid-solid interface remains inside the material's domain. One of the conditions yields the following monotonicity of the moving interface.

Lemma 1 *If the model validity condition* (1.18) *holds, then the moving interface is monotonically nondecreasing, i.e.,*

$$\dot{s}(t) \geq 0, \quad \textit{for all} \quad t \geq 0. \tag{1.20}$$

Lemma 1 is established using Hopf's Lemma and a detailed proof can be found in [60]. To satisfy the conditions (1.18) and (1.19), it is plausible to impose the following assumption on the initial values.

Assumption 1 *The initial interface position satisfies* $s_0 > 0$ *and the Lipschitz continuity of* $T_0(x)$ *holds, i.e.,*

$$0 \leq T_0(x) - T_{\mathrm{m}} \leq H(s_0 - x). \tag{1.21}$$

Assumption 1 is physically reasonable and consistent with Remark 1. Hereafter, we always impose Assumption 1 without explicitly stating.

1.3 Explicit Solutions

Neumann solution by a constant boundary temperature

A well known analytical solution of the Stefan problem is so called "Neumann solution", named after the discovery of the solution by F. Neumann around 1860 [33]. The name might be a kind of misleading because the solution is equivalent to the one under a constant Dirichlet boundary condition (not Neumann boundary condition) at $x = 0$ as a direct Stefan problem in PII. Thus, the condition is prescribed as

$$T_c(t) = T_b, \tag{1.22}$$

in PII. The Neumann solution to the equations (1.14)–(1.17) with the above condition is given by

$$T(x,t) = T_b - \frac{T_b - T_m}{\mathrm{erf}\,(\lambda)} \mathrm{erf}\left(\frac{x}{2\sqrt{\alpha t}}\right), \tag{1.23}$$

$$s(t) = 2\lambda\sqrt{\alpha t}, \tag{1.24}$$

where $\mathrm{erf}(\cdot)$ is the error function defined by

$$\mathrm{erf}(x) = \frac{2}{\sqrt{\pi}} \int_0^x e^{-t^2} dt. \tag{1.25}$$

We can see that the pair of the solution (1.23) and (1.24) satisfy the model equation (1.14)–(1.17) with the implicit parameter λ which is a solution to the following nonlinear algebraic equation

$$\sqrt{\pi}\lambda \mathrm{erf}(\lambda) e^{\lambda^2} = Ste, \tag{1.26}$$

where Ste is so called "Stefan number" defined by

$$Ste = \frac{C_p}{\Delta H^*}(T_b - T_m). \tag{1.27}$$

Since the boundary temperature condition (1.22) is reasonable and simple, this pair of solution (1.23) and (1.24) have been very popular among thermal and chemical engineers. Once we consider the inverse Stefan problem of PI by prescribing the interface solution as (1.24), the boundary heat flux is obtained as

$$q_c(t) = \frac{k(T_b - T_m)}{\mathrm{erf}(\lambda)\sqrt{\pi\alpha}}\frac{1}{\sqrt{t}}. \tag{1.28}$$

In other words, for the boundary temperature $T(0,t)$ to maintain a constant value, the boundary heat flux $q_c(t)$ must be a decaying function in time which is proportional to $\frac{1}{\sqrt{t}}$.

Case 2 : Linear growth of the interface

Another known analytical solution can be obtain by the inverse Stefan problem of both PI and PII. There, the interface dynamics is set as growing linearly in time, which can be described as

$$s(t) = At, \tag{1.29}$$

where $A > 0$ is a positive parameter. Then, one can see that the following solution of the temperature profile

$$T(x,t) = \frac{\alpha}{\beta}\left(e^{\frac{A}{\alpha}(At-x)} - 1\right) + T_m \tag{1.30}$$

satisfies the governing equations (1.10)–(1.13) (or (1.14)–(1.17)). Thus, the associated boundary condition in PI is given by

$$q_c(t) = \frac{kA}{\beta} e^{\frac{A^2}{\alpha} t}, \tag{1.31}$$

in PI, or

$$T_c(t) = \frac{\alpha}{\beta} \left(e^{\frac{A^2}{\alpha} t} - 1 \right) + T_m \tag{1.32}$$

in PII.

1.4 Mathematical Analysis

This section is devoted to a rigorous analysis which is especially of interest to mathematicians, that is, the existence and uniqueness of the classical solution. To begin, referring to [55], the definition of the classical solution is defined as follows:

Definition 1 *Under Assumption 1, a pair* $(T(x,t), s(t))$ *is the classical solution of the one-phase Stefan problem* (1.10)–(1.13) *with* $q_c(t) \geq 0$ *in PI (or* (1.14)–(1.17) *with* $T_c(t) \geq T_m$ *in PII) for all* $t < \sigma$*, where* $0 < \sigma \leq \infty$ *if*

(i) T_{xx} *and* T_t *are continuous for* $0 < x < s(t)$, $0 < t < \sigma$*;*

(ii) T *and* T_x *are continuous for* $0 \leq x \leq s(t)$, $0 < t < \sigma$*;*

(iii) T *is also continuous for* $t = 0$, $0 < x \leq s_0$ *and* $0 \leq \liminf T(x,t) \leq \limsup T(x,t) < \infty$ *as* $t \to 0$, $x \to 0$*;*

(iv) $s(t)$ *is continuously differentiable for* $0 \leq t < \sigma$*;*

(v) the equations (1.10)–(1.13) *are satisfied.*

Thus, the explicit solutions introduced in Section 1.3 are the classical solution. Again by

referring to [55], the existence and uniqueness of the classical solution can be guaranteed by the following lemma.

Lemma 2 *Assume that $q_c(t)$ in PI (or $T_c(t)$ in PII) and $T_0(x)$ are continuously differentiable functions for $\forall t > 0$ and $\forall x \in [0, s_0]$. Then there exists a unique classical solution $(T(x,t), s(t))$ of the system* (1.10)–(1.13) *provided that $q_c(t) \geq 0$ in PI (or the system* (1.14)–(1.17) *provided that $T_c(t) \geq T_m$ in PII) and Assumption 1 for all $t > 0$.*

Once the existence and uniqueness of the solution is established, the validity of the model is ensured by the following lemma.

Lemma 3 *If there is a unique classical solution of* (1.10)–(1.13)*, then for any $q_c(t) \geq 0$ in PI (or $T_c(t) \geq T_m$ in PII) for all $t < \sigma$ where $0 < \sigma \leq \infty$, the condition* (1.18) *holds, and* (1.20) *is also satisfied by Lemma 1. In addition, if $q_c(t) > 0$ in PI (or $T_c(t) > T_m$ in PII) holds then the strong inequality of* (1.18) *and* (1.20) *holds.*

The proof of Lemma 3 is based on Maximum principle as shown in [60]. Furthermore, both Definition 1 and Lemma 2 can be extended to the generalized parabolic PDE

$$T_t = \alpha(x,t)T_{xx} + b(x,t)T_x + h(x,t)T, \tag{1.33}$$

provided that $h(x,t) \leq 0$ and the functions α_x, α_{xx}, α_t, b, b_x, and h are Hölder continuous for $0 \leq x < \infty$, $t \geq 0$.

1.5 Macroscopic Energy Balance

This section provides a physical perspective of the system. The conventional thermodynamics gives the heat balance in macroscopic scale, known as the first law of the thermodynamics. For the Stefan problem, the first law of the thermodynamics is obtained by taking the integration

of the local energy balance on the whole domain as

$$\rho C_{\mathrm{p}} \int_0^{s(t)} T_t(x,t)dx = -(q(s(t),t) - q(0,t)). \tag{1.34}$$

Combining the specific heat with the latent heat, the internal energy is defined as

$$E(t) = \rho C_{\mathrm{p}} \int_0^{s(t)} (T(x,t) - T_{\mathrm{m}})dx + \rho \Delta H^* s(t). \tag{1.35}$$

Taking the time derivative of (1.35) along the solution of (1.10)–(1.13), we can see that

$$\frac{dE}{dt}(t) = q_{\mathrm{c}}(t). \tag{1.36}$$

Taking the time integration of (1.36) yields the following description of the macroscopic energy conservation law

$$E(t) - E(0) = \int_0^t q_{\mathrm{c}}(\tau)d\tau. \tag{1.37}$$

The left-hand side of (1.37) denotes the growth of internal energy, and its right-hand side denotes the external work provided by the injected heat flux. This form directly captures the classical first law of thermodynamics without heat dissipation.

1.6 Numerical Methods

This section presents the numerical method of 1D one-phase Stefan problem by referring to [102]. While there are several methods, in this book we introduce a boundary immobilization method (BIM) technique which shows an enough accurate data for 1D Stefan problem in cartesian coordinate. The idea of BIM is to scale the original coordinate on time-varying domain to the new coordinate on fixed domain. The resulting system through the scaling leads to a nonlinear coupled

PDE-ODE system. Then, we utilize some approximations for the spatial and time derivatives by finite difference and Euler method, that yields a set of nonlinear difference equations.

Algorithm development by BIM

Let us introduce the following scaling of the spatial coordinate and the associated state variable as

$$\xi := \frac{x}{s(t)}, \quad v(\xi,t) := T(x,t). \tag{1.38}$$

Then, the relations of the spatial and time derivatives are given by

$$T_x(x,t) = \frac{\partial \xi}{\partial x} v_\xi(\xi,t) = \frac{1}{s(t)} v_\xi(\xi,t), \tag{1.39}$$

$$T_{xx}(x,t) = \left(\frac{\partial \xi}{\partial x}\right)^2 v_{\xi\xi}(\xi,t) = \frac{1}{s(t)^2} v_{\xi\xi}(\xi,t), \tag{1.40}$$

$$\begin{aligned} T_t(x,t) =& \frac{\partial \xi}{\partial t} v_\xi(\xi,t) + v_t(\xi,t) = -\frac{x\dot{s}(t)}{s(t)^2} v_\xi(\xi,t) + v_t(\xi,t) \\ =& -\frac{\xi \dot{s}(t)}{s(t)} v_\xi(\xi,t) + v_t(\xi,t) \end{aligned} \tag{1.41}$$

First, we derive the numerical algorithm for Neumann boundary actuation setup in PI. Substituting the above derivatives in (1.10)–(1.13), we obtain

$$v_t(\xi,t) = \frac{\alpha}{s(t)^2} v_{\xi\xi}(\xi,t) + \frac{\xi \dot{s}(t)}{s(t)} v_\xi(\xi,t), \quad 0 < \xi < 1 \tag{1.42}$$

$$v_\xi(0,t) = -k^{-1} s(t) q_c(t), \tag{1.43}$$

$$v(1,t) = T_m, \tag{1.44}$$

$$\dot{s}(t) = -\frac{\beta}{s(t)} v_\xi(1,t), \tag{1.45}$$

The PDE state is evaluated at points $\xi = ih$ for $i = 0, 1, \cdots, N$ where N is the discretization number and $Nh = 1$. Then, the number of the elements is $N+1$. Thus, the following state variables are defined

$$v^{(i)}(t) = v(ih, t), \quad \text{for} \quad i = 0, 1, 2, \cdots, N \tag{1.46}$$

To approximate the spatial derivatives, we use the finite difference method. The first and second spacial derivatives in second-order accurate scheme are obtained by

$$v_\xi(ih, t) = \frac{v^{(i+1)}(t) - v^{(i-1)}(t)}{2h} + O(h^2), \tag{1.47}$$

$$v_{\xi\xi}(ih, t) = \frac{v^{(i+1)}(t) - 2v^{(i)}(t) + v^{(i-1)}(t)}{h^2} + O(h^2). \tag{1.48}$$

By evaluating the fixed domain PDE (1.42) at $\xi = ih$ for $i = 0, 1, \cdots, N-1$, the following N-th ODEs are derived

$$\frac{d}{dt}v^{(i)}(t) = \frac{\alpha}{h^2 s(t)^2}(v^{(i+1)}(t) - 2v^{(i)}(t) + v^{(i-1)}(t)) + \frac{i\dot{s}(t)}{2s(t)}(v^{(i+1)}(t) - v^{(i-1)}(t)), \tag{1.49}$$

A reader might notice that the above equation at $i = 0$ includes an undefined value, that is, $v^{(-1)}(t)$. This is called "fictitious value", and it is obtained by applying (1.47) to the boundary condition at $\xi = 0$ in (1.43), which yields

$$v^{(-1)}(t) = v^{(1)}(t) + 2hk^{-1}s(t)q_c(t). \tag{1.50}$$

Also, the boundary condition at $\xi = 1$ is

$$v^{(N)}(t) = T_m. \tag{1.51}$$

To describe the spatial derivative of the temperature at the moving interface position, we cannot use the central approximation since there is no position one step forward than the moving boundary. Instead, the finite difference approximation of the first derivative in second-order accurate is given as in [102];

$$\dot{s}(t) = -\frac{\beta}{s(t)} \frac{3v^{(N)}(t) - 4v^{(N-1)}(t) + v^{(N-2)}(t)}{2h}. \tag{1.52}$$

In addition, the time discretization is implemented by defining the discrete time states as

$$v_j^{(i)} = v^{(i)}(j\Delta t), \quad s_k = s(j\Delta t), \quad j = 0, 1, \cdots, M \tag{1.53}$$

where $M = \lfloor t_f/\Delta t \rfloor$ with the final time t_f. The well-known approximation is explicit Euler method (a.k.a. forward Euler method) which has a first order accuracy. Applying Euler method to (1.49) and (1.49), the numerical solution of the Stefan problem is obtained by employing the following algorithm:

Algorithm 1: Time Update for Temperature Profile and Phase Interface

Input: s_0, $\{v_0^i\}_{i=0}^N$
for $j = 0$ to M, **do**
  $v_j^{(-1)} \leftarrow v_j^{(1)} + 2hk^{-1}s_j q_c(j\Delta t)$
  $v_j^{(N)} \leftarrow T_m$
  $\dot{s}_j \leftarrow -\frac{\beta\left(3v_j^{(N)} - 4v_j^{(N-1)} + v_j^{(N-2)}\right)}{2hs_j}$
  $s_{j+1} \leftarrow s_j + \Delta t \dot{s}_j$
  for $i = 0$ to $N-1$, **do**
    $v_{j+1}^{(i)} \leftarrow v_j^{(i)} + \Delta t \left(\frac{\alpha}{h^2 s_j^2}(v_j^{(i+1)} - 2v_j^{(i)} + v_j^{(i-1)}) + \frac{i\dot{s}_j}{2s_j}(v_j^{(i+1)} - v_j^{(i-1)}) \right)$
  end for
end for
Output: $\{s_j\}_{j=1}^M$, $\{v_j^i\}_{i=0,j=1}^{N,M}$

By defining the state vector $v(t) = [v^{(0)}(t), v^{(1)}(t), \cdots, v^{(N-1)}(t)]$ and substituting the

Table 1.1: Physical properties of zinc

Description	Symbol	Value
Density	ρ	$6570\ \mathrm{kg}\cdot\mathrm{m}^{-3}$
Latent heat of fusion	ΔH^*	$112000\ \mathrm{J}\cdot\mathrm{kg}^{-1}$
Heat capacity	C_p	$390\ \mathrm{J}\cdot\mathrm{kg}^{-1}\cdot\mathrm{K}^{-1}$
Thermal conductivity	k	$116\ \mathrm{w}\cdot\mathrm{m}^{-1}$
Melting temperature	T_m	$419.5\ ^\circ$ C

boundary conditions, we obtain the nonlinear ODEs for the state vector $[\phi, s]$ as

$$\frac{d}{dt}\begin{bmatrix} v \\ s \end{bmatrix} = \begin{bmatrix} \frac{1}{s(t)^2}(Av + g(v)) \\ \frac{\beta}{2hs(t)}(-4v^{(N-1)}(t) + v^{(N-2)}(t)) \end{bmatrix} + \frac{2\alpha}{hks(t)}Bq_c(t) \tag{1.54}$$

where

$$A = \frac{\alpha}{h^2}\begin{pmatrix} -2 & 2 & 0 & \cdots & \cdots & \cdots & \cdots & \cdots & 0 \\ 1 & -2 & 1 & 0 & \cdots & \cdots & \cdots & \cdots & 0 \\ 0 & 1 & -2 & 1 & 0 & \cdots & \cdots & \cdots & 0 \\ \vdots & & & & \ddots & & & & \vdots \\ 0 & \cdots & \cdots & \cdots & \cdots & 0 & 1 & -2 & 1 \\ 0 & \cdots & \cdots & \cdots & \cdots & \cdots & 0 & 1 & -2 \end{pmatrix} \tag{1.55}$$

In the case of Dirichlet boundary actuation given in PII, the fictitious variable $v_j^{(-1)}$ is not needed since $v_j^{(0)}$ directly captures the boundary temperature $T_c(j\Delta t)$. Hence, the algorithm is replaced by $v_j^{(0} = T_c(j\Delta t)$ and i starts from 1.

Simulation result

The numerical simulation of BMI is performed using the physical parameters of zinc given in Table 1.1. We apply the Dirichelt boundary actuation setup with the constant boundary

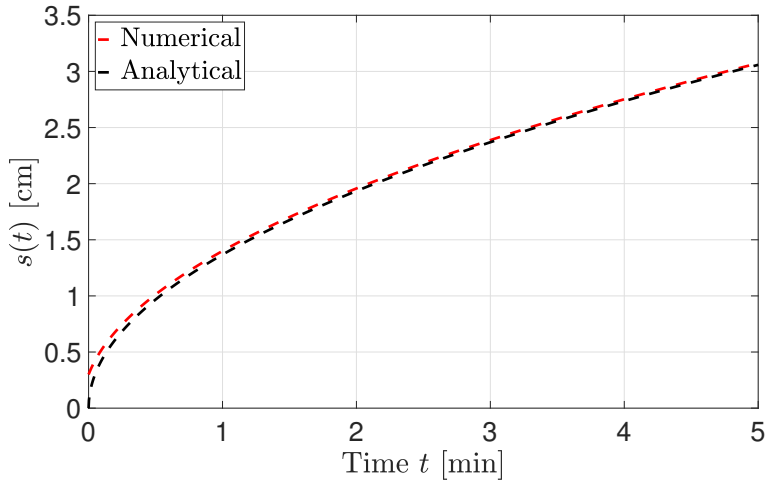

(a) Interface position dynamics of the analytical solution in (1.24) (black) and the numerical solution (red).

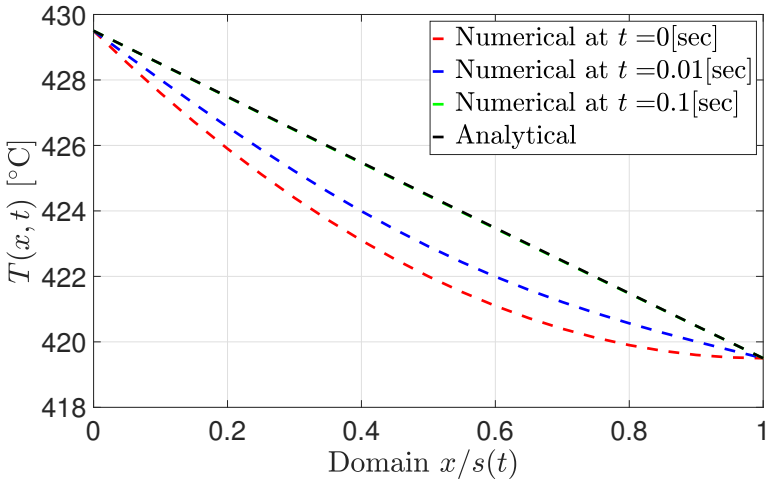

(b) Temperature profile dynamics of analytical solution in (1.23) (black) and the numerical solution at $t = 0$ (red), $t = 0.01$ (blue), $t = 0.1$ (green)

Figure 1.2: Comparison of the analytical solution and the numerical solution by Algorithm 1. The numerical solution converges to the analytical solution very quickly from an initial error.

temperature $T_b = T_m + 10$ [$^\circ C$] with $T_m = 419.5$ [°C]. As explained in Section 1.3, the explicit solution under the constant boundary temperature is given by Neumann solution. Moreover, the

solution in the scaled fixed domain is given by

$$v(\xi,t) = T_b - \frac{T_b - T_m}{\text{erf}(\lambda)}\text{erf}(\lambda\xi), \tag{1.56}$$

which is independent on time t. Hence, the numerical solution should approaches to the solution (1.56). The initial data are set as $s_0 = 3$ [mm] and $T_0(x) = (T_b - T_m)(1 - x/s_0)^2 + T_m$, which satisfies the boundary conditions. Fig. 1.2 (a) depicts the interface position dynamics of the simulation result of the numerical model and the analytical solution, which shows the good correspondence as time goes. Also, Fig. 1.2 (b) depicts the temperature profile of the numerical simulation at $t = 0$, t =0.01 [sec], $t = 0.1$[min], and the analytic solution, which illustrates that the numerical solution converges to the analytic solution as time goes.

Chapter 2

State Feedback Control Design

This chapter presents the design procedure of the control algorithm for the one-phase Stefan problem. Due to the recent advancement of software performance, a sophisticated control algorithm which is involved with highly complex computations has attained strong possibilities for practical implementations. In addition, the phase changes appear in a variety of scientific phenomena and industrial processes. Therefore, the design procedure of the control algorithm for the Stefan problem is significant for numerous applications in science and engineering (we introduce some examples in Part II).

2.1 Control Objective of Stefan Problem

This section states how the control problem is posed in the Stefan problem. Especially, we focus on PI given in Chapter 1, i.e., we consider the design of boundary heat flux $q_c(t) > 0$

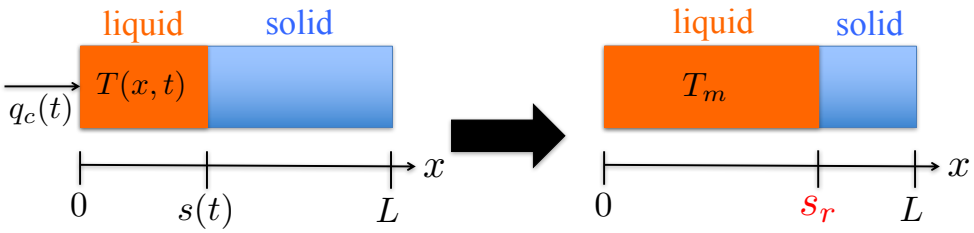

Figure 2.1: Control objective of the Stefan problem. We aim to design a heat flux input $q_c(t)$ such that the interface position $s(t)$ is driven to the setpoint position s_r.

for the state variables $(T(x,t),s(t))$ governed by the following coupled PDE-ODE system

$$T_t(x,t) = \alpha T_{xx}(x,t), \quad x \in (0,s(t)), \tag{2.1}$$

$$-kT_x(0,t) = q_c(t), \tag{2.2}$$

$$T(s(t),t) = T_m, \tag{2.3}$$

$$\dot{s}(t) = -\beta T_x(s(t),t). \tag{2.4}$$

How to achieve a desired size

In some engineering process, achieving a desired shape of the material is an important task. For instance, in manufacturing industries, the desired shape is given based on the required quality of the product. In 1D one phase Stefan problem, such a desired shape is equivalent to the desired length of the liquid material. Therefore, it is significant to consider the design of boundary heat flux to drive the liquid-solid interface position $s(t)$ to a given desired setpoint position s_r. At the desired state, both of the temperature profile and the interface position needs to be static. Such a "steady-state" solution $(T_{eq}(x), s_{eq})$ of the system (2.1)–(2.4) is given by setting $T_t = 0$ and $\dot{s}(t) = 0$ in (2.1) and (2.4) and imposing the boundary condition (2.3). Thus, the steady-state

solution satisfies

$$T''_{\mathrm{eq}}(x) = 0, \quad T_{\mathrm{eq}}(s_{\mathrm{eq}}) = T_{\mathrm{m}}, \quad T'_{\mathrm{eq}}(s_{\mathrm{eq}}) = 0, \tag{2.5}$$

which yields the steady-state temperature profile as a uniform melting temperature, i.e.,

$$T_{\mathrm{eq}}(x) = T_{\mathrm{m}} \tag{2.6}$$

for any given s_r. Thus, the objective of the control design is to achieve the following asymptotic convergence,

$$\lim_{t\to\infty} s(t) = s_{\mathrm{r}}, \tag{2.7}$$

$$\lim_{t\to\infty} T(x,t) = T_{\mathrm{m}}. \tag{2.8}$$

Setpoint restriction by an energy conservation

Clearly, the setpoint s_{r} must be chosen to satisfy $0 < s_{\mathrm{r}} < L$, as addressed in the condition (1.19). In addition, the positivity of the manipulated heat flux in Lemma 3 imposes a restriction on the setpoint given that system (2.1)–(2.4) satisfies the following energy conservation

$$\frac{d}{dt}\left(\frac{k}{\alpha}\int_0^{s(t)} (T(x,t) - T_{\mathrm{m}})dx + \frac{k}{\beta}s(t)\right) = q_{\mathrm{c}}(t). \tag{2.9}$$

Integrating (2.9) in t from 0 to ∞ and substituting (2.7) and (2.8), one can deduce that the heat flux $q_c(t)$ that drives the system (2.1)–(2.4) to the desired setpoint satisfies the following relation

$$\frac{k}{\beta}(s_{\mathrm{r}} - s_0) - \frac{k}{\alpha}\int_0^{s_0} (T_0(x) - T_{\mathrm{m}})dx = \int_0^{\infty} q_{\mathrm{c}}(t)dt. \tag{2.10}$$

From relation (2.10), one can deduce that for any positive heat flux control $q_c(t) > 0$, the internal energy for a given setpoint must be greater than the initial internal energy. Thus, the following assumption is required.

Assumption 2 *The setpoint s_r is chosen to satisfy*

$$s_0 + \frac{\beta}{\alpha}\int_0^{s_0}(T_0(x) - T_m)dx < s_r < L. \tag{2.11}$$

Therefore, Assumption 2 stands as the least restrictive condition for the choice of setpoint and can be consequently viewed as a setpoint restriction.

Open-loop setpoint control law by energy shaping perspective

For any given open-loop control law $q_c(t)$ satisfying (2.10), the asymptotical stability of the system (2.1)–(2.4) at s_r can be established and the following lemma holds.

Lemma 4 *Consider an open-loop setpoint control law $q_c^\star(t)$ which satisfies* (2.10)*. Then, the interface converges asymptotically to the prescribed setpoint s_r and consequently, conditions* (2.7) *and* (2.8) *hold.*

The proof of Lemma 4 can be derived straightforwardly from (2.10). To illustrate the introduced concept of open-loop "energy shaping control" action, we define ΔE as the left-hand side of (2.10), i.e.,

$$\Delta E = \frac{k}{\beta}(s_r - s_0) - \frac{k}{\alpha}\int_0^{s_0}(T_0(x) - T_m)dx. \tag{2.12}$$

For instance, the rectangular pulse control law given by

$$q_c^\star(t) = \left\{ \begin{array}{ll} \bar{q} & \text{for} \quad t \in [0, \Delta E/\bar{q}] \\ 0 & \text{for} \quad t > \Delta E/\bar{q} \end{array} \right\} \tag{2.13}$$

satisfies (2.12) for any choice of the boundary heat flux $\bar{q}$ and thereby, ensures the asymptotical stability of (2.1)–(2.4) to the setpoint $(T_{\mathrm{m}}, s_{\mathrm{r}})$.

Towards closed-loop feedback control

It is remarkable that adopting an open-loop control strategy such as the rectangular pulse (2.13), does not allow to improve the convergence speed. Moreover, the physical parameters of the model need to be known accurately. In engineering process, the practical implementation of an open-loop control is limited by performance and robustness issues, thus closed-loop control laws have to be designed to deal with such limitations.

In the following sections, we aim the design of closed-loop backstepping control law for the one-phase Stefan problem in order to achieve faster exponential convergence to the desired setpoint $(T_{\mathrm{m}}, s_{\mathrm{r}})$ while ensuring the robustness of the closed-loop system to the uncertainty of the physical parameters. In detail, for a given reference setpoint $(T_{\mathrm{m}}, s_{\mathrm{r}})$, we define the reference error states (u, X) as

$$u(x,t) = T(x,t) - T_{\mathrm{m}}, \quad X(t) = s(t) - s_{\mathrm{r}}, \tag{2.14}$$

respectively. Then, the reference error system associated to the coupled system (2.1)–(2.4) is written as

$$u_t(x,t) = \alpha u_{xx}(x,t), \quad 0 \leq x \leq s(t), \tag{2.15}$$

$$u_x(0,t) = -k^{-1} q_{\mathrm{c}}(t), \tag{2.16}$$

$$u(s(t),t) = 0, \tag{2.17}$$

$$\dot{X}(t) = -\beta u_x(s(t),t). \tag{2.18}$$

Hence, from the perspective of the reference error system (u, X), the objective is to design $q_c(t)$

to stabilize the state variables (u, X) at $(0, 0)$, which is a standard description in control theory.

2.2 Basic Idea of PDE Control on Fixed Boundary

Overview

In this section, we introduce a well-known method of the control design for systems described by PDEs. The method is "backstepping" which was firstly developed for nonlinear and adaptive systems [92], and successfully extended to PDE of parabolic [141, 143], hyperbolic [94, 5], delays [97, 11], and adaptive systems [100, 144, 145]. Further advances on the backstepping control of diffusion equations defined on a multidimensional space or involving in-domain coupled systems can be found in [8, 43, 160, 161]. PDE backstepping design has been utilized for the applications to oil drilling [134, 62, 167, 169], multi-agent system [59, 130], traffic control [179], battery management [118, 117], mining cables [166, 168, 170], etc. The fundamental idea of the backstepping is to introduce a "state transformation" to convert the original system to an ideal stable system, and derive the control design to be consistent with the transformation.

Results devoted to the backstepping stabilization of coupled systems described by a diffusion PDE in cascade with a linear ODE has been primarily presented in [95] with Dirichlet type of boundary interconnection and extended to Neumann boundary interconnection in [153, 156]. For systems relevant with Stefan problem, [65] designed a backstepping output feedback controller that ensures the exponential stability of an unstable parabolic PDE on *a priori* known dynamics of moving interface which is assumed to be an analytic function in time. Moreover, for PDE-ODE cascaded systems under a state-dependent moving boundary, [22] derived a local stability result for nonlinear ODEs with actuator dynamics governed by a wave PDE defined on a time- and state-dependent moving domain. Such a technique is based on the input delay and wave compensation for nonlinear ODEs designed in [98, 10] and its extension to state-dependent input delay compensation for nonlinear ODEs provided by [9]. While the results in [22] and

[9] that cover state-dependence problems do not ensure global stabilization due to a so-called feasibility condition that needs to be satisfied *a priori*, such a restriction was recently unlocked in [37] which provides a global stability result. However, the result in [37] is limited to the case of hyperbolic PDE in cascade with a nonlinear ODE.

Unstable reaction-diffusion PDE

As an introductory example of diffusion type systems of which the solution diverges in time, let us consider the following diffusion reaction PDE

$$u_t = u_{xx}(x,t) + \lambda u(x,t), \quad 0 < x < 1, \tag{2.19}$$

$$u(0,t) = 0, \tag{2.20}$$

$$u(1,t) = 0, \tag{2.21}$$

$$u(x,0) = u_0(x). \tag{2.22}$$

The solution to (2.19)–(2.21) is uniquely given by (see Section 3.1 in [99] for detail)

$$u(x,t) = \sum_{n=1}^{\infty} C_n e^{(\lambda-\pi^2 n^2)t} \sin(\pi n x). \tag{2.23}$$

where $C_n = 2\int_0^1 u_0(y)\sin(\pi n y)\,dy$. The important characteristic of the solution (2.23) is the time dependency, namely, the exponential term $e^{(\lambda-\pi^2 n^2)t}$. For the solution not to diverge, the coefficient in the exponent $\lambda - \pi^2 n^2$ needs not to be positive for all $n = 1, 2, \cdots$. Clearly, this condition holds if $\lambda \leq \pi^2$ by considering the case $n = 1$. Moreover, if $\lambda < \pi^2$ then the solution converges to zero as $t \to \infty$.

In order for the solution to converge to zero under $\lambda \geq \pi^2$, some actuation needs to be manipulated. There are two distinct types of control problems for PDEs. One is "in-domain control", which renders actuators to be located inside the domain of the PDE, resulting in the

control term to appear in PDE as a mathematical structure. The other is "boundary control", in which the actuator is located only in the boundary of the PDE. Then, the control term only appears in the boundary condition of the PDE. In general, the boundary control is more challenging to design compared to the in-domain control, and even somewhat practical setup.

Referring to [99], we consider the boundary control at $x = 1$, with defining $U(t)$ as a control input. Thus, the resulting problem we consider is

$$u_t = u_{xx}(x,t) + \lambda u(x,t), \quad 0 < x < 1, \tag{2.24}$$

$$u(0,t) = 0, \tag{2.25}$$

$$u(1,t) = U(t). \tag{2.26}$$

The "backstepping design" is one of the most systematic method for the boundary control of PDEs, which have been studied widely since the first work in [141]. The method introduces a state transformation (called "backstepping transformation") from the original state $u(x,t)$ to newly defined state $w(x,t)$ in the following form

$$w(x,t) = u(x,t) - \int_0^x k(x,y)u(y,t)dy, \tag{2.27}$$

where $k(x,y)$ is so called "gain kernel" function which is solved later. The idea of the backstepping is to design a stable "target system". Mostly, the target system is chosen to have a similar structure as the original system with canceling some undesired (or adding some desired) terms for the stabilization. For instance, in the reaction-diffusion PDE (2.24)–(2.26), the undesired term is $\lambda u(x,t)$ in (2.24) as we have seen in the analytical solution (2.23). Hence, a natural choice of the

target system is

$$w_t = w_{xx}(x,t), \quad 0 < x < 1, \tag{2.28}$$

$$w(0,t) = 0, \tag{2.29}$$

$$w(1,t) = 0. \tag{2.30}$$

The solution of the target system (2.28)–(2.28) converges to zero as we can see by substituting $\lambda = 0$ in the analytic solution (2.23). Next task is to find the gain kernel solution $k(x,y)$ in the transformation (2.27) to sustain the consistency between the original u-system (2.24)–(2.26) and the target w-system (2.28)–(2.30). Taking the first and second spacial derivatives of (2.27), we obtain

$$w_x(x,t) = u_x(x,t) - k(x,x)u(x,t) - \int_0^x k_x(x,y)u(y,t)dy, \tag{2.31}$$

$$\begin{aligned} w_{xx}(x,t) =& u_{xx}(x,t) - k(x,x)u_x(x,t) \\ & - \left(k_x(x,x) + \frac{d}{dx}k(x,x)\right)u(x,t) - \int_0^x k_{xx}(x,y)u(y,t)dy \end{aligned} \tag{2.32}$$

Taking the time derivative of (2.27) along the solution of (2.24)–(2.26) leads to

$$w_t(x,t) = u_{xx}(x,t) + \lambda u(x,t) - \int_0^x k(x,y)(u_{yy}(y,t) + \lambda u(y,t))dy \tag{2.33}$$

Using the integration by parts twice and the boundary condition (2.25),

$$\begin{aligned} \int_0^x k(x,y)u_{yy}(y,t)dy =& k(x,x)u_x(x,t) - k(x,0)u_x(0,t) - \int_0^x k_y(x,y)u_y(y,t)dy \\ =& k(x,x)u_x(x,t) - k(x,0)u_x(0,t) \\ & - k_y(x,x)u(x,t) + \int_0^x k_{yy}(x,y)u(y,t)dy \end{aligned} \tag{2.34}$$

Substituting (2.34) into (2.33), we have

$$\begin{aligned} w_t(x,t) =& u_{xx}(x,t) - k(x,x)u_x(x,t) + (k_y(x,x) + \lambda)\, u(x,t) \\ &+ k(x,0)u_x(0,t) - \int_0^x (k_{yy}(x,y) + \lambda k(x,y))\, u(y,t)dy \end{aligned} \tag{2.35}$$

Subtracting (2.32) from (2.35), we have

$$\begin{aligned} w_t(x,t) - w_{xx}(x,t) = & \left(2\frac{d}{dx}k(x,x) + \lambda\right) u(x,t) + k(x,0)u_x(0,t) \\ &+ \int_0^x (k_{xx}(x,y) - k_{yy}(x,y) - \lambda k(x,y))\, u(y,t)dy \end{aligned} \tag{2.36}$$

To satisfy target PDE (2.28), the right hand side of (2.36) must be zero for any $u(x,t)$, and thus the following conditions of the gain kernel function must be satisfied:

$$k_{xx}(x,y) - k_{yy}(x,y) = \lambda k(x,y), \tag{2.37}$$

$$k(x,0) = 0, \tag{2.38}$$

$$\frac{d}{dx}k(x,x) = -\frac{\lambda}{2}, \tag{2.39}$$

The solution to the PDE (2.37)–(2.39) is given by

$$k(x,y) = -\lambda y \frac{I_1(z)}{z}, \quad z := \sqrt{\lambda(x^2 - y^2)}. \tag{2.40}$$

where $I_1(z)$ is a modified Bessel function of the first kind defined by

$$I_1(z) = \sum_{m=0}^{\infty} \frac{1}{m!(m+1)!} \left(\frac{z}{2}\right)^{2m+1} \tag{2.41}$$

Evaluating (2.27) at $x = 1$ together with the boundary conditions of the original system (2.26)

and the target system (2.30), the control law is designed by

$$\begin{aligned} U(t) &= \int_0^1 k(1,y)u(y,t)dy \\ &= -\lambda \int_0^1 y \frac{I_1(\sqrt{\lambda(1-y^2)})}{\sqrt{\lambda(1-y^2)}} u(y,t)dy. \end{aligned} \tag{2.42}$$

The conclusion here is that, the designed backstepping feedback controller (2.42) stabilizes the unstable reaction diffusion PDE (2.24)–(2.26). This is how the design problem of PDE control is solved via backstepping. For the mathematical analysis to conclude the closed-loop stability, we need more analysis by guaranteeing the invertibility of the transformation and equivalence of the norm, but we omit it here. We refer [99] to readers for more detailed procedure.

Unstable ODE cascaded with diffusion PDE

For an example of an unstable ODE cascaded with a diffusion PDE as in Stefan problem, we consider the following system

$$u_t = u_{xx}(x,t), \quad 0 < x < 1, \tag{2.43}$$

$$u_x(0,t) = 0, \tag{2.44}$$

$$u(1,t) = U(t), \tag{2.45}$$

$$\dot{X}(t) = AX(t) + Bu(0,t). \tag{2.46}$$

where $X \in \mathbb{R}^n$ is an ODE state, $A \in \mathbb{R}^{n\times n}$ and $B \in \mathbb{R}^{n\times 1}$ are time invariant matrices of a controllable pair. If there exists an eigenvalue of the matrix A which has a strictly positive value on its real part, then there exists at least one element in the state vector X which diverges in time. In such a case, the system becomes unstable, and some actuation is needed to stabilize. If the control input can directly affect the ODE state, $u(0,t)$ in the right hand side of (2.46) is replaced by the control input $U(t)$. In such a case, a simple choice of a control input is $U(t) = KX(t)$, where $K \in \mathbb{R}^{1\times n}$

is a control gain to be chosen. Then, the closed-loop system becomes $\dot{X}(t) = (A+BK)X(t)$. Hence, by choosing K such that the closed-loop matrix $A+BK$ is "Hurwitz" matrix (i.e. all the eigenvalues have a strictly negative real part), all of the elements in the state X converge to zero, and hence the system is stabilized.

However, if the effect of the input is propagated through the heat equation, the cascaded PDE-ODE system (2.43)–(2.46) needs to be considered. The backstepping method can be applied for the control design of such systems as well. Let us introduce the following backstepping transformation

$$w(x,t) = u(x,t) - \int_0^x k(x,y)u(y,t)dy - \phi(x)^T X(t), \tag{2.47}$$

which maps to

$$w_t = w_{xx}(x,t), \quad 0 < x < 1, \tag{2.48}$$

$$w_x(0,t) = 0, \tag{2.49}$$

$$w(1,t) = 0, \tag{2.50}$$

$$\dot{X}(t) = (A+BK)X(t) + Bw(0,t). \tag{2.51}$$

where $K \in \mathbb{R}^{1\times n}$ is a control gain. The difference between u-system and w-system is on the system matrix of ODE, namely, A and $A+BK$. Since $A+BK$ is chosen to be Hurwitz matrix, ODE (2.51) is a stable system under the setting $w(0,t) \equiv 0$. In addition, the heat equation (2.48) with the boundary conditions (2.49) and (2.50) is stable system as we have discussed in (2.28)–(2.30). Hence, we can see that the target system (2.48)–(2.51) is stable. (see [95] for its strict proof using Lyapunov analysis).

Taking the derivatives of (2.47) along the solution of (2.43)–(2.46), we obtain

$$w_x(x,t) = u_x(x,t) - k(x,x)u(x,t) - \int_0^x k_x(x,y)u(y,t)dy - \phi'(x)^T X(t), \tag{2.52}$$

$$\begin{aligned} w_{xx}(x,t) =& u_{xx}(x,t) - k(x,x)u_x(x,t) - \left(k_x(x,x) + \frac{d}{dx}k(x,x)\right)u(x,t) \\ & - \int_0^x k_{xx}(x,y)u(y,t)dy - \phi''(x)^T X(t), \end{aligned} \tag{2.53}$$

$$\begin{aligned} w_t(x,t) =& u_{xx}(x,t) - k(x,x)u_x(x,t) + k_y(x,x)u(x,t) - (k_y(x,0) + \phi(x)^T B)u(0,t) \\ & - \int_0^x k_{yy}(x,y)u(y,t)dy - \phi(x)^T AX(t) \end{aligned} \tag{2.54}$$

Therefore,

$$\begin{aligned} & w_t(x,t) - w_{xx}(x,t) \\ =& \left(2\frac{d}{dx}k(x,x)\right)u(x,t) - (k_y(x,0) + \phi(x)^T B)u(0,t) \\ & + \int_0^x (k_{xx}(x,y) - k_{yy}(x,y))u(y,t)dy + (\phi''(x)^T - \phi(x)^T A)X(t) \end{aligned} \tag{2.55}$$

Substituting $x = 0$ in (2.47) and (2.52), we have

$$w(0,t) = u(0,t) - \phi(0)^T X(t), \tag{2.56}$$

$$w_x(0,t) = -k(0,0)u(0,t) - \phi'(0)^T X(t), \tag{2.57}$$

On the other hand, by the boundary condition (2.49), we need $w_x(0,t) = 0$. Also, by comparing

ODEs of (2.46) and (2.51), we require $u(0,t) = KX(t) + w(0,t)$. Therefore, (2.55)–(2.57) yields

$$k_{xx}(x,y) = k_{yy}(x,y), \tag{2.58}$$

$$k(x,x) = 0, \quad k_y(x,0) + \phi(x)^T B = 0, \tag{2.59}$$

$$\phi''(x)^T = \phi(x)^T A, \tag{2.60}$$

$$\phi(0)^T = K, \quad \phi'(0)^T = 0, \tag{2.61}$$

The solution to (2.58)–(2.61) is given by

$$\phi(x)^T = \begin{bmatrix} K & 0_{1,n} \end{bmatrix} e^{\mathcal{A}x} \begin{bmatrix} I \\ 0_{n,n} \end{bmatrix}, \tag{2.62}$$

$$k(x,y) = \int_0^{x-y} \phi(z)^T B dz. \tag{2.63}$$

where $0_{i,j} \in \mathbb{R}^{i \times j}$ is a zero matrix, $I \in \mathbb{R}^{n \times n}$ is an identity matrix, and $\mathcal{A} \in \mathbb{R}^{2n \times 2n}$ is a matrix defined by

$$\mathcal{A} = \begin{bmatrix} 0_{n,n} & A \\ I & 0_{n,n} \end{bmatrix}. \tag{2.64}$$

Evaluating (2.47) at $x = 1$, the controller design is derived as

$$\begin{aligned} U(t) &= \int_0^1 k(1,y)u(y,t)dy + \phi(1)^T X(t) \\ &= \begin{bmatrix} K & 0_{1,n} \end{bmatrix} \left\{ \int_0^1 \left(\int_0^{1-y} e^{\mathcal{A}z} \begin{bmatrix} I \\ 0_{n,n} \end{bmatrix} Bdz \right) u(y,t)dy + e^{\mathcal{A}} \begin{bmatrix} I \\ 0_{n,n} \end{bmatrix} X(t) \right\}. \end{aligned} \tag{2.65}$$

Hence, the designed controller (2.65) stabilizes PDE-ODE cascades given in (2.43)–(2.46)

Stefan-like cascaded diffusion PDE-ODE on fixed domain

Finally, we introduce PDE-ODE cascades which has a similar structure to the Stefan problem given in (2.15)–(2.18) but on fixed domain. Let us replace the moving boundary terms $s(t)$ in (2.15)–(2.18) with a constant domain length D, and consider the following system

$$u_t = \alpha u_{xx}(x,t), \quad 0 < x < D, \tag{2.66}$$

$$u_x(0,t) = -k^{-1} q_c(t), \tag{2.67}$$

$$u(D,t) = 0, \tag{2.68}$$

$$\dot{X}(t) = -\beta u_x(D,t). \tag{2.69}$$

Next, we introduce the following backstepping transformation

$$w(x,t) = u(x,t) - \int_x^D k(x,y)u(y,t)dy - \phi(x-D)^T X(t) \tag{2.70}$$

which transforms onto

$$w_t = \alpha w_{xx}(x,t), \quad 0 < x < D, \tag{2.71}$$

$$w_x(0,t) = 0, \tag{2.72}$$

$$w(D,t) = 0, \tag{2.73}$$

$$\dot{X}(t) = -cX(t) - \beta w_x(D,t). \tag{2.74}$$

Since ODE state $X \in \mathbb{R}$ is a scaler variable in this system, Hurwitz matrix discussed in the previous PDE-ODE system can be described by the coefficient $-c$ in (2.74) with a control gain

$c > 0$. Taking the derivatives of (2.70) along the solution of (2.66)–(2.69), we obtain

$$w_x(x,t) = u_x(x,t) + k(x,x)u(x,t) - \int_x^D k_x(x,y)u(y,t)dy - \phi'(x-D)^T X(t), \tag{2.75}$$

$$\begin{aligned} w_{xx}(x,t) =& u_{xx}(x,t) + k(x,x)u_x(x,t) + \left(k_x(x,x) + \frac{d}{dx}k(x,x)\right)u(x,t) \\ & - \int_x^D k_{xx}(x,y)u(y,t)dy - \phi''(x-D)^T X(t), \end{aligned} \tag{2.76}$$

$$\begin{aligned} w_t(x,t) =& \alpha u_{xx}(x,t) + \alpha k(x,x)u_x(x,t) - \alpha k_y(x,x)u(x,t) \\ & - (\alpha k(x,D) - \phi(x-D)\beta)u_x(D,t) - \alpha\int_0^x k_{yy}(x,y)u(y,t)dy. \end{aligned} \tag{2.77}$$

By (2.76) and (2.77),

$$\begin{aligned} & w_t(x,t) - \alpha w_{xx}(x,t) \\ =& -\alpha\left(2\frac{d}{dx}k(x,x)\right)u(x,t) - (\alpha k(x,D) - \phi(x-D)^T\beta)u_x(D,t) \\ & + \alpha\int_0^x (k_{xx}(x,y) - k_{yy}(x,y))u(y,t)dy + \alpha\phi''(x-D)X(t). \end{aligned} \tag{2.78}$$

Substituting $x = D$ in (2.70) and (2.75), we have

$$w(D,t) = -\phi(0)X(t), \tag{2.79}$$

$$w_x(D,t) = u_x(D,t) - \phi'(0)X(t). \tag{2.80}$$

Applying the boundary condition (2.73) to (2.79), and comparing ODE of (2.69) with (2.74) with using (2.80), the following conditions are obtained

$$\phi''(x) = 0, \quad \phi(0) = 0, \quad \phi'(0) = \frac{c}{\beta} \tag{2.81}$$

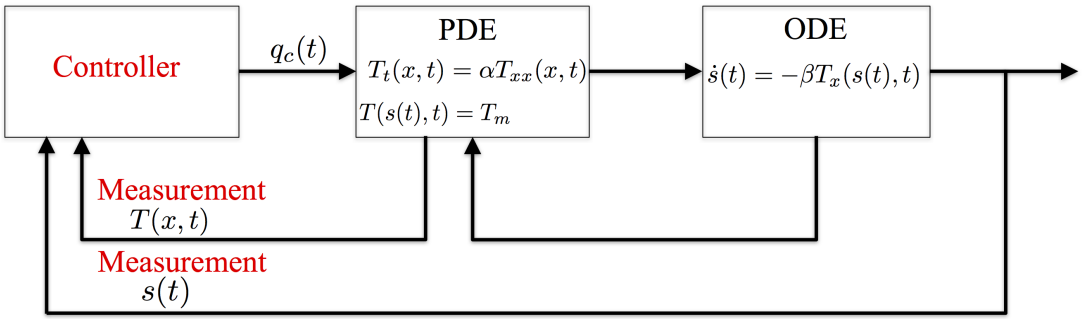

Figure 2.2: Block diagram of the state feedback closed-loop control. Both the temperature profile and the interface position are assumed to be available for the control input.

The solutions are given by

$$\phi(x) = \frac{c}{\beta}x, \tag{2.82}$$

$$k(x,y) = \frac{\beta}{\alpha}\phi(x-y) = \frac{c}{\alpha}(x-y) \tag{2.83}$$

Substituting (2.82) and (2.83) into (2.70), the backstepping transformation is derived as

$$w(x,t) = u(x,t) - \frac{c}{\alpha}\int_x^D (x-y)u(y,t)dy - \frac{c}{\beta}(x-D)X(t). \tag{2.84}$$

Evaluating the spatial derivative of (2.84) at $x = 0$ and using (2.67) and (2.72), the control law is obtained by

$$q_c(t) = -c\left(\frac{k}{\alpha}\int_0^D u(y,t)dy + \frac{k}{\beta}X(t)\right). \tag{2.85}$$

Motivated by the transformation (2.84) and the control law (2.85), in the following sections we develop the control design and its closed-loop analysis of the Stefan problem.

2.3 Backstepping Control of Stefan Problem

This section presents the main theorem of this book. We provide how the backstepping method for PDEs can be extended from fixed boundary PDE to the moving boundary PDE. Let us see the theorem first, stated in the following:

Theorem 1 *Consider a closed-loop system consisting of the plant* (2.1)–(2.4) *and the control law*

$$q_{\mathrm{c}}(t) = -c\left(\frac{k}{\alpha}\int_0^{s(t)}(T(x,t)-T_{\mathrm{m}})dx+\frac{k}{\beta}(s(t)-s_{\mathrm{r}})\right), \tag{2.86}$$

where $c>0$ is an arbitrary controller gain. Let Assumption 1 and Assumption 2 hold, and assume that the initial conditions $(T_0(x),s_0)$ are compatible with the control law. Then, the closed-loop system has a unique classical solution which satisfies the model validity conditions

$$T(x,t) > T_m, \quad \dot{s}(t) > 0, \quad \forall x \in (0,s(t)), \quad \forall t > 0, \tag{2.87}$$

$$s_0 < s(t) < s_{\mathrm{r}}, \quad \forall t > 0, \tag{2.88}$$

and is exponentially stable in the sense of the norm

$$||T-T_{\mathrm{m}}||^2_{\mathcal{H}_1} + (s(t)-s_{\mathrm{r}})^2. \tag{2.89}$$

The proof is established by the following steps.

Direct transformation

Recall the reference error (u,X)-system for the Stefan problem given by

$$u_t(x,t) = \alpha u_{xx}(x,t), \quad 0 \le x \le s(t), \tag{2.90}$$

$$-ku_x(0,t) = q_c(t), \tag{2.91}$$

$$u(s(t),t) = 0, \tag{2.92}$$

$$\dot{X}(t) = -\beta u_x(s(t),t). \tag{2.93}$$

The extension of the bacsktepping method for fixed boundary PDEs given by (2.84) to that for moving boundary PDE we developed is somewhat simple. We switch the constant boundary D in the transformation (2.84) to $s(t)$, namely, we introduce the following backstepping transformation

$$w(x,t) = u(x,t) - \frac{c}{\alpha}\int_x^{s(t)} (x-y)u(y,t)dy - \frac{c}{\beta}(x-s(t))X(t). \tag{2.94}$$

Since what differs (2.94) from (2.84) is only the time dependency of the boundary, the additional terms on the target (w,X)-system through (2.94) appears in the time derivative of w, that is

$$\begin{aligned} w_t(x,t) &= \cdots - \frac{c}{\alpha}\dot{s}(t)(x-s(t))u(s(t),t) + \frac{c}{\beta}\dot{s}(t)X(t) \\ &= \cdots + \frac{c}{\beta}\dot{s}(t)X(t) \end{aligned} \tag{2.95}$$

in which we used (2.92). Therefore, the target w-system is given by

$$w_t(x,t) = \alpha w_{xx}(x,t) + \frac{c}{\beta}\dot{s}(t)X(t), \tag{2.96}$$

$$w_x(0,t) = 0, \tag{2.97}$$

$$w(s(t),t) = 0, \tag{2.98}$$

$$\dot{X}(t) = -cX(t) - \beta w_x(s(t),t). \tag{2.99}$$

The additional term $\frac{c}{\beta}\dot{s}(t)X(t)$ in (2.96) poses a nontrivial question whether the target (w,X)-system is stable or not. We will show it later in stability analysis.

Inverse transformation

One of the benefits to use backstepping method is that the target system has easier structure to prove its stability property than the original system under the closed-loop system. To ensure the equivalent stability property between the target (w,X)-system and the original (u,X)-system, the invertibility of the transformation (2.94) needs to be guaranteed, which is nontrivial especially for nonlinear systems like Stefan problem. Suppose that the inverse transformation that maps (2.96)–(2.99) into (2.90)–(2.93) is given by the following form

$$u(x,t) = w(x,t) + \int_x^{s(t)} l(x-y)w(y,t)dy + \psi(x-s(t))X(t), \tag{2.100}$$

where $l(x-y)$, $\psi(x-s(t))$ are the kernel functions. Taking derivative of (2.100) with respect to t and x, respectively, along the solution of (2.96)–(2.99), the following relations are derived

$$\begin{aligned} u_t(x,t)-\alpha u_{xx}(x,t) =& \left\{ \frac{c}{\beta}\left(1+\int_x^{s(t)} l(x-y)dy\right) - \psi'(x-s(t)) \right\} \dot{s}(t)X(t) \\ &+ \left(\alpha l(x-s(t)) - \beta\psi(x-s(t))\right) w_x(s(t),t) \\ &- \left(c\psi(x-s(t)) + \alpha\psi''(x-s(t))\right) X(t). \end{aligned} \tag{2.101}$$

In addition, by the boundary conditions, we need

$$u(s(t),t) = \psi(0)X(t), \tag{2.102}$$

$$u_x(s(t),t) = w_x(s(t),t) + \psi'(0)X(t). \tag{2.103}$$

From (2.101)–(2.103), one can deduce that in order to recover the original system(2.90)–(2.93) for any continuous functions $(w(x,t),X(t))$, $\psi(x)$ and $l(x-y)$ must satisfy

$$\psi''(x) = -\frac{c}{\alpha}\psi(x), \quad \psi(0)=0, \quad \psi'(0)=\frac{c}{\beta}, \tag{2.104}$$

$$l(x-s(t)) = \frac{\beta}{\alpha}\psi(x-s(t)), \tag{2.105}$$

$$\psi'(x-s(t)) = \frac{c}{\beta}\left(1+\int_x^{s(t)} l(x-y)dy\right). \tag{2.106}$$

The solution to (2.104) is given by

$$\psi(x) = \frac{c}{\beta}\sqrt{\frac{\alpha}{c}}\sin\left(\sqrt{\frac{c}{\alpha}}x\right). \tag{2.107}$$

from which $l(x-y)$ can be deduced using (2.105) as

$$l(x-y) = \frac{\beta}{\alpha}\psi(x-y). \tag{2.108}$$

Fortunately, the solutions (2.110) and (2.108) satisfy the condition (2.106) as well. Hence, the inverse transformation of (2.94) is uniquely given by

$$u(x,t) = w(x,t) + \frac{\beta}{\alpha}\int_x^{s(t)} \psi(x-y)w(y,t)dy + \psi(x-s(t))X(t), \tag{2.109}$$

$$\psi(x) = \frac{c}{\beta}\sqrt{\frac{\alpha}{c}}\sin\left(\sqrt{\frac{c}{\alpha}}x\right). \tag{2.110}$$

Remark 2 *Substituting $s(t)$ by $X(t)+s_{\mathrm{r}}$ in the transformations* (2.94) *and* (2.109)*, one can easily see that the transformations* (2.94) *and* (2.109) *are nonlinear.*

The nonlinearity of the direct and inverse transformations implies that the stability properties of (u,X)-system and (w,X)-system are equivalent only if both transformations are bounded, which is shown later.

Guaranteeing the conditions of model validity

As stated in Remark 1 and Lemma 3, we should verify $q_{\mathrm{c}}(t) > 0$. Motivated by the energy conservation (2.9), we take the time derivative of (2.86) along the solution of (2.1)–(2.4), that yields

$$\begin{aligned}
\dot{q}_{\mathrm{c}}(t) =& \frac{d}{dt}\left(-c\left(\frac{k}{\alpha}\int_0^{s(t)}(T(x,t)-T_{\mathrm{m}})dx + \frac{k}{\beta}(s(t)-s_{\mathrm{r}})\right)\right),\\
=& -ck\left(\frac{1}{\alpha}\dot{s}(t)(T(s(t),t)-T_{\mathrm{m}}) + \frac{1}{\alpha}\int_0^{s(t)} T_t(x,t)dx + \frac{1}{\beta}\dot{s}(t)\right),\\
=& -ck\left(\int_0^{s(t)} T_{xx}(x,t)dx - T_x(s(t),t)\right),\\
=& ckT_x(0,t),\\
=& -cq_{\mathrm{c}}(t).
\end{aligned} \tag{2.111}$$

Solving (2.111) leads to

$$q_{\mathrm{c}}(t) = q_{\mathrm{c}}(0)e^{-ct}. \tag{2.112}$$

Since the setpoint restriction (2.11) implies $q_{\mathrm{c}}(0) > 0$, we have

$$q_{\mathrm{c}}(t) > 0, \quad \forall t \geq 0. \tag{2.113}$$

Hence, one can deduce that the closed-loop system has a unique classical solution. Then, using Lemma 3, the conditions in (2.87) are satisfied. By the control law (2.86), we have

$$\frac{k}{\beta}(s(t) - s_{\mathrm{r}}) = -\frac{q_{\mathrm{c}}(t)}{c} - \frac{k}{\alpha}\int_0^{s(t)} (T(x,t) - T_{\mathrm{m}})dx \tag{2.114}$$

Applying (2.113) and (2.87) to (2.114), we obtain $s(t) < s_{\mathrm{r}}$ for all $t > 0$. In addition, the second condition in (2.87) implies that $s_0 < s(t)$. Combining these two later inequalities leads to (2.88).

In the next section, the inequalities (2.87) and (2.88) are used to establish the Lyapunov stability of the target system (2.96)–(2.99).

Convergence of liquid length to a desired value

In the following, we prove the exponential stability of the closed-loop system based on the analysis of the target system (2.96)–(2.99). We consider a functional V_1 defined by

$$V_1 = \frac{1}{2}\int_0^{s(t)} w(x,t)^2 dx. \tag{2.115}$$

Taking the time derivative of (2.115), we have

$$\begin{aligned}
\dot{V}_1 &= \int_0^{s(t)} w(x,t)w_t(x,t)dx + \frac{1}{2}\dot{s}(t)w(s(t),t)^2 \\
&= \alpha \int_0^{s(t)} w(x,t)w_{xx}(x,t)dx + \frac{c}{\beta}\dot{s}(t)X(t)\int_0^{s(t)} w(x,t)dx \\
&= \alpha w(x,t)w_x(x,t)|_{y=0}^{y=s(t)} - \alpha \int_0^{s(t)} w_x(x,t)^2 dx + \frac{c}{\beta}\dot{s}(t)X(t)\int_0^{s(t)} w(x,t)dx \\
&= -\alpha \int_0^{s(t)} w_x(x,t)^2 dx + \frac{c}{\beta}\dot{s}(t)X(t)\int_0^{s(t)} w(x,t)dx. \qquad (2.116)
\end{aligned}$$

Next, we consider V_2 defined by

$$V_2 = \frac{1}{2}\int_0^{s(t)} w_x(x,t)^2 dx. \qquad (2.117)$$

Taking the time derivative of (2.117), we get

$$\begin{aligned}
\dot{V}_2 =& \int_0^{s(t)} w_x(x,t)w_{xt}(x,t)dx + \frac{1}{2}\dot{s}(t)w_x(s(t),t)^2 \\
=& w_x(x,t)w_t(x,t)|_{x=0}^{x=s(t)} - \int_0^{s(t)} w_{xx}(x,t)w_t(x,t)dx + \frac{1}{2}\dot{s}(t)w_x(s(t),t)^2 \\
=& w_x(s(t),t)w_t(s(t),t) - \alpha \int_0^{s(t)} w_{xx}(x,t)^2 dx \\
& - \frac{c}{\beta}\dot{s}(t)X(t)\int_0^{s(t)} w_{xx}(x,t)dx + \frac{1}{2}\dot{s}(t)w_x(s(t),t)^2 \qquad (2.118)
\end{aligned}$$

Recall the boundary condition (2.98), i.e., $w(s(t),t) = 0$. Taking the total time derivative on both sides, we obtain the following

$$\frac{d}{dt}w(s(t),t) = w_t(s(t),t) + \dot{s}(t)w_x(s(t),t) = 0, \qquad (2.119)$$

which yields

$$w_t(s(t),t) = -\dot{s}(t)w_x(s(t),t). \tag{2.120}$$

Moreover, the integration in first term in the last line in (2.118) is given by

$$\int_0^{s(t)} w_{xx}(x,t)dx = w_x(s(t),t). \tag{2.121}$$

Therefore, plugging (2.120) and (2.121) into (2.118), we arrive at

$$\dot{V}_2 = -\alpha \int_0^{s(t)} w_{xx}(x,t)^2 dx - \frac{c}{\beta}\dot{s}(t)X(t)w_x(s(t),t) - \frac{1}{2}\dot{s}(t)w_x(s(t),t)^2. \tag{2.122}$$

Next, we consider V_3 defined by

$$V_3 = \frac{1}{2}X(t)^2. \tag{2.123}$$

Using (2.99), the time derivative of (2.123) is given by

$$\begin{aligned}\dot{V}_3 =& X(t)\dot{X}(t)\\ =& -cX(t)^2 - \beta X(t)w_x(s(t),t).\end{aligned} \tag{2.124}$$

Let V be the functional defined by

$$V = V_1 + V_2 + pV_3. \tag{2.125}$$

By (2.116), (2.122), and (2.124), the time derivative of (2.125) is given by

$$\begin{aligned}\dot{V} =& -\alpha\int_0^{s(t)} w_{xx}(x,t)^2dx-\alpha\int_0^{s(t)} w_x(x,t)^2dx-pcX(t)^2-p\beta X(t)w_x(s(t),t)\\ &+\frac{c}{\beta}\dot{s}(t)X(t)\int_0^{s(t)} w(x,t)dx-\dot{s}(t)\frac{c}{\beta}X(t)w_x(s(t),t)-\frac{\dot{s}(t)}{2}w_x(s(t),t)^2.\end{aligned} \tag{2.126}$$

Using the fact that $\dot{s}(t)>0$ and applying Young's inequality yields

$$-p\beta X(t)w_x(s(t),t)\leq\frac{p}{2}\left(cX(t)^2+\frac{\beta^2}{c}w_x(s(t),t)^2\right), \tag{2.127}$$

$$\frac{c}{\beta}\dot{s}(t)X(t)\int_0^{s(t)} w(x,t)dx\leq\frac{\dot{s}(t)}{2}\left(\left(\frac{c}{\beta}X(t)\right)^2+\left(\int_0^{s(t)} w(x,t)dx\right)^2\right), \tag{2.128}$$

$$-\dot{s}(t)\frac{c}{\beta}X(t)w_x(s(t),t)\leq\frac{\dot{s}(t)}{2}\left(\left(\frac{c}{\beta}X(t)\right)^2+w_x(s(t),t)^2\right). \tag{2.129}$$

Also, by Cauchy-Schwarz inequality, we have

$$\left(\int_0^{s(t)} w(x,t)dx\right)^2\leq s_r\int_0^{s(t)} w(x,t)^2dx. \tag{2.130}$$

Applying (2.127)–(2.130) to (2.126), the following inequality on V is derived

$$\begin{aligned}\dot{V}\leq&-\alpha\int_0^{s(t)} w_{xx}(x,t)^2dx-\alpha\int_0^{s(t)} w_x(x,t)^2dx-\frac{pc}{2}X(t)^2+\frac{p\beta^2}{2c}w_x(s(t),t)^2\\ &+\dot{s}(t)\left(\frac{s_r}{2}\int_0^{s(t)} w(x,t)^2dx+\frac{c^2}{\beta^2}X(t)^2\right)\end{aligned} \tag{2.131}$$

Applying Pointcare's and Agmon's inequality which give $\int_0^{s(t)} w(x,t)^2dx\leq 4s_r^2\int_0^{s(t)} w_x(x,t)^2dx$ and $w_x(s(t),t)^2\leq 4s_r\int_0^{s(t)} w_{xx}(x,t)^2dx$, the inequality (2.131) becomes

$$\begin{aligned}\dot{V}\leq&-\left(\alpha-\frac{2p\beta^2s_r}{c}\right)\int_0^{s(t)} w_{xx}(x,t)^2dx-\alpha\int_0^{s(t)} w_x(x,t)^2dx-\frac{pc}{2}X(t)^2\\ &+\dot{s}(t)\left(\frac{s_r}{2}\int_0^{s(t)} w(x,t)^2dx+\frac{c^2}{\beta^2}X(t)^2\right).\end{aligned} \tag{2.132}$$

Therefore, by choosing $p = \frac{c\alpha}{4\beta^2 s_r}$, we arrive at

$$\begin{aligned}\dot{V} \leq & -\frac{\alpha}{8s_r^2}\int_0^{s(t)} w_x(x,t)^2 dx - \frac{\alpha}{4s_r^2}\int_0^{s(t)} w(x,t)^2 dx - \frac{pc}{2}X(t)^2 \\ & + \dot{s}(t)\left(\frac{s_r}{2}\int_0^{s(t)} w(x,t)^2 dx + \frac{c^2}{\beta^2}X(t)^2\right) \\ & \leq -bV + a\dot{s}(t)V \end{aligned} \tag{2.133}$$

where $a = \max\left\{1, \frac{8s_r c}{\alpha}\right\}$, $b = \min\left\{\frac{\alpha}{4s_r^2}, c\right\}$.

However, the second term of the right-hand side of (2.133) does not enable to directly conclude the exponential stability. To deal with it, we introduce a new Lyapunov function W defined by

$$W = Ve^{-as(t)}. \tag{2.134}$$

The time derivative of (2.134) is written as

$$\dot{W} = \left(\dot{V} - a\dot{s}(t)V\right)e^{-as(t)}, \tag{2.135}$$

and using (2.133) the following estimate can be deduced

$$\dot{W} \leq -bW. \tag{2.136}$$

Hence, $W(t) \leq W(0)e^{-bt}$, and using (2.88) and (2.134), we obtain

$$V(t) \leq e^{as_r}V(0)e^{-bt}. \tag{2.137}$$

From the definition of V in (2.125) the following holds

$$||w||^2_{\mathcal{H}_1} + pX(t)^2 \leq e^{as_r}\left(||w_0||^2_{\mathcal{H}_1} + pX(0)^2\right)e^{-bt}. \tag{2.138}$$

Finally, with the help of (2.88), the direct transformation (2.94) and its associated inverse transformation (2.109)–(2.110) combined with Young's and Cauchy-Schwarz inequalities, enable to state the existence of a positive constant $D > 0$ such that

$$||u||^2_{\mathcal{H}_1} + X(t)^2 \leq D\left(||u_0||^2_{\mathcal{H}_1} + X(0)^2\right)e^{-bt}, \tag{2.139}$$

which completes the proof of Theorem 1.

2.4 Gain Tuning to Avoid Input Saturation and Evaporation

In practical control systems, the capability of the actuator is often limited in a certain range, which is widely known as "input saturation" [64]. Particularity in Stefan problem as a melting process, the heat input should not go beyond a given upper bound, while it is feasible to assume that the lower bound is zero, i.e., the actuator does not work as a cooler. Furthermore, the liquid temperature must be lower than the boiling temperature to avoid an evaporation which is another phase transition from liquid to gas. Such an overall input and state constraint problem from control algorithm perspective can be treated by restricting the control gain. First, we state the following well known lemma for Stefan problem.

Lemma 5 *If $T_m \leq T_0(x) \leq \bar{T}_0(1 - x/s_0) + T_m$ and $0 \leq q_c(t) \leq \bar{q}$ for $\forall t \geq 0$, then*

$$T_m \leq T(x,t) \leq \bar{T}(x,t) := K(s(t) - x) + T_m, \tag{2.140}$$

where $K = \max\{\bar{q}/k, \bar{T}_0/s_0\}$ for $\forall x \in (0, s(t))$, $\forall t \geq 0$.

Proof:

Let $v(x,t) := \bar{T}(x,t) - T(x,t)$. Taking the time and second spatial derivatives yields

$$v_t = K\dot{s}(t) - T_t(x,t), \quad v_{xx} = -T_{xx}(x,t), \tag{2.141}$$

Since $0 \leq q_c(t)$, we have $\dot{s}(t) \geq 0$. Thus, we obtain

$$v_t \geq \alpha v_{xx}, \tag{2.142}$$

$$v_x(0,t) \leq 0, \quad v(s(t),t) = 0. \tag{2.143}$$

Applying maximum principle to (2.142)–(2.143), we can state that if $v(x,0) \geq 0$ for all $x \in (0, s_0)$ then $v(x,t) \geq 0$ for all $x \in (0, s(t))$ and all $t \geq 0$, which concludes Lemma 5.

Next, we state the following theorem on the input and state constraint on the closed-loop analysis of the designed control law.

Theorem 2 *Assume $\bar{T}_0 \leq \frac{s_0}{s_r}(T_b - T_m)$, where T_b is the boiling temperature. By choosing the control gain $c > 0$ as*

$$0 < c \leq \frac{1}{\Delta E} \min\left\{ \bar{q}, \frac{k(T_\mathrm{b} - T_\mathrm{m})}{s_\mathrm{r}} \right\} \tag{2.144}$$

where ΔE is defined by (2.12)*, then the designed controller satisfies the input constraint*

$$0 \leq q_\mathrm{c}(t) \leq \bar{q} \tag{2.145}$$

and the liquid temperature profile satisfies the state constraint

$$T_\mathrm{m} \leq T(x,t) \leq T_\mathrm{b}. \tag{2.146}$$

Proof:

As presented in the last section, the closed-loop control is equivalent to the explicit function $q_c(t) = q_c(0)e^{-ct}$. Hence, $q_c(t) \leq q_c(0) = c\Delta E \leq \bar{q}$ by the control gain (2.144). Moreover, applying $q_c(t) \leq q_c(0) = c\Delta E$ to Lemma 5, it holds that $T(x,t) \leq \bar{T}(x,t) := K(s(t)-x)+T_m$ with $K = \max\{c\Delta E/k, \bar{T}_0/s_0\}$. Since $s(t) \leq s_r$ is ensured, $\bar{T}(x,t)$ is bounded by $\bar{T}(x,t) \leq Ks_r + T_m$. Thus, by the control gain (2.144), the state is bounded by $T(x,t) \leq T_b$.

2.5 Robustness to Diffusivity and Latent Heat Mismatch

The proposed control law (2.86) requires the plant's parameters α and β. In practice, such parameters are identified prior to the control implementation by conducting an open-loop experiments and statistical learning methods. However, the parameters are essentially not accurate value, and hence the robustness analysis of the closed-loop systems under the parameters' uncertainties is significant to study. In other words, we account for perturbations caused by uncertainties of the thermal diffusivity and the latent heat of fusion. Thus, we consider the following closed-loop system

$$T_t(x,t) = \alpha(1+\varepsilon_1)T_{xx}(x,t), \quad 0 \leq x \leq s(t), \tag{2.147}$$

$$-kT_x(0,t) = q_c(t), \tag{2.148}$$

$$T(s(t),t) = T_m, \tag{2.149}$$

$$\dot{s}(t) = -\beta(1+\varepsilon_2)T_x(s(t),t), \tag{2.150}$$

with the control law (2.86), where ε_1 and ε_2 are parameters' perturbation such that $\varepsilon_1 > -1$ and $\varepsilon_2 > -1$.

Theorem 3 *Consider a closed-loop system* (2.147)–(2.150) *and the control law* (2.86) *under Assumption 1 and 2. Then, for any pair of perturbation* $(\varepsilon_1, \varepsilon_2)$ *such that* $\varepsilon_1 \geq \varepsilon_2$ *and for any*

control gain c satisfying $0 < c \leq c^*$ *where*

$$c^* = \left(\frac{3}{10}\right)^{1/4} \frac{\alpha}{8s_r^2} \frac{1+\varepsilon_1}{\varepsilon_1 - \varepsilon_2},$$

the closed-loop system is exponentially stable in the sense of the $\mathcal{H}_1$ *the norm* (2.89).

Proof:

The reference error system on (u, X) to the perturbed system is given by

$$u_t(x,t) = \alpha(1+\varepsilon_1)u_{xx}(x,t), \quad 0 \leq x \leq s(t), \tag{2.151}$$

$$-ku_x(0,t) = q_c(t), \tag{2.152}$$

$$u(s(t),t) = 0, \tag{2.153}$$

$$\dot{s}(t) = -\beta(1+\varepsilon_2)u_x(s(t),t), \tag{2.154}$$

Taking the spatial and time derivatives of the backstepping transformation (2.94) along the solution to the "perturbed system" (2.151)–(2.154), we obtain

$$w_x(x,t) = u_x(x,t) - \frac{c}{\alpha}\int_x^{s(t)} u(y,t)dy - \frac{c}{\beta}X(t) \tag{2.155}$$

$$w_{xx}(x,t) = u_{xx}(x,t) + \frac{c}{\alpha}u(x,t), \tag{2.156}$$

$$\begin{aligned} w_t(x,t) =& \alpha(1+\varepsilon_1)u_{xx}(x,t) + c(1+\varepsilon_1)u(x,t) \\ &+ \frac{c(\varepsilon_1 - \varepsilon_2)}{\beta(1+\varepsilon_2)}\dot{s}(t)(x - s(t)) + \frac{c}{\beta}\dot{s}(t)X(t) \end{aligned} \tag{2.157}$$

Hence, the associated target systems is derived as

$$w_t(x,t) = \alpha(1+\varepsilon_1)w_{xx}(x,t) + \frac{c}{\beta}\dot{s}(t)X(t) + \frac{c}{\beta}\frac{\varepsilon_1-\varepsilon_2}{1+\varepsilon_2}\dot{s}(t)(x-s(t)), \tag{2.158}$$

$$w_x(0,t) = 0, \tag{2.159}$$

$$w(s(t),t) = 0, \tag{2.160}$$

$$\dot{X}(t) = -c(1+\varepsilon_2)X(t) - \beta(1+\varepsilon_2)w_x(s(t),t). \tag{2.161}$$

Next, we prove that the control law (2.86) applied to the perturbed system (2.147)–(2.150), satisfies (2.113) and (2.88). Taking the time derivative of (2.86) along with (2.147)–(2.150), we arrive at

$$\dot{q}_c(t) = -c(1+\varepsilon_1)q_c(t) - ck(\varepsilon_1-\varepsilon_2)u_x(s(t),t). \tag{2.162}$$

The positivity of the control law (2.86) applied to the perturbed system (2.147)–(2.150) can be shown using a contradiction argument. Assume that there exists $t_1 > 0$ such that $q_c(t) > 0$, $\forall t \in (0,t_1)$ and $q_c(t_1) = 0$. Then, Lemma 3 leads to $u_x(s(t),t) < 0$, $\forall t \in (0,t_1)$. Since $\varepsilon_1 \geq \varepsilon_2$, (2.162) implies that

$$\dot{q}_c(t) \geq -c(1+\varepsilon_1)q_c(t), \quad \forall t \in (0,t_1). \tag{2.163}$$

Using comparison principle, (2.163) and Assumption 2 leads to

$$q_c(t_1) \geq q_c(0)e^{-c(1+\varepsilon_1)t_1} > 0. \tag{2.164}$$

Thus $q_c(t_1) \neq 0$ which is in contradiction with the assumption $q_c(t_1) = 0$. Consequently, (2.113) holds by this contradiction argument. Accordingly, (2.88) is established using (2.113) and the control law (2.86).

Now, consider V_1 defined by

$$V_1 = \frac{1}{2}||w||^2_{L_2}. \tag{2.165}$$

The time derivative is obtained by

$$\begin{aligned}\dot{V}_1 =& -\alpha(1+\varepsilon_1)||w_x||^2_{L_2} - c\bar{e}\left(\frac{c}{\beta}X(t) + w_x(s(t),t)\right)\int_0^{s(t)}(x-s(t))w(x,t)dx \\ &+ \frac{c}{\beta}\dot{s}(t)X(t)\int_0^{s(t)} w(x,t)dx.\end{aligned} \tag{2.166}$$

where $\bar{e} = \varepsilon_1 - \varepsilon_2$. By Young's and Causchy inequalities, we have

$$\begin{aligned}&- c\bar{e}\left(\frac{c}{\beta}X(t) + w_x(s(t),t)\right)\int_0^{s(t)}(x-s(t))w(x,t)dx \\ \leq& \frac{c^2\bar{e}^2}{\gamma_1}\left(\left(\frac{c}{\beta}X(t)\right)^2 + w_x(s(t),t)^2\right) + \frac{\gamma_1}{2}\int_0^{s(t)}(x-s(t))^2dx||w||^2 \\ \leq& \frac{c^2\bar{e}^2}{\gamma_1}\left(\left(\frac{c}{\beta}X(t)\right)^2 + w_x(s(t),t)^2\right) + \frac{\gamma_1 s_r^3}{6}||w||^2 \\ \leq& \frac{2\gamma_1 s_r^5}{3}||w_x||^2_{L_2} + \frac{c^2\bar{e}^2}{\gamma_1}\left(\left(\frac{c}{\beta}X(t)\right)^2 + w_x(s(t),t)^2\right).\end{aligned} \tag{2.167}$$

Choosing $\gamma_1 = \frac{3\alpha(1+\varepsilon_1)}{4s_r^5}$ and applying to (2.166), we get

$$\begin{aligned}\dot{V}_1 \leq& -\frac{\alpha(1+\varepsilon_1)}{2}||w_x||^2_{L_2} + \frac{4s_r^5c^2\bar{e}^2}{3\alpha(1+\varepsilon_1)}\left(\left(\frac{c}{\beta}X(t)\right)^2 + 4s_r||w_{xx}||^2\right) \\ &+ \frac{c}{\beta}\dot{s}(t)X(t)\int_0^{s(t)} w(x,t)dx.\end{aligned} \tag{2.168}$$

Consider V_2 defined by

$$V_2 = \frac{1}{2}\int_0^{s(t)} w_x(x,t)^2dx. \tag{2.169}$$

The time derivative is obtained by

$$\begin{aligned}\dot{V}_2 = &-\alpha(1+\varepsilon_1)||w_{xx}||_{L_2}^2 + \frac{c}{\beta}\bar{e}cX(t)w(0,t) + c\bar{e}w_x(s(t),t)w(0,t) \\ &+ \dot{s}(t)\left(-\frac{c}{\beta}X(t)w_x(s(t),t) - \frac{1}{2}w_x(s(t),t)^2\right).\end{aligned} \tag{2.170}$$

Applying Young's and Agmon's inequality leads to

$$\begin{aligned}\dot{V}_2 \leq &-\alpha(1+e_1)||w_{xx}||_{L_2}^2 + \frac{\gamma_1}{2}X(t)^2 + \frac{1}{2\gamma_1}\left(\frac{c}{\beta}\bar{e}cw(0,t)\right)^2 \\ &+ 2\gamma_2 s_r||w_{xx}||_{L_2}^2 + \frac{1}{2\gamma_2}\left(c\bar{e}w(0,t)\right)^2 + \frac{\dot{s}(t)}{2}\left(\frac{c}{\beta}X(t)\right)^2.\end{aligned} \tag{2.171}$$

Thus, choosing $\gamma_2 = \alpha(1+e_1)/4s_r$, it follows that

$$\begin{aligned}\dot{V}_2 \leq &-\frac{\alpha(1+e_1)}{2}||w_{xx}||_{L_2}^2 + \frac{\gamma_1}{2}X(t)^2 + \frac{1}{2\gamma_1}\left(\frac{c}{\beta}\bar{e}cw(0,t)\right)^2 \\ &+ \frac{2s_r c^2\bar{e}^2}{\alpha(1+e_1)}w(0,t)^2 + \dot{s}(t)\frac{c^2}{2\beta^2}X(t)^2.\end{aligned} \tag{2.172}$$

Consider Y defined by

$$Y = \frac{1}{2}X(t)^2. \tag{2.173}$$

The time derivative is obtained and bounded by

$$\begin{aligned}\dot{Y} = &-(1+\varepsilon_2)cX(t)^2 - (1+\varepsilon_2)\beta X(t)w_x(s(t),t) \\ \leq &-\frac{(1+\varepsilon_2)c}{2}X(t)^2 + \frac{2s_r(1+\varepsilon_2)\beta^2}{c}||w_{xx}||^2\end{aligned} \tag{2.174}$$

where Young's inequality and Agmon's inequality are used from the first line to the second line.

Thus, choosing $V_4 = V_2 + pY$, with setting p as $p = \frac{c\alpha(1+\varepsilon_1)}{8s_r(1+\varepsilon_2)\beta^2}$, we have

$$\begin{aligned}\dot{V}_4 \leq & -\frac{\alpha(1+\varepsilon_1)}{4}||w_{xx}||_{L_2}^2 - p\frac{(1+\varepsilon_2)c}{2}X(t)^2 + \frac{\gamma_1}{2}X(t)^2 \\ & + \frac{1}{2\gamma_1}\left(\frac{c}{\beta}\bar{e}cw(0,t)\right)^2 + \frac{2s_rc^2\bar{e}^2}{\alpha(1+\varepsilon_1)}w(0,t)^2 + \dot{s}(t)\frac{c^2}{2\beta^2}X(t)^2. \end{aligned} \tag{2.175}$$

Choosing $\gamma_1 = p\frac{(1+e_2)c}{2}$, we get

$$\begin{aligned}\dot{V}_4 \leq & -\frac{\alpha(1+e_1)}{4}||w_{xx}||_{L_2}^2 - p\frac{(1+e_2)c}{4}X(t)^2 \\ & + \frac{10c^2\bar{e}^2s_r}{\alpha(1+e_1)}w(0,t)^2 + \dot{s}(t)\frac{c^2}{2\beta^2}X(t)^2. \end{aligned} \tag{2.176}$$

Let V be the overall Lyapunov functional defined by

$$V = dV_1 + V_4. \tag{2.177}$$

The time derivative satisfies the following inequality

$$\begin{aligned}\dot{V} \leq & -d\left(\frac{\alpha(1+e_1)}{2} - \frac{40c^2\bar{e}^2s_r^2}{d\alpha(1+e_1)}\right)||w_x||_{L_2}^2 + d\left\{\frac{c}{\beta}\dot{s}(t)X(t)\int_0^{s(t)}w(x,t)dx\right\} \\ & - \frac{\alpha(1+e_1)}{4}\left(1 - \frac{16ds_rf(\bar{e})}{\alpha(1+e_1)}\right)||w_{xx}||_{L_2}^2 \\ & - \frac{c^2\alpha(1+e_1)}{32\beta^2s_r}\left(1 - \frac{32ds_rf(\bar{e})}{\alpha(1+e_1)}\right)X(t)^2 + \dot{s}(t)\frac{c^2}{2\beta^2}X(t)^2, \end{aligned} \tag{2.178}$$

where $f(\bar{e}) = \frac{4s_r^5c^2\bar{e}^2}{3\alpha(1+e_1)}$. Setting $d = \frac{160c^2\bar{e}^2s_r^2}{\alpha^2(1+e_1)^2}$ leads to

$$\begin{aligned}\dot{V} \leq & -d\left(\frac{\alpha(1+\varepsilon_1)}{4}\right)||w_x||_{L_2}^2 - \frac{\alpha(1+\varepsilon_1)}{12}\left(4 - \left(\frac{c}{c^*}\right)^4\right)||w_{xx}||_{L_2}^2 \\ & - \frac{c^2}{\beta^2}\frac{\alpha(1+\varepsilon_1)}{64s_{\mathrm{r}}}\left(2 - \left(\frac{c}{c^*}\right)^4\right)X(t)^2 + \dot{s}(t)\left\{d^2s_{\mathrm{r}}^2||w||_{L_2}^2 + \frac{c^2}{\beta^2}X(t)^2\right\}. \end{aligned} \tag{2.179}$$

From (2.179) we deduce that for all $0 < c < c^*$, there exists positive parameters a and b such that

$$\dot{V} \leq -bV + a\dot{s}(t)V. \tag{2.180}$$

The exponential stability of the target system (2.158)–(2.161) can be straightforwardly established following the proof procedure used in (2.134)–(2.138), which completes the proof of Theorem 3.

2.6 Numerical Simulation

Following the numerical method presented in Section 1.6, the simulation of the closed-loop system is obtained by rendering the feedback control law to the boundary heat input at every time sequence. The initial values are set to s_0 = 1 [cm], $T_0(x) = \bar{T}(1 - x/s_0) + T_{\mathrm{m}}$ with $\bar{T}$ = 100 [C°], and the setpoint is chosen as s_{r} = 35 [cm] which satisfies the setpoint restriction (2.11).

Comparison of the pulse input and the backstepping control law

Fig. 2.3 shows the responses of the plant (2.147)–(2.150) with the open-loop pulse input (2.13) (dashed line) and the backstepping control law (2.86) (solid line). The time window of the open-loop pulse input is set to 50 [min]. The gain of the backstepping control law is chosen sufficiently small, c=0.001, to avoid numerical instabilities. Fig. 2.3 (a) shows the response of $s(t)$ without the parameters perturbations, i.e. $(\varepsilon_1, \varepsilon_2) = (0, 0)$ and clearly demonstrates that $s(t)$ converges to s_{r} applying both rectangular pulse input and backstepping control law. However, the convergence speed is faster with the backstepping control. Moreover, from the dynamics of $s(t)$ under parameters' perturbations $(\varepsilon_1, \varepsilon_2) = (0.3, -0.2)$ shown in Fig. 2.3 (b), it can be seen that the convergence of $s(t)$ to s_{r} is only achieved with the backstepping control law. On both Fig. 2.3 (a) and Fig. 2.3 (b), the responses with the backstepping control law show that the interface position converges faster without the overshoot beyond the setpoint, i.e., $\dot{s}(t) > 0$ and

$s_0 < s(t) < s_\mathrm{r}, \forall t > 0$.

Closed-loop system's validity with respect to the physical constraints

The dynamics of the controller $q_\mathrm{c}(t)$ and the temperature at the initial interface $T(s_0,t)$ with the backstepping control law (2.86) are described in Fig. 2.4 (a) and Fig. 2.4 (b), respectively, for the system without parameter's uncertainties, i.e., $(\varepsilon_1,\varepsilon_2) = (0,0)$ (red) and the system with parameters' mismatch $(\varepsilon_1,\varepsilon_2) = (0.3,-0.2)$ (blue). As presented in Fig. 2.4 (a), the boundary heat controller $q_\mathrm{c}(t)$ remains positive, i.e. $q_\mathrm{c}(t) > 0$ in both cases. Moreover, Fig. 2.4 (b) shows that $T(s_0,t)$ converges to T_m with $T(s_0,t) > T_\mathrm{m}$ for the system with accurate parameters and the system with uncertainties on the parameters. Physically, Fig. 2.4 (b) means that the temperature at the initial interface's location increases away above the melting temperature T_m, which enables the melting of the solid-phase to the setpoint s_r. After this significant transient dynamics, $T(s_0,t)$ settles back to T_m. An identical behavior is observed when the system is subject to parameters' uncertainty. Therefore, the numerical results are consistent with our theoretical result.

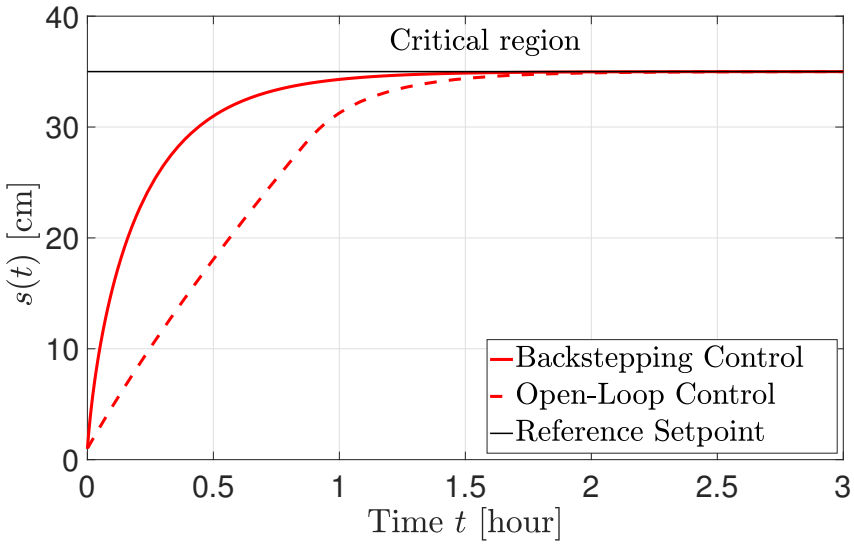

(a) The plots with accurate parameters $(\varepsilon_1, \varepsilon_2) = (0, 0)$. Our backstepping control achieves the faster convergence of the interface position.

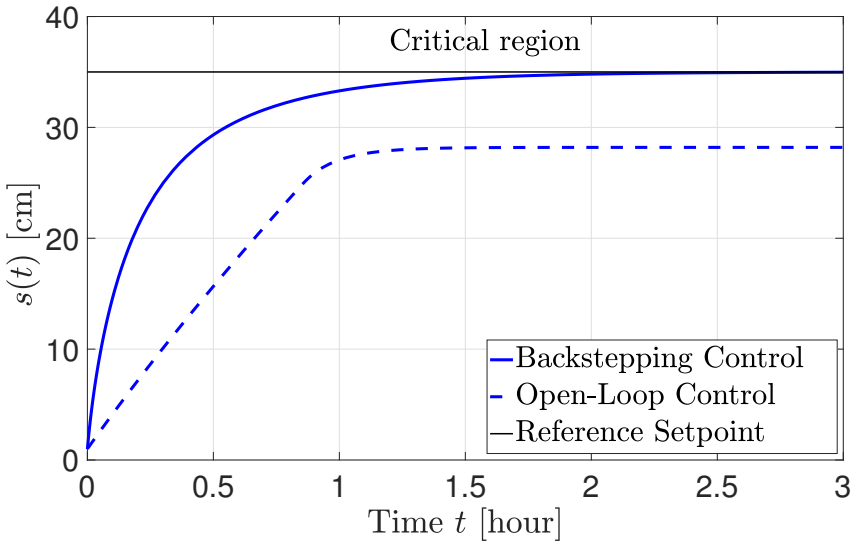

(b) The plots under parameters perturbation $(\varepsilon_1, \varepsilon_2) = (0.3, -0.2)$. Our backstepping control is robust to uncertainties of the system parameters.

Figure 2.3: The moving interface responses of the plant (2.147)–(2.150) with the open-loop pulse input (2.13) (dashed line) and the backstepping control law (2.86) (solid line) in Neumann boundary actuation.

2.7 Boundary Temperature Actuation

Some actuators such as a thermo-electric cooler require the direct controlling of the temperature at the boundary, which corresponds to a Dirichlet boundary control problem [16],

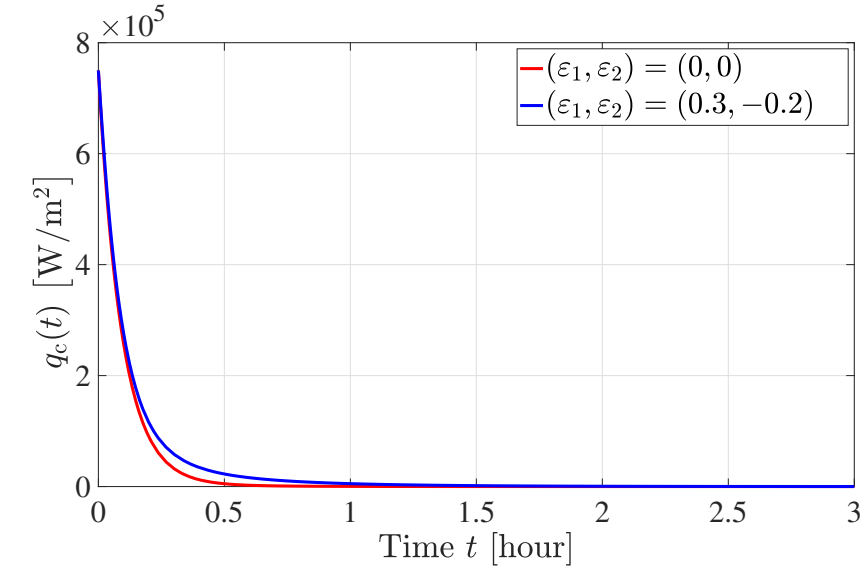

(a) Positivity of the controller remains, i.e., $q_c(t) > 0$.

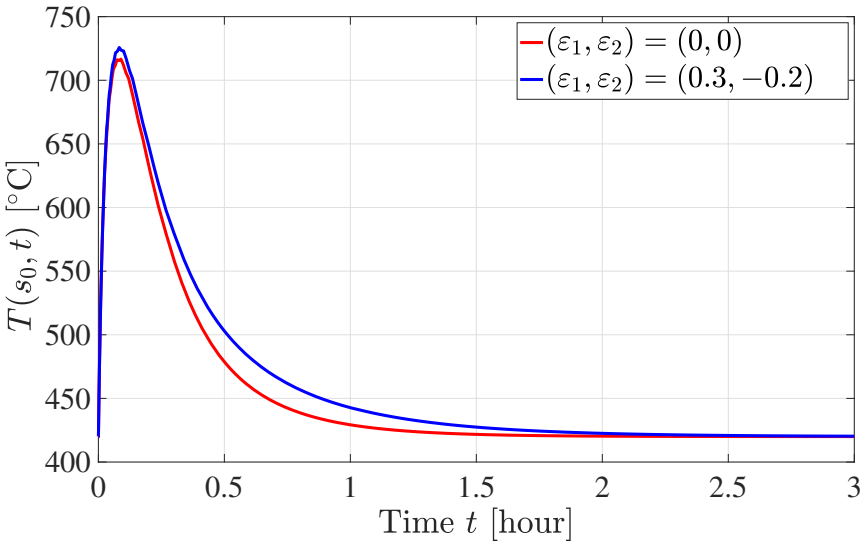

(b) $T(s_0, t)$ warms up from T_m and returns to it.

Figure 2.4: The closed-loop responses with accurate parameters (red) and parameters perturbation (blue) under the backstepping control in Neumann boundary actuation.

noted as PII in Section 1.2. In this section, backstepping feedback control for PII is developed.

We define the control problem consisting of the following system:

$$T_t(x,t) = \alpha T_{xx}(x,t), \quad 0 \le x \le s(t), \tag{2.181}$$

$$T(0,t) = T_{\mathrm{c}}(t) + T_{\mathrm{m}}, \tag{2.182}$$

$$T(s(t),t) = T_{\mathrm{m}}, \tag{2.183}$$

$$\dot{s}(t) = -\beta T_x(s(t),t), \tag{2.184}$$

where $T_{\mathrm{c}}(t)$ is a controlled temperature relative to the melting temperature. As shown in Lemma 3, the designed temperature controller needs to ensure the positivity, i.e., the following conditions are required to hold as physical constraints

$$T_{\mathrm{c}}(t) > 0, \tag{2.185}$$

$$s_0 < s(t) < s_r, \tag{2.186}$$

Setpoint restriction

For boundary temperature control, the conservation law obeys the following

$$\frac{d}{dt}\left(\frac{1}{\alpha}\int_0^{s(t)} x(T(x,t) - T_{\mathrm{m}})dx + \frac{1}{2\beta}s(t)^2\right) = T_{\mathrm{c}}(t). \tag{2.187}$$

Considering the same control objective

$$s(t) \to s_r, \quad T(x,t) \to T_m, \tag{2.188}$$

taking the limit of (2.187) from 0 to ∞ yields

$$\Delta E = \int_0^{\infty} T_{\mathrm{c}}(t)dt, \tag{2.189}$$

where $\Delta E := \frac{1}{2\beta}(s_{\mathrm{r}}^2 - s_0^2) - \frac{1}{\alpha}\int_0^{s_0} x(T_0(x) - T_{\mathrm{m}})dx$. Hence, by imposing the physical constraint (2.185), the least restrictive condition for the choice of setpoint is derived, and the open-loop stabilization is presented in the following.

Lemma 6 *Consider an open-loop setpoint control law $T_{\mathrm{c}}^{\star}(t)$ which satisfies* (2.189)*. Then, for any setpoint s_{r} satisfying*

$$s_{\mathrm{r}} > \sqrt{s_0^2 + \frac{2\beta}{\alpha}\int_0^{s_0} x(T_0(x) - T_{\mathrm{m}})dx}, \tag{2.190}$$

the control objective (2.188) *is satisfied.*

As in Section 2.1, a simple rectangular pulse input achieves (2.188). Such a control action given by

$$T_{\mathrm{c}}^{\star}(t) = \left\{ \begin{array}{ll} \bar{T} & \text{for} \quad t \in [0, \Delta E/\bar{T}] \\ 0 & \text{for} \quad t > \Delta E/\bar{T} \end{array} \right\}, \tag{2.191}$$

stands as an open-loop "energy shaping" approach.

State feedback controller design

Firstly, we suppose that the physical parameters are accurately known and state the following theorem.

Theorem 4 *Consider a closed-loop system consisting of the plant* (2.181)–(2.184) *and the control law*

$$T_{\mathrm{c}}(t) = -c\left(\frac{1}{\alpha}\int_0^{s(t)} x\,(T(x,t) - T_{\mathrm{m}})\,dx + \frac{1}{\beta}s(t)\,(s(t) - s_{\mathrm{r}})\right), \tag{2.192}$$

where $c > 0$ is the controller gain under Assumption 1. Then, for any reference setpoint s_{r} and

control gain c which satisfy

$$s_{\mathrm{r}} > s_0 + \frac{\beta}{\alpha}\int_0^{s_0} \frac{x}{s_0}(T_0(x) - T_{\mathrm{m}})dx, \tag{2.193}$$

$$c \leq \frac{\alpha}{2\sqrt{2}s_{\mathrm{r}}}, \tag{2.194}$$

respectively, the closed-loop system is exponentially stable in the sense of the norm (2.89)*.*

Proof:

We use the same backstepping transformation as in (2.94), which leads to the following target system

$$w_t(x,t) = \alpha w_{xx}(x,t) + \frac{c}{\beta}\dot{s}(t)X(t), \tag{2.195}$$

$$w(0,t) = 0, \tag{2.196}$$

$$w(s(t),t) = 0, \tag{2.197}$$

$$\dot{X}(t) = -cX(t) - \beta w_x(s(t),t) \tag{2.198}$$

and the control law (2.192).

Next, we show that the physical constraints (2.185) and (2.186) are insured if (2.193) holds. Taking the time derivative of (2.192), we have

$$\dot{T}_{\mathrm{c}}(t) = -cT_{\mathrm{c}}(t) - \frac{c}{\beta}\dot{s}(t)X(t). \tag{2.199}$$

Assume that $\exists t_2$ such that $T_{\mathrm{c}}(t) > 0$, $\forall t \in (0,t_2)$ and $T_{\mathrm{c}}(t_2) = 0$. Then, by Lemma 3, we get $u(x,t) > 0$ and $\dot{s}(t) > 0$ for $\forall t \in (0,t_2)$. Hence, $s(t) > s_0 > 0$. Applying these inequalities to (2.192), we deduce $X(t) < 0, \quad \forall t \in (0,t_2)$. Hence, (2.199) verifies the differential inequality $\dot{T}_{\mathrm{c}}(t) > -cT_{\mathrm{c}}(t), \quad \forall t \in (0,t_2)$. Comparison principle and (2.193) yield $T_{\mathrm{c}}(t_2) > T_{\mathrm{c}}(0)e^{-ct_2} > 0$ in contradiction to $T_{\mathrm{c}}(t_2) = 0$. Therefore, $\nexists t_2$ such that $T_{\mathrm{c}}(t) > 0$ for $\forall t \in (0,t_2)$ and $T_{\mathrm{c}}(t_2) = 0$,

which implies $T_{\mathrm{c}}(t) > 0$, $\forall t > 0$ assuming (2.193).

Finally, we consider a functional

$$V = \frac{d}{2}||w||_{L_2}^2 + \frac{1}{2}||w_x||_{L_2}^2 + \frac{p}{2}X(t)^2. \tag{2.200}$$

With an appropriate choice of the positive parameters d and p, the time derivative of (2.200) yields

$$\begin{aligned}\dot{V} \leq & -\left(\frac{\alpha}{2} - \sqrt{2}cs_{\mathrm{r}}\right)||w_{xx}||^2 - \frac{d\alpha}{2(4s_{\mathrm{r}}^2+1)}||w||_{\mathcal{H}_1}^2 \\ & - \frac{\alpha c^2}{4\beta^2}X(t)^2 + \dot{s}(t)\left(\frac{c^2}{\beta^2}X(t)^2 + \frac{d^2 s_{\mathrm{r}}^2}{2}||w||^2\right).\end{aligned} \tag{2.201}$$

Thus, choosing the controller gain to satisfy (2.194), it can be verified that there exist positive constants b and a such that

$$\dot{V} \leq -bV + a\dot{s}(t)V. \tag{2.202}$$

Similarly in the Neumann boundary actuation case, under the physical constraint (2.185), the exponential stability of the target system (2.195)–(2.198) can be established from the inequality (2.202), which completes the proof of Theorem 4.

Robustness to parameters' uncertainty

Next, we investigate the controller (2.192) to perturbations on the plant's physical parameters α and β, considering the following perturbed system

$$T_t(x,t) = \alpha(1+\varepsilon_1)T_{xx}(x,t), \quad 0 \le x \le s(t), \tag{2.203}$$

$$T(0,t) = T_{\rm c}(t) + T_{\rm m}, \tag{2.204}$$

$$T(s(t),t) = T_{\rm m}, \tag{2.205}$$

$$\dot{s}(t) = -\beta(1+\varepsilon_2)T_x(s(t),t) \tag{2.206}$$

where ε_1 and ε_2 are perturbation parameters such that $\varepsilon_1 > -1$ and $\varepsilon_2 > -1$.

Theorem 5 *Consider the closed-loop system consisting of the plant* (2.203)–(2.206) *and the control law* (2.192) *under the assumption on* (2.193) *to hold. Then, for any perturbations* $(\varepsilon_1, \varepsilon_2)$ *which satisfy* $\varepsilon_1 \ge \varepsilon_2$*, there exists* $\bar{c}^* > 0$ *such that for all controller gain c satisfying* $0 < c \le \bar{c}^*$*, the closed-loop system is exponentially stable in the sense of the norm* (2.89)*.*

Proof:

By the same transformation (2.94), the target *w*-system is given by

$$w_t(x,t) = \alpha(1+\varepsilon_1)w_{xx}(x,t) + \frac{c}{\beta}\dot{s}(t)X(t) + \frac{c}{\beta}\frac{\varepsilon_1-\varepsilon_2}{1+\varepsilon_2}\dot{s}(t)(x-s(t)), \tag{2.207}$$

$$w(0,t) = 0, \tag{2.208}$$

$$w(s(t),t) = 0, \tag{2.209}$$

$$\dot{X}(t) = -c(1+\varepsilon_2)X(t) - \beta(1+\varepsilon_2)w_x(s(t),t). \tag{2.210}$$

To prove the physical constraints (2.185) and (2.186), taking the time derivative of (2.192)

along the system (2.203)–(2.206), we obtain

$$\begin{aligned}\dot{T}_{\mathrm{c}}(t) =& -c(1+\varepsilon_1)T_{\mathrm{c}}(t) - \frac{c}{\beta}\dot{s}(t)X(t) \\ & - c(\varepsilon_1-\varepsilon_2)u_x(s(t),t). \end{aligned} \tag{2.211}$$

Thus, the inequality $\varepsilon_1 \geq \varepsilon_2$ enables to state the positivity of the controller $T_{\mathrm{c}}(t) > 0$ and the physical constraints (2.185) and (2.186) are verified.

Finally, we consider the functional defined in (2.200). After lengthy calculation and applying inequalities in a similar way to Section 2.5, with an appropriate choice of d and p and imposing $c < c_1$ where $c_1 := \frac{\alpha(1+\varepsilon_2)}{2\sqrt{2}s_{\mathrm{r}}}$, we have

$$\begin{aligned}\dot{V} \leq & -\frac{d\alpha(1+\varepsilon_1)}{4}||w_x||_{L_2}^2 - \frac{\alpha(1+\varepsilon_1)}{8}\left(2-Ac^3\right)||w_{xx}||_{L_2}^2 \\ & - \frac{c^2\alpha(1+\varepsilon_1)}{32\beta^2 s_{\mathrm{r}}}\left(2-Ac^3-Bc\right)X(t)^2 \\ & + \dot{s}(t)\left\{d^2 s_{\mathrm{r}}^2||w||_{L_2}^2 + \frac{c^2}{\beta^2}X(t)^2\right\}. \end{aligned} \tag{2.212}$$

where $A = \frac{2^9\sqrt{2}s_{\mathrm{r}}^6(1+s_{\mathrm{r}})(\varepsilon_1-\varepsilon_2)^2}{3\alpha^3(1+\varepsilon_1)^2(1+\varepsilon_2)}$, $B = \frac{16\sqrt{2}s_{\mathrm{r}}^2}{\alpha(1+\varepsilon_2)}$. Let c_2 be a positive root of $Ac_2^3 + Bc_2 = 1$. Then, for $0 < \forall c < \bar{c}^* := \min\{c_1, c_2\}$, there exists positive constants $\bar{a}$ and $\bar{b}$ which verifies $\dot{V} \leq -\bar{b}V + \bar{a}\dot{s}(t)V$, which concludes Theorem 5.

Numerical simulation

Numerical simulation is studied for the designed Dirichlet boundary actuation. Analogous plots to the ones given in Section 2.6 are depicted in Fig. 2.5 and 2.6, respectively. Basically we can observe the similar good performance and properties to the ones for Neumann boundary actuations in terms of the convergence to the setpoint and the validity of the physical constraints.

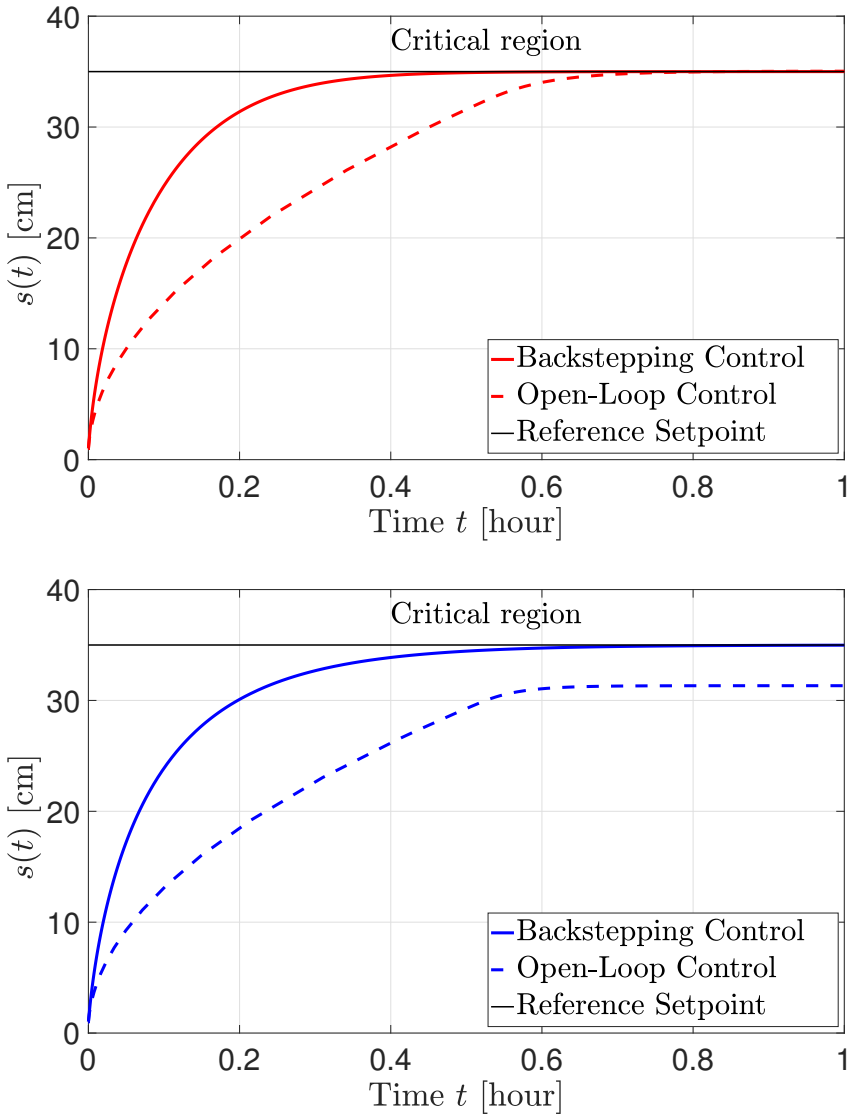

Figure 2.5: The moving interface response of the plant (2.181)–(2.184) with the open-loop pulse input (2.191) (dashed line) and the backstepping control law (2.192) (solid line), under the accurate parameters $(\varepsilon_1, \varepsilon_2) = (0, 0)$ (top) and under the parameters perturbation $(\varepsilon_1, \varepsilon_2) = (0.3, -0.2)$. We can observe the faster convergence and the parametric robustness of our backstepping control law.

2.8 Stefan-Like Problem with Dirichlet Interconnection

In this section, we study whether the procedure for control design and analysis of the Stefan problem can be applicable to an analogous moving boundary problem. Specifically, one

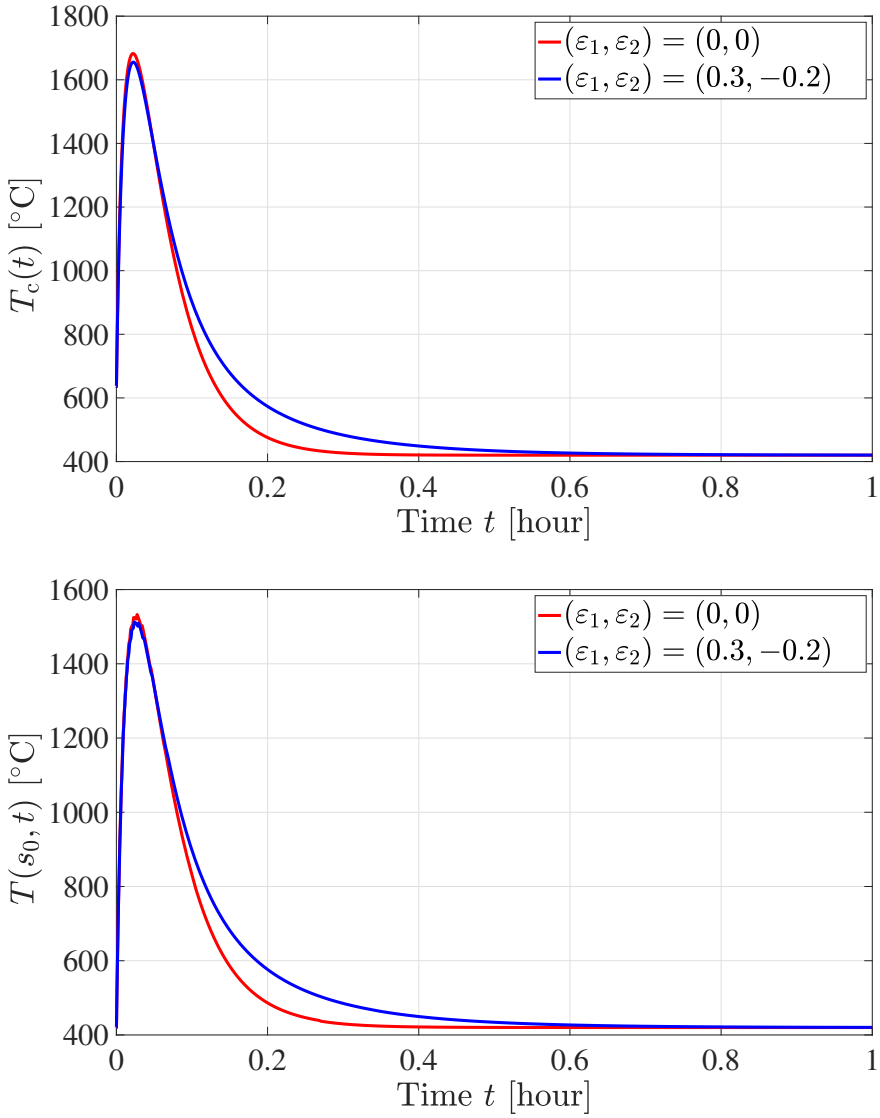

Figure 2.6: The closed-loop responses with accurate parameters (red) and parameters perturbation (blue) under the backstepping control in Dirichlet boundary actuation. Both positivity of the control input and the constraints of temperature are validated.

might be interested in the following diffusion PDE under Dirhichlet interconnection on the

moving boundary dynamics

$$u_t(x,t) = \alpha u_{xx}(x,t), \quad 0 < x < s(t) \tag{2.213}$$

$$u(0,t) = U(t), \tag{2.214}$$

$$u_x(s(t),t) = 0, \tag{2.215}$$

$$\dot{s}(t) = -\beta u(s(t),t). \tag{2.216}$$

The dynamics (2.216) leads to the shrinking moving interface under the positivity of PDE state, contrary to the Stefan problem. Applying maximum principle, the following lemma is stated.

Lemma 7 *If $u_0(x) > 0$ and $U(t) > 0$ for all $t > 0$, then $u(x,t) > 0$, $\forall x \in (0, s(t))$ and $\dot{s}(t) < 0$, $\forall t > 0$.*

Therefore, we consider the stabilization of the interface position $s(t)$ driven "back" to a setpoint s_r. The following theorem is presented.

Theorem 6 *Assume $s_0 > 0$, $u_0(x) > 0$ for $\forall x \in (0, s_0)$, and the setpoint is chosen to satisfy*

$$0 < s_r < s_0 - \frac{\beta}{\alpha} \int_0^{s_0} x u_0(x) dx. \tag{2.217}$$

Then the closed-loop system under the control law

$$U(t) = -c \left(\frac{1}{\alpha} \int_0^{s(t)} x u(x,t) dx - \frac{1}{\beta} (s(t) - s_r) \right), \tag{2.218}$$

satisfies the following properties

$$U(t) > 0, \quad u(x,t) > 0, \tag{2.219}$$

$$\dot{s}(t) < 0, \tag{2.220}$$

$$s_r < s(t) < s_0, \tag{2.221}$$

and is exponentially stable in the norm

$$||u||_{L_2}^2 + (s(t) - s_r)^2. \tag{2.222}$$

Proof:

Taking the time derivative of the control law (2.218), we have

$$\dot{U}(t) = c\frac{\dot{s}(t)^2}{\alpha\beta}s(t) - cU(t). \tag{2.223}$$

We prove $s(t) > s_r > 0$. Assume there exists $t^* > 0$ such that $s(t) > s_r$ for $\forall t \in [0, t^*)$ and $s(t^*) = s_r$. Then, (2.223) yields $\dot{U}(t) > -cU(t)$ for $\forall t \in [0, t^*]$, which leads to $U(t) > U(0)e^{-ct}$ for $\forall t \in [0, t^*]$. By Lemma 7, it holds that $u(x,t) > 0$, $\forall x \in (0, s(t))$, $\forall t \in [0, t^*)$. Thus, by (2.218), we have

$$U(0)e^{-ct} < \frac{c}{\beta}(s(t) - s_r), \quad \forall t \in [0, t^*). \tag{2.224}$$

Since $U(0) > 0$ due to the setpoint condition (2.217), the inequality (2.224) contradicts with the imposed assumption $s(t^*) = s_r$. Thus, there does not exist such a finite time t^*, which yields $s(t) > s_r$ for $\forall t > 0$. Applying this to (2.223) and using comparison principle, the inequalities (2.219) are satisfied. By Lemma 7, the inequality (2.220) is derived, and finally (2.221) is proved by applying these inequalities to (2.218).

Next, we consider the following transformation

$$w(x,t) = u(x,t) + \frac{c}{\alpha}\int_x^{s(t)} (y - x)u(y,t)dy - \frac{c}{\beta}X(t). \tag{2.225}$$

Taking the time and spatial derivatives, we obtain the following target system

$$w_t(x,t) = \alpha w_{xx}(x,t) + \frac{c}{\alpha}\dot{s}(t)(s(t)-x)\left(\frac{c}{\beta}X(t) + w(s(t),t)\right), \tag{2.226}$$

$$w(0,t) = 0, \tag{2.227}$$

$$w_x(s(t),t) = 0, \tag{2.228}$$

$$\dot{X}(t) = -cX(t) - \beta w(s(t),t). \tag{2.229}$$

Finally we prove the stability of the target system (2.226)–(2.229) by utilizing the proven inequalities (2.220) and (2.221). Consider

$$V_1 = \frac{1}{2\alpha}||w||^2 = \frac{1}{2\alpha}\int_0^{s(t)} w(x,t)^2 dx. \tag{2.230}$$

The time derivative is given by

$$\begin{aligned}\dot{V}_1 = &-\int_0^{s(t)} w_x(x,t)^2 dx + \frac{\dot{s}(t)}{2\alpha}w(s(t),t)^2 \\ &+ \frac{c}{\alpha^2}\dot{s}(t)\left(\frac{c}{\beta}X(t) + w(s(t),t)\right)\int_0^{s(t)}(s(t)-x)w(x,t)dx.\end{aligned} \tag{2.231}$$

By Young's inequality with the help of $\dot{s}(t) < 0$, we have

$$\begin{aligned}&\dot{s}(t)\left(\frac{c}{\beta}X(t) + w(s(t),t)\right)\int_0^{s(t)}(s(t)-x)w(x,t)dx \\ \leq &-\frac{\dot{s}(t)}{2}\left(\gamma\left(\frac{c}{\beta}X(t) + w(s(t),t)\right)^2 + \frac{1}{\gamma}\left(\int_0^{s(t)}(s(t)-x)w(x,t)dx\right)^2\right) \\ \leq &-\dot{s}(t)\left(\frac{c^2\gamma}{\beta^2}X(t)^2 + \gamma w(s(t),t)^2 + \frac{s(t)^3}{2\gamma}||w||^2\right).\end{aligned} \tag{2.232}$$

Applying (2.232) to (2.231), the following bound is obtained

$$\begin{aligned}\dot{V}_1 \leq & -\int_0^{s(t)} w_x(x,t)^2 dx + \frac{\dot{s}(t)}{2\alpha} w(s(t),t)^2 \\ & -\dot{s}(t)\frac{c}{\alpha^2}\left(\frac{c^2\gamma}{\beta^2}X(t)^2 + \gamma w(s(t),t)^2 + \frac{s(t)^3}{2\gamma}||w||^2\right). \end{aligned} \tag{2.233}$$

Setting $\gamma = \frac{\alpha}{2c}$ leads to

$$\dot{V}_1 \leq -||w_x||^2 - \dot{s}(t)\frac{c}{\alpha^2}\left(\frac{c\alpha}{2\beta^2}X(t)^2 + \frac{cs(t)^3}{\alpha}||w||^2\right). \tag{2.234}$$

Consider

$$Y = \frac{1}{2}X(t)^2. \tag{2.235}$$

Taking the time derivative and applying Young's and Agmon's inequalities yield

$$\dot{Y} = -cX(t)^2 + \beta X(t)w(s(t),t) \leq -\frac{c}{2}X(t)^2 + \frac{2\beta^2 s_0}{c}||w_x||^2. \tag{2.236}$$

Therefore, by defining $V = V_1 + pY$ with $p = \frac{c}{4\beta^2 s_0}$, we have

$$\begin{aligned}\dot{V} \leq & -\frac{1}{2}||w_x||^2 - \frac{pc}{2}X(t)^2 - \dot{s}(t)\left(\frac{c^2}{2\alpha\beta^2}X(t)^2 + \frac{c^2 s_0^3}{\alpha^3}||w||^2\right) \\ \leq & -aV - b\dot{s}(t)V. \end{aligned} \tag{2.237}$$

As in the previous way, consider $W = Ve^{bs(t)}$ and taking the time derivative with applying (2.237), it holds that

$$\dot{W} \leq -aW. \tag{2.238}$$

Thus, by (2.220) and (2.221), the following estimate of the norm is derived

$$V \leq V_0 e^{b(s_0 - s_r)} e^{-at}, \tag{2.239}$$

from which we conclude the exponential stability stated in Theorem 6.

Numerical simulation is studied by using the same value of α and β as of zinc. Fig. 2.7 shows that under the closed-loop system the interface position is driven from $s_0 = 10$ [cm] to the setpoint $s_r = 2$ [cm] without overshoot. Fig. 2.8 illustrates that the designed controller maintains the positivity as proven in the theorem.

2.9 Conclusion and Remarks

While the numerical analysis of the one-phase Stefan problem is broadly covered in the literature, their control related problems have been addressed relatively fewer. In addition to it, most of the proposed control approaches are based on finite-dimensional approximations with the assumption of an explicitly given moving boundary dynamics [35],[7],[125]. Diffusion-reaction processes with an explicitly known moving boundary dynamics are investigated in [7] based on the concept of inertial manifold [28] and the partitioning of the infinite dimensional dynamics into slow and fast finite dimensional modes. Motion planning boundary control has been adopted in [125] to ensure asymptotic stability of a one-dimensional one-phase nonlinear Stefan problem assuming a prior known moving boundary and deriving the manipulated input from the solutions of the inverse problem. However, the series representation introduced in [125] leads to highly complex solutions that reduce controller design possibilities.

For control objectives, infinite-dimensional frameworks that lead to significant challenges in the process characterization have been developed for the stabilization of the temperature profile and the moving interface of the Stefan problem. An enthalpy-based boundary feedback control law that ensures asymptotical stability of the temperature profile and the moving boundary at the

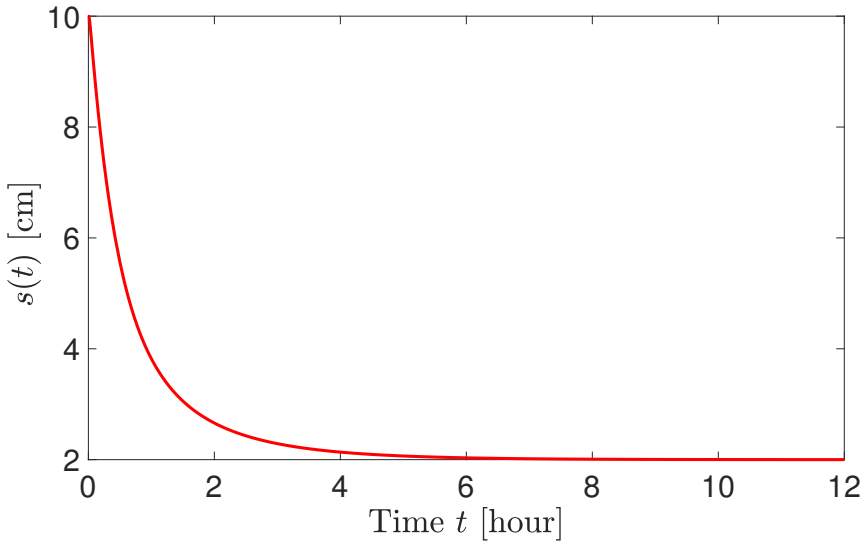

Figure 2.7: The interface response of the Stefan-like problem with Dirichlet interconnection. $s(t)$ is driven back to the setpoint $s_r = 2$ [cm]

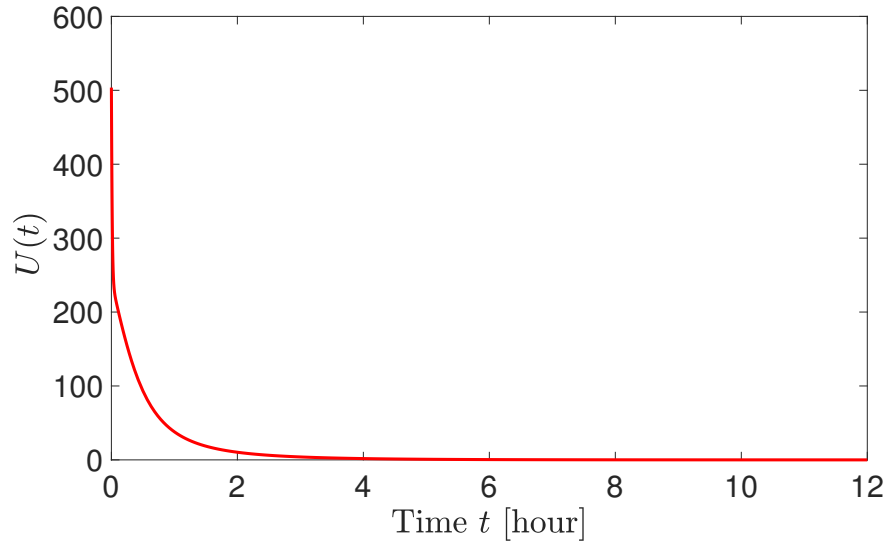

Figure 2.8: The closed-loop response of the control input of the Stefan-like problem with Dirichlet interconnection. Positivity of $U(t)$ is maintained.

desired reference, has been employed in [127]. Lyapunov analysis is performed in [110] based on a geometric control approach which enables to adjust the position of a liquid-solid interface to the desired setpoint while exponentially stabilizing the L_2-norm of the distributed temperature. However, the results in [110] are stated based on physical assumptions on the liquid temperature

being greater than the melting point, which needs to be guaranteed by proving strictly positive boundary input. The significant contribution of the proposed method using backstepping is to prove all the physical properties which needs to be addressed and global exponential stability of the closed-loop system by focusing on the stability analysis of the target system.

This chapter presented control designs for the one-phase Stefan problem via backstepping method. The novelties of our results are summarized below.

1. A new approach to globally stabilizing a class of nonlinear parabolic PDEs with moving boundary via a nonlinear backstepping transformation is proposed.

2. The closed-loop responses satisfy the physical constraints needed for the validity of the model.

3. A novel formulation of the Lyapunov function for moving boundary PDEs was applied and it showed the exponential stability of the closed loop system.

Even though our state feedback controller for the Neumann boundary actuation is same as the one proposed in [128], we ensure the exponential stability of the interface and temperature in $\mathcal{H}_1$ norm, which is stronger than the asymptotical stability presented in [128]. The application of extremum seeking control with static maps to the Stefan problem following the recent results of [119] could be an interesting design that can be applied to the optimization of phase-change phenomena in building use [103].

2.10 Acknowledgement

Chapters 2, in part, is a reprint of the material as it appears in:

- S. Koga, M. Diagne, S. Tang, and M. Krstic, "Backstepping Control of the One-Phase Stefan Problem", *American Control Conference*, 2016,

- S. Koga, M. Diagne, and M. Krstic, "Control and State Estimation of the One-Phase Stefan Problem via Backstepping Design", *IEEE Transactions on Automatic Control*, vol. 64, no. 2, pp. 510-525, 2019.

The dissertation author was the primary investigators and author of these papers. The author would like to thank Mamadou Diagne and Shuxia Tang for their collaboration.

Chapter 3

State Estimation Design

The state feedback control presented in Chapter 2 requires the entire profile of the temperature in the liquid phase as a given information. Some imaging-based sensors such as thermographic camera (a.k.a. infrared camera or IR camera) enables to capture the temperature profile, however, they include relatively higher noise than single point thermal sensors such as thermocouples. Thus, estimating the entire temperature profile given a boundary measurement is a significant task for the real implementation of the control algorithm. Generally speaking, such a problem to estimate variables of interest given some measured value is widely known as ”state estimation”. One of the most popular state estimation methods is ”Kalman filter” which is an optimal filter in linear dynamical systems with white Gaussian noise in the model and measurements. Another well known method is ”Luenberger observer” which stabilizes the estimation error at zero in linear deterministic systems. In finite dimensional systems, the observer gain is designed by means of pole placement or linear matrix inequality. In this book, we focus on the state estimation of the Stefan problem by Luenberger-type observer with designing the observer gain via the backstepping method.

3.1 Basic Idea of PDE Estimation on Fixed Boundary

Consider the unstable reaction-diffusion PDE presented in Section 2.2

$$u_t = u_{xx}(x,t) + \lambda u(x,t), \quad 0 < x < 1, \tag{3.1}$$

$$u(0,t) = 0, \tag{3.2}$$

$$u(1,t) = U(t), \tag{3.3}$$

where $U(t)$ is a time-varying input which can be either an open-loop forcing or a feedback control. Suppose that a boundary flux $u_x(0,t)$ is available for measurement $y(t)$:

$$y(t) = u_x(0,t) \tag{3.4}$$

The observer is constructed as a copy of the plant (3.1)–(3.3) plus the product of the observer gain and the measurement error, given by

$$\hat{u}_t = \hat{u}_{xx}(x,t) + \lambda \hat{u}(x,t) + p_1(x)(y(t) - \hat{u}_x(0,t)), \quad 0 < x < 1, \tag{3.5}$$

$$\hat{u}(0,t) = 0, \tag{3.6}$$

$$\hat{u}(1,t) = U(t), \tag{3.7}$$

The objective is to find the gain function $p_1(x)$ such that $\hat{u}$ converges to u. First, we introduce the estimation error variable defined by

$$\tilde{u} = u - \hat{u} \tag{3.8}$$

Subtraction of (3.5)–(3.7) from (3.1)–(3.3) yields the estimation error dynamics as

$$\tilde{u}_t = \tilde{u}_{xx}(x,t) + \lambda \tilde{u}(x,t) - p_1(x)\tilde{u}_x(0,t), \quad 0 < x < 1, \tag{3.9}$$

$$\tilde{u}(0,t) = 0, \tag{3.10}$$

$$\tilde{u}(1,t) = 0, \tag{3.11}$$

Consider the backstepping transformation from a newly defined variable $\tilde{w}$ to the estimation error $\tilde{u}$, given by

$$\tilde{u} = \tilde{w} - \int_0^x p(x,y)\tilde{w}(y)dy \tag{3.12}$$

where $\tilde{w}$ obeys the following stable diffusion PDE

$$\tilde{w}_t = \tilde{w}_{xx}, \quad 0 < x < 1, \tag{3.13}$$

$$\tilde{w}(0,t) = 0, \tag{3.14}$$

$$\tilde{w}(1,t) = 0. \tag{3.15}$$

Taking the spatial and time derivatives of (3.12), we obtain

$$\begin{aligned}\tilde{u}_{xx} =& \tilde{w}_{xx} - p(x,x)\tilde{w}_x(x) - \left(\frac{d}{dx}p(x,x) + p_x(x,x)\right)\tilde{w}(x) \\ & - \int_0^x p_{xx}(x,y)\tilde{w}(y)dy\end{aligned} \tag{3.16}$$

$$\begin{aligned}\tilde{u}_t =& \tilde{w}_{xx} - p(x,x)\tilde{w}_x(x) + p(x,0)\tilde{w}_x(0) + p_y(x,x)\tilde{w}(x) \\ & - \int_0^x p_{yy}(x,y)\tilde{w}(y)dy\end{aligned} \tag{3.17}$$

Thus,

$$\begin{aligned}\tilde{u}_t - \tilde{u}_{xx} - \lambda\tilde{u} + p_1(x)\tilde{u}_x(0,t) =& (p_1(x) + p(x,0))\tilde{w}_x(0) + \left(2\frac{d}{dx}p(x,x) - \lambda\right)\tilde{w}(x) \\ &+ \int_0^x (p_{xx}(x,y) - p_{yy}(x,y) + \lambda p(x,y))\tilde{w}(y)dy \end{aligned} \tag{3.18}$$

By boundary condition, we get

$$p(1,y) = 0 \tag{3.19}$$

Therefore,

$$p_{xx} - p_{yy} = -\lambda p, \tag{3.20}$$

$$\frac{d}{dx}p(x,x) = \frac{\lambda}{2}, \tag{3.21}$$

$$p(1,y) = 0, \tag{3.22}$$

Introduce a change of coordinates

$$\bar{x} = 1 - y, \quad \bar{y} = 1 - x, \quad \bar{p}(\bar{x},\bar{y}) = p(x,y), \tag{3.23}$$

we have

$$\bar{p}_{\bar{x}\bar{x}} - \bar{p}_{\bar{y}\bar{y}} = \lambda\bar{p}, \tag{3.24}$$

$$\frac{d}{d\bar{x}}\bar{p}(\bar{x},\bar{x}) = -\frac{\lambda}{2}, \tag{3.25}$$

$$\bar{p}(x,0) = 0 \tag{3.26}$$

This PDE (3.24) and the boundary conditions (3.25), (3.26) are equivalent to the one introduced

in (2.37)–(2.39). Hence, taking back to the original coordinate x and y, the solution is given by

$$p(x,y) = -\lambda(1-x)\frac{I_1(z)}{z}, \quad z := \sqrt{\lambda((1-y)^2-(1-x)^2)} \tag{3.27}$$

The observer gain is given by

$$p_1(x) = -p(x,0) = \lambda(1-x)\frac{I_1\left(\sqrt{\lambda(1-(1-x)^2)}\right)}{\sqrt{\lambda(1-(1-x)^2)}}, \tag{3.28}$$

3.2 Temperature Profile Estimation for the Stefan Problem

In this section, we develop the observer design of temperature profile for the Stefan problem given available measurements of the interface position and the temperature gradient at the interface. While measuring the temperature gradient at the interface lacks on the practical feasibility in sensing technique, the estimator under the setting is relatively easy and enables the analysis of the output feedback control.

Recall the Stefan problem modeling the liquid temperature dynamics under the melting, described by

$$T_t(x,t) = \alpha T_{xx}(x,t), \quad x \in (0, s(t)), \tag{3.29}$$

$$-kT_x(0,t) = q_c(t), \tag{3.30}$$

$$T(s(t),t) = T_m, \tag{3.31}$$

$$\dot{s}(t) = -\beta T_x(s(t),t), \tag{3.32}$$

Denoting the estimates of the temperature $\hat{T}(x,t)$, the following theorem holds:

Theorem 7 *Consider the plant* (3.29)–(3.32) *with the measurements*

$$Y_1(t) = s(t), \quad Y_2(t) = T_x(s(t),t), \tag{3.33}$$

and the following observer

$$\hat{T}_t(x,t) = \alpha \hat{T}_{xx}(x,t) + p_1(x,Y_1(t)) \left(Y_2(t) - \hat{T}_x(Y_1(t),t)\right), \tag{3.34}$$

$$-k\hat{T}_x(0,t) = q_c(t), \tag{3.35}$$

$$\hat{T}(Y_1(t),t) = T_m, \tag{3.36}$$

where $x \in [0, Y_1(t)]$*, and the observer gain* $p_1(x,Y_1(t))$ *is*

$$p_1(x,Y_1(t)) = -\lambda Y_1(t) \frac{I_1\left(\sqrt{\frac{\lambda}{\alpha}(Y_1(t)^2 - x^2)}\right)}{\sqrt{\frac{\lambda}{\alpha}(Y_1(t)^2 - x^2)}}, \tag{3.37}$$

with a gain parameter $\lambda > 0$*. Assume that the model validity condition* $T(x,t) \geq T_m$ *is satisfied. Then, for all* $\lambda > 0$*, the observer error system has a unique classical solution and is exponentially stable in the sense of the norm*

$$||T - \hat{T}||^2_{\mathcal{H}_1}. \tag{3.38}$$

Since the observer PDE (3.34)–(3.35) is a cascaded system of the plant PDE-ODE (3.29)–(3.32), the observer state $\hat{T}(x,t)$ admits a classical solution only if the plant states $(T(x,t), s(t))$ admits a classical solution. Note that the observer gain (3.37) is dependent on the measured value $Y_1(t) = s(t)$, which renders the derivation of the observer gain require *online* computation.

Observer gain derivation by backstepping transformation

Let us define the estimation error state $\tilde{u}$ as

$$\tilde{u}(x,t) = T(x,t) - \hat{T}(x,t). \tag{3.39}$$

Subtraction of (3.34)–(3.36) from (3.29)–(3.31) leads to the estimation error system given by

$$\tilde{u}_t(x,t) = \alpha\tilde{u}_{xx}(x,t) - p_1(x,s(t))\tilde{u}_x(s(t),t), \tag{3.40}$$

$$\tilde{u}_x(0,t) = 0, \tag{3.41}$$

$$\tilde{u}(s(t),t) = 0. \tag{3.42}$$

As for the full-state feedback case, the following backstepping transformation for moving boundary PDEs

$$\tilde{u}(x,t) = \tilde{w}(x,t) + \int_x^{s(t)} P(x,y)\tilde{w}(y,t)dy, \tag{3.43}$$

is constructed to convert the following exponentially stable target system

$$\tilde{w}_t(x,t) = \alpha\tilde{w}_{xx}(x,t) - \lambda\tilde{w}(x,t), \tag{3.44}$$

$$\tilde{w}_x(0,t) = 0, \tag{3.45}$$

$$\tilde{w}(s(t),t) = 0, \tag{3.46}$$

into the $\tilde{u}$-system (3.40)–(3.42). Taking the derivative of (3.43) with respect to t and x along the solution of (3.44)–(3.46), respectively, for any continuous function $\tilde{w}(x,t)$, the gain kernel $P(x,y)$

and the observer gain $p_1(x,s(t))$ must satisfy

$$P_{xx}(x,y)-P_{yy}(x,y)+\frac{\lambda}{\alpha}P(x,y)=0, \tag{3.47}$$

$$P(x,x)=\frac{\lambda}{2\alpha}x, \tag{3.48}$$

$$P_x(0,y)=0, \tag{3.49}$$

$$p_1(x,s(t))=-\alpha P(x,s(t)), \tag{3.50}$$

in order to map (3.40)–(3.42) into (3.44)–(3.46). Introduce the change of coordinates and the state as

$$\bar{x}=y, \quad \bar{y}=x, \quad \bar{P}(\bar{x},\bar{y})=-P(x,y), \quad \bar{\lambda}=\frac{\lambda}{\alpha}. \tag{3.51}$$

Then, the system (3.47)–(3.49) is rewritten using the new coordinates as

$$\bar{P}_{\bar{x}\bar{x}}-\bar{P}_{\bar{y}\bar{y}}=\bar{\lambda}\bar{P}, \tag{3.52}$$

$$\bar{P}(\bar{x},\bar{x})=-\frac{\bar{\lambda}}{2}\bar{x}, \tag{3.53}$$

$$\bar{P}_{\bar{y}}(\bar{x},0)=0. \tag{3.54}$$

The solution to (3.52)–(3.54) is obtained (see eq. (4.64)–(4.66) in [99]). Taking back to the original coordinates and variables, the gain kernel function is solved as

$$P(x,y)=\frac{\lambda}{\alpha}y\frac{I_1\left(\sqrt{\frac{\lambda}{\alpha}(y^2-x^2)}\right)}{\sqrt{\frac{\lambda}{\alpha}(y^2-x^2)}}. \tag{3.55}$$

Finally, using (3.50), the observer gain (3.37) is derived.

Inverse transformation

The inverse transformation is formulated as

$$\tilde{w}(x,t) = \tilde{u}(x,t) - \int_x^{s(t)} Q(x,y)\tilde{u}(y,t)dy, \tag{3.56}$$

where the gain kernel $Q(x,y)$ satisfies

$$Q_{xx}(x,y) - Q_{yy}(x,y) = \frac{\lambda}{\alpha}Q(x,y), \tag{3.57}$$

$$Q(x,x) = \frac{\lambda}{2\alpha}x, \tag{3.58}$$

$$Q_x(0,y) = 0. \tag{3.59}$$

The solution to (3.57)–(3.59) is written as

$$Q(x,y) = \frac{\lambda}{\alpha}y\frac{J_1\left(\sqrt{\frac{\lambda}{\alpha}(y^2-x^2)}\right)}{\sqrt{\frac{\lambda}{\alpha}(y^2-x^2)}}, \tag{3.60}$$

where $J_1(x)$ is a Bessel function of the first kind.

Temperature profile estimate converges to the real temperature

To show the stability of the target $\tilde{w}$-system (3.44)–(3.46), we consider a functional

$$\tilde{V} = \frac{1}{2}||\tilde{w}||^2_{\mathcal{H}_1}. \tag{3.61}$$

Taking the time derivative of (3.61) along the solution of (3.44)–(3.46) leads to

$$\dot{\tilde{V}} = -\alpha||\tilde{w}_x||^2_{\mathcal{H}_1} - \lambda||\tilde{w}||^2_{\mathcal{H}_1} - \frac{\dot{s}(t)}{2}\tilde{w}_x(s(t),t)^2. \tag{3.62}$$

As stated in Lemma 1 in Section 1.2, the model validity condition $T(x,t) \geq T_m$ leads to $\dot{s}(t) \geq 0$. Hence, the following differential inequality in $\tilde{V}$ is derived from (3.62):

$$\dot{\tilde{V}} \leq -\lambda \tilde{V}. \tag{3.63}$$

Hence, $\tilde{w}$-system (3.44)–(3.46) is exponentially stable, which induces the exponential stability of the original $\tilde{u}$-system (3.40)–(3.42), which completes the proof of Theorem 7.

Algorithm development of the designed observer

The designed observer (3.34)–(3.36) obeys the PDE on moving boundary, however, the numerical model needs to be described by a finite dimensional state in a discrete time. Following the procedure in Section 1.6, the scaled PDE on the fixed domain is firstly derived, which requires the information on $s(t)$ and $\dot{s}(t)$. Through the available measurements, these variables are obtained by $Y_1(t)$ and $-\beta Y_2(t)$. Since the observer utilizes the measured values as inputs, the fixed domain PDE observer can be expressed by

$$\begin{aligned}
\hat{v}_t(\xi,t) =& \frac{\alpha}{Y_1(t)^2}\hat{v}_{\xi\xi}(\xi,t) - \frac{\xi\beta Y_2(t)}{Y_1(t)}\hat{v}_\xi(\xi,t) \\
&+ p_1(\xi, Y_1(t))\left(Y_2(t) - \frac{\hat{v}_\xi(1,t)}{Y_1(t)}\right), \quad 0 < \xi < 1 \qquad (3.64)\\
\hat{v}_\xi(0,t) =& -k^{-1}Y_1(t)q_c(t), \qquad (3.65)\\
\hat{v}(1,t) =& T_m, \qquad (3.66)
\end{aligned}$$

Hence, the available measurements enable to design not only moving boundary PDE observer but also the equivalent fixed domain PDE observer. After the spatial discretization by finite difference and the time discretization by explicit Euler methods as in BIM, the observer algorithm is described by the following structure.

Algorithm 2: Time Update for Estimating Temperature Profile

Input: $\{\hat{v}_0^i\}_{i=0}^N, \{Y_{1,j}\}_{j=0}^M, \{Y_{2,j}\}_{j=0}^M$

for $j = 0$ to M, **do**

$\hat{v}_j^{(-1)} \leftarrow \hat{v}_j^{(1)} + 2hk^{-1}Y_{1,j}q_c(j\Delta t)$

$\hat{v}_j^{(N)} \leftarrow T_m$

$\hat{Y}_{2,j} \leftarrow \frac{3\hat{v}_j^{(N)} - 4\hat{v}_j^{(N-1)} + \hat{v}_j^{(N-2)}}{2hY_{1,j}}$

for $i = 0$ to $N-1$, **do**

$z \leftarrow \sqrt{\frac{\lambda}{\alpha}Y_{1,j}^2(1-(ih)^2)}$

$p_1 \leftarrow -\lambda Y_{1,j}\frac{I_1(z)}{z}$

$\hat{v}_{j+1}^{(i)} \leftarrow$

$\hat{v}_j^{(i)} + \Delta t\left(\frac{\alpha}{h^2Y_{1,j}^2}(\hat{v}_j^{(i+1)} - 2\hat{v}_j^{(i)} + \hat{v}_j^{(i-1)}) - \frac{i\beta Y_{2,j}}{2Y_{1,j}}(\hat{v}_j^{(i+1)} - \hat{v}_j^{(i-1)}) + p_1\left(Y_{2,j} - \hat{Y}_{2,j}\right)\right)$

end for

end for

Output: $\{\hat{v}_j^i\}_{i=0,j=1}^{N,M}$

3.3 Observer-Based Output Feedback Control Design

An output feedback control law is constructed using the reconstruction of the estimated temperature profile through the exponentially convergent observer (3.34)–(3.35) with the measurements as shown in Fig. 3.1 and the following theorem holds:

Theorem 8 *Consider the closed-loop system* (3.29)–(3.32) *with the measurements* $Y_1(t) = s(t)$, $Y_2(t) = T_x(s(t),t)$, *and the observer* (3.34)–(3.35) *under the output feedback control law*

$$q_c(t) = -c\left(\frac{k}{\alpha}\int_0^{s(t)}\left(\hat{T}(x,t) - T_m\right)dx + \frac{k}{\beta}\left(s(t) - s_r\right)\right). \tag{3.67}$$

Assuming that the Lipschitz constant H in Assumption 1 ($0 \le T_0(x) - T_m \le H(s_0 - x)$*) is known, for any initial temperature estimation* $\hat{T}_0(x)$, *any gain parameter of the observer* λ, *and any*

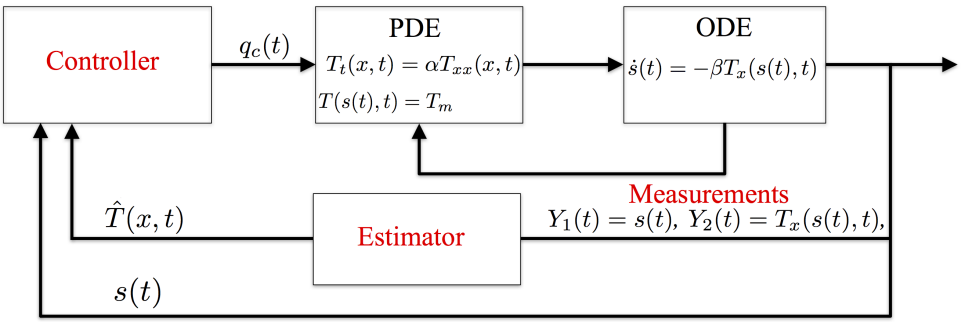

Figure 3.1: Block diagram of observer design and output feedback. Here, the interface position and the temperature gradient at the interface position are assumed to be available.

setpoint s_{r} *satisfying*

$$T_{\mathrm{m}} + \hat{H}_l(s_0 - x) \leq \hat{T}_0(x) \leq T_{\mathrm{m}} + \hat{H}_u(s_0 - x), \tag{3.68}$$

$$\lambda < \frac{4\alpha}{s_0^2}\frac{\hat{H}_l - H}{\hat{H}_u}, \tag{3.69}$$

$$s_{\mathrm{r}} > s_0 + \frac{\beta s_0^2}{2\alpha}\hat{H}_u, \tag{3.70}$$

respectively, where the parameters $\hat{H}_u$ *and* $\hat{H}_l$ *satisfy* $\hat{H}_u \geq \hat{H}_l > H$*, the closed-loop system is exponentially stable in the sense of the norm*

$$||T - \hat{T}||^2_{\mathcal{H}_{\mathrm{l}}} + ||T - T_{\mathrm{m}}||^2_{\mathcal{H}_{\mathrm{l}}} + (s(t) - s_{\mathrm{r}})^2. \tag{3.71}$$

Backstepping transformation

For the output feedback analysis, we introduce the estimator state of a reference error $\hat{u}$ by defining

$$\hat{u} = \hat{T} - T_m \tag{3.72}$$

Then, $\hat{u}$-system is described by

$$\hat{u}_t(x,t) = \alpha\hat{u}_{xx}(x,t) + p_1(x,Y_1(t))\left(Y_2(t) - \hat{u}_x(Y_1(t),t)\right), \tag{3.73}$$

$$-k\hat{u}_x(0,t) = q_c(t), \tag{3.74}$$

$$\hat{u}(Y_1(t),t) = 0, \tag{3.75}$$

with the observer gain p_1 in (3.37). We can see that the estimation error state defined by (3.39) is equivalent to the estimation error in a reference error state, namely, $\tilde{u} = T - \hat{T} = u - \hat{u}$. Since $\tilde{u}$-system in (3.40)–(3.42) is independent on the control input $U(t)$, by separation principle, the output feedback controller is designed by utilizing the estimator state $\hat{u}$ instead of the plant state u in the full-state feedback control. The transformation of the variables $(\hat{u},X)$ into $(\hat{w},X)$ is performed using the gain kernel functions of backstepping transformation in state feedback control. Thus, we consider

$$\hat{w}(x,t) = \hat{u}(x,t) - \frac{c}{\alpha}\int_x^{s(t)} (x-y)\hat{u}(y,t)dy - \frac{c}{\beta}(x-s(t))X(t). \tag{3.76}$$

Note that $\hat{w} \neq w - \tilde{w}$ due to the different transformation between $\hat{w}$ and $\tilde{w}$. Taking the derivatives of (3.76) along with the solution of (3.73)–(3.75) with the help of the transformation (3.43), the associated target system is obtained by

$$\hat{w}_t(x,t) = \alpha\hat{w}_{xx}(x,t) + \frac{c}{\beta}\dot{s}(t)X(t) + f(x,s(t))\tilde{w}_x(s(t),t), \tag{3.77}$$

$$\hat{w}_x(0,t) = 0, \tag{3.78}$$

$$\hat{w}(s(t),t) = 0, \tag{3.79}$$

$$\dot{X}(t) = -cX(t) - \beta\hat{w}_x(s(t),t) - \beta\tilde{w}_x(s(t),t), \tag{3.80}$$

where

$$f(x,s(t)) = P(x,s(t)) - \frac{c}{\alpha}\int_x^{s(t)} (x-y)P(y,s(t))dy - c(s(t)-x). \tag{3.81}$$

Evaluating the spatial derivative of (3.76) at $x = 0$, we derive the output feedback controller as

$$q_{\mathrm{c}}(t) = -c\left(\frac{k}{\alpha}\int_0^{s(t)} \hat{u}(x,t)dx + \frac{k}{\beta}X(t)\right). \tag{3.82}$$

After lengthy calculation, one can see that the inverse transformation is also equivalent to the one of the state feedback control, namely

$$\hat{u}(x,t) = \hat{w}(x,t) + \frac{\beta}{\alpha}\int_x^{s(t)} \psi(x-y)\hat{w}(y,t)dy + \psi(x-s(t))X(t), \tag{3.83}$$

where the gain kernel (2.110).

Observer gain restriction for positivity of heat input

As presented in Chapter 2, the closed loop system must verify the two physical constraints

$$q_{\mathrm{c}}(t) > 0, \quad \forall t > 0 \tag{3.84}$$

$$s_0 < s(t) < s_{\mathrm{r}}, \quad \forall t > 0. \tag{3.85}$$

We derive sufficient conditions to guarantee that the physical constraints (3.84) and (3.85) are not violated when the output feedback control law (3.82) is applied to the plant. First, we state the following lemma.

Lemma 8 *Suppose that* $\tilde{w}(0,t) < 0$. *Then, the solution to* (3.44)–(3.46) *satisfies* $\tilde{w}(x,t) < 0$, $\forall x \in (0, s(t))$, $\forall t > 0$.

The proof of Lemma 8 is constructed using the maximum principle [121]. Next, we state the

following lemma.

Lemma 9 *For any initial temperature estimate $\hat{T}_0(x)$ and any observer gain parameter λ satisfying* (3.68) *and* (3.69)*, respectively, the following properties hold:*

$$\tilde{u}(x,t) < 0,\ \tilde{u}_x(s(t),t) > 0,\ \forall x \in (0,s(t)), \quad \forall t > 0. \tag{3.86}$$

Proof:

Lemma 8 states that if $\tilde{w}(x,0) < 0$, then $\tilde{w}(x,t) < 0$. In addition, from (3.43), $\tilde{w}(x,t) < 0$ leads to $\tilde{u}(x,t) < 0$ due to the positivity of the solution to the gain kernel (3.55). Therefore, with the help of (3.56), we deduce that $\tilde{u}(x,t) < 0$ if the following holds

$$\tilde{u}(x,0) < \int_x^{s_0} Q(x,y)\tilde{u}(y,0)dy, \quad \forall x \in (0,s_0). \tag{3.87}$$

Considering the bound of the solution (3.60) under the condition (3.68), the sufficient condition for (3.87) to hold is given by (3.69), which restricts the gain λ. Thus, we have shown that conditions (3.68) and (3.69) lead to $\tilde{u}(x,t) < 0$, $\forall x \in (0,s(t))$, $\forall t > 0$. In addition, from the boundary condition (3.42) and Hopf's lemma, it follows that $\tilde{u}_x(s(t),t) > 0$.

The final step is to prove that the output feedback closed-loop system satisfies the physical constraint (3.84).

Proposition 1 *Suppose the initial values $\hat{T}_0(x)$ and s_0 satisfy* (3.68) *and the setpoint s_r is chosen to satisfy* (3.70)*. Then, the physical constraints* (3.84) *and* (3.85) *are satisfied by the closed-loop system consisting of the plant* (3.29)–(3.32)*, the observer* (3.34)–(3.36) *and the output feedback control law* (3.67)*.*

Proof:

Taking the time derivative of (3.82) along with the solution (3.73)–(3.75), with the help of the

observer gain (3.50), we obtain

$$\dot{q}_{\mathrm{c}}(t) = -cq_{\mathrm{c}}(t) + \left(1 + \int_0^{s(t)} P(x,s(t))dx\right)\tilde{u}_x(s(t),t). \tag{3.88}$$

From the positivity of the gain kernel solution (3.55) and the Neumann boundary value (3.86), the following differential inequality holds

$$\dot{q}_{\mathrm{c}}(t) \geq -cq_{\mathrm{c}}(t). \tag{3.89}$$

Hence, if the initial values satisfy $q_{\mathrm{c}}(0) > 0$, equivalently (3.70) is satisfied from (3.82) and (3.68), we get

$$q_{\mathrm{c}}(t) > 0, \quad \forall t > 0. \tag{3.90}$$

Then, using (3.86) given in Lemma 9 and the positivity of $u(x,t)$ (see Lemma 3), the following inequality is established:

$$\hat{u}(x,t) > 0, \quad \forall x \in (0,s(t)), \quad \forall t > 0. \tag{3.91}$$

Finally, substituting the inequalities (3.90) and (3.91) into (3.82), we arrive at $X(t) < 0$, $\forall t > 0$, which guarantees that the second physical constraint (3.85) is satisfied.

Convergence of estimation error and the liquid length

We prove the stability of the overall closed-loop system under the output feedback. We consider

$$\hat{V}_1 = \frac{1}{2}\int_0^{s(t)} \hat{w}(x,t)^2 dx. \tag{3.92}$$

The time derivative yields

$$\begin{aligned}\dot{\hat{V}}_1 =& -\alpha\int_0^{s(t)} \hat{w}_x(x,t)^2 dx + \frac{c}{\beta}\dot{s}(t)X(t)\int_0^{s(t)} \hat{w}(x,t)dx \\ &+ \int_0^{s(t)} f(x,s(t))\hat{w}(x,t)dx\tilde{w}_x(s(t),t), \qquad (3.93)\\ \leq& -\alpha\int_0^{s(t)} \hat{w}_x(x,t)^2 dx + \dot{s}(t)\left(\frac{c^2}{2\beta^2}X(t) + \frac{s_r}{2}\int_0^{s(t)} \hat{w}(x,t)^2 dx\right) \\ &+ \frac{\gamma_0}{2}\left(\int_0^{s(t)} f(x,s(t))^2 dx\right)\left(\int_0^{s(t)} \hat{w}(x,t)^2 dx\right) + \frac{1}{2\gamma_0}\tilde{w}_x(s(t),t)^2, \qquad (3.94)\end{aligned}$$

where we used $\dot{s}(t) > 0$ and Young's inequalities. Let $A_1 = \sup_{s_0 \leq s(t) \leq s_r}\int_0^{s(t)} f(x,s(t))^2 dx$. By Poincare's inequality, we obtain

$$\begin{aligned}\dot{\hat{V}}_1 \leq& -\frac{\alpha}{2}\int_0^{s(t)} \hat{w}_x(x,t)^2 dx + \dot{s}(t)\left(\frac{c^2}{2\beta^2}X(t) + \frac{s_r}{2}\int_0^{s(t)} \hat{w}(x,t)^2 dx\right) \\ &+ \frac{2s_r^2 A_1}{\alpha}\tilde{w}_x(s(t),t)^2, \qquad (3.95)\end{aligned}$$

where we chose $\gamma_0 = \alpha/4s_r^2 A_1$. Next, we consider

$$\hat{V}_2 = \frac{1}{2}\int_0^{s(t)} \hat{w}_x(x,t)^2 dx. \tag{3.96}$$

The time derivative leads to

$$\begin{aligned}\dot{\hat{V}}_2 =& -\alpha\int_0^{s(t)}\hat{w}_{xx}(x,t)^2dx-\frac{c}{\beta}\dot{s}(t)X(t)\hat{w}_x(s(t),t)-\frac{\dot{s}(t)}{2}\hat{w}_x(s(t),t)^2\\&-\{f(s(t),s(t))\hat{w}_x(s(t),t)+f_x(0,s(t))\hat{w}(0,t)\\&+\int_0^{s(t)}f_{xx}(x,s(t))\hat{w}(x,t)dx\Big\}\tilde{w}_x(s(t),t).\end{aligned}\tag{3.97}$$

Applying Young's and Poincare's inequalities with the help of $\dot{s}(t)>0$, we have

$$\begin{aligned}\dot{\hat{V}}_2 \leq& -\frac{\alpha}{2}\int_0^{s(t)}\hat{w}_{xx}(x,t)^2dx+\dot{s}(t)\left(\frac{c^2}{2\beta^2}X(t)^2\right)+2s_r\left(\gamma_2+\gamma_3 s_r A_2\right)\int_0^{s(t)}\hat{w}_x(x,t)^2dx\\&+\left(\frac{2s_r f(s(t),s(t))^2}{\alpha}+\frac{f_x(0,s(t))^2}{2\gamma_2}+\frac{1}{2\gamma_3}\right)\tilde{w}_x(s(t),t)^2\end{aligned}\tag{3.98}$$

where $A_2=\max_{s_0\leq s(t)\leq s_r}\int_0^{s(t)}f_{xx}(x,s(t))^2dx$ and γ_2 and γ_3 are positive parameters to be determined. Let Y be a Lyapunov function such that

$$Y=\frac{1}{2}X(t)^2\tag{3.99}$$

Taking time derivative and applying Young's inequality,

$$\dot{Y}\leq-\frac{c}{2}X(t)^2+\frac{\beta^2}{c}\hat{w}_x(s(t),t)^2+\frac{\beta^2}{c}\tilde{w}_x(s(t),t)^2\tag{3.100}$$

We define the Lyapunov functional

$$\hat{V}=\hat{V}_1+\hat{V}_2+pY,\tag{3.101}$$

where $p > 0$ is to be determined. Then, combining the inequalities, we get

$$\begin{aligned}\dot{\hat{V}} \leq & -\left(\frac{\alpha}{2}-\frac{4p\beta^2 s_r}{c}\right)\int_0^{s(t)}\hat{w}_{xx}(x,t)^2dx-\left(\frac{\alpha}{2}-2s_r\left(\gamma_2+\gamma_3 s_r A_2\right)\right)\int_0^{s(t)}\hat{w}_x(x,t)^2dx \\ & -\frac{pc}{2}X(t)^2+\dot{s}(t)\left(\frac{c^2}{\beta^2}X(t)+\frac{s_r}{2}\int_0^{s(t)}\hat{w}(x,t)^2dx\right) \\ & +\left(\frac{2s_r f(s(t),s(t))^2}{\alpha}+\frac{f_x(0,s(t))^2}{2\gamma_2}+\frac{1}{2\gamma_3}+\frac{2s_r^2A_1}{\alpha}+\frac{p\beta^2}{c}\right)\tilde{w}_x(s(t),t)^2 \end{aligned} \tag{3.102}$$

Choosing

$$p=\frac{c\alpha}{16\beta^2 s_r},\quad \gamma_2=\frac{\alpha}{16s_r},\quad \gamma_3=\frac{\alpha}{16s_r^2A_2}, \tag{3.103}$$

we obtain

$$\begin{aligned}\dot{\hat{V}} \leq & -\frac{\alpha}{4}\int_0^{s(t)}\hat{w}_{xx}(x,t)^2dx-\frac{\alpha}{4}\int_0^{s(t)}\hat{w}_x(x,t)^2dx-\frac{pc}{2}X(t)^2 \\ & +\dot{s}(t)\left(\frac{c^2}{\beta^2}X(t)+\frac{s_r}{2}\int_0^{s(t)}\hat{w}(x,t)^2dx\right) \\ & +\left(\frac{2s_r f(s(t),s(t))^2}{\alpha}+\frac{8s_r f_x(0,s(t))^2}{\alpha}+\frac{8s_r^2A_2}{\alpha}+\frac{2s_r^2A_1}{\alpha}+\frac{\alpha}{16s_r}\right)\tilde{w}_x(s(t),t)^2. \end{aligned} \tag{3.104}$$

Thus, defining $V_{all}=\hat{V}+d\tilde{V}$, we have

$$\begin{aligned}\dot{V}_{all} \leq & -\frac{\alpha}{16s_r^2}\int_0^{s(t)}\hat{w}_x(x,t)^2dx-\frac{\alpha}{16s_r^2}\int_0^{s(t)}\hat{w}(x,t)^2dx-\frac{pc}{2}X(t)^2 \\ & +\dot{s}(t)\left(\frac{c^2}{\beta^2}X(t)+\frac{s_r}{2}\int_0^{s(t)}\hat{w}(x,t)^2dx\right) \\ & -\left[\frac{d\alpha}{4s_r}-\left(\frac{2s_r f(s(t),s(t))^2}{\alpha}+\frac{8s_r f_x(0,s(t))^2}{\alpha}+\frac{8s_r^2A_2}{\alpha}+\frac{2s_r^2A_1}{\alpha}+\frac{\alpha}{16s_r}\right)\right]\tilde{w}_x(s(t),t)^2 \\ & -d(\lambda+\alpha)\int_0^{s(t)}\tilde{w}_x(x,t)^2dx-d\lambda\int_0^{s(t)}\tilde{w}(x,t)^2dx. \end{aligned} \tag{3.105}$$

Choosing d sufficiently large, we arrive at

$$\dot{V}_{all} \leq -bV_{all} + a\dot{s}(t)V_{all}, \tag{3.106}$$

where

$$a = \max\left\{s_r^2, \frac{c^2}{p\beta^2}\right\}, \quad b = \min\left\{\frac{\alpha}{8s_r^2}, c, 2\lambda\right\}. \tag{3.107}$$

As we have studied stability analysis of state feedback, the inequality (3.106) with the help of $\dot{s}(t) > 0$ and $s_0 < s(t) < s_r$ leads to the exponential stability of $(\tilde{w}, \hat{w}, X)$-system. By the invertibility and boundedness of the transformations, we deduce the proof of Theorem 8.

Numerical simulation

We use parameters of zinc given in Table 1.1 in Section 1.6. The initial interface is set to $s_0 = 1$ [cm], and the setpoint is chosen as $s_r = 35$ [cm]. The initial estimation of the temperature profile is set to $\hat{T}_0(x) = \bar{\hat{T}}(1 - x/s_0) + T_{\rm m}$ with $\bar{\hat{T}}$ = 30 [C$^\circ$] while the initial temperature is set to $T_0(x) = \bar{T}(1 - x/s_0) + T_{\rm m}$ with $\bar{T}$ = 10 [C$^\circ$], and the observer gain is chosen as λ = 0.01. Then, the restriction on $\hat{T}_0(x)$, λ, and $s_{\rm r}$ described in (3.68)–(3.70) are satisfied. The control gain is chosen as $c = 0.001$.

The dynamics of the moving interface $s(t)$, the output feedback controller $q_{\rm c}(t)$, and the temperature at the initial interface $T(s_0, t)$ are depicted in Fig. 3.2. The first plot shows that the interface $s(t)$ converges to the setpoint $s_{\rm r}$ without overshoot which is guaranteed in Proposition 1. The second figure shows that the output feedback controller remains positive as stated in Proposition 1. The model validity can be seen in the third figure, which illustrates $T(s_0, t)$ increases from the melting temperature $T_{\rm m}$ to enable melting of material and settles back to its equilibrium. Fig. 3.3 shows a short-time dynamics of the temperature profile (solid) and

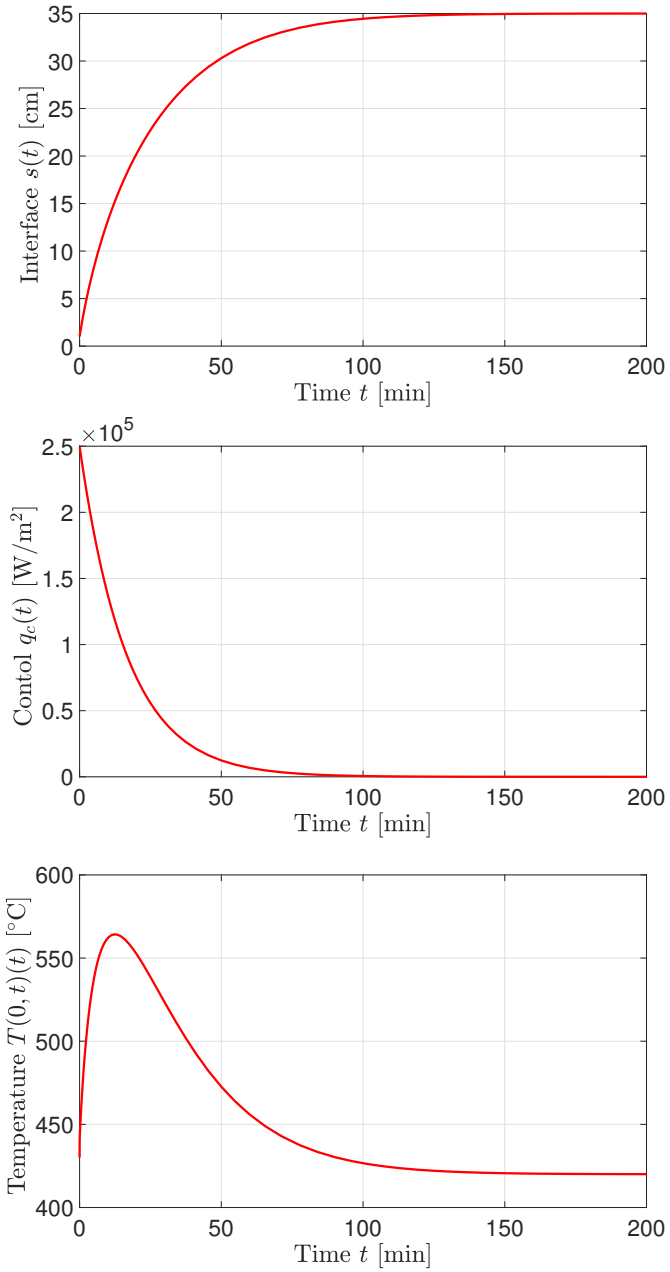

Figure 3.2: Simulation of the closed-loop system (3.29)–(3.32) and the estimator (3.34)–(3.37) with the output feedback control law (3.67).

the estimated temperature (dash). Clearly, the estimated temperature converges to the the true temperature quickly.

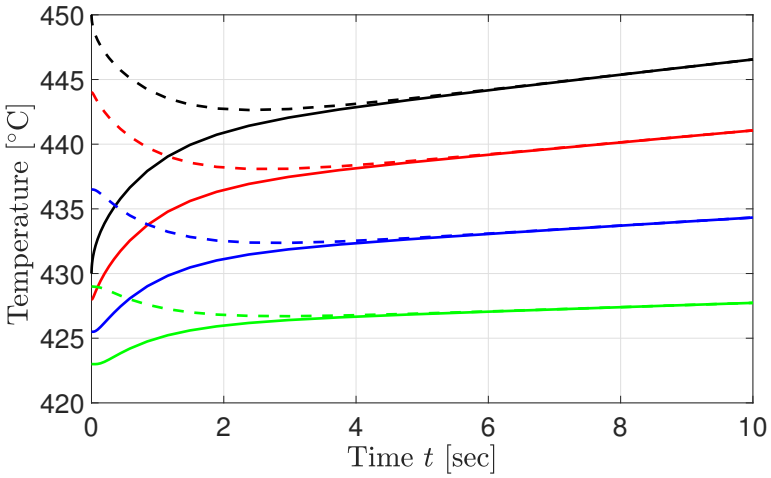

Figure 3.3: Time evolution of true temperature (solid) and the estimate (dash) at $x = 0$ (black), $x = s(t)/4$ (red), $x = s(t)/2$ (blue), and $x = 3s(t)/4$ (green), respectively.

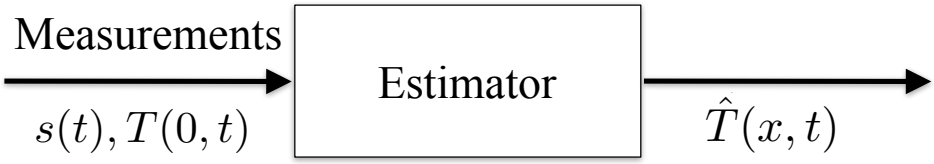

Figure 3.4: The estimation problem measuring a boundary temperature and the interface position.

3.4 State Estimation under More Practical Sensors

We also develop the temperature profile estimation design under the available measurement on the liquid temperature at the fixed domain instead of the temperature gradient at the interface proposed in the last sections. This setup is much more practical while the drawback is that the analysis for the output feedback control has not been established yet due to the challenge on proving the physical constraints. Nevertheless, we can show the analysis of the convergent observer by proving the stability of the estimation error state.

We consider the same system in last sections, (3.29)–(3.32). The following observer is designed with the statement on the theorem.

Theorem 9 *Consider the plant* (3.29)–(3.32) *with the measurements*

$$Y_1(t) = s(t), \quad Y_2(t) = T(0,t), \tag{3.108}$$

and the following observer

$$\hat{T}_t(x,t) = \alpha \hat{T}_{xx}(x,t) + p_1(x, Y_1(t)) \left(Y_2(t) - \hat{T}(0,t) \right), \tag{3.109}$$

$$\hat{T}_x(0,t) = -\frac{q_c(t)}{k} + p_2(Y_1(t)) \left(Y_2(t) - \hat{T}(0,t) \right), \tag{3.110}$$

$$\hat{T}(Y_1(t),t) = T_m, \tag{3.111}$$

where $x \in [0, Y_1(t)]$*, and the observer gains are*

$$p_1(x, Y_1(t)) = \lambda Y_1(t)(Y_1(t) - x) \frac{I_2\left(\sqrt{\frac{\lambda}{\alpha} \{ Y_1(t)^2 - (x - Y_1(t))^2 \}} \right)}{Y_1(t)^2 - (x - Y_1(t))^2}, \tag{3.112}$$

$$p_2(Y_1(t)) = -\frac{\lambda}{2\alpha} Y_1(t) \tag{3.113}$$

with a gain parameter $\lambda > 0$*. Assume that the model validity condition* $T(x,t) \geq T_m$ *is satisfied. Then, for all* $\lambda > 0$*, the observer error system is exponentially stable in the sense of the norm* $||T - \hat{T}||^2_{\mathcal{H}_1}$.

Let $\tilde{u}(x,t) = T(x,t) - \hat{T}(x,t)$ be an estimation error variable. Then, we have a system for error variable as

$$\tilde{u}_t(x,t) = \alpha \tilde{u}_{xx}(x,t) - p_1(x, s(t)) \tilde{u}(0,t), \quad 0 < x < s(t) \tag{3.114}$$

$$\tilde{u}_x(0,t) = -p_2(x, s(t)) \tilde{u}(0,t), \tag{3.115}$$

$$\tilde{u}(s(t),t) = 0 \tag{3.116}$$

Unlike the procedure in Section 3.2, we cannot establish a good target system using the same

form of the transformation. Instead, as developed in the state feedback design in Chapter 2, we first consider the observer design for the analogous system on the fixed domain and develop the observer gain with the associated backstepping transformation. After that, we apply the analogous gain and transformation on the moving boundary to the error system (3.114)–(3.116), and prove the stability of the associated target system on the moving boundary.

Fixed domain design

Consider the analogous estimation error system on the fixed domain $x \in (0, D)$ given by

$$\tilde{u}_t(x,t) = \alpha \tilde{u}_{xx}(x,t) - p_1(x,D)\tilde{u}(0,t), \quad 0 < x < D \tag{3.117}$$

$$\tilde{u}_x(0,t) = -p_2(D)\tilde{u}(0,t), \tag{3.118}$$

$$\tilde{u}(D,t) = 0, \tag{3.119}$$

Introduce the transformation

$$\tilde{u}(x,t) = w(x,t) + \int_0^x P(x,y)w(y,t)dy, \tag{3.120}$$

which transforms into

$$w_t(x,t) = \alpha w_{xx}(x,t) - \lambda w(x,t), \tag{3.121}$$

$$w_x(0,t) = 0, \tag{3.122}$$

$$w(D,t) = 0. \tag{3.123}$$

Taking time and spatial derivatives of (3.120), the conditions for the gain kernel and the observer gain are obtained by

$$P_{xx}(x,y) - P_{yy}(x,y) = -\frac{\lambda}{\alpha}P(x,y), \tag{3.124}$$

$$P(x,x) = -\frac{\lambda}{2\alpha}(x-D), \tag{3.125}$$

$$P(D,y) = 0, \tag{3.126}$$

$$p_1(x,D) = -\alpha P_y(x,0), \tag{3.127}$$

$$p_2(D) = -P(0,0). \tag{3.128}$$

The solution to the gain kernel PDE is derived as

$$P(x,y) = \lambda'(D-x)\frac{I_1\left(\sqrt{\lambda'\{(D-y)^2-(D-x)^2\}}\right)}{\sqrt{\lambda'\{(D-y)^2-(D-x)^2\}}}. \tag{3.129}$$

By the differentiation formula for the Bessel functions, we have $\frac{d}{dz}\left(\frac{I_1(z)}{z}\right) = \frac{I_2(z)}{z}$. Using this formula and some calculus, the observer gains in (3.127) and (3.128) are described by

$$p_1(x,D) = \alpha\lambda'^2 D(D-x)\frac{I_2(z)}{z^2}, \quad z = \sqrt{\lambda'\{D^2-(D-x)^2\}}, \tag{3.130}$$

$$p_2(D) = -\frac{\lambda}{2\alpha}D. \tag{3.131}$$

Then, in the similar manner, we have

$$w(x,t) = \tilde{u}(x,t) + \int_0^x Q(x,y)\tilde{u}(y,t)dy, \tag{3.132}$$

which leads to the conditions of

$$Q_{xx}(x,y)-Q_{yy}(x,y)=\frac{\lambda}{\alpha}Q(x,y), \tag{3.133}$$

$$Q(x,x)=\frac{\lambda}{2\alpha}(x-D), \tag{3.134}$$

$$Q(D,y)=0. \tag{3.135}$$

The solution is

$$Q(x,y)=P(x,y,-\lambda)=-\lambda'(D-x)\frac{J_1\left(\sqrt{\lambda'\{(D-y)^2-(D-x)^2\}}\right)}{\sqrt{\lambda'\{(D-y)^2-(D-x)^2\}}}. \tag{3.136}$$

Analogous observer design on moving boundary domain

Referring to the result of fixed domain, we apply the backstepping observer design of

$$\hat{u}_t(x,t)=\alpha\hat{u}_{xx}(x,t)+p_1(x,s(t))(u(0,t)-\hat{u}(0,t)),\quad 0<x<s(t) \tag{3.137}$$

$$\hat{u}(s(t),t)=0, \tag{3.138}$$

$$\hat{u}_x(0,t)=-q_c(t)/k+p_2(s(t))(u(0,t)-\hat{u}(0,t)), \tag{3.139}$$

with gains

$$p_1(x,s(t))=\frac{\lambda^2}{\alpha}s(t)(x-s(t))\frac{I_2\left(\sqrt{\frac{\lambda}{\alpha}\{s(t)^2-(x-s(t))^2\}}\right)}{\sqrt{\frac{\lambda}{\alpha}\{s(t)^2-(x-s(t))^2\}}}, \tag{3.140}$$

$$p_2(s(t))=-\frac{\lambda}{2\alpha}s(t). \tag{3.141}$$

Now, we look at the original model in moving boundary coordinate. Consider the invertible transformation

$$\tilde{w}(x,t) = \tilde{u}(x,t) + \int_0^x Q(x-s(t), y-s(t))\tilde{u}(y,t)dy, \tag{3.142}$$

$$\tilde{u}(x,t) = \tilde{w}(x,t) + \int_0^x P(x-s(t), y-s(t))\tilde{w}(y,t)dy. \tag{3.143}$$

Then, the target system has the form of

$$\begin{aligned}\tilde{w}_t(x,t) =& \alpha\tilde{w}_{xx}(x,t) - \lambda\tilde{w}(x,t) \\ & - \dot{s}(t)\int_0^x q(\bar{x},\bar{y})\left(\tilde{w}(y,t) + \int_0^y P(\bar{y},\bar{z})\tilde{w}(z,t)dz\right)dy, \end{aligned}\tag{3.144}$$

$$\tilde{w}(s(t),t) = 0, \tag{3.145}$$

$$\tilde{w}_x(0,t) = 0, \tag{3.146}$$

where $\bar{x} = x - s(t)$, $\bar{y} = y - s(t)$, and $q(\bar{x},\bar{y}) = Q_x(x,y) + Q_y(x,y)$.

We prove that the target $\tilde{w}$-system in (3.144)–(3.146) is stable under $\dot{s}(t) > 0$ and $s(t) < s_r$. Consider the Lyapunov function

$$\tilde{V}_1 = \frac{1}{2}||\tilde{w}||^2 \tag{3.147}$$

The time derivative is given by

$$\begin{aligned}\dot{\tilde{V}}_1 =& -\alpha\int_0^{s(t)} \tilde{w}_x(x,t)^2 dx - \lambda\int_0^{s(t)} \tilde{w}(x,t)^2 dx \\ & - \dot{s}(t)\int_0^{s(t)} \tilde{w}(x,t)\left(\int_0^x q(\bar{x},\bar{y})\left(\tilde{w}(y,t) + \int_0^y P(\bar{y},\bar{z})\tilde{w}(z,t)dz\right)dy\right)dx. \end{aligned}\tag{3.148}$$

Define $\bar{q} = \max_{(x,y)\in[0,s_r]} q(\bar{x},\bar{y})^2$ and $\bar{p} = \max_{(y,z)\in[0,s_r]} P(\bar{y},\bar{z})$. Applying Young's Cauchy Schwarz inequalities to the second line of (3.148) with the help of $\dot{s}(t) > 0$ and $s(t) \le s_r$, the following

inequality is derived

$$\dot{\tilde{V}}_1 \leq -\alpha||\tilde{w}_x||^2 - \lambda||\tilde{w}||^2 + \frac{\dot{s}(t)}{2}\left(1 + 2\bar{q}s_r^2(1+\bar{p}^2 s_r^2)\right)||\tilde{w}||^2. \tag{3.149}$$

Consider

$$\tilde{V}_2 = \frac{1}{2}\int_0^{s(t)} \tilde{w}_x(x,t)^2 dx. \tag{3.150}$$

The time derivative is obtained by

$$\dot{\tilde{V}}_2 = -\alpha||\tilde{w}_{xx}||^2 - \lambda||\tilde{w}_x||^2 - \frac{\dot{s}(t)}{2}\tilde{w}_x(s(t),t)^2 + \dot{s}(t)\int_0^{s(t)} \Phi(w(x,t),s(t),x), \tag{3.151}$$

where

$$\Phi := \int_0^{s(t)} \tilde{w}_{xx}(x,t)\left(\int_0^x q(\bar{x},\bar{y})\left(\tilde{w}(y,t) + \int_0^y P(\bar{y},\bar{z})\tilde{w}(z,t)dz\right)dy\right)dx. \tag{3.152}$$

Calculating integration by parts twice leads to

$$\begin{aligned}\Phi =& \tilde{w}_x(s(t),t)\left(\int_0^{s(t)} q(0,\bar{y})\left(\tilde{w}(y,t) + \int_0^y P(\bar{y},\bar{z})\tilde{w}(z,t)dz\right)dy\right) \\ &+ \tilde{w}(0,t)\left(\frac{d}{dx}\left(\int_0^x q(\bar{x},\bar{y})\left(\tilde{w}(y,t) + \int_0^y P(\bar{y},\bar{z})\tilde{w}(z,t)dz\right)dy\right)\right)|_{x=0} \\ &+ \int_0^{s(t)} \tilde{w}(x,t)\left(\frac{d^2}{dx^2}\left(\int_0^x q(\bar{x},\bar{y})\left(\tilde{w}(y,t) + \int_0^y P(\bar{y},\bar{z})\tilde{w}(z,t)dz\right)dy\right)dx\right).\end{aligned} \tag{3.153}$$

We calculate

$$\frac{d}{dx}\int_0^x q(\bar{x},\bar{y})\left(\tilde{w}(y,t) + \int_0^y P(\bar{y},\bar{z})\tilde{w}(z,t)dz\right)dy|_{x=0} = q(s(t),s(t))\tilde{w}(0,t) \tag{3.154}$$

Here, we see that $q(s(t),s(t)) = Q_x(0,0) + Q_y(0,0) = \left(\frac{d}{dx}Q(x,x)\right)|_{x=0} = \frac{\lambda}{2\alpha}$. Moreover,

$$\begin{aligned}
&\frac{d^2}{dx^2}\left(\int_0^x q(\bar{x},\bar{y})\left(\tilde{w}(y,t) + \int_0^y P(\bar{y},\bar{z})\tilde{w}(z,t)dz\right)dy\right) \\
=&q(\bar{x},\bar{x})\tilde{w}_x(x,t) + (q(\bar{x},\bar{x})P(\bar{x},\bar{x}) - 2q_{\bar{x}}(\bar{x},\bar{x}) - q_{\bar{y}}(\bar{x},\bar{x}))\tilde{w}(x,t) \\
&- \int_0^x \left((2q_{\bar{x}}(\bar{x},\bar{x}) + q_{\bar{y}}(\bar{x},\bar{x}))P(\bar{x},\bar{z}) + q(\bar{x},\bar{x})P_{\bar{x}}(\bar{x},\bar{z}) + q_{\bar{x}}(\bar{x},\bar{z})\right)\tilde{w}(z,t)dz \\
&- \int_0^x q_{\bar{x}}(\bar{x},\bar{y})\left(\int_0^y P(\bar{y},\bar{z})\tilde{w}(z,t)dz\right)dy. \qquad (3.155)
\end{aligned}$$

In addition, we have

$$\int_0^{s(t)} q(\bar{x},\bar{x})\tilde{w}(x,t)\tilde{w}_x(x,t)dx = -\frac{\lambda}{4\alpha}\tilde{w}(0,t)^2 + \frac{1}{2}(q_{\bar{x}}(\bar{x},\bar{x}) + q_{\bar{y}}(\bar{x},\bar{x}))\tilde{w}(x,t)^2dx. \qquad (3.156)$$

Thus,

$$\begin{aligned}
\Phi =&\tilde{w}_x(s(t),t)\left(\int_0^{s(t)} q(0,\bar{y})\left(\tilde{w}(y,t) + \int_0^y P(\bar{y},\bar{z})\tilde{w}(z,t)dz\right)dy\right) + \frac{\lambda}{4\alpha}\tilde{w}(0,t)^2 \\
&+ \int_0^{s(t)} (q(\bar{x},\bar{x})P(\bar{x},\bar{x}) - \frac{3}{2}q_{\bar{x}}(\bar{x},\bar{x}) - \frac{1}{2}q_{\bar{y}}(\bar{x},\bar{x}))\tilde{w}(x,t)^2dx \\
&+ \int_0^{s(t)} \tilde{w}(x,t)I(\tilde{w}(x,t),x,s(t))dx, \qquad (3.157)
\end{aligned}$$

where

$$\begin{aligned}
&I(w(x,t),x,s(t)) \\
=&-\int_0^x \left((2q_{\bar{x}}(\bar{x},\bar{x}) + q_{\bar{y}}(\bar{x},\bar{x}))P(\bar{x},\bar{z}) + q(\bar{x},\bar{x})P_{\bar{x}}(\bar{x},\bar{z}) + q_{\bar{x}}(\bar{x},\bar{z})\right)\tilde{w}(z,t)dz \\
&- \int_0^x q_{\bar{x}}(\bar{x},\bar{y})\left(\int_0^y P(\bar{y},\bar{z})\tilde{w}(z,t)dz\right)dy. \qquad (3.158)
\end{aligned}$$

Applying Young's and Cauchy-Schwarz inequality, we can show that there exist positive constants

M_1, M_2, M_3 such that

$$\tilde{w}_x(s(t),t)\left(\int_0^{s(t)} q(0,\bar{y})\left(\tilde{w}(y,t)+\int_0^y P(\bar{y},\bar{z})\tilde{w}(z,t)dz\right)dy\right) \leq \frac{1}{2}\tilde{w}_x(s(t),t)^2 + M_1||\tilde{w}||^2, \tag{3.159}$$

$$\int_0^{s(t)} (q(\bar{x},\bar{x})P(\bar{x},\bar{x}) - \frac{3}{2}q_{\bar{x}}(\bar{x},\bar{x}) - \frac{1}{2}q_{\bar{y}}(\bar{x},\bar{x}))\tilde{w}(x,t)^2 dx \leq M_2||\tilde{w}||^2, \tag{3.160}$$

$$\int_0^{s(t)} \tilde{w}(x,t)I(\tilde{w}(x,t),x,s(t))dx \leq M_3||\tilde{w}||^2 \tag{3.161}$$

Furthermore, by Agmon's inequality, it holds $w(0,t)^2 \leq 4s_r||\tilde{w}||^2$. Therefore, applying all these inequalities to (3.157) leads to

$$\Phi \leq \frac{1}{2}\tilde{w}_x(s(t),t)^2 + \frac{\lambda s_r}{\alpha}||\tilde{w}_x||^2 + (M_1+M_2+M_3)||\tilde{w}||^2. \tag{3.162}$$

Applying (3.162) to (3.151), we arrive at

$$\dot{\tilde{V}}_2 \leq -\alpha||\tilde{w}_{xx}||^2 - \lambda||\tilde{w}_x||^2 + \dot{s}(t)\left(\frac{\lambda s_r}{\alpha}||\tilde{w}_x||^2 + (M_1+M_2+M_3)||\tilde{w}||^2\right) \tag{3.163}$$

Thus, defining $\tilde{V} = \tilde{V}_1 + \tilde{V}_2$ and $b = \frac{\alpha}{4s_r^2} + \lambda$, we can see that there exists a positive constant $a > 0$ such that the following inequality holds

$$\dot{\tilde{V}} \leq -b\tilde{V} + a\dot{s}(t)\tilde{V}, \tag{3.164}$$

from which we conclude Theorem 9.

Improvement of the designed observer for numerical algorithm

From the numerical algorithm perspective, the designed observer (3.109)–(3.111) is not implementable using BIM due to the following reason. Through scaling the spatial domain, the

equivalent observer on a fixed domain $\xi \in [0,1]$ is written as

$$\begin{aligned}\hat{v}_t(\xi,t) =& \frac{\alpha}{Y_1(t)^2}\hat{v}_{\xi\xi}(\xi,t) - \frac{\xi\beta v_\xi(1,t)}{Y_1(t)}\hat{v}_\xi(\xi,t) \\ &+ p_1(\xi,Y_1(t))\left(Y_2(t)-\hat{v}(0,t)\right), \quad 0<\xi<1 \end{aligned} \tag{3.165}$$

$$\hat{v}_\xi(0,t) = -k^{-1}Y_1(t)q_c(t) + Y_1(t)p_2(Y_1(t))(T(0,t)-\hat{T}(0,t)), \tag{3.166}$$

$$\hat{v}(1,t) = T_m, \tag{3.167}$$

The problem is that we need to know the state $v_\xi(1,t)$ in the second term of the first line in (3.165), which is not the available variable under the current setting, unlike the setting on last sections. Therefore, for the numerical model, we should replace $v_\xi(1,t)$ by the estimated variable $\hat{v}_\xi(1,t)$. In other words, instead of (3.165), the fixed domain PDE we calculate is

$$\begin{aligned}\hat{v}_t(\xi,t) =& \frac{\alpha}{Y_1(t)^2}\hat{v}_{\xi\xi}(\xi,t) - \frac{\xi\beta\hat{v}_\xi(1,t)}{Y_1(t)}\hat{v}_\xi(\xi,t) \\ &+ p_1(\xi,Y_1(t))\left(Y_2(t)-\hat{v}(0,t)\right), \quad 0<\xi<1 \end{aligned} \tag{3.168}$$

The theoretical analysis of the fixed-domain PDE observer (3.168) is still an open problem. The observer algorithm is given in Algorithm 3.

3.5 Estimation of Both Temperature Profile and Moving Interface by Measuring Only a Boundary Temperature

The most challenging setup for the state estimation of 1D one-phase Stefan problem is to estimate both temperature profile and moving interface position given a measured value of single boundary temperature. This is not only mathematically challenging, but also practically important in some industrial processes such as steel casting as developed in [127]. We have

Algorithm 3: Time Update for Estimating Temperature Profile

Input: $\{\hat{v}_0^i\}_{i=0}^N, \{Y_{1,j}\}_{j=0}^M, \{Y_{2,j}\}_{j=0}^M$

for $j = 0$ to M, **do**

$p_2 \leftarrow -\frac{\lambda}{2\alpha} Y_{1,j}$

$\hat{v}_j^{(-1)} \leftarrow \hat{v}_j^{(1)} + 2hY_{1,j}(k^{-1}q_c(j\Delta t) - p_2(Y_{2,j} - \hat{v}_j^{(0)}))$

$\hat{v}_j^{(N)} \leftarrow T_m$

$\hat{w}_j \leftarrow \frac{3\hat{v}_j^{(N)} - 4\hat{v}_j^{(N-1)} + \hat{v}_j^{(N-2)}}{2hY_{1,j}}$

for $i = 0$ to $N-1$, **do**

$z \leftarrow \sqrt{\frac{\lambda}{\alpha} Y_{1,j}^2 (1 - (1 - (ih)^2))}$

$p_1 \leftarrow \frac{\lambda^2}{\alpha} Y_{1,j}^2 (1 - ih) \frac{I_2(z)}{z^2}$

$\hat{v}_{j+1}^{(i)} \leftarrow$

$\hat{v}_j^{(i)} + \Delta t \left(\frac{\alpha}{h^2 Y_{1,j}^2} (\hat{v}_j^{(i+1)} - 2\hat{v}_j^{(i)} + \hat{v}_j^{(i-1)}) - \frac{i\beta\hat{w}_j}{2Y_{1,j}} (\hat{v}_j^{(i+1)} - \hat{v}_j^{(i-1)}) + p_1 \left(Y_{2,j} - \hat{v}_j^{(0)} \right) \right)$

end for

end for

Output: $\{\hat{v}_j^i\}_{i=0,j=1}^{N,M}$

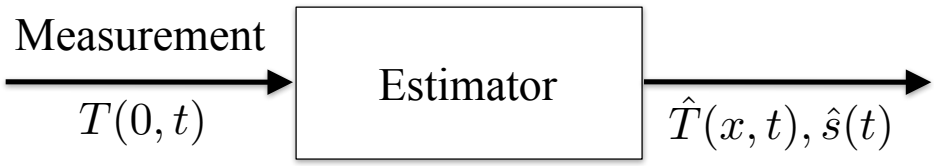

Figure 3.5: The estimation problem measuring only a boundary temperature. The problem is challenging due to the requirement to estimate the interface position.

not established a mathematically rigorous result for this problem, however, suggest an observer design and investigate the performance in numerical simulation. Thus, we state the following "conjecture" for the observer design.

Conjecture Consider the plant (3.29)–(3.32) with the measurement

$$Y(t) = T(0,t), \tag{3.169}$$

and the following PDE observer

$$\hat{T}_t(x,t) = \alpha \hat{T}_{xx}(x,t) + p_1(x,\hat{s}(t))\left(Y(t) - \hat{T}(0,t)\right), \tag{3.170}$$

$$\hat{T}_x(0,t) = -\frac{q_c(t)}{k} + p_2(\hat{s}(t))\left(Y(t) - \hat{T}(0,t)\right), \tag{3.171}$$

$$\hat{T}(\hat{s}(t),t) = T_m, \tag{3.172}$$

with the ODE observer

$$\dot{\hat{s}}(t) = -\beta \hat{T}_x(\hat{s}(t),t) + l(Y(t) - \hat{T}(0,t)) \tag{3.173}$$

where $x \in [0, Y_1(t)]$, the observer gains p_1, p_2 are given in (3.112), (3.113) with a gain parameter $\lambda > 0$, and $l > 0$ is a gain parameter. Then, there exist $\lambda^* > 0$ and l^* such that $\forall \lambda \in (0, \lambda^*)$ and $\forall l \in (0, l^*)$ the estimation error system is exponentially stable in the norm $||T - \hat{T}||_{L_2}^2 + (s - \hat{s})^2$.

Following the procedure in last section, the fixed domain PDE observer for numerical algorithm is given by the following

$$\hat{v}_t(\xi,t) = \frac{\alpha}{\hat{s}(t)^2}\hat{v}_{\xi\xi}(\xi,t) - \frac{\xi \dot{\hat{s}}(t)}{\hat{s}(t)}\hat{v}_\xi(\xi,t) + p_1(\xi,\hat{s}(t))\left(Y(t) - \hat{v}(0,t)\right), \tag{3.174}$$

for $\xi \in (0,1)$. Thus, the numerical algorithm is described by Algorithm 4.

We study the performance of the observer in numerical simulation using parameters of zinc and tuning the gain parameters λ and l. Also, we compare with the observer design suggested in [127], which is given by a copy of the plant for PDE observer and the same structure in (3.173) for ODE observer. Fig. 3.6 depicts the simulation results and its comparison, as stated in its caption, which illustrates the better performance of the proposed estimation compared to the method in [127].

Algorithm 4: Time Update for Estimating Temperature Profile and Interface Position ($i = 0, \cdots, N$ for spatial discretization and $j = 0, \cdots, M$ for time discretization)

Input: $\{\hat{v}_0^i\}_{i=0}^N, \hat{s}_0, \{Y_j\}_{j=0}^M$
for $j = 0$ to M, **do**
$p_2 \leftarrow -\frac{\lambda}{2\alpha}\hat{s}_j$
$\hat{v}_j^{(-1)} \leftarrow \hat{v}_j^{(1)} + 2hk^{-1}\hat{s}_j q_c(j\Delta t) - \hat{s}_j p_2(Y_j - \hat{v}_j^{(0)})$
$\hat{v}_j^{(N)} \leftarrow T_m$
$\hat{w}_j \leftarrow -\beta\frac{3\hat{v}_j^{(N)} - 4\hat{v}_j^{(N-1)} + \hat{v}_j^{(N-2)}}{2h\hat{s}_j} + l(Y_j - \hat{v}_j^{(0)})$
$p_1 \leftarrow \frac{\lambda^2}{8\alpha}\hat{s}_j^2$
$\hat{v}_{j+1}^{(0)} \leftarrow \hat{v}_j^{(0)} + \Delta t\left(\frac{\alpha}{h^2\hat{s}_j^2}(\hat{v}_j^{(1)} - 2\hat{v}_j^{(0)} + \hat{v}_j^{(-1)}) + p_1\left(Y_j - \hat{v}_j^{(0)}\right)\right)$
for $i = 1$ to $N-1$, **do**
$z \leftarrow \sqrt{\frac{\lambda}{\alpha}\hat{s}_j^2(1-(1-(ih)^2))}$
$p_1 \leftarrow \frac{\lambda^2}{\alpha}\hat{s}_j^2(1-ih)\frac{I_2(z)}{z^2}$
$\hat{v}_{j+1}^{(i)} \leftarrow$
$\hat{v}_j^{(i)} + \Delta t\left(\frac{\alpha}{h^2\hat{s}_j^2}(\hat{v}_j^{(i+1)} - 2\hat{v}_j^{(i)} + \hat{v}_j^{(i-1)}) + \frac{i\hat{w}_j}{2\hat{s}_j}(\hat{v}_j^{(i+1)} - \hat{v}_j^{(i-1)}) + p_1\left(Y_j - \hat{v}_j^{(0)}\right)\right)$
end for
$\hat{s}_{j+1} \leftarrow \hat{s}_j + \Delta t\hat{w}_j$
end for
Output: $\{\hat{v}_j^i\}_{i=0,j=1}^{N,M}$

State Estimation by Extended Kalman Filter

This section presents the state estimation algorithm by Extended Kalman Filter (EKF). While we have not incorporated a stochastic noise in the system, in reality the noise should appear in most of the value and observations. Since we have introduced the model reduction by spatial and time discretization, it is natural to incorporate the system noise. In addition, the observation is idealized to directly measure the surface concentration which can be inversely calculated from the output voltage. The observation of the output voltage has a stochastic noise in general, so we

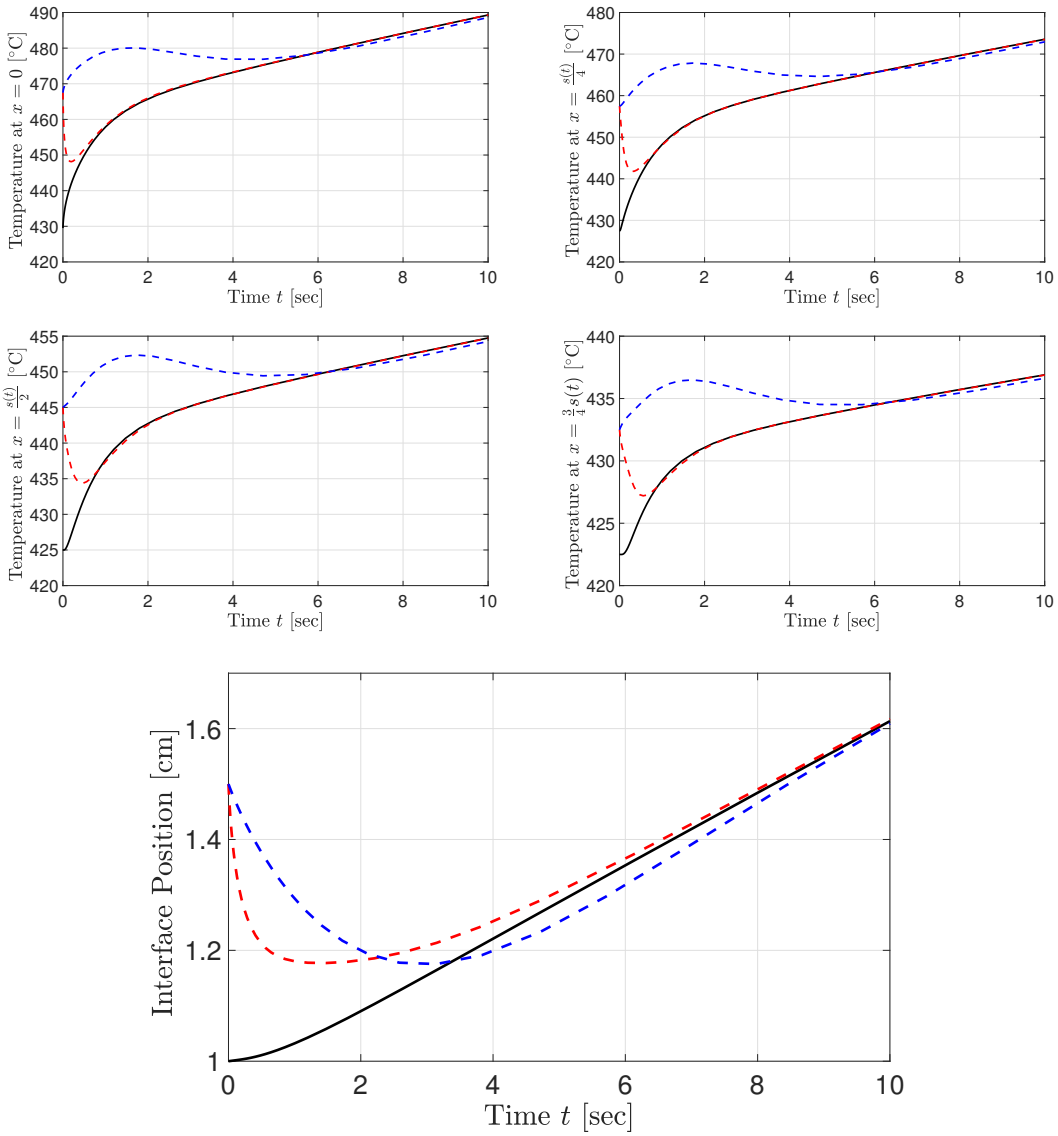

Figure 3.6: Dynamics of the true states (black solid), estimation by Algorithm 4 (red dash), and estimation using the method in [127] (blue dash), respectively. The upper four figures show the temperature at $x = 0, s(t)/4, s(t)/2, 3s(t)/4$, and the lower figure shows the interface position, respectively. We can observe that for all the states, estimation by Algorithm 4 achieves faster convergence to the true states.

should also incorporate the stochastic noise in the observation. Hence, we write the form of

$$z_{k+1} = f(z_k) + w_k, \tag{3.175}$$

$$y_k = Cz_k + v_k \tag{3.176}$$

where

$$z_k = [v_k, s_k], \tag{3.177}$$

$$f(z_k) = z_k + \Delta t \bar{f}(z_k), \tag{3.178}$$

$$C = [1, 0, \cdots, 0, 0, 0] \tag{3.179}$$

, and w_k and v_k are white Gaussian noises in $w_k \sim \mathcal{N}(0, W_k)$ and $v_k \sim \mathcal{N}(0, V_k)$. Based on this model description, EKF algorithm is given in the following.

State Estimation Algorithm by EKF

$\hat{x}_k^- \cdots$ priori estimate (using meas. up to previous time)

$\hat{x}_k^+ \cdots$ posteriori estimate (using meas. up to current time)

(i) [Initialization] For $k = 0$, set

$$\hat{x}_0^+ = E[x_0], \quad \Sigma_0^+ = E[(x_0 - E[x_0])(x_0 - E[x_0])^T]$$

For $k = 1, 2, \cdots$, compute

(ii) [Time update]

Define Jacobian matrices : $A_{k-1} = \frac{\partial f(x)}{\partial x}|_{x=\hat{x}_{k-1}^+}$

State estimate time update: $\hat{x}_k^- = f(\hat{x}_{k-1}^+)$

Error covariance time update: $\Sigma_k^- = A_{k-1}\Sigma_{k-1}^+ A_{k-1}^T + W_k$

(iii) [Measurement update]

Kalman gain: $L_k = \Sigma_k^- C^T [C\Sigma_k^- C^T + V_k]$

State estimate measurement update: $\hat{x}_k^+ = \hat{x}_k^- + L_k[y_k - C\hat{x}^-]$

Error covariance measurement update: $\Sigma_k^+ = (I - L_k C_k)\Sigma_k^-$

$$\bar{f}(z_k) = \begin{bmatrix} \frac{1}{s_k^2}(Av_k + g(v_k)) \\ \frac{1}{s_k} c^\top v_k \end{bmatrix} + \frac{1}{s_k} \begin{bmatrix} B \\ 0 \end{bmatrix} q_{c,k} \tag{3.180}$$

where $A \in \mathbb{R}^{N\times N}, B \in \mathbb{R}^{N\times 1}, c \in \mathbb{R}^{N\times 1}$,

$$A = \frac{\alpha}{h^2} \begin{pmatrix} -2 & 2 & 0 & \cdots & \cdots & \cdots & \cdots & \cdots & 0 \\ 1 & -2 & 1 & 0 & \cdots & \cdots & \cdots & \cdots & 0 \\ 0 & 1 & -2 & 1 & 0 & \cdots & \cdots & \cdots & 0 \\ \vdots & & & & \ddots & & & & \vdots \\ 0 & \cdots & \cdots & \cdots & \cdots & 0 & 1 & -2 & 1 \\ 0 & \cdots & \cdots & \cdots & \cdots & \cdots & 0 & 1 & -2 \end{pmatrix} \tag{3.181}$$

$$B = \frac{2\alpha}{hk} \begin{pmatrix} 1 & 0 & 0 & \cdots & \cdots & \cdots & \cdots & \cdots & 0 \end{pmatrix}^\top, \tag{3.182}$$

$$g = \frac{1}{2} c^\top v_k G v_k, \tag{3.183}$$

$$c = \frac{\beta}{2h} \begin{pmatrix} 0 & 0 & \cdots & \cdots & \cdots & \cdots & 0 & -1 & 4 \end{pmatrix}^\top, \tag{3.184}$$

$$G = \begin{pmatrix} 0 & 0 & 0 & \cdots & \cdots & \cdots & \cdots & \cdots & 0 \\ -1 & 0 & 1 & 0 & \cdots & \cdots & \cdots & \cdots & 0 \\ 0 & -2 & 0 & 2 & 0 & \cdots & \cdots & \cdots & 0 \\ \vdots & & & & \ddots & & & & \vdots \\ 0 & \cdots & \cdots & \cdots & 0 & -(N-3) & 0 & (N-3) & 0 \\ 0 & \cdots & \cdots & \cdots & \cdots & 0 & -(N-2) & 0 & (N-2) \\ 0 & \cdots & \cdots & \cdots & \cdots & \cdots & 0 & -(N-1) & 0 \end{pmatrix} \tag{3.185}$$

Thus,

$$\frac{\partial f}{\partial z_k} = I + \Delta t \begin{pmatrix} \frac{1}{s_k^2}(A + \frac{\partial g}{\partial v_k}) & -\frac{2}{s_k^3}(Av_k + g(v_k)) - \frac{1}{s_k^2}Bq_{c,k} \\ \frac{1}{s_k}c^\top & -\frac{1}{s_k^2}c^\top v_k \end{pmatrix}, \tag{3.186}$$

$$\frac{\partial g}{\partial z_k} = \frac{1}{2}(c(Gv_k)^\top + c^\top v_k G) \tag{3.187}$$

3.6 Estimation under Boundary Temperature Actuation

One characteristic of PDEs under boundary control is that the observer design becomes slightly different when the actuation is changed from Neumann to Dirichlet even under the same measurements. We reconsider the Stefan problem under boundary temperature actuation discussed in Section 2.7, descried by

$$T_t(x,t) = \alpha T_{xx}(x,t), \quad 0 \le x \le s(t), \tag{3.188}$$

$$T(0,t) = T_{\mathrm{c}}(t) + T_{\mathrm{m}}, \tag{3.189}$$

$$T(s(t),t) = T_{\mathrm{m}}, \tag{3.190}$$

$$\dot{s}(t) = -\beta T_x(s(t),t). \tag{3.191}$$

The observer design is replaced by the following.

Corollary 1 *Consider the plant* (3.188)–(3.191) *with measurements* $Y_1(t) = s(t)$, $Y_2(t) = T_x(s(t),t)$, *and the following observer*

$$\hat{T}_t(x,t) = \alpha \hat{T}_{xx}(x,t) + p_2(x, Y_1(t)) \left(Y_2(t) - \hat{T}_x(Y_1(t),t)\right), \tag{3.192}$$

$$\hat{T}(0,t) = T_{\mathrm{c}}(t) + T_{\mathrm{m}}, \tag{3.193}$$

$$\hat{T}(Y_1(t),t) = T_{\mathrm{m}}, \tag{3.194}$$

where $x \in [0, Y_1(t)]$, and the observer gain $p_2(x, Y_1(t))$ is

$$p_2(x, Y_1(t)) = -\lambda x \frac{I_1\left(\sqrt{\frac{\lambda}{\alpha}(Y_1(t)^2 - x^2)}\right)}{\sqrt{\frac{\lambda}{\alpha}(Y_1(t)^2 - x^2)}}, \tag{3.195}$$

with an observer gain $\lambda > 0$. Assume that the two physical constraints $\dot{s}(t) > 0$ and $s_0 < s(t) < s_r$ are satisfied. Then, for all $\lambda > 0$, the observer error system has a unique classical solution and is exponentially stable in the sense of the norm (3.38).

The proof procedure is same as that in Section 3.2. Let us define the estimation error state $\tilde{u} := T - \hat{T}$. Then, the estimation error system is

$$\tilde{u}_t(x,t) = \alpha \tilde{u}_{xx}(x,t) - p_2(x, s(t))\tilde{u}_x(s(t),t), \quad 0 < x < s(t) \tag{3.196}$$

$$\tilde{u}(s(t),t) = 0, \tag{3.197}$$

$$\tilde{u}(0,t) = 0. \tag{3.198}$$

Consider the transformation

$$\tilde{u}(x,t) = \tilde{w}(x,t) + \int_x^{s(t)} P(x,y)\tilde{w}(y,t)dy, \tag{3.199}$$

which maps onto

$$\tilde{w}_t(x,t) = \alpha \tilde{w}_{xx}(x,t) - \lambda \tilde{w}(x,t), \tag{3.200}$$

$$\tilde{w}(s(t),t) = 0, \tag{3.201}$$

$$\tilde{w}(0,t) = 0. \tag{3.202}$$

It is easy to see that the target $\tilde{w}$-system (3.200)–(3.202) is exponentially stable under the conditions $\dot{s}(t) > 0$ and $s_0 < s(t) < s_r$. Through taking derivatives and imposing boundary

conditions, the gain kernel and the observer gain must satisfy

$$P_{xx}(x,y) - P_{yy}(x,y) = -\frac{\lambda}{\alpha}P(x,y), \tag{3.203}$$

$$P(x,x) = \frac{\lambda}{2\alpha}x, \tag{3.204}$$

$$P(0,y) = 0, \tag{3.205}$$

$$p_2(x,s(t)) = -\alpha P(x,s(t)). \tag{3.206}$$

The solution of the PDE is written as

$$P(x,y) = \frac{\lambda}{\alpha}x\frac{I_1\left(\sqrt{\frac{\lambda}{\alpha}(y^2-x^2)}\right)}{\sqrt{\frac{\lambda}{\alpha}(y^2-x^2)}}. \tag{3.207}$$

Substituting the solution (3.207) into the condition (3.206) leads to the observer gain (3.195). By the same technique, we can see that the inverse transformation is uniquely given by

$$\tilde{w}(x,t) = \tilde{u}(x,t) - \int_x^{s(t)} Q(x,y)\tilde{u}(y,t)dy, \tag{3.208}$$

where

$$Q(x,y) = \frac{\lambda}{\alpha}x\frac{J_1\left(\sqrt{\frac{\lambda}{\alpha}(y^2-x^2)}\right)}{\sqrt{\frac{\lambda}{\alpha}(y^2-x^2)}}. \tag{3.209}$$

Due to the invertibility of the transformation, the stability property of $\tilde{u}$-system is equivalent to that of $\tilde{w}$-system, which proves Corollary 1.

The corresponding output feedback controller is designed using the state observer (3.192)–(3.195).

Corollary 2 *Consider the closed-loop system consisting of the plant* (3.188)–(3.191)*, the mea-*

surements $Y_1(t) = s(t)$ *and* $Y_2(t) = T_x(s(t),t)$*, the observer* (3.192)–(3.194)*, and the output feedback control law*

$$T_{\rm c}(t) = -c\left(\frac{1}{\alpha}\int_0^{Y_1(t)} x\left(\hat{T}(x,t) - T_{\rm m}\right)dx + \frac{1}{\beta}Y_1(t)\left(Y_1(t) - s_{\rm r}\right)\right). \tag{3.210}$$

With c*,* $\hat{T}_0(x)$*,* λ *satisfying* (3.68)*, and* (3.69)*, respectively, and* $s_{\rm r}$ *satisfying* $s_{\rm r} > s_0 + \frac{\beta s_0^2}{6\alpha}\hat{H}_u$*, the closed-loop system is exponentially stable in the sense of the norm* (3.71)*.*

The proof of Corollary 2 can be established by following the methodology presented in Section 3.3.

3.7 Summary

This chapter provides the novel state estimation method for the one-phase Stefan problem with moving boundary. Several problem setups have been provided based on available measurements and the performance properties. Table 3.1 summarizes these properties of each design with showing the application field to be used in the latter half of the dissertation. Briefly speaking, there is essentially tradeoff between the convergence speed of the estimator and its applicability to the output feedback control design for the sake of maintaining the positivity. Therefore, if the primal objective of the estimator is to estimate some unmeasured variable as fast as possible without the need of the control, Designs 2, 5, 6 are useful. On the contrary, if the primal objective of the estimator is to use it for output feedback control, Designs 3 and 4 are useful.

3.8 Acknowledgement

Chapters 3, in part, is a reprint of the material as it appears in:

- S. Koga, M. Diagne, and M. Krstic, "Output Feedback Control of the One-Phase Stefan

Table 3.1: Properties of each estimation design.

	Measurements	Stability proof	Fast conver.	Output FB	Applications
Design 1	$s, T_x(s(t)), q_c$	✓	✓	✓	
Design 2	$s, T(0), q_c$	✓	✓		
Design 3	$s, T(0), q_c$	✓		✓	Polymer 3D-print.
Design 4	s, q_c	✓		✓	Metal 3D-print.
Design 5	$s, T(0)$	✓	✓		Sea ice
Design 6	$T(0), q_c$		✓		Batteries

Problem", *IEEE Conference on Decision and Control*, 2016,

- S. Koga, M. Diagne, and M. Krstic, "Control and State Estimation of the One-Phase Stefan Problem via Backstepping Design", *IEEE Transactions on Automatic Control*, vol. 64, no. 2, pp. 510-525, 2019.

The dissertation author was the primary investigators and author of these papers. The author would like to thank Mamadou Diagne for the collaboration.

Chapter 4

Extended Models and Design

4.1 Melting with Advection and Heat Transfer of Newton's Law

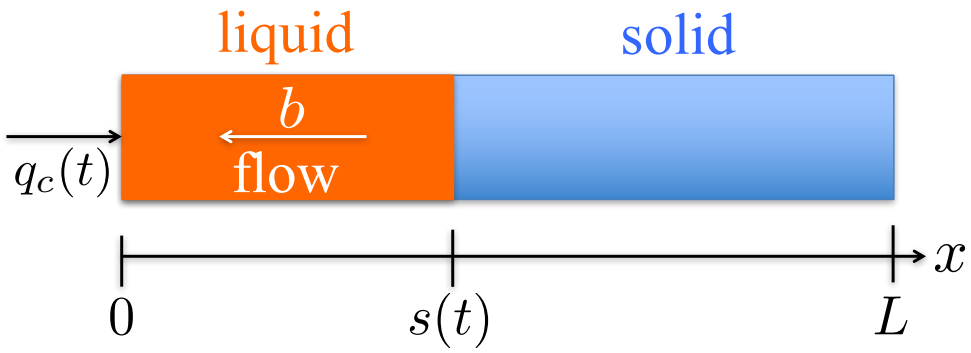

Figure 4.1: Schematic of the one-phase Stefan problem with flowing liquid. We consider both counter-convection ($b > 0$) and regular-convection ($b < 0$).

We also consider that in the liquid phase there is a fluid flow described by a velocity field, representing the movement of the material. This configuration is shown in Fig. 4.1. Moreover, the heat transfer through the environment can be modeled by following Newton's law of convective heat. Here we assume that the ambient temperature is same as the melting temperature. As a

consequence, by defining the reference error variables $u(x,t) = T(x,t) - T_{\mathrm{m}}$ and $X(t) = s(t) - s_{\mathrm{r}}$ analogously to the last chapter, we have the following model of the Stefan problem:

$$u_t(x,t) = \alpha u_{xx}(x,t) + b u_x(x,t) - h u(x,t), \quad 0 < x < s(t), \tag{4.1}$$

$$-k u_x(0,t) = q_{\mathrm{c}}(t), \tag{4.2}$$

$$u(s(t),t) = 0, \tag{4.3}$$

$$\dot{X}(t) = -\beta u_x(s(t),t). \tag{4.4}$$

where b is an advection velocity which can be either positive or negative, $h > 0$ is the heat transfer coefficient. The stability property of Stefan PDE depends on the sign of the advection velocity b. The control objective is same as the one in Chapter 2, namely, $u(x,t) \to 0$ and $X(t) \to 0$ as $t \to \infty$. We design the control law and provide the following theorem.

Theorem 10 *Consider the closed-loop system consisting of the plant* (4.1)–(4.4) *and the control law*

$$q_{\mathrm{c}}(t) = -k\left(\gamma u(0,t) + \frac{\beta}{\alpha}\int_0^{s(t)} f(x)u(x,t)dx + f(s(t))X(t)\right). \tag{4.5}$$

where

$$f(x) = \frac{c}{\beta(d_1 - d_2)}\left((d_1 - \gamma)e^{-d_1 x} - (d_2 + \gamma)e^{-d_2 x}\right), \tag{4.6}$$

$$d_1 = \frac{-b + \sqrt{b^2 + 4\alpha h}}{2\alpha}, \quad d_2 = \frac{-b - \sqrt{b^2 + 4\alpha h}}{2\alpha}, \tag{4.7}$$

and γ *and* c *are arbitral gain parameters satisfying* $\gamma > \max\left\{0, -\frac{b}{2\alpha}\right\}$ *and* $c > 0$*. Suppose that the setpoint is chosen to satisfy*

$$s_{\mathrm{r}} > s_0 + \frac{\beta}{\alpha}\int_0^{s_0} \frac{f(x)}{f(s_0)} u(x,0)dx. \tag{4.8}$$

Then, the closed-loop system satisfies the model validity conditions (1.18) *and* (1.20) *and is exponentially stable in the sense of the norm*

$$||T(x,t)-T_{\mathrm{m}}||^2_{\mathcal{H}_{\mathrm{I}}(0,s(t))}+(s(t)-s_{\mathrm{r}})^2. \tag{4.9}$$

The proof of Theorem 10 is established through the remainder of this section and Appendix C.2.

Analogous PDE-ODE cascade with constant domain

We consider an analogous PDE-ODE cascade with constant domain to the Stefan system (4.1)–(4.4), similarly to the procedure in Chapter 2, that is

$$u_t(x,t) = \alpha u_{xx}(x,t)+bu_x(x,t)-hu(x,t), \quad 0<x<D, \tag{4.10}$$

$$u_x(0,t) = U(t), \tag{4.11}$$

$$u(D,t) = 0, \tag{4.12}$$

$$\dot{X}(t) = -\beta u_x(D,t). \tag{4.13}$$

Let us introduce the transformation

$$w(x,t) = u(x,t)-\frac{\beta}{\alpha}\int_x^D \phi(x-y)u(y,t)dy-\phi(x-D)X(t), \tag{4.14}$$

which maps to

$$w_t(x,t) = \alpha w_{xx}(x,t) + b w_x(x,t) - h w(x,t), \quad 0 < x < D \tag{4.15}$$

$$w_x(0,t) = \gamma w(0,t), \tag{4.16}$$

$$w(D,t) = 0, \tag{4.17}$$

$$\dot{X}(t) = -cX(t) - \beta w_x(D,t). \tag{4.18}$$

Taking the spatial and time derivatives of (4.14) yields

$$\begin{aligned} w_x(x,t) =& u_x(x,t) + \frac{\beta}{\alpha}\phi(0)u(x,t) \\ & - \frac{\beta}{\alpha}\int_x^D \phi'(x-y)u(y,t)dy - \phi'(x-D)X(t), \end{aligned} \tag{4.19}$$

$$\begin{aligned} w_{xx}(x,t) =& u_{xx}(x,t) + \frac{\beta}{\alpha}(\phi(0)u_x(x,t) + \phi'(0)u(x,t)) \\ & - \frac{\beta}{\alpha}\int_x^D \phi''(x-y)u(y,t)dy - \phi''(x-D)X(t), \end{aligned} \tag{4.20}$$

and

$$\begin{aligned} w_t(x,t) =& \alpha u_{xx}(x,t) + b u_x(x,t) - h u(x,t) \\ & - \beta\left(\phi(x-D)u_x(D,t) - \phi(0)u_x(x,t) + \phi'(x-D)u(D,t)\right. \\ & \left. -\phi'(0)u(x,t) + \int_x^D \phi''(x-y)u(y,t)dy\right) \\ & - \frac{\beta b}{\alpha}\left(\phi(x-D)u(D,t) - \phi(0)u(x,t) + \int_x^D \phi'(x-y)u(y,t)dy\right) \\ & + \frac{\beta h}{\alpha}\int_x^D \phi(x-y)u(y,t)dy + \phi(x-D)\beta u_x(D,t) \end{aligned} \tag{4.21}$$

Hence, by (4.14), (4.19)–(4.21), we have

$$\begin{aligned} & w_t(x,t) - \alpha w_{xx}(x,t) - b w_x(x,t) + h w(x,t) \\ &= \left(\alpha\phi''(x-D) + b\phi'(x-D) - h\phi(x-D)\right) X(t) \end{aligned} \tag{4.22}$$

Hence, the solution of the gain kernel satisfies

$$\alpha\phi''(x-D) + b\phi'(x-D) - h\phi(x-D) = 0, \tag{4.23}$$

$$\phi(0) = 0, \quad \phi'(0) = \frac{c}{\beta} \tag{4.24}$$

The solution is described as

$$\phi(x) = \frac{c}{\beta(d_1 - d_2)} \left(e^{d_1 x} - e^{d_2 x}\right), \tag{4.25}$$

$$\phi'(x) = \frac{c}{\beta(d_1 - d_2)} \left(d_1 e^{d_1 x} - d_2 e^{d_2 x}\right) \tag{4.26}$$

where d_1, d_2 are

$$d_1 = \frac{-b + \sqrt{b^2 + 4\alpha h}}{2\alpha}, \tag{4.27}$$

$$d_2 = \frac{-b - \sqrt{b^2 + 4\alpha h}}{2\alpha} \tag{4.28}$$

Then, $d_1 > 0$ and $d_2 < 0$. Hence, $\phi'(x) > 0$. Finally, by (4.14) and (4.19), to satisfy (4.16), we require

$$\begin{aligned} & w_x(x,t) - \gamma w(0,t) \\ =& U(t) - \frac{\beta}{\alpha} \int_0^D \phi'(-y) u(y,t) dy - \phi'(-D) X(t), \\ & - \gamma \left(u(0,t) - \frac{\beta}{\alpha} \int_0^D \phi(-y) u(y,t) dy - \phi(-D) X(t) \right) = 0, \end{aligned} \tag{4.29}$$

which leads to the control design

$$U(t) = \gamma u(0,t) + \frac{\beta}{\alpha}\int_0^D f(x)u(x,t)dy + f(D)X(t), \tag{4.30}$$

where

$$\begin{aligned} f(x) =& \phi'(-x) - \gamma\phi(-x), \\ =& \frac{c}{\beta(d_1-d_2)}\left((d_1-\gamma)e^{-d_1 x} - (d_2+\gamma)e^{-d_2 x}\right). \end{aligned} \tag{4.31}$$

Control design for Stefan system with advection and heat transfer

We design the controller for the Stefan system with advection and heat loss governed by (4.1)–(4.4). As presented in Chapter 2, we introduce the transformation which replaces the domain D in (4.14) by the moving boundary $s(t)$, given by

$$w(x,t) = u(x,t) - \frac{\beta}{\alpha}\int_x^{s(t)} \phi(x-y)u(y,t)dy - \phi(x-s(t))X(t), \tag{4.32}$$

where ϕ is given by (4.25). Then, applying (4.32) to (4.1)–(4.4), the target system is easily shown as

$$\begin{aligned} w_t(x,t) =& \alpha w_{xx}(x,t) + b w_x(x,t) - h w(x,t) \\ &+ \dot{s}(t)\phi'(x-s(t))X(t), \quad 0 < x < s(t) \end{aligned} \tag{4.33}$$

$$w_x(0,t) = \gamma w(0,t), \tag{4.34}$$

$$w(s(t),t) = 0, \tag{4.35}$$

$$\dot{X}(t) = -cX(t) - \beta w_x(s(t),t). \tag{4.36}$$

Moreover, replacing $U(t) \to -q_c(t)/k$ and $D \to s(t)$ in (4.30), the control design for the Stefan system is given by

$$q_c(t) = -k\left(\gamma u(0,t) + \frac{\beta}{\alpha}\int_0^{s(t)} f(x)u(x,t)dx + f(s(t))X(t)\right). \tag{4.37}$$

Physical constraint

To prove the physical constraint under the closed-loop system, we introduce a variable $Z(t)$ defined by

$$\begin{aligned} Z(t) =& \frac{q_c}{k} + \gamma u(0,t) && (4.38)\\ =& -\frac{\beta}{\alpha}\int_0^{s(t)} f(x)u(x,t)dx - f(s(t))X(t). && (4.39) \end{aligned}$$

Taking the time derivative of $Z(t)$, we get

$$\begin{aligned} \dot{Z}(t) =& -\frac{\beta}{\alpha}\int_0^{s(t)} f(x)u_t(x,t)dx - f(s(t))\dot{X}(t) - \dot{s}(t)f'(s(t))X(t),\\ =& -\beta\left(f(s(t))u_x(s(t),t) - f(0)u_x(0,t) + f'(0)u(0,t) + \int_0^{s(t)} f''(x)u(x,t)dy\right)\\ & -\frac{\beta}{\alpha}\left(-bf(0)u(0) - \int_0^{s(t)}(bf'(x) + hf(x))u(x,t)dx\right) + \beta f(s(t))u_x(s(t),t)\\ & -\dot{s}(t)f'(s(t))X(t),\\ =& \beta f(0)u_x(0,t) - \frac{\beta}{\alpha}\left(\alpha f'(0) - bf(0)\right)u(0,t)\\ & -\frac{\beta}{\alpha}\int_0^{s(t)}(\alpha f''(x) - bf'(x) - hf(x))u(x,t)dx - \dot{s}(t)f'(s(t))X(t), \end{aligned} \tag{4.40}$$

Here, by $f(x) = \phi'(-x) - \gamma\phi(-x)$, we can see that

$$f(0) = \phi'(0) - \gamma\phi(0) = \frac{c}{\beta}, \tag{4.41}$$

$$f'(x) = -\phi''(-x) + \gamma\phi'(-x) = \left(\frac{b}{\alpha} + \gamma\right)\phi'(-x) - \frac{h}{\alpha}\phi(-x), \tag{4.42}$$

$$f''(x) = \phi'''(-x) - \gamma\phi''(-x) = -\frac{b}{\alpha}\phi''(-x) + \left(\frac{h}{\alpha} - \gamma\right)\phi'(-x), \tag{4.43}$$

and thus

$$\alpha f'(x) - bf(x) = \alpha\gamma\phi'(-x) - (h - b\gamma)\,\phi(-x), \tag{4.44}$$

which leads to

$$\frac{\beta}{\alpha}(\alpha f'(0) - f(0)) = \gamma c. \tag{4.45}$$

Moreover,

$$\begin{aligned}
&\alpha f''(x) - bf'(x) - hf(x) \\
=&\left(\alpha\phi'''(-x) + b\phi''(-x) - h\phi'(-x)\right) - \gamma\left(\alpha\phi''(-x) + b\phi'(-x) - h\phi(-x)\right) \\
=&0.
\end{aligned} \tag{4.46}$$

Thus, (4.40) is led to

$$\begin{aligned}
\dot{Z}(t) =& c(u_x(0,t) - \gamma u(0,t)) - \dot{s}(t)f'(s(t))X(t) \\
=& -cZ(t) - \dot{s}(t)f'(s(t))X(t).
\end{aligned} \tag{4.47}$$

We prove $Z(t) > 0$ by contradiction approach. Assume that there exists $t^* > 0$ such that

$$Z(t) > 0, \quad \forall t \in (0, t^*), \qquad Z(t^*) = 0. \tag{4.48}$$

By Maximum principle and Hopf's lemma, we get $u(x,t) > 0$ and $\dot{s}(t) > 0$ for all $x \in (0, s(t))$ and $t \in (0, t^*)$. Thus, we have $s(t) > s_0 > 0$, $\forall t \in (0, t^*)$. In addition, using (4.39) and knowing that $f(x) > 0$, it leads to $X(t) < 0$, $\forall t \in (0, t^*)$. Therefore, (4.47) leads to

$$\dot{Z}(t) > -cZ(t), \quad \forall t \in (0, t^*). \tag{4.49}$$

Gronwall's inequality leads to the inequality regarding the solution of the differential equation, written as $Z(t) \geq Z(0)e^{-ct}, \quad \forall t \in (0, t^*]$. Thus, we have $Z(t^*) \geq Z(0)e^{-ct^*} > 0$, which contradicts with the assumption (4.48). Hence,

$$Z(t) > 0, \quad \forall t \geq 0 \tag{4.50}$$

is proved. Then, by Maximum principle, it holds

$$u(x,t) > 0, \quad \forall x \in (0, s(t), \quad \forall t \geq 0, \quad u_x(s(t),t) < 0, \quad \forall t \geq 0, \tag{4.51}$$

$$\dot{s}(t) > 0, \quad \forall t \geq 0. \tag{4.52}$$

Imposing (4.50) and (4.51) on (4.39), we obtain

$$X(t) < 0, \quad \forall t \geq 0. \tag{4.53}$$

Thus, the following condition holds:

$$0 < s(t) < s_{\mathrm{r}}, \quad \forall t \geq 0. \tag{4.54}$$

Finally, with the help of the conditions (4.52) and (4.54), as proven in Appendix C.2, the exponential stability of the closed-loop system is ensured, which completes the proof of Theorem 10.

4.2 Actuator Delay Compensation

In the presence of actuator delay, a delay compensation technique has been developed intensively for many classes of systems using a backstepping transformation [97]: see [94] for linear ODE systems and [98] for nonlinear ODE systems. Using the Lyapunov method, [93] presented the several analysis of the predictor-based feedback control for ODEs such as robustness with respect to the delay mismatch and disturbance attenuation. To deal with systems under unknown and arbitrary large actuator delay, a Lyapunov-based delay-adaptive control design was developed in [19, 20] for both linear and nonlinear ODEs with certain systems, and [18] extended the design for trajectory tracking of uncertain linear ODEs. For control of unstable parabolic PDE under a long input delay, [96] designed the stabilizing controller by introducing two backstepping transformations for the stabilization of the unstable PDE and the compensation of the delay. By the similar technique, in [157] the coupled diffusion PDE-ODE system in the presence of the actuator delay is stabilized. Implementation issues on the predictor-based feedback are covered in [72] by studying the closed-loop analysis under the sampled-data control.

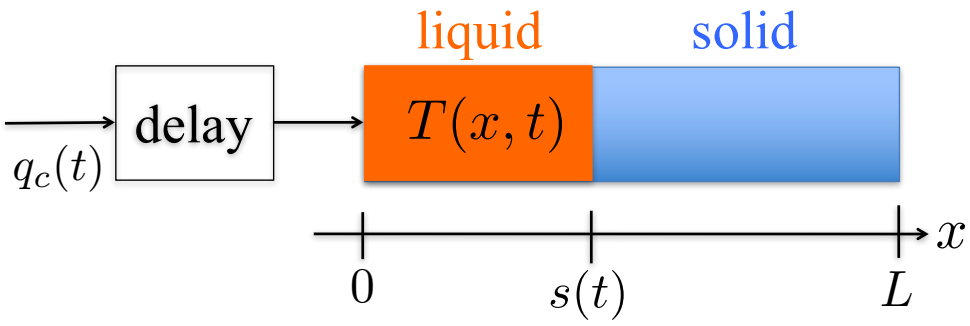

Figure 4.2: Schematic of the one-phase Stefan problem with actuator delay.

Problem Setup and Main Result

Here we impose an actuator delay which is caused by several reasons such as computational time or communication delay. Specifically, the communication delay takes place during the time in which the signals are transmitted from sensors to the controller and from the controller to the actuator, and the computational delay is caused during the time when the controller completes the computation after receiving the signals from the sensors. This configuration is shown in Fig. 4.2. Thus, the Stefan problem with the actuator delay is formulated as follows;

$$T_t(x,t) = \alpha T_{xx}(x,t), \quad 0 \le x \le s(t), \tag{4.55}$$

$$-kT_x(0,t) = q_{\rm c}(t-D), \tag{4.56}$$

$$T(s(t),t) = T_{\rm m}, \tag{4.57}$$

$$\dot{s}(t) = -\beta T_x(s(t),t), \tag{4.58}$$

and the initial values

$$s(0) = s_0, \quad T(x,0) = T_0(x), \ \ \forall x \in [0,s_0], \quad q_{\rm c}(t) = q_{\rm c,0}(t), \quad \forall t \in [-D,0) \tag{4.59}$$

where D is the time delay of the input. Since the boundary input (4.56) is now described by $q_{\mathrm{c}}(t-D)$, all the statements in Lemma 2 and 3 are replaced by $q_{\mathrm{c}}(t-D)$. Thus, the boundary input is needed to be a bounded piecewise continuous function with generating nonnegative heat, i.e.,

$$q_{\mathrm{c}}(t-D) \geq 0, \quad \forall t > 0. \tag{4.60}$$

Hence, we require the following assumption.

Assumption 3 *The past input $q_{\mathrm{c},0}(t)$ for $t \in [-D, 0)$ is a bounded piecewise continuous function and maintains nonnegative, i.e.*

$$q_{\mathrm{c},0}(t) \geq 0, \quad \forall t \in [-D, 0). \tag{4.61}$$

With Assumption 3, the model validity conditions (1.18) and (1.20) remain if $q_{\mathrm{c}}(t) \geq 0$ for $\forall t > 0$.

The control objective is same as Chapter 2. As addressed in Section 2.1, we study the energy growth. The plant (4.55)–(4.58) obeys the following energy conservation law:

$$\frac{d}{dt}\left(\frac{k}{\alpha}\int_0^{s(t)}(T(x,t)-T_{\mathrm{m}})dx + \frac{k}{\beta}s(t) + \int_{t-D}^{t} q_{\mathrm{c}}(\theta)d\theta\right) = q_{\mathrm{c}}(t). \tag{4.62}$$

The control objective is achieved if and only if the following limit is satisfied:

$$\lim_{t\to\infty}\left(\frac{k}{\alpha}\int_0^{s(t)}(T(x,t)-T_{\mathrm{m}})dx + \frac{k}{\beta}s(t) + \int_{t-D}^{t} q_{\mathrm{c}}(\theta)d\theta\right) = \frac{k}{\beta}s_{\mathrm{r}}, \tag{4.63}$$

which can be derived by substituting $T(x,t) \to T_{\mathrm{m}}$, $s(t) \to s_{\mathrm{r}}$, and $q_c(t) \to 0$ into the left hand side of (4.63). Taking integration of (4.62) from $t = 0$ to $t = \infty$ with the help of $q_{\mathrm{c}}(t) > 0$ for $t > 0$ and (4.63), the following assumption on the setpoint is provided.

Assumption 4 *The setpoint is chosen to satisfy*

$$s_{\mathrm{r}} > s_0 + \beta \left(\int_{-D}^{0} \frac{q_{\mathrm{c}}(t)}{k} dt + \frac{1}{\alpha} \int_{0}^{s_0} (T_0(x) - T_{\mathrm{m}}) dx \right). \tag{4.64}$$

Next, we state our main result.

Theorem 1 *Under Assumptions 3-4, the closed-loop system consisting of the plant* (4.55)–(4.58) *and the control law*

$$q_{\mathrm{c}}(t) = -c \left(\int_{t-D}^{t} q_{\mathrm{c}}(\theta) d\theta + \frac{k}{\alpha} \int_{0}^{s(t)} (T(x,t) - T_{\mathrm{m}}) dx + \frac{k}{\beta} (s(t) - s_{\mathrm{r}}) \right), \tag{4.65}$$

where $c > 0$ *is an arbitral control gain, maintains the model validity conditions* (1.18) *and* (1.20) *and is exponentially stable in the sense of the norm*

$$||T(x,t) - T_{\mathrm{m}}||^2_{\mathcal{H}_1(0,s(t))} + (s(t) - s_{\mathrm{r}})^2 + \int_{t-D}^{t} q_{\mathrm{c}}(\theta)^2 d\theta + \int_{t-D}^{t} \dot{q}_{\mathrm{c}}(\theta)^2 d\theta. \tag{4.66}$$

The proof of Theorem 1 is established through the remainder of this section and the stability proof given in Appendix C.

Backstepping Transformation

Change of variables

Introduce reference error variables defined by

$$u(x,t) := T(x,t) - T_{\mathrm{m}}, \quad X(t) := s(t) - s_{\mathrm{r}}. \tag{4.67}$$

Next, we introduce a variable

$$v(x,t) = \frac{q_c(t-x-D)}{k}, \quad \forall x \in [-D,0]. \tag{4.68}$$

Here, the variable $x \in [-D,0]$ in (4.68) is not the spatial coordinate $x \in (0,s(t))$ of the system (4.55)–(4.58), but a newly introduced variable for an alternative representation of the delayed input, as introduced in [96]. Hence, the variable $q_c(t-x-D)$ in (4.68) still represents the boundary heat input (not an input acting on the space $x \in (0,s(t))$), during the time period from $t-D$ to t. Then, (4.68) gives the boundary values of current input $v(-D,t) = q_c(t)/k$ and delayed input $v(0,t) = q_c(t-D)/k$, and $v(x,t)$ satisfies a transport PDE. Hence, the coupled (v,u,X)-system is described as

$$v_t(x,t) = -v_x(x,t), \quad -D < x < 0 \tag{4.69}$$

$$v(-D,t) = q_c(t)/k, \tag{4.70}$$

$$u_x(0,t) = -v(0,t), \tag{4.71}$$

$$u_t(x,t) = \alpha u_{xx}(x,t), \quad 0 < x < s(t) \tag{4.72}$$

$$u(s(t),t) = 0, \tag{4.73}$$

$$\dot{X}(t) = -\beta u_x(s(t),t). \tag{4.74}$$

Now, the control objective is to design $q_c(t)$ to stabilize the coupled (v,u,X)-system at the origin.

Direct transformation

We consider backstepping transformations for the coupled PDEs-ODE system as

$$w(x,t) = u(x,t) - \frac{c}{\alpha}\int_x^{s(t)} (x-y)u(y,t)dy - \frac{c}{\beta}(x-s(t))X(t), \tag{4.75}$$

$$z(x,t) = v(x,t) + c\int_x^0 v(y,t)dy + \frac{c}{\alpha}\int_0^{s(t)} u(y,t)dy + \frac{c}{\beta}X(t). \tag{4.76}$$

The transformation (4.75) is the same nonlinear transformation as the one proposed in Section 2.3 for delay-free Stefan problem. The formulation of (4.76) is motivated by a design in fixed domain introduced in [96]. Taking derivatives of (4.75) and (4.76) in x and t along with the solution of the system (4.69)–(4.74), we have

$$w_x(x,t) = u_x(x,t) - \frac{c}{\alpha}\int_x^{s(t)} u(y,t)dy - \frac{c}{\beta}X(t), \tag{4.77}$$

$$z_x(x,t) = v_x(x,t) - cv(x,t), \tag{4.78}$$

$$\begin{aligned} z_t(x,t) &= -v_x(x,t) - c\int_x^0 v_y(y,t)dy + c\int_0^{s(t)} u_{yy}(y,t)dy - cu_x(s(t),t), \\ &= -v_x(x,t) + cv(x,t). \end{aligned} \tag{4.79}$$

By (4.78) and (4.79), we get $z_t(x,t) = -z_x(x,t)$. In addition, by substituting $x = 0$ in (4.76) and (4.77), $w_x(0,t) = -z(0,t)$ holds. On the other hand, because w transformation does not depend on v, w system is not changed from the delay-free target system given in Section 2.3. Thus, the

target (z,w,X)-system is obtained by

$$z_t(x,t) = -z_x(x,t), \quad -D < x < 0 \tag{4.80}$$

$$z(-D,t) = 0, \tag{4.81}$$

$$w_x(0,t) = -z(0,t), \tag{4.82}$$

$$w_t(x,t) = \alpha w_{xx}(x,t) + \frac{c}{\beta}\dot{s}(t)X(t), \quad 0 < x < s(t) \tag{4.83}$$

$$w(s(t),t) = 0, \tag{4.84}$$

$$\dot{X}(t) = -cX(t) - \beta w_x(s(t),t). \tag{4.85}$$

The control design is achieved through evaluating (4.76) at $x = -D$ together with the boundary conditions (4.70) and (4.81), which yields

$$q_c(t) = -ck\left(\int_{-D}^{0} v(y,t)dy + \frac{1}{\alpha}\int_{0}^{s(t)} u(y,t)dy + \frac{1}{\beta}X(t)\right). \tag{4.86}$$

Finally, substituting the definitions (4.67) and (4.68) in (4.86), the control law (4.65) is obtained.

In a similar manner, the inverse transformations are obtained by

$$u(x,t) = w(x,t) + \frac{\beta}{\alpha}\int_{x}^{s(t)} \psi(x-y)w(y,t)dy + \psi(x-s(t))X(t), \tag{4.87}$$

$$v(x,t) = z(x,t) - \int_{x}^{0} \mu(x-y)z(y,t)dy - \frac{\beta}{\alpha}\mu(x)\int_{0}^{s(t)} \zeta(y)w(y,t)dy - \zeta(s(t))\mu(x)X(t), \tag{4.88}$$

where

$$\psi(x) = \frac{\sqrt{c\alpha}}{\beta}\sin\left(\sqrt{\frac{c}{\alpha}}x\right), \tag{4.89}$$

$$\mu(x) = ce^{cx}, \quad \zeta(x) = \frac{1}{\beta}\cos\left(\sqrt{\frac{c}{\alpha}}x\right). \tag{4.90}$$

Physical constraints

Next, we prove that the closed-loop system with the control law (4.65) guarantees some important properties.

Lemma 1 *With Assumption 4, the control law* (4.65) *for the system* (4.55)–(4.58) *generates a positive input signal, i.e.,*

$$q_{\mathrm{c}}(t) > 0, \quad \forall t > 0. \tag{4.91}$$

Proof:

Taking the time derivative of (4.65) together with the solution of (4.55)–(4.58), we obtain

$$\begin{aligned}
\dot{q}_{\mathrm{c}}(t) &= -c\left(q_{\mathrm{c}}(t) - q_{\mathrm{c}}(t-D) + k\int_0^{s(t)} T_{xx}(x,t)dx - kT_x(s(t),t)\right), \\
&= -c\left(q_{\mathrm{c}}(t) - q_{\mathrm{c}}(t-D) - kT_x(0,t)\right), \\
&= -cq_{\mathrm{c}}(t).
\end{aligned} \tag{4.92}$$

The differential equation (4.92) yields

$$q_{\mathrm{c}}(t) = q_{\mathrm{c}}(0)e^{-ct}. \tag{4.93}$$

Additionally, substituting $t = 0$ into the control law (4.65) leads to

$$q_{\mathrm{c}}(0) = -c\left(\int_{-D}^{0} q_{\mathrm{c}}(\theta)d\theta + \frac{k}{\alpha}\int_0^{s_0}(T_0(x) - T_{\mathrm{m}})dx + \frac{k}{\beta}(s_0 - s_{\mathrm{r}})\right), \tag{4.94}$$

Hence, Assumption 4 leads to

$$q_{\mathrm{c}}(0) > 0. \tag{4.95}$$

Applying (4.95) to (4.93), the positivity of the controller (4.91) is satisfied.

Hence, the model validity conditions (1.18) and (1.20) hold, i.e.,

$$T(x,t) \geq T_{\mathrm{m}} \quad \text{for all} \quad x \in [0, s(t)]. \tag{4.96}$$

$$\dot{s}(t) \geq 0, \quad \forall t > 0, \tag{4.97}$$

By the control law (4.65), the following relation holds under the closed-loop system:

$$\frac{k}{\beta}(s(t) - s_{\mathrm{r}}) = -\frac{1}{c}q_{\mathrm{c}}(t) - \int_{t-D}^{t} q_{\mathrm{c}}(\theta)d\theta - \frac{k}{\alpha}\int_{0}^{s(t)} (T(x,t) - T_{\mathrm{m}})dx, \tag{4.98}$$

Applying (4.91) and (4.96) to the control law (4.65), it holds

$$s_0 < s(t) < s_{\mathrm{r}}, \quad \forall t > 0. \tag{4.99}$$

Relation between the designed control law and a state prediction

As developed in some literature for ODE systems, the delay compensated control via the method of backstepping is known to be equivalent to the predictor-based feedback where the control law is derived to stabilize the future state called "predictor state", see Section 2 in [97] for instance. Hence, one might have a question whether our delay compensated control is also equivalent to the predictor-based feedback. This is not a trivial question in the case of Stefan problem due to the complicated structure of ODE dynamics whose state is the domain of the PDE.

The nominal control design for delay-free Stefan problem developed in [82] is given by

$$\bar{q}_{\mathrm{c}}(t) = -c\left(\frac{k}{\alpha}\int_{0}^{s(t)} (T(x,t) - T_{\mathrm{m}})dx + \frac{k}{\beta}(s(t) - s_{\mathrm{r}})\right), \tag{4.100}$$

where we defined the notation $\bar{q}_{\mathrm{c}}(t)$ to distinguish with the delay compensated control law (4.65).

Thus, our interest lies in proving $q_{\mathrm{c}}(t) \equiv \bar{q}_{\mathrm{c}}(t+D)$ because $\bar{q}_{\mathrm{c}}(t+D)$ is the prediction of the nominal control. We start from the expression of $\bar{q}_{\mathrm{c}}(t+D)$ which can be described as

$$\bar{q}_{\mathrm{c}}(t+D) = -c\left(\frac{k}{\alpha}\int_0^{s(t+D)}(T(x,t+D)-T_{\mathrm{m}})dx + \frac{k}{\beta}(s(t+D)-s_{\mathrm{r}})\right). \tag{4.101}$$

Integrating ODE dynamics $\dot{s}(t) = -\beta T_x(s(t),t)$ given in (4.58) from t to $t+D$ yields

$$s(t+D) = s(t) - \beta\int_t^{t+D} T_x(s(\tau),\tau)d\tau. \tag{4.102}$$

Next, integrating PDE dynamics $T_t = \alpha T_{xx}$ given in (4.55) in time from t to $t+D$ leads to $T(x,t+D) = T(x,t) + \alpha\int_t^{t+D} T_{xx}(x,\tau)d\tau$. Furthermore, integrating the both sides in space from 0 to $s(t+D)$, we obtain

$$\begin{aligned}
&\int_0^{s(t+D)}(T(x,t+D)-T_{\mathrm{m}})dx \\
=&\int_0^{s(t+D)}(T(x,t)-T_{\mathrm{m}})dx + \alpha\int_0^{s(t+D)}\int_t^{t+D} T_{xx}(x,\tau)d\tau dx, \\
=&\int_0^{s(t+D)}(T(x,t)-T_{\mathrm{m}})dx + \alpha\int_t^{t+D}(T_x(s(t+D),\tau)-T_x(0,\tau)d\tau, \\
=&\int_0^{s(t+D)}(T(x,t)-T_{\mathrm{m}})dx + \alpha\int_t^{t+D} T_x(s(t+D),\tau)d\tau + \frac{\alpha}{k}\int_{t-D}^{t} q_c(\xi)d\xi.
\end{aligned} \tag{4.103}$$

Therefore, substituting (4.102) and (4.103) into (4.101), we get

$$\begin{aligned}
\bar{q}_{\mathrm{c}}(t+D) = -c\Bigg(&\frac{k}{\alpha}\int_0^{s(t+D)}(T(x,t)-T_{\mathrm{m}})dx + k\int_t^{t+D}(T_x(s(t+D),\tau)-T_x(s(\tau),\tau))d\tau \\
&+\int_{t-D}^{t} q_c(\xi)d\xi + \frac{k}{\beta}(s(t)-s_{\mathrm{r}})\Bigg).
\end{aligned} \tag{4.104}$$

Consequently, it remains to consider the following term

$$\begin{aligned}
&\int_t^{t+D} (T_x(s(t+D),\tau) - T_x(s(\tau),\tau))d\tau \\
=&\int_t^{t+D} \int_{s(\tau)}^{s(t+D)} T_{xx}(x,\tau)dxd\tau, \\
=&\frac{1}{\alpha}\int_{s(t)}^{s(t+D)} \int_t^{s^{-1}(x)} T_\tau(x,\tau)d\tau dx, \\
=&\frac{1}{\alpha}\int_{s(t)}^{s(t+D)} \left(T(x,s^{-1}(x)) - T(x,t)\right) dx. \qquad (4.105)
\end{aligned}$$

where we switched the order of the integrations in time and space from the first line to the second line with defining the inverse function $s^{-1}(x)$. The existence and uniqueness of $s^{-1}(x)$ is guaranteed due to the continuous and monotonically increasing property of $s(t)$ provided $q_c(t) > 0$. Thus, boundary condition $T(s(t),t) = T_m$, $\forall t \geq 0$ given in (4.57) implies $T(x,s^{-1}(x)) = T_m$ from which (4.105) is given by

$$\int_t^{t+D} (T_x(s(t+D),\tau) - T_x(s(\tau),\tau))d\tau = -\frac{1}{\alpha}\int_{s(t)}^{s(t+D)} (T(x,t) - T_m)\, dx. \qquad (4.106)$$

Substituting (4.106) into (4.104), we arrive at

$$\bar{q}_{\rm c}(t+D) = -c\left(\frac{k}{\alpha}\int_0^{s(t)} (T(x,t) - T_{\rm m})dx + \int_{t-D}^{t} q_c(\xi)d\xi + \frac{k}{\beta}(s(t) - s_{\rm r})\right) \equiv q_{\rm c}(t). \qquad (4.107)$$

Therefore, we conclude that the delay compensated control (4.65) is indeed the prediction of the nominal control law (4.100).

Robustness to delay mismatch

The results established up to the last section are based on the control design with utilizing the exact value of the actuator delay. However, in practice, there is an error between the exact time delays and the identified delays. Hence, guaranteeing the performance of the controller

under the small delay mismatch is important. In this section, $D > 0$ is denoted as the identified time delay and ΔD is denoted as the delay mismatch (can be either positive or negative), which yields $D + \Delta D$ as the exact time delay from the controller to the plant. Thus, the system we focus on is described by

$$T_t(x,t) = \alpha T_{xx}(x,t), \quad x \in (0, s(t)), \tag{4.108}$$

$$-kT_x(0,t) = q_c(t - (D + \Delta D)), \tag{4.109}$$

$$T(s(t),t) = T_m, \tag{4.110}$$

$$\dot{s}(t) = -\beta T_x(s(t),t), \tag{4.111}$$

with the control law given in (4.65) which utilizes the identified delay D. Since the control law is not changed, the same backstepping transformation in (4.75) and (4.76) can be applied, but the target (z,w,X)-system needs to be redescribed due to the modification of (4.109). The theorem for the robustness to delay mismatch is provided under the restriction on the control gain, as stated in the following.

Theorem 2 *Under Assumptions 3-4, there exists a positive constant $\bar{c} > 0$ such that $\forall c \in (0, \bar{c})$ the closed-loop system consisting of the plant* (4.108)–(4.111) *and the control law* (4.65) *maintains the model validity conditions* (1.18) *and* (1.20) *and is exponentially stable in the sense of the norm* (4.66).

An important characteristic to note in Theorem 2 is that the existence of $\bar{c}$ is ensured for any given ΔD as long as $D + \Delta D > 0$. An analogous description with respect to the small delay mismatch is given in the following corollary.

Corollary 1 *Under Assumptions 3-4, for any given $c > 0$ there exist positive constants $\underline{\varepsilon} > 0$ and $\bar{\varepsilon} > 0$ such that $\forall \Delta D \in (-\underline{\varepsilon}, \bar{\varepsilon})$ the closed-loop system* (4.108)–(4.111)*,* (4.65) *satisfies the same model validity and stability property as Theorem 2.*

The proof of Theorem 2 can be seen in [84], and is emitted here.

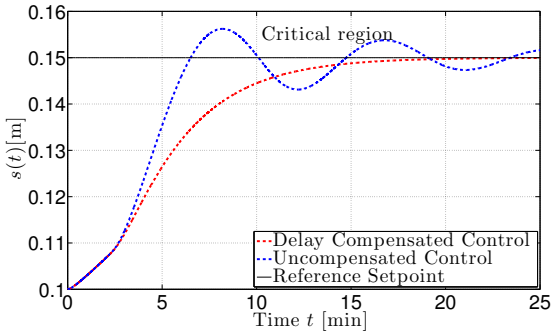

(a) Delay compensated control achieves the monotonic convergence of $s(t)$ to the setpoint s_{r} without overshooting, i.e. $\dot{s}(t) > 0$, $s_0 < s(t) < s_{\mathrm{r}}$.

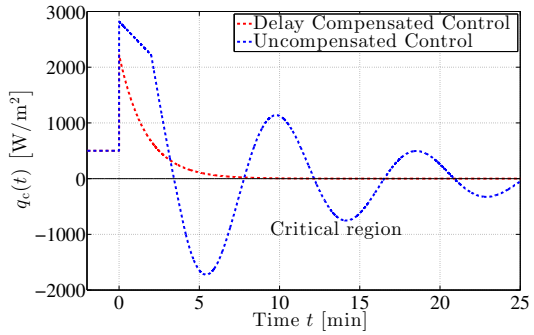

(b) Delay compensated control keeps injecting positive heat, i.e. $q_c(t) > 0$.

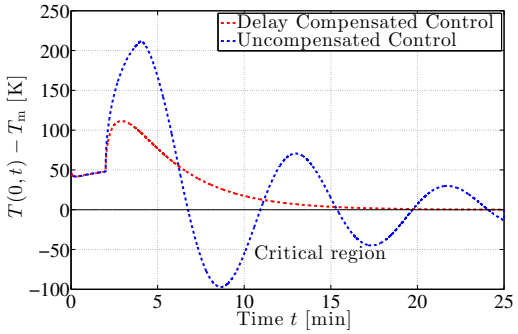

(c) $T(0,t)$ converges to the melting temperature T_{m} with maintaining $T(0,t) > T_{\mathrm{m}}$.

Figure 4.3: The closed-loop response of (4.55)-(4.58) with the delay compensated control law (4.65) (red) and the uncompensated control law (4.100) (blue).

Numerical Simulation

We study the simulation of the proposed delay compensated controller under the accurate value on the delay and the delay mismatch.

Exact Compensation

The performance of the proposed delay compensated controller is investigated by comparing to the performance of the nominal controller (4.100). The time delay, the past heat input, and the initial values are set as $D = 2$ [min], $q_{\mathrm{c}}(t) = 500$ [W/m] for $\forall t \in [-D, 0)$, $s_0 = 0.1$ [m], and $T_0(x) = \bar{T}(1 - x/s_0) + T_{\mathrm{m}}$ with $\bar{T} = 50$ [K]. The setpoint and the controller gain are chosen as $s_{\mathrm{r}} = 0.15$ m and $c = 0.01$/s, which satisfies the setpoint restriction (4.64).

Fig. 4.3 shows the simulation results of the closed-loop system of the plant (4.55)–(4.58) with the proposed delay compensated control (4.65) (red) and the uncompensated control law (4.100) (blue). The closed-loop responses of the moving interface $s(t)$, the boundary heat control $q_{\mathrm{c}}(t)$, and the boundary temperature $T(0,t)$ are depicted in Fig. 4.3 (a)–(c), respectively. As stated in their captions, the proposed delay compensated controller ensures all the derived conditions with the convergence of the interface position to the setpoint, while the uncompensated control does not provide such a behavior. Hence, the numerical result is consistent with the theoretical result, and the proposed controller achieves better performances than the uncompensated controller under the actuator delay.

Robustness to Delay Mismatch

To evaluate the delay robustness, the performance of the proposed controller is investigated under the delay mismatch. First, the simulation is conducted with the underestimated delay mismatch where the time delay from the actuator to the plant is 60 [sec] while the compensating time delay in the controller is $D = 30$ [sec], i.e., the delay mismatch is $\Delta D = 30$ [sec]. The closed-loop responses are depicted in Fig. 4.4 with the choices of the control gain $c = 0.01$ [1/sec]

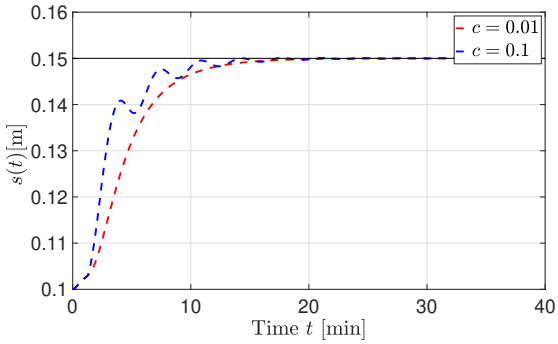

(a) Monotonicity of the interface dynamics is satisfied with smaller gain, but is violated with larger gain.

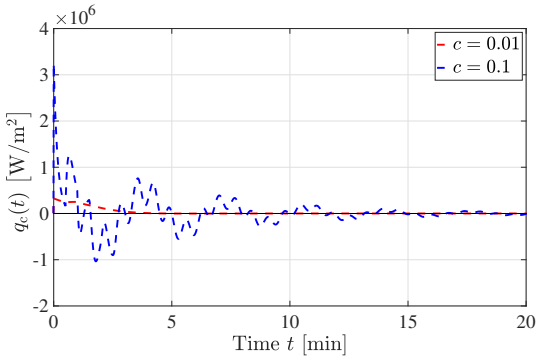

(b) Positivity of the heat input is satisfied with smaller gain, but is violated with larger gain.

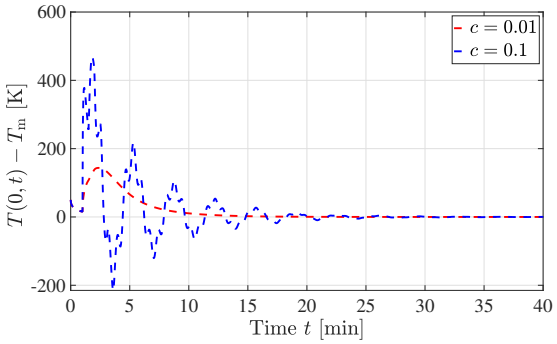

(c) The boundary temperature keeps above the melting temperature with smaller gain, while it reaches below the melting temperature with larger gain, which violates the temperature condition for the liquid phase.

Figure 4.4: The closed-loop response under the "underestimated" delay mismatch with $D = 30$ [sec] and $\Delta D = 30$ [sec]. The simulations are conducted with the control gain $c = 0.01$ [/sec] (red) and $c = 0.1$ [/sec] (blue). The delay-robustness is observed only with smaller gain in terms of the model validity.

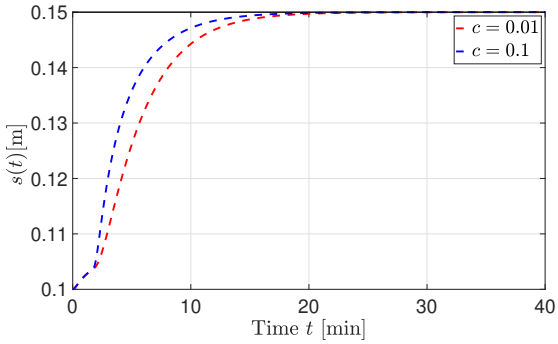

(a) The interface position converges to the setpoint without overshooting.

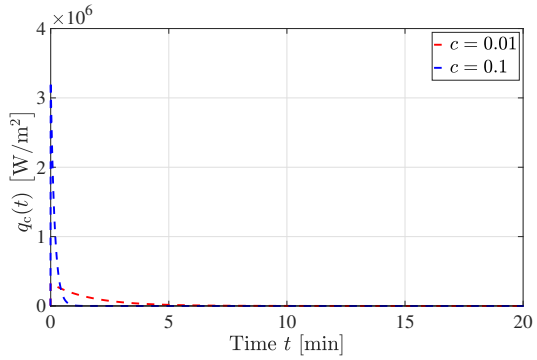

(b) The heat input maintains positive.

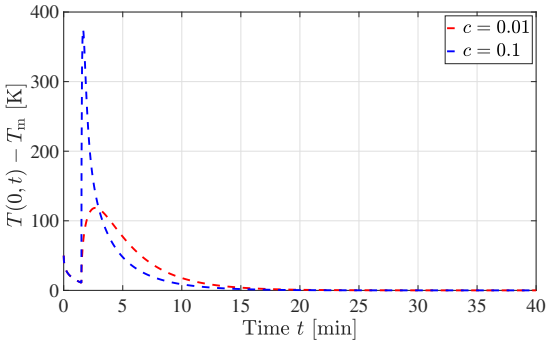

(c) The boundary temperature is greater than melting temperature, which satisfies the temperature condition for the liquid phase.

Figure 4.5: The closed-loop response under the "overestimated" delay mismatch with $D = 90$ [sec] and $\Delta D = -30$ [sec]. The simulations are conducted with the control gain $c = 0.01$ [/sec] (red) and $c = 0.1$ [/sec] (blue). In this case, all the constraints for the model validity are satisfied with both smaller gain and larger gain.

(red) and $c = 0.1$ [1/sec] (blue). Fig. 4.4 (a) illustrates the convergence of the interface position to the setpoint, however, the monotonicity of the interface dynamics is violated with larger gain

(red). From Fig. 4.4 (b) and (c) we can observe that the positivity of the control input and the temperature condition for the liquid phase are satisfied only with the lower gain (blue) for all time, while the simulation with the larger gain (red) violates these conditions too. Hence, with the underestimated delay mismatch, the robustness is well illustrated for sufficiently small gain $c > 0$, which is consistent with Theorem 2.

Next, we have studied the simulation with the over-estimated delay mismatch with the same value of the time delay from the actuator to the plant 60 [sec] but the compensating time delay in the controller is $D = 90$ [sec], i.e., the delay mismatch is $\Delta D =$ -30 [sec]. The closed-loop responses are depicted in Fig. 4.5 with the same choices of the control gain as in simulation of underestimated delay mismatch. While the magnitude of the delay mismatch is same as the one conducted in the underestimated delay mismatch, we can observe from Fig. 4.5 (b) and (c) that the positivity of the control input and the temperature condition for the model validity are satisfied for all time with both smaller control gain (red) and larger control gain (blue). Although Theorem 2 guarantees these properties only for sufficiently small control gain $c > 0$, the numerical results illustrate that the restriction on the control gain to satisfy these properties is not equivalent between the underestimated and over-estimated delay mismatch.

Indeed, as far as we have investigated the numerical results with the over-estimated delay mismatch using other values of the control gain c and the delay perturbation ΔD, the positivity of the control input is satisfied for every cases and the convergence of the interface position to the setpoint is depicted without overshooting. These observations from the numerical simulation leads us to conjecture that the delay-compensated controller might exhibit greater sensitivity to delay mismatch when it is underestimated rather than over-estimated in terms of the model validation. Hence, once the user is faced with some range of the uncertainty in the actuator delay, it is better to choose small control gain $c > 0$, and additionally, it might be better to choose larger value of the compensating delay in the controller to be conservative.

4.3 What Can We Guarantee If the Solid Phase Remains? - ISS

While all the aforementioned results are based on the one-phase Stefan problem which neglects the cooling heat caused by the solid phase, an analysis on the system incorporating the cooling heat at the liquid-solid interface has not been established. The one-phase Stefan problem with a prescribed heat flux at the interface was studied in [140]. The author proved the existence and uniqueness of the solution with a prescribed heat input at the fixed boundary by verifying positivity conditions on the interface position and temperature profile using a similar technique as in [55].

Regarding the added heat flux at the interface as the heat loss induced by the remaining other phase dynamics, it is reasonable to treat the prescribed heat flux as the disturbance of the system. The norm estimate of systems with a disturbance is often analyzed in terms of Input-to-State Stability (ISS) [149], which serves as a criterion for the robustness of the controller or observer design [6, 54]. The characterizations of ISS have been investigated in [147, 148], which have been utilized for the derivation of small gain theorems [66, 67]. Recently, the ISS for infinite dimensional systems with respect to the boundary disturbance was developed in [73, 74, 76] using the spectral decomposition of the solution of linear parabolic PDEs in one dimensional spatial coordinate with Strum-Liouville operators. An analogous result for the diffusion equations with a radial coordinate in n-dimensional balls is shown in [23] with proposing an application to robust observer design for battery management systems [118].

We incorporate the heat loss at the interface in the one-phase Stefan problem, as a cooling effect from the solid phase. Here, we assume that the heat loss is a time-varying function, unlike the two-phase Stefan problem which models the heat loss by the solid phase temperature that is

state-dependent. Hence, we consider the following model

$$T_t(x,t) = \alpha T_{xx}(x,t), \quad 0 \le x \le s(t), \tag{4.112}$$

$$-kT_x(0,t) = q_{\mathrm{c}}(t), \tag{4.113}$$

$$T(s(t),t) = T_{\mathrm{m}}, \tag{4.114}$$

$$\dot{s}(t) = -\beta T_x(s(t),t) - \frac{\beta}{k} q_{\mathrm{f}}(t), \tag{4.115}$$

where $q_{\mathrm{f}}(t) \ge 0$ is a magnitude of the heat loss. The coefficient β/k is added from the physical modeling, which yields the consistency in the physical unit. We impose the following assumption on the heat loss.

Assumption 5 *The heat loss remains non-negative, bounded, and continuous for all $t \ge 0$, and the total energy is also bounded, i.e.,*

$$q_{\mathrm{f}}(t) \ge 0, \quad \forall t > 0, \tag{4.116}$$

$$\exists M > 0, \quad s.t. \quad \int_0^\infty q_{\mathrm{f}}(t)\mathrm{d}t < M. \tag{4.117}$$

One critical difference of the system (4.112)–(4.115) from the systems we have studied in previous sections is that the monotonicity of the interface dynamics does not hold, i.e.,

$$\dot{s}(t) \not\gtrless 0 \tag{4.118}$$

which can cause the following scenario:

$$s(t) \searrow 0 \tag{4.119}$$

even under a physically reasonable situation. Namely, even if we keep injecting a positive heat into the liquid phase, the material can be completely frozen to the solid phase due to the heat loss.

Such a situation can be explained in the following lemma proven in [140]:

Lemma 10 *Provided that $q_{\mathrm{c}}(t) \geq 0$ for all $t \geq 0$, there exists $\sigma > 0$ such that for any $\bar{t} \leq \sigma$ where $0 < \sigma \leq \infty$, there is a unique classical solution of the system* (4.112)–(4.115). *If $\sigma \neq \infty$, then $s(\sigma) = 0$.*

However, to validate the physical model under the feedback control, we need to show

$$s(t) > 0, \quad \forall t \geq 0. \tag{4.120}$$

Hence, the condition (4.120) stands as an additional constraint to hold under the closed-loop system. Here, the heat loss $q_{\mathrm{f}}(t)$ is an unknown variable, and we study how the norm estimate is described under the feedback control law designed in Section 2.3, namely, the control law is

$$q_{\mathrm{c}}(t) = -c\left(\frac{k}{\alpha}\int_0^{s(t)}(T(x,t)-T_{\mathrm{m}})\mathrm{d}x + \frac{k}{\beta}(s(t)-s_{\mathrm{r}})\right), \tag{4.121}$$

We impose the same assumption on the setpoint position as follows.

Assumption 6 *The setpoint is chosen to satisfy*

$$s_{\mathrm{r}} > s_0 + \frac{\beta}{\alpha}\int_0^{s_0}(T_0(x)-T_{\mathrm{m}})\mathrm{d}x. \tag{4.122}$$

Finally, we impose the following condition of the control gain.

Assumption 7 *The control gain c is chosen sufficiently large to satisfy $c > \frac{\beta}{ks_{\mathrm{r}}}\bar{q}_{\mathrm{f}}$, where $\bar{q}_{\mathrm{f}} := \sup_{0\leq t\leq\infty}\{q_{\mathrm{f}}(t)\}$.*

The controller is feedback design of liquid temperature profile and the interface position $(T(x,t), s(t))$. The heat loss $q_{\mathrm{f}}(t)$ is regarded as a disturbance, and the norm estimate of the reference error is derived in a sense of input-to-state stability, as stated in the following theorem.

Theorem 11 *Under Assumptions 5–7, the closed-loop system consisting of* (4.112)–(4.115) *with the control law* (4.121) *satisfies the model validity conditions* (1.18) *and* (4.120)*, and is ISS with respect to the heat loss $q_{\mathrm{f}}(t)$ at the interface, i.e., there exist a class-$\mathcal{KL}$ function ζ and a class-$\mathcal{K}$ function η such that the following estimate holds:*

$$\Psi(t) \leq \zeta(\Psi(0),t) + \eta\left(\sup_{\tau\in[0,t]} |q_{\mathrm{f}}(\tau)|\right), \tag{4.123}$$

for all $t \geq 0$, in the L_2 norm

$$\Psi(t) = \left(\int_0^{s(t)} (T(x,t) - T_{\mathrm{m}})^2 \,\mathrm{d}x + (s(t) - s_r)^2\right)^{\frac{1}{2}}. \tag{4.124}$$

Moreover, there exist positive constants $M_1 > 0$ and $M_2 > 0$ such that the explicit functions of ζ and η are given by

$$\zeta(\Psi(0),t) = M_1 \Psi(0) e^{-\lambda t}, \tag{4.125}$$

$$\eta(\sup_{\tau\in[0,t]} |q_{\mathrm{f}}(\tau)|) = M_2 \sup_{\tau\in[0,t]} |q_{\mathrm{f}}(\tau)|, \tag{4.126}$$

where $\lambda = \frac{1}{32}\min\left\{\frac{\alpha}{s_{\mathrm{r}}^2}, c\right\}$, which ensures the exponentially ISS.

Backstepping transformation

Let $u(x,t)$ and $X(t)$ be reference error variables defined by

$$u(x,t) := T(x,t) - T_{\mathrm{m}}, \tag{4.127}$$

$$X(t) := s(t) - s_r. \tag{4.128}$$

Then, the system (4.112)–(4.115) is rewritten as

$$u_t(x,t) = \alpha u_{xx}(x,t), \tag{4.129}$$

$$u_x(0,t) = -\frac{q_c(t)}{k}, \tag{4.130}$$

$$u(s(t),t) = 0, \tag{4.131}$$

$$\dot{X}(t) = -\beta u_x(s(t),t) - d(t), \tag{4.132}$$

where $d(t) = \frac{\beta}{k} q_f(t)$.

We apply the following backstepping transformation

$$w(x,t) = u(x,t) - \frac{\beta}{\alpha}\int_x^{s(t)} \phi(x-y)u(y,t)dy - \phi(x-s(t))X(t), \tag{4.133}$$

where the gain kernel ϕ is given by

$$\phi(x) = \frac{c}{\beta}x - \varepsilon. \tag{4.134}$$

Then, one can derive the following target system

$$w_t(x,t) = \alpha w_{xx}(x,t) + \dot{s}(t)\phi'(x-s(t))X(t) + \phi(x-s(t))d(t), \tag{4.135}$$

$$w_x(0,t) = \frac{\beta}{\alpha}\phi(0)u(0), \tag{4.136}$$

$$w(s(t),t) = \varepsilon X(t), \tag{4.137}$$

$$\dot{X}(t) = -cX(t) - \beta w_x(s(t),t) - d(t). \tag{4.138}$$

Inverse transformation

Consider the following inverse transformation

$$u(x,t) = w(x,t) - \frac{\beta}{\alpha}\int_x^{s(t)} \psi(x-y)w(y,t)\mathrm{d}y - \psi(x-s(t))X(t). \tag{4.139}$$

Taking the derivatives of (4.139) in x and t along (4.135)-(4.138), to match with (4.129)-(4.132), we obtain the gain kernel solution as

$$\psi(x) = e^{rx}\left(p_1 \sin(\omega x) + \varepsilon\cos(\omega x)\right), \tag{4.140}$$

where

$$r = \frac{\beta\varepsilon}{2\alpha}, \quad \omega = \sqrt{\frac{4\alpha c - (\varepsilon\beta)^2}{4\alpha^2}}, \tag{4.141}$$

$$p_1 = -\frac{1}{2\alpha\beta\omega}\left(2\alpha c - (\varepsilon\beta)^2\right), \tag{4.142}$$

and $0 < \varepsilon < 2\frac{\sqrt{\alpha c}}{\beta}$ is to be chosen later. Finally, using the inverse transformation, the boundary condition (4.143) is rewritten as

$$w_x(0,t) = -\frac{\beta}{\alpha}\varepsilon\left[w(0,t) - \frac{\beta}{\alpha}\int_0^{s(t)} \psi(-y)w(y,t)\mathrm{d}y - \psi(-s(t))X(t)\right]. \tag{4.143}$$

In other words, the target (w,X)-system is described by (4.135), (4.137), (4.138), and (4.143). Note that the boundary condition (4.137) and the kernel function (4.134) are modified from the one in Section 2.3, while the control design is equivalent. The target system derived in Section 2.3 requires $\mathcal{H}_1$-norm analysis for stability proof. However, with the prescribed heat loss at the interface, $\mathcal{H}_1$-norm analysis fails to show the stability due to the non-monotonic moving boundary dynamics. The modification of the boundary condition (4.137) enables to prove the stability in L_2 norm as shown later.

Analysis of closed-loop system

Here, we prove the well-posedness of the closed-loop solution and the positivity conditions of the state variables.

Taking the time derivative of the control law (4.121) along with the energy conservation leads to the following differential equation

$$\dot{q}_{\mathrm{c}}(t) = -cq_{\mathrm{c}}(t) + cq_{\mathrm{f}}(t), \tag{4.144}$$

which has the explicit solution as the following open-loop control:

$$q_{\mathrm{c}}(t) = q_0 e^{-ct} + c\int_0^t e^{-c(t-\tau)} q_{\mathrm{f}}(\tau)\mathrm{d}\tau, \tag{4.145}$$

where

$$q_0 = -c\left(\frac{k}{\alpha}\int_0^{s_0}(T_0(x) - T_{\mathrm{m}})\mathrm{d}x + \frac{k}{\beta}(s_0 - s_{\mathrm{r}})\right). \tag{4.146}$$

Hence, the closed-loop solution is equivalent to to the open-loop solution with (4.145). Since Assumption 6 leads to $q_0 > 0$, the open-loop controller (4.145) remains positive and continuous for all $t > 0$ by Assumption 5. Hence, applying Lemma 10, we can show that there exists $\sigma > 0$ such that for any $\bar{t} \leq \sigma$ where $0 < \sigma \leq \infty$, there is a unique classical solution of the system (4.112)–(4.115).

Next, we show $\sigma = \infty$ by contradiction. Suppose there exists $0 < \sigma < \infty$ such that $s(\sigma) = 0$. Let $E(t)$ be an internal energy of the physical system defined by

$$E(t) = \frac{k}{\alpha}\int_0^{s(t)} (T(x,t) - T_{\mathrm{m}})\,\mathrm{d}x + \frac{k}{\beta}s(t). \tag{4.147}$$

Note that $E(\sigma) = 0$ holds by the imposed assumption. Taking the time derivative of (4.147) yields

the energy conservation

$$\dot{E}(t) = q_{\mathrm{c}}(t) - q_{\mathrm{f}}(t). \tag{4.148}$$

In addition, the time derivative of (4.145) yields

$$\dot{q}_{\mathrm{c}}(t) = -c\left(q_{\mathrm{c}}(t) - q_{\mathrm{f}}(t)\right). \tag{4.149}$$

Combining these two and taking integration on both sides gives

$$E(t) = E(0) - \frac{1}{c}(q_{\mathrm{c}}(t) - q_{\mathrm{c}}(0)). \tag{4.150}$$

By (4.146) and (4.147), we get

$$q_0 = -c\left(E(0) - \frac{k}{\beta}s_{\mathrm{r}}\right). \tag{4.151}$$

Substituting this and (4.145) into (4.150), we have

$$E(t) = e^{-ct}\left[E(0) + \frac{ks_{\mathrm{r}}}{\beta}(e^{ct} - 1) - \int_0^t e^{c\tau}q_{\mathrm{f}}(\tau)\mathrm{d}\tau\right]. \tag{4.152}$$

Let $f(t)$ be a function in time defined by

$$f(t) = E(0) + \frac{ks_{\mathrm{r}}}{\beta}(e^{ct} - 1) - \int_0^t e^{c\tau}q_{\mathrm{f}}(\tau)\mathrm{d}\tau. \tag{4.153}$$

Since $E(t) = e^{-ct}f(t)$, we can see that $E(t) > 0$ for all $t > 0$ if and only if $f(t) > 0$ for all $t > 0$. By (4.153), we have $f(0) = E(0) > 0$. Taking the time derivative of (4.153) yields

$$f'(t) = e^{ct}\left(\frac{ks_{\mathrm{r}}c}{\beta} - q_{\mathrm{f}}(t)\right). \tag{4.154}$$

By Assumption 7, (4.154) leads to $f'(t) > 0$ for all $t > 0$. Therefore, $f(t) > 0$ for all $t > 0$, and we conclude $E(t) > 0$ for all $t > 0$ which contradicts with the imposed assumption $s(\sigma) = 0$ where $\sigma \neq \infty$. Hence, the existence and uniqueness of the solution holds globally $\forall t \geq 0$.

Since the open-loop system has a unique solution, the closed-loop solution has a unique solution as well. Thus, the following properties hold:

$$q_c(t) > 0, \tag{4.155}$$

$$u(x,t) > 0, \quad u_x(s(t),t) < 0, \tag{4.156}$$

$$s(t) > 0. \tag{4.157}$$

Moreover, applying (4.155) and (4.156) to (4.121), the following condition is derived

$$0 < s(t) < s_r. \tag{4.158}$$

ISS Proof

To conclude the ISS of the original system, first we show the ISS of the target system (4.135), (4.137), (4.138), and (4.143) with respect to the disturbance $d(t)$. We consider

$$V(t) = \frac{1}{2\alpha}||w||^2 + \frac{\varepsilon}{2\beta}X(t)^2. \tag{4.159}$$

Then, as proven in Appendix C.4, for a sufficiently small $\varepsilon > 0$, the following inequality is derived:

$$\dot{V}(t) \leq -bV(t) + \Gamma d(t)^2 + a|\dot{s}(t)|V(t), \tag{4.160}$$

where $a = \frac{2\beta\varepsilon}{\alpha}\max\left\{1, \frac{\alpha c^2 s_r}{2\beta^3\varepsilon^3}\right\}$, $b = \frac{1}{8}\min\left\{\frac{\alpha}{s_r^2}, c\right\}$, and $\Gamma = \frac{\varepsilon}{\beta c} + \frac{2s_r^3}{\alpha^2}\left(\frac{cs_r}{\beta} + \varepsilon\right)^2$. Let $z(t)$ be defined by

$$z(t) := s(t) + 2\int_0^t d(\tau)\mathrm{d}\tau. \tag{4.161}$$

By (4.117) and (4.158), we have

$$0 < z(t) < \bar{z} := s_r + \frac{2\beta M}{k} \tag{4.162}$$

The time derivative of (4.161) is given by

$$\dot{z}(t) = -\beta u_x(s(t),t) + d(t) \tag{4.163}$$

Since $\dot{s}(t) = -\beta u_x(s(t),t) - d(t)$ and recalling $u_x(s(t),t) < 0$ and $d(t) > 0$, the following inequality holds:

$$|\dot{s}(t)| \leq -\beta u_x(s(t),t) + d(t) = \dot{z}(t). \tag{4.164}$$

Applying (4.164) to (4.160) leads to

$$\dot{V}(t) \leq -bV(t) + \Gamma d(t)^2 + a\dot{z}(t)V(t). \tag{4.165}$$

Consider the following functional

$$W(t) = V(t)e^{-az(t)}. \tag{4.166}$$

Taking the time derivative of (4.166) with the help of (4.165) and applying (4.162), we deduce

$$\dot{W}(t) \leq -bW(t) + \Gamma d(t)^2. \tag{4.167}$$

Since (4.167) leads to the statement that either $\dot{W}(t) \leq -\frac{b}{2}W(t)$ or $W(t) \leq \frac{2}{b}\Gamma d(t)^2$ is true, following the procedure in [149] (proof of Theorem 5 in Section 3.3), one can derive

$$W(t) \leq W(0)e^{-\frac{b}{2}t} + \frac{2}{b}\Gamma \sup_{\tau\in[0.t]} d(\tau)^2. \tag{4.168}$$

By (4.166), we have $V(t) = W(t)e^{az(t)}$. Applying (4.168), we get $V(t) \leq e^{az(t)}W(0)e^{-\frac{b}{2}t} + \frac{2}{b}\Gamma \sup_{\tau\in[0.t]} d(\tau)^2$. Again by (4.166), we have $W(0) = V(0)e^{-az(0)}$. Combining these two with the help of (4.162), finally we obtain the following estimate on the L_2 norm of the target system

$$V(t) \leq V(0)e^{a\bar{z}}e^{-\frac{b}{2}t} + \frac{2}{b}\Gamma e^{a\bar{z}} \sup_{\tau\in[0.t]} d(\tau)^2. \tag{4.169}$$

Due to the invertibility of the transformation from (u,X) to (w,X) together with the boundedness of the domain $0 < s(t) < s_r$, there exist positive constants $\underline{M} > 0$ and $\overline{M} > 0$ such that the following inequalities hold:

$$\underline{M}\Psi(t)^2 \leq V(t) \leq \overline{M}\Psi(t)^2, \tag{4.170}$$

where $\Psi(t)$ is the L_2 norm of the original system defined in (4.124). Finally, applying (4.170) to (4.169), one can derive the norm estimate on the original (T,s)-system as $\Psi(t) \leq \sqrt{\frac{\overline{M}e^{a\bar{z}}}{\underline{M}}}\Psi(0)e^{-\frac{b}{4}t} + \sqrt{\frac{2\Gamma e^{a\bar{z}}}{b\underline{M}}} \sup_{\tau\in[0.t]} d(\tau)$, which completes the proof of Theorem 11.

Table 4.1: Physical properties of the liquid paraffin.

Description	Symbol	Value
Density	ρ	$790\ \mathrm{kg}\cdot\mathrm{m}^{-3}$
Latent heat of fusion	ΔH^*	$210\ \mathrm{J}\cdot\mathrm{g}^{-1}$
Heat Capacity	C_p	$2.38\ \mathrm{J}\cdot\mathrm{g}^{-1}\cdot{}^\circ\mathrm{C}^{-1}$
Melting Temperature	T_m	$37.0\ ^\circ\mathrm{C}$
Thermal conductivity	k	$0.220\ \mathrm{W}\cdot\mathrm{m}^{-1}$

Numerical Simulation

Simulation results are performed for the one-phase Stefan problem by considering a cylinder of paraffin whose physical properties are given in Table 4.1. The setpoint and the initial values are chosen as $s_\mathrm{r} = 2$ [cm], $s_0 = 0.1$ [cm], and $T_0(x) - T_\mathrm{m} = \bar{T}_0(1 - x/s_0)$ with $\bar{T}_0 = 1$ [°C]. Then, the setpoint restriction is satisfied.

The control gain is set as $c = 5.0 \times 10^{-3}$[/s], and the heat loss at the interface is set as

$$q_\mathrm{f}(t) = \bar{q}_\mathrm{f} e^{-Kt}, \tag{4.171}$$

where $K = 5.0 \times 10^{-6}$ [/s]. The closed-loop responses for $\bar{q}_\mathrm{f} = 1.0 \times 10^2$[W/m^2] (red), 2.0×10^2[W/m^2] (blue), and 3.0×10^3[W/m^2] (green) are implemented as depicted in Fig. 4.6. Fig. 4.6 (a) shows the dynamics of the interface, which illustrates the convergence to the setpoint with an error due to the unknown heat loss at the interface. This error becomes larger as $\bar{q}_\mathrm{f}$ gets larger, which is consistent with the ISS result. In addition, the property $0 < s(t) < s_\mathrm{r}$ is observed. Fig. 4.6 (b) shows the dynamics of the proposed closed-loop control law, and Fig. 4.6 (c) shows the dynamics of the boundary temperature $T(0,t)$. Hence, we can observe that the simulation results are consistent with the theoretical result we prove for the model validity conditions and ISS.

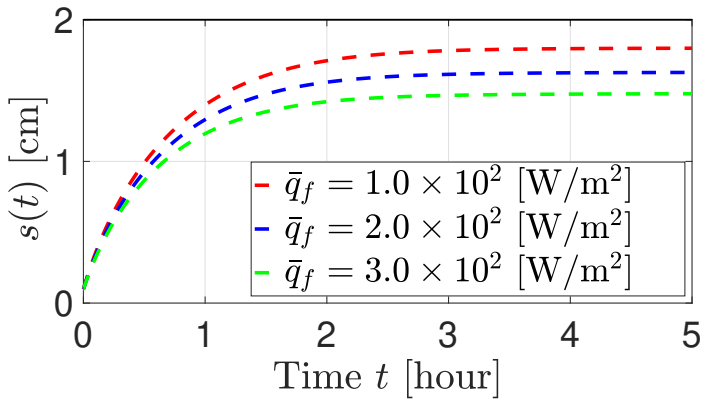

(a) Convergence of the interface is observed with offsets from the setpoint depending on the magnitude of the heat loss.

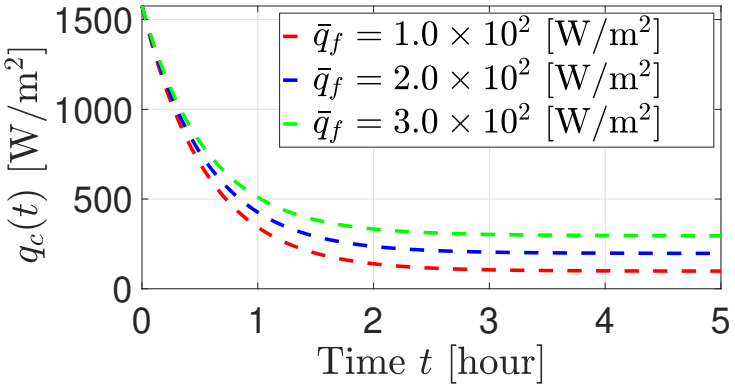

(b) Positivity of the closed-loop controller maintains.

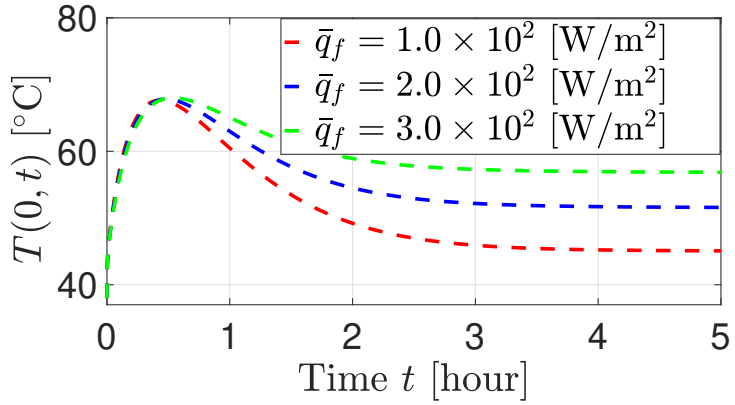

(c) The model validity of the boundary liquid temperature holds, i.e., $T(0,t) > T_{\mathrm{m}}$.

Figure 4.6: The responses of the system (4.112)–(4.115) with the heat loss $q_{\mathrm{f}}(t) = \bar{q}_{\mathrm{f}} e^{-Kt}$ under the feedback control law (4.121).

4.4 Sampled-Data Design

The aforementioned results assumed the control input to be varying continuously in time; however, in practical implementation of the control systems it is impossible to dynamically change the control input continuously in time due to limitations of the sensors, actuators, and software. Instead, the control input can be adjusted at each sampling time at which the measured states are obtained or the actuator is manipulated. One of the most fundamental and well known method to design such a "sampled-data" control is the so-called "emulation design" that applies "Zero-Order-Hold" (ZOH) to the nominal "continuous-time" control law. A general result for nonlinear ODEs to guarantee the global stability of the closed-loop system under such a ZOH-based sampled-data control was studied in [68], and the sampled-data observer design under discrete-time measurement is developed in [69] by introducing inter-sampled output predictor. As further extensions, the stability of the sampled-data control for general nonlinear ODEs under actuator delay is shown in [71, 72] by applying predictor-based feedback developed in [97], and results for a linear parabolic PDE are given in [75] by employing Sturm-Liouville operator theory. The sampled-data control for parabolic PDEs has been intensively developed by Fridman and coworkers by utilizing linear matrix inequalities [4, 57, 58, 136]. However, none of the existing work on the sampled-data control has studied the class of the Stefan problem described by a parabolic PDE with state-dependent moving boundaries "(a nonlinear system)".

We consider the one-phase Stefan problem in Section 2.3:

$$T_t(x,t) = \alpha T_{xx}(x,t), \quad 0 \le x \le s(t), \tag{4.172}$$

$$-kT_x(0,t) = q_{\mathrm{c}}(t), \tag{4.173}$$

$$T(s(t),t) = T_{\mathrm{m}}, \tag{4.174}$$

$$\dot{s}(t) = -\beta T_x(s(t),t), \tag{4.175}$$

In practical implementation, the actuation value cannot be changed continuously in time. Instead, by obtaining the measured value as signals discretely in time, the control value needs to be implemented at each sampling time. One of the most typical design for such a sampled-data control is the application of "Zero-Order-Hold"(ZOH) to the nominal continuous time control law. Through ZOH, during the time intervals between each sampling, the control maintains the value at the previous sampling time. Let t_j be the j-th sampling time for $j = 0, 1, 2, \cdots,$, and τ_j be defined by

$$\tau_j = t_{j+1} - t_j. \tag{4.176}$$

The application of ZOH to the nominal control law (4.121) leads to the following design for the sampled-data control

$$q_{\mathrm{c}}(t) = -c\left(\frac{k}{\alpha}\int_0^{s(t_j)}(T(x,t_j)-T_{\mathrm{m}})\mathrm{d}x + \frac{k}{\beta}(s(t_j)-s_r)\right), \quad \forall t \in [t_j, t_{j+1}), \tag{4.177}$$

of which the right hand side is constant during the time interval $t \in [t_j, t_{j+1})$. Let us denote $q_j = q_{\mathrm{c}}(t)$ for $t \in [t_j, t_{j+1})$. Hereafter, all the variables with subscript j denote the variables at $t = t_j$. We introduce the following assumptions on the sampling scheduling.

Assumption 8 *The sampling schedule has a finite upper diameter and a positive lower diameter, i.e., there exist constants* $0 < r \leq R$ *such that*

$$\sup_{j\in\mathcal{Z}^+}\{\tau_j\} \leq R, \tag{4.178}$$

$$\inf_{j\in\mathcal{Z}^+}\{\tau_j\} \geq r. \tag{4.179}$$

Our main theorem is given next.

Theorem 3 *Consider the closed-loop system* (4.172)–(4.175)*,* (4.177) *under Assumptions 6, 8.*

Then for every $0 < r \leq R < 1/c$*, there exists a constant* $M := M(r)$ *such that the closed-loop system has a unique solution satisfying the following estimate:*

$$\Psi(t) \leq M\Psi(0)\exp(-bt), \tag{4.180}$$

where $b = \frac{1}{8}\min\left\{\frac{\alpha}{s_r^2}, c\right\}$*, for all* $t \geq 0$*, in the* L_2 *norm* $\Psi(t) = \int_0^{s(t)} (T(x,t) - T_{\mathrm{m}})^2 \,\mathrm{d}x + (s(t) - s_r)^2$.

The positive constant M in (4.180) has a dependency on $r > 0$ as

$$M(r) = M_1 + \frac{M_2}{1 - (1 - cr)^2 e^{\frac{cr}{8}}}, \tag{4.181}$$

for some positive constants $M_1 > 0$ and $M_2 > 0$ that are not dependent on $r > 0$.

Analysis of the closed-loop system

We introduce the following reference error states:

$$u(x,t) = T(x,t) - T_{\mathrm{m}}, \quad X(t) = s(t) - s_r. \tag{4.182}$$

The governing equations (4.172)–(4.175) are rewritten as the following reference error system

$$u_t(x,t) = \alpha u_{xx}(x,t), \tag{4.183}$$

$$u_x(0,t) = -q_{\mathrm{c}}(t)/k, \tag{4.184}$$

$$u(s(t),t) = 0, \tag{4.185}$$

$$\dot{X}(t) = -\beta u_x(s(t),t). \tag{4.186}$$

Define the internal energy of the reference error system as follows:

$$\widetilde{E}(t) = \frac{k}{\alpha}\int_0^{s(t)} u(x,t)\mathrm{d}x + \frac{k}{\beta}X(t). \tag{4.187}$$

Taking the time derivative of (4.187) along the solution of (4.183)–(4.186) leads to

$$\frac{\mathrm{d}}{\mathrm{d}t}\widetilde{E}(t) = q_{\mathrm{c}}(t). \tag{4.188}$$

Noting that $q_{\mathrm{c}}(t)$ is constant for $t \in [t_j, t_{j+1})$ as $q_{\mathrm{c}}(t) = q_j$ under ZOH-based sampled-data control, taking the integration of (4.188) from $t = t_j$ to $t = t_{j+1}$ yields

$$\widetilde{E}_{j+1} - \widetilde{E}_j = \tau_j q_j, \tag{4.189}$$

where $\widetilde{E}_j = \widetilde{E}(t_j)$ and $\tau_j = t_{j+1} - t_j$. The sampled-data control (4.177) and the internal energy (4.187) at each sampling time satisfy the following relation:

$$q_j = -c\widetilde{E}_j. \tag{4.190}$$

Substituting (4.190) into (4.189), we obtain

$$\widetilde{E}_{j+1} = \left(1 - c\tau_j\right)\widetilde{E}_j, \tag{4.191}$$

which leads to the explicit solution as follows:

$$\widetilde{E}_j = \widetilde{E}_0 \prod_{i=0}^{j-1} \left(1 - c\tau_i\right). \tag{4.192}$$

Substituting (4.192) into (4.190) yields

$$q_{\mathrm{c}}(t) = q_j = q_0 \prod_{i=0}^{j-1} (1 - c\tau_i), \quad \forall t \in [t_j, t_{j+1}), \quad \forall j \in \mathcal{Z}^+ \tag{4.193}$$

where

$$q_0 = -c \left(\frac{k}{\alpha} \int_0^{s_0} (T_0(x) - T_{\mathrm{m}}) \mathrm{d}x + \frac{k}{\beta} (s_0 - s_r) \right). \tag{4.194}$$

Therefore, the closed-loop system under the sampled-data feedback control (4.177) is equivalent to the open-loop solution with the control input (4.193). Moreover, under Assumptions 6, 8, and the fact that $c < \frac{1}{R}$, the input (4.193) is shown to be a bounded piecewise continuous function and $q_{\mathrm{c}}(t) \geq 0$ for all $t \geq 0$. Thus, the existence and uniqueness of the solution is ensured.

One can deduce

$$\dot{s}(t) > 0, \quad \forall t \geq 0, \tag{4.195}$$

and thus $s_0 < s(t)$ for all $t \geq 0$. Integrating (4.188) from $t = t_j$ to $t \in [t_j, t_{j+1})$ leads to

$$\widetilde{E}(t) - \widetilde{E}_j = (t - t_j) q_j, \quad \forall t \in [t_j, t_{j+1}). \tag{4.196}$$

With the help of (4.190) and (4.192), equation (4.196) yields

$$\widetilde{E}(t) = \big(1 - c(t - t_j)\big) \widetilde{E}_j, \quad \forall t \in [t_j, t_{j+1}). \tag{4.197}$$

By Assumption 8 and since $c < \frac{1}{R}$, we have $0 < c < \frac{1}{\tau_j}$ for all $j \in \mathcal{Z}^+$. In addition, for all $t \in [t_j, t_{j+1})$ and for all $j \in \mathcal{Z}^+$, it holds $t - t_j \leq \tau_j$. Hence, we have $1 - c(t - t_j) > 0$, for all

$t \in [t_j, t_{j+1})$ and for all $j \in \mathcal{Z}^+$. Applying this to (4.197) and noting that

$$\widetilde{E}_j < 0, \quad \forall j \in \mathcal{Z}^+, \tag{4.198}$$

one can obtain

$$\widetilde{E}(t) < 0, \quad \forall t \geq 0. \tag{4.199}$$

Substituting (4.199) into (4.187) and applying $u(x,t) > 0$ for all $x \in (0, s(t))$ and $t \geq 0$, we have

$$X(t) < 0, \quad \forall t \geq 0, \tag{4.200}$$

which leads to

$$s_0 < s(t) < s_r, \quad \forall t \geq 0. \tag{4.201}$$

Target system

We use the same backstepping transformation as (4.133) (4.134). Thus, we get the target system

$$w_t(x,t) = \alpha w_{xx}(x,t) + \dot{s}(t)\phi'(x - s(t))X(t), \tag{4.202}$$

$$w(s(t),t) = \varepsilon X(t), \tag{4.203}$$

$$\dot{X}(t) = -cX(t) - \beta w_x(s(t),t). \tag{4.204}$$

The boundary condition at $x = 0$ is obtained by

$$w_x(0,t) = -\frac{q_c(t)}{k} - \frac{\beta}{\alpha}\varepsilon u(0,t) - \frac{c}{\alpha}\int_0^{s(t)} u(y,t)\mathrm{d}y - \frac{c}{\beta}X(t). \tag{4.205}$$

Substituting the design of the sampled-data control $q_c(t) = q_j = -c\widetilde{E}_j$ for all $t \in [t_j, t_{j+1})$ and for all $j \in \mathcal{Z}^+$, and recalling the definition of $\widetilde{E}(t)$ in (4.187), the boundary condition (4.205) can be written as

$$w_x(0,t) = -\frac{c}{k}\left(\widetilde{E}(t) - \widetilde{E}_j\right) - \frac{\beta}{\alpha}\varepsilon u(0,t). \tag{4.206}$$

Moreover, substituting (4.197), we can describe (4.206) as

$$w_x(0,t) = f(t) - \frac{\beta}{\alpha}\varepsilon u(0,t), \tag{4.207}$$

where $f(t)$ is an explicit function in time defined by

$$f(t) = \frac{c^2}{k}\widetilde{E}_j \cdot (t - t_j), \quad \forall t \in [t_j, t_{j+1}), \quad j \in \mathcal{Z}^+. \tag{4.208}$$

The closed form representation of (4.207) using variables (w,X) is given by using the same inverse transformation as (4.139) (4.140), which yields

$$w_x(0,t) = f(t) - \frac{\beta}{\alpha}\varepsilon\left[w(0,t) - \frac{\beta}{\alpha}\int_0^{s(t)} \psi(-y)w(y,t)\mathrm{d}y - \psi(-s(t))X(t)\right]. \tag{4.209}$$

Therefore, the closed form of the target (w,X)-system is described by (4.202), (4.203), (4.204), and (4.209).

Stability proof

For a given $t \geq 0$, we define the most recent sampling number as

$$n := \{n \in \mathcal{Z}^+ | t_n \leq t < t_{n+1}\}, \tag{4.210}$$

and we firstly apply Lyapunov method for the time interval $t \in [t_j, t_{j+1})$ for all $j = 0, 1, \cdots, n-1$, and next for the interval from t_n to t. For both cases, we consider

$$V = \frac{1}{2\alpha}||w||^2 + \frac{\varepsilon}{2\beta}X(t)^2. \tag{4.211}$$

where $||w||$ denotes L_2 norm defined by $||w|| = \sqrt{\int_0^{s(t)} w(x,t)^2 \mathrm{d}x}$. As proven in Appendix C.4, and applying $\dot{s}(t) > 0$, for a sufficiently small $\varepsilon > 0$, the following inequality is derived:

$$\dot{V} \leq -bV + 2s_r f(t)^2 + a\dot{s}(t)V, \tag{4.212}$$

where

$$b = \frac{1}{8}\min\left\{\frac{\alpha}{s_r^2}, c\right\}, \quad a = \frac{2\beta\varepsilon}{\alpha}\max\left\{1, \frac{\alpha c^2 s_r}{2\beta^3\varepsilon^3}\right\}. \tag{4.213}$$

Consider the following functional

$$W = Ve^{-as(t)}. \tag{4.214}$$

Taking the time derivative of (4.214) with the help of (4.212), we deduce

$$\begin{aligned}\dot{W} &\leq -bW + 2s_r f(t)^2 e^{-as(t)} \\ &\leq -bW + 2s_r f(t)^2.\end{aligned} \tag{4.215}$$

(i) For $t \in [t_j, t_{j+1})$, for all $j = 0, 1, \cdots, n-1$,

Applying comparison principle to (4.215) for $t \in [t_j, t_{j+1})$ leads to

$$W(t) \leq W(t_j)e^{-b(t-t_j)} + 2s_r e^{-bt}\int_{t_j}^{t} e^{b\tau} f(\tau)^2 \mathrm{d}\tau. \tag{4.216}$$

Setting $t = t_{j+1}$ and recalling $f(t) = \frac{c^2}{k}\widetilde{E}_j(t-t_j), \forall t \in [t_j, t_{j+1})$, we get

$$W_{j+1} \leq W_j e^{-b\tau_j} + \frac{2c^4 s_r}{k^2} e^{-b\tau_j} \widetilde{E}_j^2 I_j, \tag{4.217}$$

where $W_j = W(t_j)$, and I_j is defined by

$$I_j := \int_{t_j}^{t_{j+1}} e^{b(\tau - t_j)} (\tau - t_j)^2 \mathrm{d}\tau. \tag{4.218}$$

Then, by introducing the variable $s = b(\tau - t_j)$ and integration by substitution, with the help of $b\tau_j < \frac{1}{8} c\tau_j < \frac{1}{8}$ for all $j \in \mathcal{Z}^+$ derived by (4.213), Assumption 8 and the fact that $c < \frac{1}{R}$, one can derive the following inequality:

$$I_j = \frac{1}{b^3} \int_0^{b\tau_j} e^s s^2 \mathrm{d}s \leq \frac{J}{b^3}, \tag{4.219}$$

where J is defined by $J := \int_0^{\frac{1}{8}} e^s s^2 \mathrm{d}s$. Applying (4.219) to (4.217) yields

$$W_{j+1} \leq W_j e^{-b\tau_j} + B_j, \tag{4.220}$$

where B_j is defined by

$$B_j = \frac{2Jc^4 s_r}{k^2 b^3} e^{-b\tau_j} \widetilde{E}_j^2. \tag{4.221}$$

Applying (4.220) from $j = n-1$ to $j = 0$ inductively, we get

$$W_n \leq W_0 e^{-b\sum_{i=0}^{n-1} \tau_i} + B_{n-1} + \sum_{i=0}^{n-2} B_i e^{-b\sum_{j=i+1}^{n-1} \tau_j}. \tag{4.222}$$

By (4.221) and the solution of $\widetilde{E}_j$ given in (4.192), we have

$$\begin{aligned}
&\sum_{i=0}^{n-2} B_i e^{-b\sum_{j=i+1}^{n-1}\tau_j} \\
\leq &\frac{2Jc^4 s_r \widetilde{E}_0^2 e^{-b\sum_{j=0}^{n-1}\tau_j}}{k^2 b^3}\left(1+\sum_{i=1}^{n-2}\left(\prod_{k=0}^{i-1}(1-c\tau_k)^2\right)e^{b\sum_{j=0}^{i-1}\tau_j}\right) \\
\leq &\frac{2Jc^4 s_r \widetilde{E}_0^2 e^{-b\sum_{j=0}^{n-1}\tau_j}}{k^2 b^3}\left(1+\sum_{i=1}^{n-2}\left(\prod_{k=0}^{i-1}(1-c\tau_k)^2 e^{b\tau_k}\right)\right). \qquad (4.223)
\end{aligned}$$

Since $b=\frac{1}{8}\min\left\{\frac{\alpha}{s_r^2},c\right\}<\frac{c}{8}$, by using $r=\inf_{j\in\mathcal{Z}^+}\{\tau_j\}>0$ given in Assumption 8, the following inequality holds

$$(1-c\tau_i)^2 e^{b\tau_i} \leq (1-cr)^2 e^{\frac{cr}{8}} := \delta < 1, \quad \forall j \in \mathcal{Z}^+. \qquad (4.224)$$

Thus, the inequality (4.223) leads to

$$\begin{aligned}
\sum_{i=0}^{n-2} B_i e^{-b\sum_{j=i+1}^{n-1}\tau_j} \leq &\frac{2Jc^4 s_r \widetilde{E}_0^2 e^{-b\sum_{j=0}^{n-1}\tau_j}}{k^2 b^3}\left(1+\sum_{i=1}^{n-2}\delta^i\right) \\
\leq &\frac{2Jc^4 s_r \widetilde{E}_0^2}{k^2 b^3(1-\delta)} e^{-b\sum_{j=0}^{n-1}\tau_j}. \qquad (4.225)
\end{aligned}$$

In the similar way, we get

$$B_{n-1} \leq \frac{2Jc^4 s_r \widetilde{E}_0^2}{k^2 b^3(1-\delta)} e^{-b\sum_{j=0}^{n-1}\tau_j}. \qquad (4.226)$$

Recalling that $\tau_j = t_{j+1} - t_j$ and $t_0 = 0$, we get $\sum_{j=0}^{n-1}\tau_j = t_n$. Applying (4.225) and (4.226) to (4.222), we arrive at

$$W_n \leq (W_0 + A\widetilde{E}_0^2) e^{-bt_n}. \qquad (4.227)$$

where $A = \frac{2Jc^4 s_r}{k^2 b^3 (1-\delta)}$.

(ii) For $t \in [t_n, t_{n+1})$,

Applying comparison principle to (4.215) from t_n to $t \in [t_n, t_{n+1})$, we get

$$\begin{aligned} W(t) \leq & W_n e^{-b(t-t_n)} + B_n e^{-b(t-t_{n+1})} \\ \leq & W_n e^{-b(t-t_n)} + A\widetilde{E}_0^2 e^{-bt}. \end{aligned} \tag{4.228}$$

Finally, combining (4.227) and (4.228), the following bound is obtained

$$W(t) \leq (W_0 + 2A\widetilde{E}_0^2) e^{-bt}. \tag{4.229}$$

Recalling the relation $W = Ve^{-as(t)}$ defined in (4.214), and applying $0 < s(t) < s_r$, the norm estimate for W in (4.229) leads to the following estimate for V:

$$V(t) \leq e^{as_r}(V_0 + 2A\widetilde{E}_0^2) e^{-bt}. \tag{4.230}$$

We consider the L_2-norm of (u, X)-system defined by

$$\Psi(t) = \int_0^{s(t)} u(x,t)^2 \mathrm{d}x + X(t)^2. \tag{4.231}$$

Due to the invertibility of the transformation from (u, X) to (w, X) together with the boundedness of the domain $0 < s(t) < s_r$, there exist positive constants $\underline{M} > 0$ and $\overline{M} > 0$ such that the following inequalities hold:

$$\underline{M}\Psi(t) \leq V(t) \leq \overline{M}\Psi(t). \tag{4.232}$$

Moreover, due to the definition of the reference energy $\widetilde{E}(t) = \frac{k}{\alpha}\int_0^{s(t)} u(x,t)\mathrm{d}x + \frac{k}{\beta}X(t)$ given in

(4.187), using Young's and Cauchy Schwarz inequalities one can show that

$$\widetilde{E}_0^2 \leq K\Psi_0, \tag{4.233}$$

where $K = 2k^2 \max\{\frac{s_r}{\alpha^2}, \frac{1}{\beta^2}\}$. Applying (4.232) and (4.233) to (4.230), we deduce that there exists positive constant $M > 0$ such that the following inequality holds

$$\Psi(t) \leq M\Psi_0 e^{-bt}, \tag{4.234}$$

which completes the proof of Theorem 3.

Numerical Simulation

We use the same physical parameters of paraffin, the initial conditions, and the setpoint as those used in the last section for ISS. We consider periodic sampling with period given by $\tau_j = R = 10$ [min], for all $j \in \mathbb{Z}$. The control gain is set as $c = 5.0 \times 10^{-3}$/s, by which the requirement $R < \frac{1}{c}$ is satisfied. The time responses of the interface position, the control input, and the boundary temperature under the closed-loop system are depicted in Fig. 4.7 (a)–(c), respectively. Fig. 4.7 (a) illustrates that the interface position $s(t)$ converges to the setpoint s_r monotonically and smoothly without overshooting, i.e., $\dot{s}(t) > 0$ and $s_0 < s(t) < s_r$ hold for all $t \geq 0$. Fig. 4.7 (b) shows that the proposed sampled-data control law maintains constant positive value for every sampling period and is monotonically decreasing to zero. Fig. 4.7 (c) illustrates that the boundary temperature $T(0,t)$ keeps greater than the melting temperature T_{m} with accompanying "spikes" at every sampling time $t = \tau_j$ up to 2 hours. Such spikes are caused by the large drop of the control input $q_{\mathrm{c}}(t)$ at sampling time observed from Fig. 4.7 (b), which affects the boundary temperature directly as given in the boundary condition. Therefore, the numerical results are consistent with the theoretical results we have established for the required

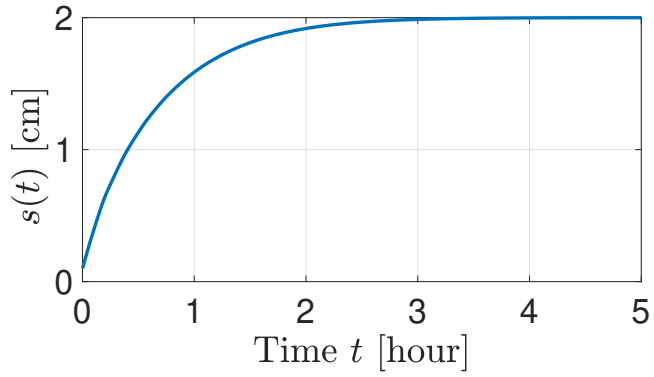

(a) Convergence of the interface to the setpoint is observed without the overshoot.

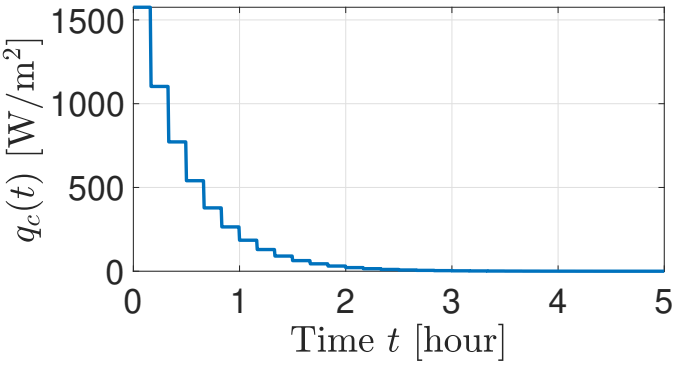

(b) The sampled-data controller maintains positive value.

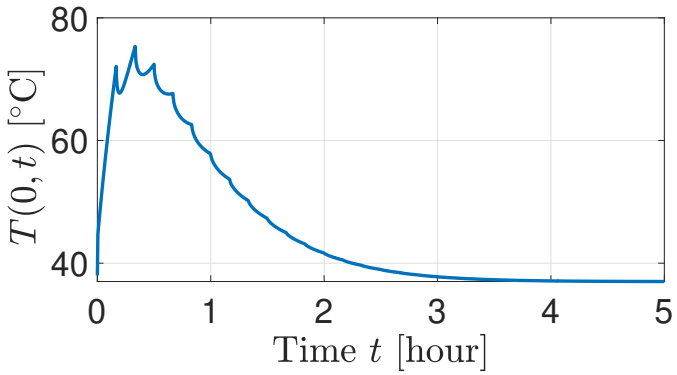

(c) The boundary temperature accompanies "spikes" at every sampling time.

Figure 4.7: The responses of the system (4.172)–(4.175) under the ZOH-based sampled-data control (4.177).

properties and in Theorem 3 for the closed-loop stability.

4.5 Acknowledgment

Chapter 4, in part, is a reprint of the material as it appears in:

- S. Koga, R. Vazquez, and M. Krstic, "Backstepping Control of the Stefan Problem with Flowing Liquid", *American Control Conference*, 2017,

- S. Koga and M. Krstic, "Delay-Compensated Control of the Stefan Problem", *IEEE Conference on Decision and Control*, 2017,

- S. Koga, D. Bresch-Pietri, and M. Krstic, "Delay-Compensated Control of the Stefan Problem and Robustness to Delay Mismatch", *International Journal of Robust and Nonlinear Control*, vol. 30, no. 6, pp. 2304-2334, 2020,

- S. Koga, I. Karafyllis, and M. Krstic, "Input-to-State Stability for the Control of Stefan Problem with Respect to Heat Loss", *American Control Conference*, 2018,

- S. Koga, I. Karafyllis, and M. Krstic, "Towards Implementation of PDE Control for Stefan System: Input-to-State Stability and Sampled-Data Design", *Automatica*, under review.

The dissertation author was the primary investigators and author of this paper. The author would like to thank Rafael Vazquez, Delphine Bresch-Pietri, and Iasson Karafyllis for their collaboration.

Chapter 5

Two-Phase Stefan Problem

Recall that in Section 4.3 we deal with a non-monotonic interface dynamics by incorporating a heat loss at the interface in the one-phase Stefan problem. However, such a heat loss should be physically modeled by the heat flux from the solid phase, which renders additional PDE of the solid phase temperature, and the control design to asymptotically stabilize such a PDE-ODE-PDE system is quite challenging, let alone for Stefan systems of moving boundary.

5.1 Description of the Physical Model

The two-phase Stefan problem describes the repetitive model of the phase change phenomena of melting and freezing (solidification) process. As depicted in Fig. 5.1, two complementary time-varying sub-domains $x \in [0, s(t)]$ and $x \in [s(t), L]$ are occupied by the liquid phase and the solid phase, respectively. Let $T_{\mathrm{l}}(x,t)$ and $T_{\mathrm{s}}(x,t)$ be the temperature profiles of liquid and solid, respectively, and $s(t)$ be the position of the interface between liquid and solid. Then, the energy conservation and heat transfer laws give the following PDE-ODE-PDE model of the temperature

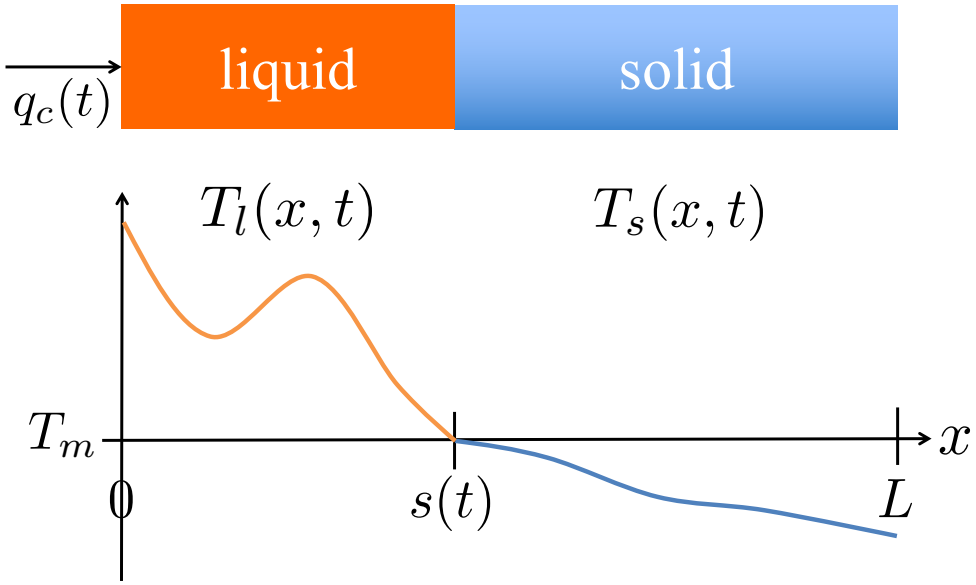

Figure 5.1: Schematic of the two-phase Stefan problem. The temperature profiles of both the liquid phase and the solid phase are dynamic.

profile

$$\frac{\partial T_{\mathrm{l}}}{\partial t}(x,t) = \alpha_{\mathrm{l}} \frac{\partial^2 T_{\mathrm{l}}}{\partial x^2}(x,t), \quad 0 < x < s(t), \tag{5.1}$$

$$\frac{\partial T_{\mathrm{s}}}{\partial t}(x,t) = \alpha_{\mathrm{s}} \frac{\partial^2 T_{\mathrm{s}}}{\partial x^2}(x,t), \quad s(t) < x < L, \tag{5.2}$$

$$\frac{\partial T_{\mathrm{l}}}{\partial x}(0,t) = -\frac{q_{\mathrm{c}}(t)}{k_{\mathrm{l}}}, \quad \frac{\partial T_{\mathrm{s}}}{\partial x}(L,t) = 0, \tag{5.3}$$

$$T_{\mathrm{l}}(s(t),t) = T_{\mathrm{m}}, \quad T_{\mathrm{s}}(s(t),t) = T_{\mathrm{m}} \tag{5.4}$$

$$\gamma \dot{s}(t) = -k_{\mathrm{l}} \frac{\partial T_{\mathrm{l}}}{\partial x}(s(t),t) + k_{\mathrm{s}} \frac{\partial T_{\mathrm{s}}}{\partial x}(s(t),t), \tag{5.5}$$

with the initial data $T_{\mathrm{l},0}(x) := T_{\mathrm{l}}(x,0)$, $T_{\mathrm{s},0}(x) := T_{\mathrm{s}}(x,0)$, $s_0 := s(0)$, where $q_{\mathrm{c}}(t) > 0$ is a boundary heat input. Here, $\alpha_i = \frac{k_i}{\rho_i c_i}$, where ρ_i, c_i, k_i for $i \in \{\mathrm{l}, \mathrm{s}\}$ are the density, the heat capacity, the thermal conductivity, and the heat transfer coefficient, respectively and the subscripts "l" and "s" are associated to the liquid or solid phase, respectively. Also, $\gamma = \rho_{\mathrm{l}} \Delta H^*$ where ΔH^* denotes the latent heat of fusion.

5.2 Difficulties by Non-Monotonic Interface Dynamics

There are underlying assumptions to validate the model (5.1)-(5.5). First, the liquid phase is not frozen to the solid phase from the boundary $x = 0$. This condition is ensured if the liquid temperature $T_{\mathrm{l}}(x,t)$ is greater than the melting temperature T_{m}. Second, in a similar manner, the solid phase is not melt to the liquid phase from the boundary $x = L$, which is ensured if the solid temperature $T_{\mathrm{s}}(x,t)$ is less than the melting temperature. Third, the material is not completely melt or frozen to single phase through the disappearance of the other phase. This condition is guaranteed if the interface position remains inside the material's domain. In addition, these conditions are also required for the well-posedness (existence and uniqueness) of the solution in this model. Taking into account of these model validity conditions, we emphasize the following remark.

Remark 3 *To keep the physical state of each phase meaningful, the following conditions must be maintained:*

$$T_{\mathrm{l}}(x,t) \geq T_{\mathrm{m}}, \quad \forall x \in (0, s(t)), \quad \forall t > 0, \tag{5.6}$$

$$T_{\mathrm{s}}(x,t) \leq T_{\mathrm{m}}, \quad \forall x \in (s(t), L), \quad \forall t > 0, \tag{5.7}$$

$$0 < s(t) < L, \quad \forall t > 0. \tag{5.8}$$

For model validity, we state the following assumption and lemma.

Assumption 9 $0 < s_0 < L$, $T_{\mathrm{l},0}(x)$ *and* $T_{\mathrm{s},0}(x)$ *are piecewise continuous functions, and there exist Lipschitz constants* $H_{\mathrm{l}} > 0$ *and* $H_{\mathrm{s}} > 0$ *such that*

$$T_{\mathrm{m}} \leq T_{\mathrm{l},0}(x) \leq T_{\mathrm{m}} + H_{\mathrm{l}}(s_0 - x), \quad \forall x \in [0, s_0], \tag{5.9}$$

$$T_{\mathrm{m}} + H_{\mathrm{s}}(s_0 - x) \leq T_{\mathrm{s},0}(x) \leq T_{\mathrm{m}}, \quad \forall x \in [s_0, L]. \tag{5.10}$$

The existence and uniqueness of the two-phase Stefan problem was proven in [25] (Theorem 1 in p.4 and Theorem 4 in p.8) by employing the maximum principle, which is stated in the following lemma.

Lemma 2 *Under Assumption 9, and provided that $q_{\mathrm{c}}(t)$ is a piecewise continuous function that satisfies*

$$q_{\mathrm{c}}(t) \geq 0, \quad \forall t \in [0, t^*), \tag{5.11}$$

there exists a finite time $\bar{t} := \sup_{t\in(0,t^*)}\{t | s(t) \in (0,L)\} > 0$ such that a classical solution to (5.1)–(5.5) *exists, is unique, and satisfies the model validity condition* (5.6)–(5.8) *for all $t \in (0,\bar{t})$. Moreover, if $t^* = \infty$ and it holds*

$$0 < \gamma s_\infty + \int_0^t q_{\mathrm{c}}(s)ds < \gamma L, \tag{5.12}$$

for all $t \geq 0$, where

$$s_\infty := s_0 + \frac{k_{\mathrm{l}}}{\alpha_{\mathrm{l}}\gamma}\int_0^{s_0}(T_{\mathrm{l},0}(x) - T_{\mathrm{m}})\mathrm{d}x + \frac{k_{\mathrm{s}}}{\alpha_{\mathrm{s}}\gamma}\int_{s_0}^{L}(T_{\mathrm{s},0}(x) - T_{\mathrm{m}})\mathrm{d}x, \tag{5.13}$$

then $\bar{t} = \infty$, namely, the well-posedness and the model validity conditions are satisfied for all $t \geq 0$.

The variable s_∞ defined in (5.13) is $s_\infty = \lim_{t\to\infty} s(t)$ under the zero input $q_{\mathrm{c}}(t) \equiv 0$ for all $t \geq 0$. For (5.12) to hold for all $t \geq 0$, we at least require it to hold at $t = 0$, which leads to the following assumption.

Assumption 10 *The initial conditions that appear in s_∞ in* (5.13) *satisfy*

$$0 < s_\infty < L. \tag{5.14}$$

5.3 State Feedback Control Design

As in the last chapters, the control objective is to stabilize the temperature profile and the interface position (T_l, T_s, s) at a reference setpoint (T_m, T_m, s_r). We approach this problem by means of *energy shaping control*, that is originally developed for underactuated mechanical systems such as robot manipulators [49]. The thermal internal energy of the total system in (5.1)–(5.5) is given by

$$E(t) = \frac{k_\mathrm{l}}{\alpha_\mathrm{l}} \int_0^{s(t)} (T_\mathrm{l}(x,t) - T_\mathrm{m})\mathrm{d}x + \frac{k_\mathrm{s}}{\alpha_\mathrm{s}} \int_{s(t)}^{L} (T_\mathrm{s}(x,t) - T_\mathrm{m})\mathrm{d}x + \gamma s(t), \tag{5.15}$$

which includes the specific heat of both liquid and solid phases and the latent heat. Taking the time derivative of (5.15) along the solution of (5.1)–(5.5), one can obtain the energy conservation law formulated as

$$\frac{d}{dt}E(t) = q_\mathrm{c}(t). \tag{5.16}$$

To achieve the control objective, the internal energy (5.15) must converge to the following setpoint energy

$$\lim_{t\to\infty} E(t) = \gamma s_\mathrm{r}. \tag{5.17}$$

Taking the time integration of (5.16) from $t = 0$ to ∞, and imposing the input constraint (5.11) required for the model validity as stated in Lemma 2, in order to achieve (5.17) we deduce that the following restriction on the setpoint *neccesary*:

Assumption 11 *The setpoint s_r is chosen to satisfy*

$$s_\infty < s_\mathrm{r} < L. \tag{5.18}$$

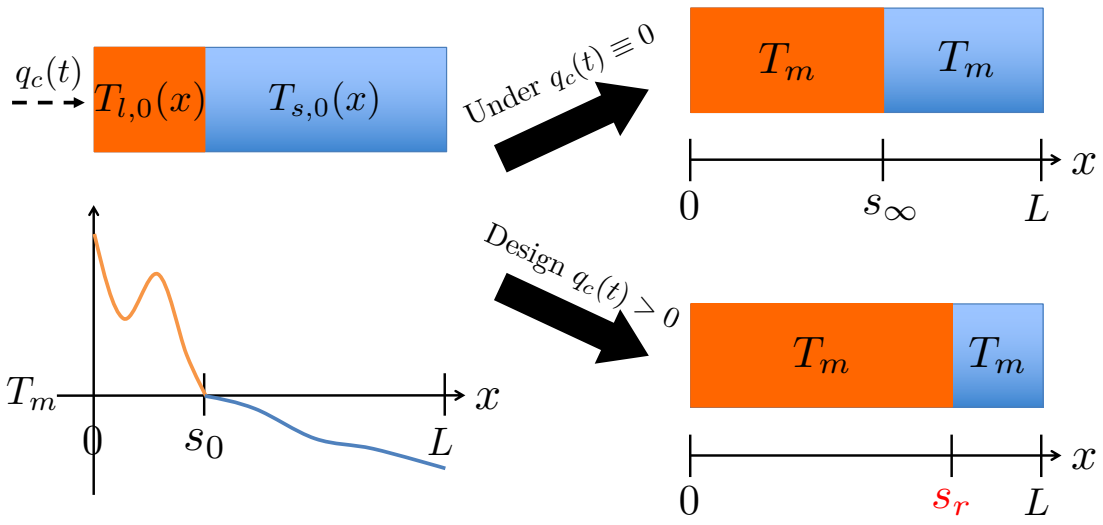

Figure 5.2: Illustration of Assumptions 9–11 and control objective.

A graphic illustration of Assumptions 1-3 and the control objective is depicted in Fig. 5.2. With Assumption 11, due to the energy conservation (5.16), the following control law

$$q_{\mathrm{c}}(t) = -c(E(t) - E_{\mathrm{r}}), \tag{5.19}$$

$$= -c\left(\frac{k_{\mathrm{l}}}{\alpha_{\mathrm{l}}}\int_0^{s(t)}(T_{\mathrm{l}}(x,t) - T_{\mathrm{m}})\mathrm{d}x + \frac{k_{\mathrm{s}}}{\alpha_{\mathrm{s}}}\int_{s(t)}^{L}(T_{\mathrm{s}}(x,t) - T_{\mathrm{m}})\mathrm{d}x + \gamma(s(t) - s_{\mathrm{r}})\right), \tag{5.20}$$

drives the internal energy $E(t)$ to the reference energy E_{r}. We state the following theorem.

Theorem 4 *Under Assumptions 9–11, the closed-loop system consisting of the plant* (5.1)–(5.5) *and the control law* (5.20) *where* $c > 0$ *is an arbitrary controller gain, maintains the conditions* (5.6)–(5.8)*, and there exists a positive constant* $M > 0$ *such that the following exponential stability estimate holds:*

$$\Psi(t) \leq M\Psi(0)e^{-dt} \tag{5.21}$$

for all $t \geq 0$*, where* $d = \frac{1}{2}\min\left\{\frac{\alpha_l}{2L^2}, \frac{\alpha_s}{L^2}, c\right\}$*, in the* L_2*-norm*

$$\Psi(t) = \int_0^{s(t)} (T_l(x,t) - T_m)^2 \mathrm{d}x + \int_{s(t)}^{L} (T_s(x,t) - T_m)^2 \mathrm{d}x + (s(t) - s_r)^2. \tag{5.22}$$

Error variables relative to melting temperature

Let $u(x,t)$ and $v(x,t)$ be reference error temperature profiles of the liquid and the solid phase, respectively, defined as

$$u(x,t) = T_l(x,t) - T_m, \quad v(x,t) = T_s(x,t) - T_m. \tag{5.23}$$

Then the system (5.1)–(5.5) is rewritten as

$$u_t(x,t) = \alpha_l u_{xx}(x,t), \quad 0 < x < s(t) \tag{5.24}$$

$$u_x(0,t) = -\frac{q_c(t)}{k_l}, \quad u(s(t),t) = 0, \tag{5.25}$$

$$v_t(x,t) = \alpha_s v_{xx}(x,t), \quad s(t) < x < L \tag{5.26}$$

$$v_x(L,t) = 0, \quad v(s(t),t) = 0, \tag{5.27}$$

$$\dot{s}(t) = -\beta_l u_x(s(t),t) + \beta_s v_x(s(t),t). \tag{5.28}$$

The system (5.24)–(5.28) shows the two PDEs coupling with the ODE describing the moving boundary. The stabilization of states (u,v,s) at $(0,0,s_r)$ is aimed by designing the control law of $q_c(t)$ in (5.25), however, the multiple PDEs are difficult to deal with as themselves in general.

Change of variable to absorb the solid phase into the interface

To reduce the complexity of the system's structure in (5.24)–(5.28), we introduce another change of variable. Let $X(t)$ be a state variable defined by

$$X(t) = s(t) - s_r + \frac{\beta_s}{\alpha_s} \int_{s(t)}^{L} v(x,t)dx. \tag{5.29}$$

Taking the time derivative of (5.29) and with the help of (5.26)–(5.28), we get $\dot{X}(t) = -\beta_l u_x(s(t),t)$ which eliminates v-dependency in ODE dynamics (5.28). Thus, (u,v,s)-system in (5.24)–(5.28) can be reduced to (u,X)-system as

$$u_t(x,t) = \alpha_l u_{xx}(x,t), \quad 0 < x < s(t) \tag{5.30}$$

$$u_x(0,t) = -\frac{q_c(t)}{k_l}, \quad u(s(t),t) = 0, \tag{5.31}$$

$$\dot{X}(t) = -\beta_l u_x(s(t),t). \tag{5.32}$$

Therefore, the control problem is now redescribed as designing the boundary control $q_c(t)$ in (5.31) to stabilize the (u,X)-system in (5.30)–(5.32) at the zero states $(0,0)$, which is equivalent problem as in the stabilization of the one-phase Stefan problem studied in Section 2.3. The main difference with Section 2.3 is that the monotonicity of the velocity of the moving interface, i.e. $\dot{s}(t) > 0$, is not guaranteed in the two-phase Stefan problem due to the reversible melting and freezing process.

Backstepping transformation

We use the same backstepping transformation as (4.133) (4.134), namely,

$$w(x,t) = u(x,t) - \frac{\beta_l}{\alpha_l}\int_x^{s(t)} \phi(x-y)u(y,t)dy - \phi(x-s(t))X(t), \tag{5.33}$$

$$\phi(x) = \frac{1}{\beta_l}(cx-\varepsilon), \tag{5.34}$$

where $\varepsilon > 0$ is a parameter to be determined in the stability analysis. Thus, the associated target system is derived as

$$w_t(x,t) = \alpha_l w_{xx}(x,t) + \frac{c}{\beta_l}\dot{s}(t)X(t), \tag{5.35}$$

$$w(s(t),t) = \frac{\varepsilon}{\beta_l}X(t), \tag{5.36}$$

$$\dot{X}(t) = -cX(t) - \beta_l w_x(s(t),t). \tag{5.37}$$

Taking the derivative of (5.33) in x, we obtain

$$w_x(x,t) = u_x(x,t) - \frac{\varepsilon}{\alpha_l}u(x,t) - \frac{c}{\alpha_l}\int_x^{s(t)} u(y,t)dy - \frac{c}{\beta_l}X(t). \tag{5.38}$$

For a standard backstepping procedure, the boundary condition at $x = 0$ of the target system leads to the control design. If we chose $w_x(0,t) = 0$, we obtain a stable target system in the case of fixed domain. However, the Stefan problem imposes the heat input to maintain positive in order to guarantee the model validity condition. The choice of $w_x(0,t) = 0$ leads to the control design which does not ensure the positivity. Instead, by the energy conservation law (5.15), (5.16), we can see that the following choice of the state feedback controller ensures the positivity

$$q_c(t) = -c\left(\frac{1}{\alpha_l}\int_0^{s(t)} u(y,t)dy + X(t)\right), \tag{5.39}$$

as developed in "*energy shaping control*". Hence, we design the control law with respect to $X(t)$ as (5.39) and obtain the boundary condition of the target system. Setting $x = 0$ in (5.38) and applying (5.39), the boundary condition at $x = 0$ is obtained by

$$w_x(0,t) = -\frac{\varepsilon}{\alpha_l} u(0,t), \tag{5.40}$$

of which the right hand side should be rewritten with respect to (w,X) by using the same inverse transformation as (4.139) (4.140).

$$w_x(0,t) = -\frac{\varepsilon}{\alpha_l}\left[w(0,t) - \frac{\beta_l}{\alpha_l}\int_0^{s(t)} \psi(-y)w(y,t)dy - \psi(-s(t))X(t)\right]. \tag{5.41}$$

Therefore, the target (w,X)-system is written as (5.35)–(5.37) and (5.41) as a closed form. Note that this target (w,X)-system is not a standard choice due to its complicated structure through the coupling between each state. Nevertheless, the target system is proven to satisfy the exponential stability estimate in L_2 norm with the help of the properties derived in the next section.

5.4 Analysis of the Closed-Loop System

Guaranteeing the conditions of the model validity

Analogously to the problems so far, we prove the positivity of input. Taking the time derivative of the control law (5.39) along the solution of the system yields

$$\dot{q}_c(t) = -cq_c(t). \tag{5.42}$$

Hence, the state feedback control law achieves the same solution as the exponentially decaying function in time, described by

$$q_c(t) = q_c(0)e^{-ct}. \tag{5.43}$$

Since Assumption 11 is equivalent with $q_c(0) > 0$, (5.43) ensures

$$q_c(t) > 0, \quad \forall t > 0, \tag{5.44}$$

Applying Lemma 2 directly leads to

$$u(x,t) > 0, \quad u_x(s(t),t) < 0, \tag{5.45}$$

$$v(x,t) < 0, \quad v_x(s(t),t) < 0, \tag{5.46}$$

$$0 < s(t) < L. \tag{5.47}$$

Stability analysis for the liquid phase with modified interface

We show the stability of (w,X)-system given in (5.35)–(5.37) and (5.41) by using the same approach as the one in Section 4.3 for $d(t) = 0$. Namely, by considering the Lyapunov function

$$V(t) = \frac{1}{2\alpha_l}||w||^2 + \frac{\varepsilon}{2\beta_l^2}X(t)^2, \tag{5.48}$$

where the L_2 norm is denoted as $||w|| := \sqrt{\int_0^{s(t)} w(x,t)^2 dx}$, we can derive that for sufficiently small ε the time derivative satisfies the following inequality:

$$\begin{aligned}\dot{V} \leq & -\frac{1}{8L^2}||w||^2 - \frac{c\varepsilon}{4\beta_l^2}X(t)^2 \\ & + \frac{|\dot{s}(t)|}{2\alpha_l}\left(\left(\frac{\varepsilon}{\beta_l}X(t)\right)^2 + 2\frac{c}{\beta_l}\left|\int_0^{s(t)} w(x,t)dx X(t)\right|\right). \end{aligned} \tag{5.49}$$

Since $u_x(s(t),t) < 0$ and $v_x(s(t),t) < 0$ by (5.45) and (5.46), we have $|\dot{s}(t)| \leq -\beta_l u_x(s(t),t) - \beta_s v_x(s(t),t)$. Let us introduce

$$z(t) := X(t) + \frac{\beta_s}{\alpha_s}\int_{s(t)}^{L} v(x,t)dx < 0, \tag{5.50}$$

where the negativity follows from (5.46) and (5.47). Taking the time derivative of (5.50) yields

$$\dot{z}(t) = -\beta_l u_x(s(t),t) - \beta_s v_x(s(t),t) > 0, \tag{5.51}$$

where the positivity follows from (5.45) and (5.46). Applying this inequality and Young's and Cauchy Schwarz inequalities to the last term of (5.49), we arrive at

$$\begin{aligned}\dot{V} \leq & -\frac{1}{8L^2}||w||^2 - \frac{c\varepsilon}{4\beta_l^2}X(t)^2 + \frac{\dot{z}(t)}{2\alpha_l}\left(\frac{c^2L}{\varepsilon^2}||w||^2 + 2\frac{\varepsilon^2}{\beta_l^2}X(t)^2\right) \\ \leq & -bV + a\dot{z}(t)V, \end{aligned} \tag{5.52}$$

where $b = \min\left\{\frac{\alpha_l}{4L^2}, \frac{c}{2}\right\}$, $a = \frac{1}{2\alpha_l}\max\left\{\frac{2\alpha_l c^2 L}{\varepsilon^2}, 4\varepsilon\right\}$. Consider the following functional

$$W = Ve^{-az(t)}. \tag{5.53}$$

Taking the time derivative of (5.53) and applying (5.52), one can deduce the following differential inequality:

$$\dot{W} = \left(\dot{V} - a\dot{z}(t)V\right) e^{-az(t)} \leq -bW. \tag{5.54}$$

Hence, $W(t) \leq W_0 e^{-bt}$ is satisfied, which leads to

$$V(t) \leq e^{a(z(t)-z(0))} V_0 e^{-bt} \leq \delta V_0 e^{-bt}, \tag{5.55}$$

where δ is defined as a constant which bounds $\delta > e^{-az(0)}$, of which the existence is ensured by Assumptions 9-11. Hence, (w,X)-system is shown to be exponentially stable.

Consider the Lyapunov function

$$V_1 = ||u||^2 = \int_0^{s(t)} u(x,t)^2 dx. \tag{5.56}$$

Due to the invertibility of the transformations, there exist positive constants $\underline{M} > 0$, $\bar{M} > 0$ such that the following norm equivalence between (u,X)-system and (w,X)-system holds:

$$\underline{M}\left(V_1(t) + X(t)^2\right) \leq V(t) \leq \bar{M}\left(V_1(t) + X(t)^2\right). \tag{5.57}$$

Hence, by (5.55), the following exponential stability estimate of the (u,X)-system is shown:

$$V_1(t) + X(t)^2 \leq \frac{\bar{M}}{\underline{M}} \delta \left(V_1(0) + X(0)\right) e^{-bt}. \tag{5.58}$$

Stability analysis for the solid phase

Let V_2 be the L_2-norm of the reference error of the solid temperature v defined by

$$V_2(t) = ||v||^2 = \int_{s(t)}^{L} v(x,t)^2 dx. \tag{5.59}$$

Taking the time derivative of (5.59) along the solution of (5.26)–(5.27), and applying Poincare's inequality with the help of $0 < s(t) < L$, we obtain

$$\begin{aligned} \dot{V}_2 =& -\alpha_s \int_{s(t)}^{L} v_x(x,t)^2 dx, \\ \leq& -\frac{\alpha_s}{2(L-s(t))^2} V_2 < -\frac{\alpha_s}{2L^2} V_2. \end{aligned} \tag{5.60}$$

By comparison principle, the differential inequality (5.60) yields the following exponential decay of the norm

$$V_2(t) \leq V_2(0) e^{-\frac{\alpha_s}{2L^2} t}. \tag{5.61}$$

Stability of overall liquid-interface-solid system

Applying Young's and Cauchy Schwartz inequalities to the definition of X given in (5.29) with the help of $0 < s(t) < L$ yields the following norm estimate

$$X(t)^2 \leq 2Y(t) + \frac{2L\beta_s^2}{\alpha_s^2} V_2, \tag{5.62}$$

where we defined $Y(t) = |s(t) - s_r|^2$. On the other hand, the bound of $Y(t)$ with respect to $X(t)^2$ and V_2 are also obtained the similar manner to (5.62), which yields

$$Y(t) \leq 2X(t)^2 + \frac{2L\beta_s^2}{\alpha_s^2} V_2. \tag{5.63}$$

Finally, summing the norms of the liquid temperature, the interface position, and the solid temperature, respectively, and applying (5.63), (5.55), (5.61), and (5.62), we can see that there exists a positive constant M such that the following estimate of the norm holds:

$$\begin{aligned} &V_1(t)+Y(t)+V_2(t) \\ \leq &M\left(V_1(0)+Y(0)+V_2(0)\right)e^{-\min\left\{b,\frac{\alpha_s}{2L^2}\right\}t}, \end{aligned} \tag{5.64}$$

which completes the proof of Theorem 4.

5.5 Robustness to Uncertainties of Physical Parameters

The control design (5.20) requires the physical parameters of both the liquid and solid phases, however, in practice these parameters are uncertain. Guaranteeing the robustness of the stability of the closed-loop system with respect to such parametric uncertainties is significant. Suppose that the proposed control law is replaced by

$$\begin{aligned} q_{\mathrm{c}}(t) = -c\Bigg(&\frac{k_{\mathrm{l}}}{\alpha_{\mathrm{l}}}(1+\varepsilon_{\mathrm{l}})\int_0^{s(t)}(T_{\mathrm{l}}(x,t)-T_{\mathrm{m}})\mathrm{d}x \\ &+\frac{k_{\mathrm{s}}}{\alpha_{\mathrm{s}}}(1+\varepsilon_{\mathrm{s}})\int_{s(t)}^{L}(T_{\mathrm{s}}(x,t)-T_{\mathrm{m}})\mathrm{d}x+\gamma(1+\varepsilon_{\mathrm{f}})(s(t)-s_{\mathrm{r}})\Bigg), \end{aligned} \tag{5.65}$$

where ε_{l}, ε_{s}, and ε_{f} are the uncertainties of physical parameters satisfying $\varepsilon_{\mathrm{l}} > -1$, $\varepsilon_{\mathrm{s}} \geq -1$, and $\varepsilon_{\mathrm{f}} \geq -1$. We state the following theorem.

Theorem 5 *Under Assumptions 9, 10, and assuming that the setpoint is chosen to satisfy* $q_{\mathrm{c}}(0) > 0$ *with* (5.65) *and* $s_{\mathrm{r}} < L$*, consider the closed-loop system consisting of the plant* (5.1)–(5.5) *and the control law* (5.65)*. Then, for any perturbations* $(\varepsilon_{\mathrm{l}}, \varepsilon_{\mathrm{s}}, \varepsilon_{\mathrm{f}})$ *satisfying*

$$\varepsilon_{\mathrm{l}} \geq \varepsilon_{\mathrm{f}} \geq \varepsilon_{\mathrm{s}}, \tag{5.66}$$

there exists $R > 0$ *such that if*

$$\left| \frac{\varepsilon_{\mathrm{f}} - \varepsilon_{\mathrm{l}}}{1 + \varepsilon_{\mathrm{l}}} \right| < R, \tag{5.67}$$

then the closed-loop system maintains model validity (5.6)-(5.8) *and the exponential stability at the origin holds for the norm defined in* (5.22).

Theorem 5 implies that if we know lower and upper bounds of the physical parameters as $\underline{k}_{\mathrm{l}} \leq k_{\mathrm{l}} \leq \overline{k}_{\mathrm{l}}$, $\underline{\alpha}_{\mathrm{l}} \leq \alpha_{\mathrm{l}} \leq \overline{\alpha}_{\mathrm{l}}$, and $\underline{\gamma} \leq \gamma \leq \overline{\gamma}$, then the most conservative choice of the control law to satisfy the condition (5.66) is given by

$$q_{\mathrm{c}}(t) = -c \left(\frac{\overline{k}_{\mathrm{l}}}{\underline{\alpha}_{\mathrm{l}}} \int_0^{s(t)} (T_{\mathrm{l}}(x,t) - T_{\mathrm{m}}) \mathrm{d}x + \underline{\gamma}(s(t) - s_{\mathrm{r}}) \right), \tag{5.68}$$

which does not incorporate the solid phase temperature. This design requires less information than the exact feedback design (5.20), however, the conditions $q_{\mathrm{c}}(0) > 0$ and $s_{\mathrm{r}} < L$, which lead to

$$s_0 + \frac{\overline{k}_{\mathrm{l}}}{\underline{\alpha}_{\mathrm{l}} \underline{\gamma}} \int_0^{s_0} (T_{\mathrm{l},0}(x) - T_{\mathrm{m}}) \mathrm{d}x < s_{\mathrm{r}} < L, \tag{5.69}$$

are more restrictive than Assumption 11 for the unperturbed design (5.20), which causes a tradeoff between the parameters' uncertainty and the restriction of the setpoint.

The proof of Theorem 5 is established by following similar steps.

Closed-loop analysis

First, we derive an analogous result on the properties of the closed-loop system to those derived in Section 5.4 by employing contradiction approach twice. Assume that there exists a

finite time $t^* > 0$ such that

$$q_{\mathrm{c}}(t) > 0, \quad \forall t \in [0, t^*), \tag{5.70}$$

$$q_{\mathrm{c}}(t^*) = 0. \tag{5.71}$$

Then, by Lemma 2, for $t \in (0, \bar{t})$ where $\bar{t} := \sup_{t \in (0,t^*)} \{t | s(t) \in (0, L)\}$, the solution exists and unique with satisfying (5.6)–(5.8). If $\bar{t} < t^*$, then it implies $s(\bar{t}) = 0$ or $s(\bar{t}) = L$ hold. However, under Assumption 10 and $q_{\mathrm{c}}(t) > 0$ for all $t \in [0, t^*)$, it holds that

$$s(t) > s_\infty > 0, \quad \forall t \in (0, t^*), \tag{5.72}$$

and hence $s(\bar{t}) \neq 0$. Moreover, applying $q_{\mathrm{c}}(t) > 0$ and (5.6) and (5.7) for all $t \in (0, \bar{t})$ to the feedback design (5.65), one can see that $s(\bar{t}) \neq L$. Hence, $\bar{t} = t^*$. Taking the time derivative of the control law (5.65), we get the following differential equation:

$$\begin{aligned} \dot{q}_{\mathrm{c}}(t) =& -c(1+\varepsilon_{\mathrm{l}})q_{\mathrm{c}}(t) - (\varepsilon_{\mathrm{l}} - \varepsilon_{\mathrm{f}})ck_{\mathrm{l}} \frac{\partial T_{\mathrm{l}}}{\partial x}(s(t), t) \\ &+ (\varepsilon_{\mathrm{s}} - \varepsilon_{\mathrm{f}})ck_{\mathrm{s}} \frac{\partial T_{\mathrm{s}}}{\partial x}(s(t), t), \qquad (5.73) \\ \geq& -c(1+\varepsilon_{\mathrm{l}})q_{\mathrm{c}}(t), \quad \forall t \in (0, t^*), \qquad (5.74) \end{aligned}$$

where the inequality from (5.73) to (5.74) follows from (5.66) and Hopf's lemma with the help of (5.6) and (5.7) for all $t \in (0, t^*)$. Therefore, applying comparison principle to (5.74), one can show that

$$q_{\mathrm{c}}(t) > q_{\mathrm{c}}(0)e^{-ct}, \quad \forall t \in (0, t^*), \tag{5.75}$$

which leads to the contradiction with the imposed assumption (5.71). Thus, there does not exist such t^*, from which we conclude

$$q_{\mathrm{c}}(t) \geq 0, \quad \forall t \geq 0, \tag{5.76}$$

and the well-posedness and the conditions (5.6)–(5.8) holds for all $t \geq 0$.

Next, we prove the stability of the perturbed closed-loop in the similar manner as the proof of Theorem 4. Let $\bar{c} = c(1+\varepsilon_{\mathrm{l}})$, and redefine the gain kernel function as $\phi = \frac{1}{\beta_{\mathrm{l}}}(\bar{c}x - \varepsilon)$ associated with the backstepping transformation (5.33). Then, the target systems is described as

$$w_t(x,t) = \alpha_{\mathrm{l}} w_{xx}(x,t) + \frac{\bar{c}}{\beta_{\mathrm{l}}} \dot{s}(t) X(t), \tag{5.77}$$

$$w(s(t),t) = \frac{\varepsilon}{\beta_{\mathrm{l}}} X(t), \tag{5.78}$$

$$\dot{X}(t) = -\bar{c}X(t) - \beta_{\mathrm{l}} w_x(s(t),t), \tag{5.79}$$

and the boundary condition at $x = 0$ is given by

$$w_x(0,t) = -\frac{\varepsilon}{\alpha_{\mathrm{l}}} u(0,t) + d(t), \tag{5.80}$$

where $d(t)$ is the perturbation caused by the parametric uncertainties, given by

$$d(t) = \frac{\varepsilon_{\mathrm{s}} - \varepsilon_{\mathrm{f}}}{1+\varepsilon_{\mathrm{l}}} \frac{\bar{c} k_{\mathrm{s}}}{k_{\mathrm{l}} \alpha_{\mathrm{s}}} \int_{s(t)}^{L} v(x,t)\mathrm{d}x + \frac{\varepsilon_{\mathrm{f}} - \varepsilon_{\mathrm{l}}}{1+\varepsilon_{\mathrm{l}}} \frac{\bar{c}}{k_{\mathrm{l}}} X(t). \tag{5.81}$$

We consider the Lyapunov function defined by (5.48). The time derivative of $V(t) = \frac{1}{2\alpha_{\mathrm{l}}}||w||^2 +$

$\frac{\varepsilon}{2\beta_1^2}X(t)^2$ along the perturbed target system (5.77)–(5.80) satisfies the following inequality

$$\begin{aligned}\dot{V} \leq & -\left(1-\frac{2\varepsilon L}{\alpha_1}\left(3+\frac{32\bar{c}L^2}{\alpha_1}\right)\right)||w_x||^2 \\ & -\frac{\varepsilon}{\beta_1^2}\left(\frac{\bar{c}}{2}-\frac{\varepsilon^2}{\alpha_1}\left(3+\frac{32\bar{c}L^2}{\alpha_1}\right)\right)X(t)^2 - w(0,t)d(t), \\ & +\frac{\dot{s}(t)}{2\alpha_1}\left(\left(\frac{\varepsilon}{\beta_1}X(t)\right)^2+2\frac{\bar{c}}{\beta_1}\int_0^{s(t)}w(x,t)\mathrm{d}xX(t)\right). \end{aligned} \tag{5.82}$$

Applying Young's and Agmon's inequalities, the perturbation is bounded by

$$\begin{aligned}-w(0,t)d(t) \leq & \frac{1}{8L}w(0,t)^2+2Ld(t)^2, \\ \leq & \frac{1}{4L}w(s(t),t)^2+\frac{1}{2}||w_x||^2+2Ld(t)^2, \\ \leq & \frac{\varepsilon^2}{4L}X(t)^2+\frac{1}{2}||w_x||^2+2Ld(t)^2. \end{aligned} \tag{5.83}$$

Moreover, applying Young's and Cauchy Schwarz inequalities to the square of (5.81), we get

$$d(t)^2 = 2\left(\frac{\varepsilon_s-\varepsilon_f}{1+\varepsilon_1}\frac{\bar{c}k_s}{k_1\alpha_s}\right)^2 L\int_{s(t)}^{L}v(x,t)^2\mathrm{d}x+2\left(\frac{\varepsilon_f-\varepsilon_1}{1+\varepsilon_1}\frac{\bar{c}}{k_1}\right)^2 X(t)^2. \tag{5.84}$$

Applying (5.83) and (5.84) to (5.82), we can see that there exists sufficiently small $\varepsilon > 0$ such that the following inequality holds

$$\begin{aligned}\dot{V} \leq & -\frac{1}{16L^2}||w||^2-\bar{c}\left(\frac{\varepsilon}{4\beta_1^2}-\frac{4L\bar{c}}{k_1^2}\left|\frac{\varepsilon_f-\varepsilon_1}{1+\varepsilon_1}\right|^2\right)X(t)^2 \\ & +4L^2\left(\frac{\varepsilon_s-\varepsilon_f}{1+\varepsilon_1}\frac{\bar{c}k_s}{k_1\alpha_s}\right)^2\int_{s(t)}^{L}v(x,t)^2\mathrm{d}x \\ & +\frac{\dot{s}(t)}{2\alpha_1}\left(\left(\frac{\varepsilon}{\beta_1}X(t)\right)^2+2\frac{c}{\beta_1}\int_0^{s(t)}w(x,t)\mathrm{d}xX(t)\right). \end{aligned} \tag{5.85}$$

Therefore, if

$$\left|\frac{\varepsilon_f-\varepsilon_l}{1+\varepsilon_l}\right|^2<\frac{\varepsilon k_l^2}{32\beta_l^2 L\bar{c}}, \tag{5.86}$$

then the differential inequality (5.85) is led to

$$\begin{aligned}\dot{V}\leq&-\frac{1}{16L^2}||w||^2-\frac{\varepsilon\bar{c}}{8\beta_l^2}X(t)^2+4L^2\left(\frac{\varepsilon_s-\varepsilon_f}{1+\varepsilon_l}\frac{\bar{c}k_s}{k_l\alpha_s}\right)^2\int_{s(t)}^{L}v(x,t)^2\mathrm{d}x\\&+\frac{\dot{s}(t)}{2\alpha_l}\left(\left(\frac{\varepsilon}{\beta_l}X(t)\right)^2+2\frac{c}{\beta_l}\int_0^{s(t)}w(x,t)\mathrm{d}xX(t)\right).\end{aligned} \tag{5.87}$$

Since v-system is equivalent to the one in previous sections, the time derivative of $V_2=||v||^2$ satisfies the inequality (5.60), which is

$$\dot{V}_2\leq-\frac{\alpha_s}{2L^2}V_2. \tag{5.88}$$

Combining (5.60) and (5.87) with applying comparison principle, one can derive that there exist positive constants $M_1>0$ and $d_1>0$ such that the following decay of the norm holds

$$V(t)+V_2(t)\leq M_1(V(0)+V_2(0))e^{-d_1t}. \tag{5.89}$$

Using the procedure in the last section, we conclude Theorem 5.

5.6 Numerical Simulation

Simulation results are performed by considering a zinc whose physical parameters are given in Table 1. Under the identical choice of the physical parameters in the plant and control, we compare the performance of the proposed design in (5.20) (hereafter "two-phase design") and

Table 5.1: Physical properties of zinc of both the liquid phase and the solid phase.

Description	Symbol	Value
Liquid density	ρ_l	$6570\ \mathrm{kg \cdot m^{-3}}$
Solid density	ρ_s	$6890\ \mathrm{kg \cdot m^{-3}}$
Liquid heat capacity	c_l	$390\ \mathrm{J \cdot kg^{-1} \cdot K^{-1}}$
Solid heat capacity	c_s	$390\ \mathrm{J \cdot kg^{-1} \cdot K^{-1}}$
Liquid thermal conductivity	k_l	$130\ \mathrm{W \cdot m^{-1}}$
Solid thermal conductivity	k_s	$100\ \mathrm{W \cdot m^{-1}}$
Melting temperature	T_m	420 °C
Latent heat of fusion	ΔH^*	$120{,}000\ \mathrm{J \cdot kg^{-1}}$

the design

$$q_\mathrm{c}(t) = -c\left(\frac{k_\mathrm{l}}{\alpha_\mathrm{l}}\int_0^{s(t)}(T_\mathrm{l}(x,t)-T_\mathrm{m})\mathrm{d}x+\gamma(s(t)-s_\mathrm{r})\right), \tag{5.90}$$

(hereafter "one-phase design"). The stability under the "one-phase design" is guaranteed by Theorem 5 for the robustness analysis of the closed-loop system under the restriction of the setpoint to satisfy $q_\mathrm{c}(0) \geq 0$ for (5.90).

The material's length, the initial interface position, and the setpoint position are chosen as L = 1.0 m, s_0 = 0.4 m, and s_r = 0.5 m. The initial temperature profiles are set as $T_{\mathrm{l},0}(x) = \bar{T}_{\mathrm{l},0}(1-x/s_0)+T_\mathrm{m}$ and $T_{\mathrm{s},0}(x) = \bar{T}_{\mathrm{s},0}(1-(L-x)/(L-s_0))+T_\mathrm{m}$ with $\bar{T}_{\mathrm{l},0}$ = 10 °C and $\bar{T}_{\mathrm{s},0}$ = –200 °C. Then, the setpoint restrictions for both "two-phase design" and "one-phase design" are satisfied. The control gain is set as $c = 1.0 \times 10^{-2}$/s.

The closed-loop responses are implemented as depicted in Fig 5.3a-5.3c for both "two-phase design" (solid) and "one-phase design" (dash). Fig 5.3a shows the dynamics of the interface $s(t)$. We can observe that $s(t)$ decreases at first due to the freezing caused by the initial temperature of the solid phase, and after some time the interface position increases and converges to the setpoint owing to the melting heat input. Moreover, the interface dynamics under the "two-phase design" achieves faster convergence than that under the "one-phase design" with having a little

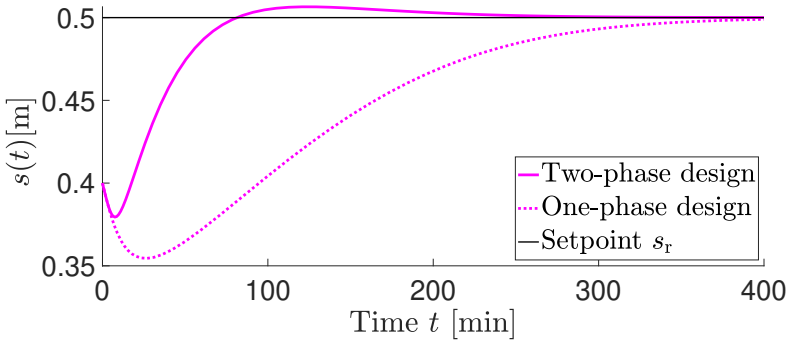

(a) Convergence of the interface to the setpoint s_{r} is observed for both controls, however, the proposed two-phase design achieves faster convergence as seen in the settling time in Fig. 5.4.

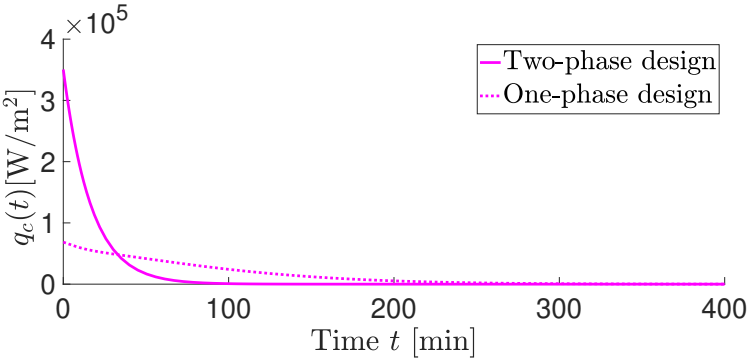

(b) Positivity of the heat input is satisfied for both control designs.

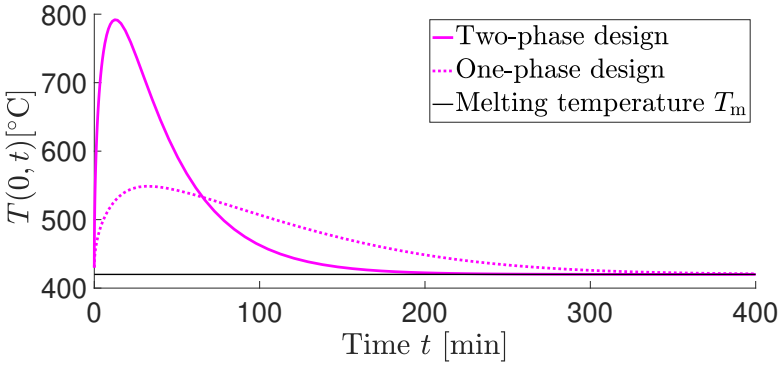

(c) The boundary temperature maintains above the melting temperature, and hence there is no appearance of a new solid phase from the controlled boundary $x = 0$ in the liquid phase.

Figure 5.3: The closed-loop responses under the proposed "two-phase" design (pink solid) and the "one-phase" design (pink dash).

overshoot as seen from Fig. 5.3a. Fig 5.3b shows the dynamics of the closed-loop control, and Fig 5.3c shows the dynamics of the boundary temperature of the liquid phase $T_{\mathrm{l}}(0,t)$. Fig 5.3b

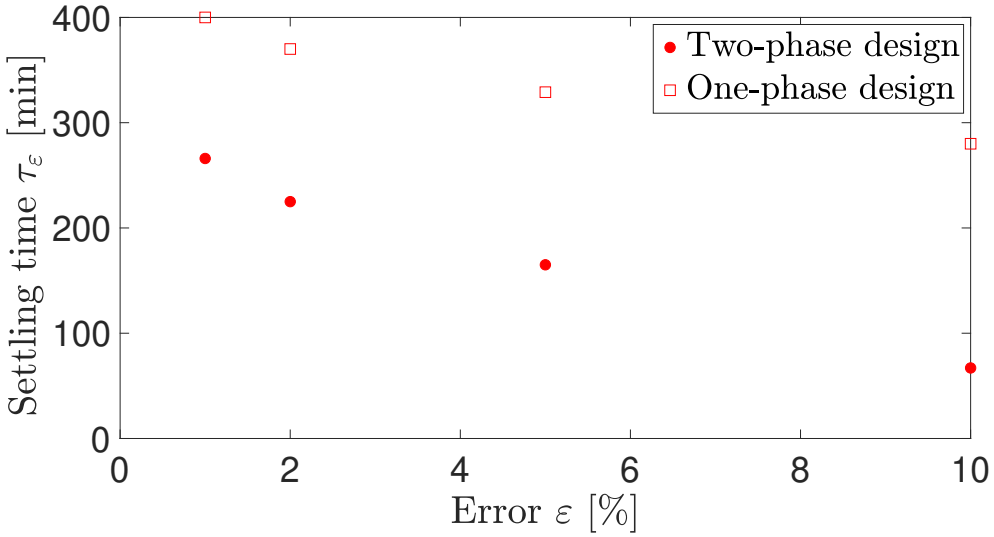

Figure 5.4: Settling time of the interface convergence in Fig. 5.3 (a) with respect to the error ε.

illustrates the positivity of the heat input $q_c(t) > 0$, and Fig. 5.3c illustrates the liquid boundary temperature being greater than the melting temperature, both of which are consistent with the derived properties. Hence, we can observe that the simulation results are consistent with the theoretical result we prove as model validity conditions and the stability analysis.

To compare the performance on the convergence speed between "two-phase design" and "one-phase design," we investigate the settling time τ_ε with respect to the error ε [%] of the interface position relative to the setpoint, mathematically defined by

$$\tau_\varepsilon := \inf_{\tau \geq 0} \left\{ \tau \middle| |s(t) - s_r| \leq |s_0 - s_r| \frac{\varepsilon}{100}, \quad \forall t \geq \tau \right\}. \tag{5.91}$$

Fig. 5.4 shows the value of τ_ε with $\varepsilon = 10, 5, 2, 1$ [%]. From the figure, it is observed that the convergence speed of "two-phase design" compared to the speed of the "one-phase design" is approximately four times faster for ε = 10[%], two times faster for ε = 5 [%], one and half times faster for both ε = 2 [%] and 1 [%], respectively. Hence, Fig. 5.4 validates superior performance of the proposed "two-phase design" compared to the "one-phase design".

5.7 Conclusion and Future Work

In this chapter, we presented the full state feedback control law of a single heat boundary input for the two-phase Stefan problem to stabilize the moving interface position at a desired setpoint. The main contribution is that we theoretically prove the global exponential stability of the closed-loop system of the two-phase Stefan problem with designing the state feedback control law by employing energy shaping and backstepping. While our present result is only on the stabilization of the moving interface at the setpoint with restricting the equillibrium temperature to only the uniform melting temperature, the simultaneous stabilization of the interface position and the temperature profile at arbitrary setpoint and temperature profiles following recent results in [177] for traffic congestion control with moving shockwave is considered as our future work. The application of extremum seeking control for online optimization of static maps to the Stefan problem following the recent results of [119, 51] is also a potential direction.

5.8 Acknowledgement

Chapter 5, in part, is a reprint of the material as it appears in:

- S. Koga and M. Krstic, "Control of the Two-Phase Stefan Problem via Single-Boundary Heat Input", *IEEE Conference on Decision and Control*, 2018,
- S. Koga and M. Krstic, "Single-Boundary Control of the Two-Phase Stefan System", *Systems & Control Letters*, vol. 135, p. 104573, 2020.

The dissertation author was the primary investigators and author of this paper.

Chapter 6

Sea Ice

6.1 Importance of the Arctic Sea Ice for Global Climate Model

The Arctic sea ice has been studied intensively in the field of climate and geoscience. One of the main reasons is due to ice-albedo feedback which influences climate dynamics through the high reflectivity of sea ice. The other reason is the rapid decline of the Arctic sea ice extent in the recent decade shown in several observations. These observations motivate the investigation of future sea ice amount. Several studies have developed a computational model of the Arctic sea ice and performed numerical simulations of the model with initial sea ice temperature profile. However, the spatially distributed temperature in sea ice is difficult to recover in realtime using a limited number of thermal sensors. Hence, the online estimation of the sea ice temperature profile based on some available measurements is crucial for the prediction of the sea ice thickness.

A thermodynamic model for the Arctic sea ice was firstly developed in [112] (hereafter MU71), in which the authors investigated the correspondence between the annual cycle pattern acquired from the simulation and empirical data of [159]. The model involves a temperature diffusion equation evolving on a spatial domain defined as the sea ice thickness. Due to melting or freezing phenomena, the aforementioned spatial domain is time-varying. Such a model is

called “Stefan problem” [60] which is described by a parabolic partial differential equation (PDE) with a state-dependent moving boundary driven by a Neumann boundary value.

Refined models of MU71 have been suggested in literature. For instance, [138] proposed a numerical model to achieve faster and accurate computation of MU71 by discretizing the temperature profile into some layers and neglecting the salinity effect. An energy-conserving model of MU71 was introduced in [15] by taking into account an internal brine pocket melting on surface ablation and the vertically varying salinity profile. Their thermodynamic model was demonstrated by [14] using a global climate model with a Lagrangian ice thickness distribution. Combining these two models, [173] developed an energy-conserving three-layer model of sea ice by treating the upper half of the ice as a variable heat capacity layer.

Remote sensing techniques have been employed to obtain the Arctic sea ice data in several studies. In [61], the authors suggested an algorithm to calculate sea ice surface temperature using the satellite measured brightness temperatures, which provided an excellent measurement of the actual surface temperature of the sea ice during the Arctic cold period. The Arctic sea ice thickness data were acquired in [105] through a satellite called ”ICESat” during 2003-2008 and compared with the data in [133] observed by a submarine during 1958-2000. More recent data describing the evolution of the sea ice thickness have been collected between 2010 and 2014 from the satellite called ”CryoSat-2” [104].

On the other hand, state estimation has been studied as a specific type of data assimilation which utilizes the numerical model along with the measured value. For finite dimensional systems associated with noisy measurements, a well-known approach is Kalman Filter. Another well-known method is the Luenberger type state observer, which reconstructs the state variable from partially measured variables. For the application to sea ice, [52] developed an adjoint-based method as an iterative state and parameter estimation for the coupled sea ice-ocean in the Labrador Sea and Baffin Bay to minimize an uncertainty-weighted model-data misfit in a least-square sense as suggested in [175], using Massachusetts Institute of Technology general

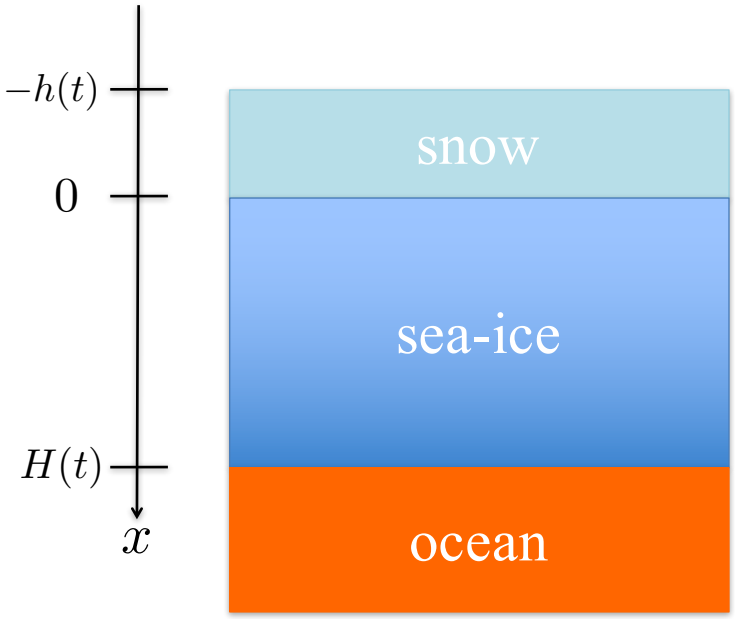

Figure 6.1: Schematic of the vertical one-dimensional model of the Arctic sea ice.

circulation model (MITgcm) developed in [111]. In [53], the same methodology was applied to reconstruct the global ocean and ice concentration. Their sea ice model is based on the zero-layer approximation of the numerical model in [138], which is a crude model lacking internal heat storage and promoting fast melting.

6.2 Thermodynamic Model of Arctic Sea Ice

The thermodynamic model of MU71 describes the time evolution of the sea ice temperature profile in the vertical axis along with its thickness, which also evolves in time due to accumulation or ablation caused by energy balance.

Fig. 6.1 provides a schematic of the Arctic sea ice model. During the seasons other than summer (July and August), the sea ice is covered by snow, and the surface position of the snow also evolves in time. Let $T_{\mathrm{s}}(x,t)$, $T_{\mathrm{i}}(x,t)$ denote the temperature profile of snow and sea ice, and $h(t)$ and $H(t)$ denote the thickness of snow and sea ice. The total incoming heat flux from the

atmosphere is denoted by F_{a}, and the heat flux from the ocean is denoted by F_{w}. The Arctic sea ice model suggested by MU71 gives governing equations of a Stefan-type free boundary problem formulated as

$$\begin{aligned} F_{\mathrm{a}} - I_0 - \sigma(T_{\mathrm{s}}(-h(t),t)+273)^4 + k_{\mathrm{s}}\frac{\partial T_{\mathrm{s}}}{\partial x}(-h(t),t) & \\ = \begin{cases} 0, & \text{if} \quad T_{\mathrm{s}}(-h(t),t) < T_{\mathrm{m1}}, \\ -q\dot{h}(t), & \text{if} \quad T_{\mathrm{s}}(-h(t),t) = T_{\mathrm{m1}}, \end{cases} & \end{aligned} \tag{6.1}$$

$$\rho_{\mathrm{s}} c_0 \frac{\partial T_{\mathrm{s}}}{\partial t}(x,t) = k_{\mathrm{s}}\frac{\partial^2 T_{\mathrm{s}}}{\partial x^2}(x,t), \forall x \in (-h(t),0), \tag{6.2}$$

$$T_{\mathrm{s}}(0,t) = T_{\mathrm{i}}(0,t), \tag{6.3}$$

$$k_{\mathrm{s}}\frac{\partial T_{\mathrm{s}}}{\partial x}(0,t) = k_0\frac{\partial T_{\mathrm{i}}}{\partial x}(0,t), \tag{6.4}$$

$$\rho c_{\mathrm{i}}(T_{\mathrm{i}},S)\frac{\partial T_{\mathrm{i}}}{\partial t}(x,t) = k_{\mathrm{i}}(T_{\mathrm{i}},S)\frac{\partial^2 T_{\mathrm{i}}}{\partial x^2}(x,t) + I_0\kappa_{\mathrm{i}}e^{-\kappa_{\mathrm{i}}x}, \ \ \forall x \in (0,H(t)), \tag{6.5}$$

$$T_{\mathrm{i}}(H(t),t) = T_{\mathrm{m2}}, \tag{6.6}$$

$$q\dot{H}(t) = k_{\mathrm{i}}\frac{\partial T_{\mathrm{i}}}{\partial x}(H(t),t) - F_{\mathrm{w}}, \tag{6.7}$$

where I_0, σ, k_{s}, ρ_{s}, c_0, k_0, ρ, T_{m1}, T_{m2}, and q are solar radiation penetrating the ice, Stefan-Boltzmann constant, thermal conductivity of snow, density of snow, heat capacity of pure ice, thermal conductivity of pure ice, density of pure ice, melting point of surface snow, melting point of bottom sea ice, and latent heat of fusion, respectively. The total heat flux from the air is given by

$$F_{\mathrm{a}} = (1-\alpha)F_{\mathrm{r}} + F_{\mathrm{L}} + F_{\mathrm{s}} + F_{\mathrm{l}}, \tag{6.8}$$

where F_{r}, F_{L}, F_{s}, F_{l}, and α denote the incoming solar short-wave radiation, the long-wave radiation from the atmosphere and clouds, the flux of sensible heat, the latent heat in the adjacent air, and the surface albedo, respectively. The heat capacity and thermal conductivity of the sea ice are

affected by the salinity as

$$c_{\mathrm{i}}(T_{\mathrm{i}},S(x)) = c_0 + \frac{\gamma_1 S(x)}{T_{\mathrm{i}}(x,t)^2},\ k_{\mathrm{i}}(T_{\mathrm{i}},S(x)) = k_0 + \frac{\gamma_2 S(x)}{T_{\mathrm{i}}(x,t)}, \tag{6.9}$$

where $S(x)$ denotes the salinity in the sea ice. γ_1 and γ_2 represent the weight parameters. The thermodynamic model (6.1)-(6.7) allows us to predict the future thickness $(h(t),H(t))$ and the temperature profile $(T_{\mathrm{s}},T_{\mathrm{i}})$ given the accurate initial data. However, from a practical point of view, it is not feasible to obtain a complete temperature profile due to a limited number of thermal sensors. To deal with the problem, the estimation algorithm is designed so that the state estimation converges to the actual state starting from an initial estimate.

6.3 Annual Cycle Simulation of Sea Ice Thickness

For the computation, we use boundary immobilization method and finite difference semi-discretization [102] with 100-point mesh in space, and the resulting approximated ODEs are calculated by using MATLAB ode15 solver.

Input Parameters

The input parameters are taken from [112] in SI units and Table 6.1 shows the monthly averaged values of heat fluxes coming from the atmosphere for each month. Table 6.2 shows the physical parameters of snow and sea ice. Following [15], the salinity profile is described by

$$S(x) = A\left[1-\cos\left\{\pi\left(\frac{x}{H(t)}\right)^{\frac{n}{m+\frac{x}{H(t)}}}\right\}\right], \tag{6.10}$$

where $A = 1.6$, $n = 0.407$, and $m = 0.573$.

Table 6.1: Average monthly values for the energy fluxes.

Symbol	F_{r}	F_{L}	F_{s}	F_{l}	α
Unit	W/m^2	W/m^2	W/m^2	W/m^2	
Jan.	0	168	19.0	0	$\cdots$
Feb.	0	166	12.3	-0.323	$\cdots$
Mar.	30.7	166	11.6	-0.484	0.83
Apr.	160	187	4.68	-1.45	0.81
May.	286	244	-7.26	-7.43	0.82
Jun.	310	291	-6.30	-11.3	0.78
Jul.	220	308	-4.84	-10.3	0.64
Aug.	145	302	-6.46	-10.7	0.69
Sep.	59.7	266	-2.74	-6.30	0.84
Oct.	6.46	224	1.61	-3.07	0.85
Nov.	0	181	9.04	-0.161	$\cdots$
Dec.	0	176	12.8	-0.161	$\cdots$

Table 6.2: Physical parameters of snow and sea ice.

Symbol	**Meaning**	**Unit**	**Value**
ρ_{s}	density (snow)	kg/m^3	330
k_s	conductivity (snow)	W/m/°C	0.31
ρ	density (ice)	kg/m^3	917
c_0	heat capacity (ice)	J/kg/°C	2110
k_0	conductivity (ice)	W/m/°C	2.034
γ_1	weight of heat capacity	kJ °C/kg	18.0
γ_2	weight of conductivity	W/m	0.117
I_0	solar radiation	W/m^2	1.59
κ_{i}	penetration rate	/m	1.5
T_{m1}	melting temperature of sea ice at surface	°C	-0.1
T_{m2}	melting temperature of sea ice at bottom	°C	-1.8

Simulation Test of MU71

Using the given data, firstly the simulation of (6.1)-(6.7) is performed and showed in Fig. 6.2 to recover the evolution of $h(t)$ and $H(t)$ in the annual season as in [112]. The dynamic behavior of the snow surface and the bottom of sea ice are shown in Fig. 6.2 (a), and the time evolution of the temperature profile in sea ice is illustrated in Fig. 6.2 (b). We can see that both of Fig. 6.2 (a) and (b) have a good agreement with the simulation results shown in [112].

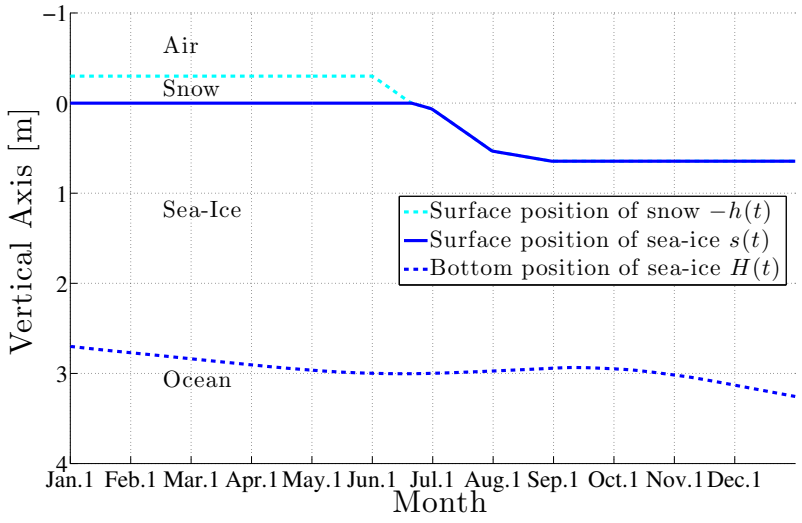

(a) Thickness evolution of the snow and sea ice.

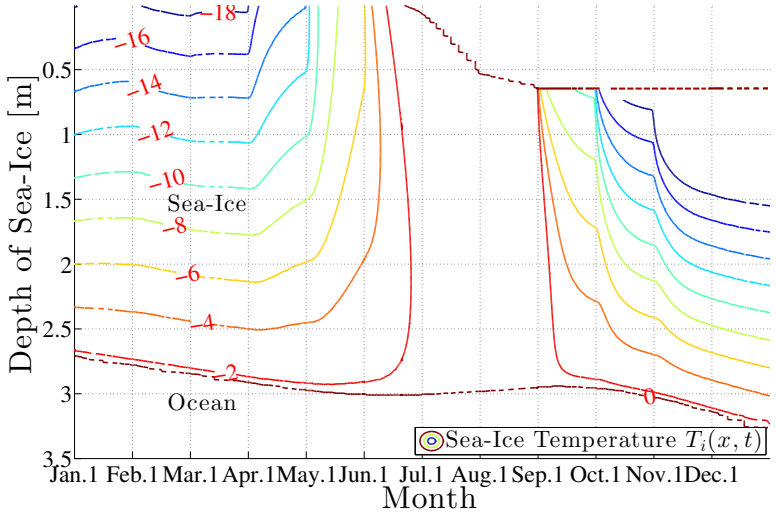

(b) Time evolution of temperature profile in sea ice.

Figure 6.2: Simulation tests of the plant (6.1)–(6.7) on annual cycle. Both (a) and (b) are in good agreement with the simulation results in [112].

6.4 Temperature Profile Estimation

In this section, we derive the estimation algorithm utilizing some available measurements and show the exponential convergence of the designed estimation to a simplified sea ice model.

The ice thickness and surface temperature are measured in several studies [61, 105, 133]. It is indeed typical to check observability before observer design, at least for systems on a constant domain (see [118] for instance). Here, we start with the observer design that is accompanied by a proof of exponential stability, which ensures the states' detectability.

Simplification of the Model

For the sake of the design and stability proof, we give a simplification on the system (6.1)-(6.7). The effect of the salinity profile on the physical parameters is assumed to be sufficiently small so that it can be negligible, i.e. $S(x) = 0$. Therefore, the heat equation of the sea ice temperature (6.5) is rewritten as

$$\frac{\partial T_{\mathrm{i}}}{\partial t}(x,t) = D_{\mathrm{i}} \frac{\partial^2 T_{\mathrm{i}}}{\partial x^2}(x,t) + \bar{I}_0 \kappa_{\mathrm{i}} e^{-\kappa_{\mathrm{i}} x},\ \forall x \in (0, H(t)), \tag{6.11}$$

where the diffusion coefficient is defined as $D_{\mathrm{i}} = k_0/\rho c_0$. Next, we impose the following assumptions.

Assumption 12 *The thickness $H(t)$ is positive and upper bounded, i.e. there exists $\bar{H} > 0$ such that $0 < H(t) < \bar{H}$, for all $t \geq 0$.*

Assumption 13 *$\dot{H}(t)$ is bounded, i.e., there exists $M > 0$ such that $|\dot{H}(t)| < M$, for all $t \geq 0$.*

According to [105], the observation data of the sea ice's thickness from the 1950s to 2008 show that the maximum value including the uncertainty is less than 5[m]. Moreover, the largest variation of the thickness in a snow-covered season of a year essentially happens from December to March as an accumulation, and most of the literature shows at most 20 [cm] accumulation per month. Hence, conservatively it is plausible to set $\bar{H} = 10$ [m], and $M = 50[\text{cm/Month}] = 1.9 \times 10^{-7}[\text{m/s}]$.

Mathematically, the existence of the classical solution of the simple Stefan problem given by (6.11) and (6.6)–(6.7) has been established in literature. We refer the readers to follow [60] for the detailed explanation. The solution of the original sea ice model (6.1)–(6.7) has not been studied due to its high complexity.

Observer Structure

Suppose that the sea ice thickness and the ice surface temperature are obtained as measurements $\mathcal{Y}_1(t)$ and $\mathcal{Y}_2(t)$, i.e.

$$\mathcal{Y}_1(t) = H(t), \quad \mathcal{Y}_2(t) = T_{\mathrm{i}}(0,t). \tag{6.12}$$

The state estimate $\hat{T}_{\mathrm{i}}$ of the sea ice temperature is governed by a copy of the plant (6.11) and (6.6)-(6.7) plus the error injection of $H(t)$, namely, as follows:

$$\frac{\partial \hat{T}_{\mathrm{i}}}{\partial t}(x,t) = D_{\mathrm{i}} \frac{\partial^2 \hat{T}_{\mathrm{i}}}{\partial x^2}(x,t) + \bar{I}_0 \kappa_{\mathrm{i}} e^{-\kappa_{\mathrm{i}} x} - p_1(x,t)\left(\mathcal{Y}_1(t) - \hat{H}(t)\right), \ \forall x \in (0, H(t)) \tag{6.13}$$

$$\hat{T}_{\mathrm{i}}(0,t) = \mathcal{Y}_2(t) - p_2(t)\left(\mathcal{Y}_1(t) - \hat{H}(t)\right), \tag{6.14}$$

$$\hat{T}_{\mathrm{i}}(H(t),t) = T_{\mathrm{m2}} - p_3(t)\left(\mathcal{Y}_1(t) - \hat{H}(t)\right), \tag{6.15}$$

$$\dot{\hat{H}}(t) = p_4(t)\left(\mathcal{Y}_1(t) - \hat{H}(t)\right) + \beta \frac{\partial \hat{T}_{\mathrm{i}}}{\partial x}(\mathcal{Y}_1(t),t) - \frac{F_{\mathrm{w}}}{q}, \tag{6.16}$$

where $\beta := \frac{k_{\mathrm{i}}}{q}$. Next, we define the estimation error states as

$$\tilde{T}(x,t) := -(T_{\mathrm{i}}(x,t) - \hat{T}_{\mathrm{i}}(x,t)), \quad \tilde{H}(t) := H(t) - \hat{H}(t), \tag{6.17}$$

where the negative sign is added to be consistent with the description developed in Chapter 3 for the liquid phase. Subtraction of the observer system (6.13)-(6.16) from the system (6.11) and

(6.6)-(6.7) yields the estimation error system as

$$\frac{\partial \tilde{T}}{\partial t}(x,t) = D_{\mathrm{i}} \frac{\partial^2 \tilde{T}}{\partial x^2}(x,t) - p_1(x,t)\tilde{H}(t),\ \forall x \in (0, H(t)) \tag{6.18}$$

$$\tilde{T}(0,t) = -p_2(t)\tilde{H}(t), \tag{6.19}$$

$$\tilde{T}(H(t),t) = -p_3(t)\tilde{H}(t), \tag{6.20}$$

$$\dot{\tilde{H}}(t) = -p_4(t)\tilde{H}(t) - \beta \frac{\partial \tilde{T}}{\partial x}(H(t),t). \tag{6.21}$$

Our goal is to design the observer gains $p_1(x,t)$, $p_2(t)$, $p_3(t)$, $p_4(t)$ so that the temperature error $\tilde{T}$ converges to zero. The main theorem of this paper is stated as follows.

Theorem 12 *Let Assumptions 12 and 13 hold. Consider the estimation error system* (6.18)-(6.21) *with the design of the observer gains*

$$p_1(x,t) = \frac{c\lambda x}{\beta} \frac{I_1(z)}{z} + \left(\frac{\varepsilon H(t)}{D_{\mathrm{i}}} - \frac{3}{\beta} \right) \lambda^2 x \frac{I_2(z)}{z^2} + \frac{\lambda^3 x^3}{D_{\mathrm{i}} \beta} \frac{I_3(z)}{z^3}, \tag{6.22}$$

$$p_2(t) = 0, \tag{6.23}$$

$$p_3(t) = -\frac{\lambda}{2\beta} H(t) - \varepsilon, \tag{6.24}$$

$$p_4(t) = c - \frac{\lambda}{2} \left(1 - \frac{\lambda H(t)^2}{8 D_{\mathrm{i}}} \right) + \frac{\beta \lambda}{2 D_{\mathrm{i}}} \varepsilon H(t), \tag{6.25}$$

where $\lambda > 0$, $c > 0$, *and* $\varepsilon > 0$ *are positive free parameters,* z *is defined by*

$$z := \sqrt{\bar{\lambda}(H(t)^2 - x^2)}, \tag{6.26}$$

where $\bar{\lambda} := \frac{\lambda}{D_{\mathrm{i}}}$, *and* $I_j(\cdot)$ *denotes the modified Bessel function of the* j*-th kind. Then, there exist positive constants* $c^* > 0$ *and* $\tilde{M} > 0$ *such that, for all* $c > c^*$, *the norm*

$$\Phi(t) := \int_0^{H(t)} \tilde{T}(x,t)^2 dx + \tilde{H}(t)^2 \tag{6.27}$$

satisfies the following exponential decay

$$\Phi(t) \leq \tilde{M}\Phi(0)e^{-\min\{\lambda,c\}t}, \tag{6.28}$$

namely, the origin of the estimation error system is exponentially stable in the spatial L_2 norm.

Remark 4 *The observer gains* (6.22)-(6.25) *include the thickness $H(t)$, so the gains are not precomputed offline, but are easily calculated* online*, along with the state estimation. Owing to the slow dynamics of the sea ice model, the computation time is much less than the time step size, which enables the real-time computation of the proposed observer.*

Remark 5 *The measurements* (6.12) *are assumed to be noiseless; however, in practice, the measured data accompany with some noise. Preferably the observer needs pre-filtering to deal with the noisy measurements.*

To handle the discrete-time measurements in practice as in [129], the designed observer should be discretized in time such as Euler or Runge-Kutta methods so that the estimation can be computed at every sampling of the discrete-time measurements. The free parameters λ, c, and ε have their physical units [1/s], [1/s], and [°C/m], respectively. Hence we can see the consistency of the physical units in the estimation error system (6.18)–(6.21) together with (6.22)–(6.25).

Gain Derivation via State Transformation

For the estimation error system (6.18)–(6.21), we apply the following invertible transformations:

$$\tilde{T}(x,t) = w(x,t) - \int_x^{H(t)} q(x,y)w(y,t)dy - \psi(x,H(t))\tilde{H}(t), \tag{6.29}$$

$$w(x,t) = \tilde{T}(x,t) - \int_x^{H(t)} r(x,y)\tilde{T}(y,t)dy - \phi(x,H(t))\tilde{H}(t), \tag{6.30}$$

which map the estimation error system (6.18)-(6.21) into the following target system:

$$w_t(x,t) = D_{\rm i} w_{xx}(x,t) - \lambda w(x,t) - \dot{H}(t) f(x,H(t)) \tilde{H}(t), \quad \forall x \in (0,H(t)) \tag{6.31}$$

$$w(0,t) = 0, \tag{6.32}$$

$$w(H(t),t) = \varepsilon \tilde{H}(t), \tag{6.33}$$

$$\dot{\tilde{H}}(t) = -c\tilde{H}(t) - \beta w_x(H(t),t), \tag{6.34}$$

where $f(x,H(t))$ is to be determined. Taking the first and second spatial derivatives of the transformation (6.29), we get

$$\begin{aligned} \tilde{T}_x(x,t) =& w_x(x,t) + q(x,x)w(x,t) \\ & - \int_x^{H(t)} q_x(x,y)w(y,t)dy - \psi_x(x,H(t))\tilde{H}(t), \end{aligned} \tag{6.35}$$

$$\begin{aligned} \tilde{T}_{xx}(x,t) =& w_{xx}(x,t) + q(x,x)w_x(x,t) + \left(q_x(x,x) + \frac{d}{dx} q(x,x) \right) w(x,t) \\ & - \int_x^{H(t)} q_{xx}(x,y)w(y,t)dy - \psi_{xx}(x,H(t))\tilde{H}(t). \end{aligned} \tag{6.36}$$

Next, taking the time derivative of (6.29) along the solution of the target system (6.31)–(6.34), using integration by parts, and substituting the boundary condition (6.33), we get

$$\begin{aligned} \tilde{T}_t(x,t) =& D_{\rm i} w_{xx}(x,t) + D_{\rm i} q(x,x) w_x(x,t) - (\lambda + D_{\rm i} q_y(x,x)) w(x,t) \\ & + (\beta \psi(x,H(t)) - D_{\rm i} q(x,H(t))) w_x(H(t),t) \\ & + (D_{\rm i} \varepsilon q_y(x,H(t)) + c\psi(x,H(t)))\tilde{H}(t) \\ & + \int_x^{H(t)} (\lambda q(x,y) - D_{\rm i} q_{yy}(x,y)) w(y,t) dy \\ & - \dot{H}(t)\tilde{H}(t) \Big(\varepsilon q(x,H(t)) + \psi_H(x,H(t)) \\ & + f(x,H(t)) - \int_x^{H(t)} q(x,y) f(y,H(t)) dy \Big). \end{aligned} \tag{6.37}$$

Thus, by (6.36) and (6.37), we have

$$\begin{aligned}
&\tilde{T}_t(x,t) - D_{\mathrm{i}}\tilde{T}_{xx}(x,t) + p_1(x,t)\tilde{H}(t) \\
=&-\left(\lambda + 2D_{\mathrm{i}}\frac{d}{dx}q(x,x)\right)w(x,t) \\
&+ (\beta\psi(x,H(t)) - D_{\mathrm{i}}q(x,H(t)))w_x(H(t),t) \\
&+ (D_{\mathrm{i}}\varepsilon q_y(x,H(t)) + D_{\mathrm{i}}\psi_{xx}(x,H(t)) + c\psi(x,H(t)) + p_1(x,t))\tilde{H}(t) \\
&+ \int_x^{H(t)} (\lambda q(x,y) + D_{\mathrm{i}}q_{xx}(x,y) - D_{\mathrm{i}}q_{yy}(x,y))w(y,t)dy \\
&- \dot{H}(t)\tilde{H}(t)\left(\varepsilon q(x,H(t)) + \psi_H(x,H(t))\right. \\
&\left.+ f(x,H(t)) - \int_x^{H(t)} q(x,y)f(y,H(t))dy\right).
\end{aligned} \tag{6.38}$$

Substituting $x = 0$ and $x = H(t)$ into (6.29), we get

$$\begin{aligned}
\tilde{T}(0,t) + p_2(t)\tilde{H}(t) =& -\int_0^{H(t)} q(0,y)w(y,t)dy \\
&+ (p_2(t) - \psi(0,H(t)))\tilde{H}(t),
\end{aligned} \tag{6.39}$$

$$\tilde{T}(H(t),t) + p_3(t)\tilde{H}(t) = (\varepsilon - \psi(H,H) + p_3(t))\tilde{H}(t). \tag{6.40}$$

Moreover, substituting $x = H(t)$ into (6.35) yields

$$\begin{aligned}
&\dot{\tilde{H}}(t) + p_4(t)\tilde{H}(t) + \beta\tilde{T}_x(H(t),t) \\
=&(p_4(t) - c + \beta(\varepsilon q(H(t),H(t)) - \psi_x(H(t),H(t))))\tilde{H}(t).
\end{aligned} \tag{6.41}$$

Therefore, for the equations (6.18)–(6.21) to hold, the gain kernel functions must satisfy the following conditions:

$$q_{xx}(x,y) - q_{yy}(x,y) = -\bar{\lambda} q(x,y), \tag{6.42}$$

$$\frac{d}{dx} q(x,x) = -\frac{\bar{\lambda}}{2}, \quad q(0,y) = 0, \tag{6.43}$$

$$\beta \psi(x,H(t)) = D_{\mathrm{i}} q(x,H(t)), \tag{6.44}$$

and the observer gains must satisfy

$$p_1(x,t) = -D_{\mathrm{i}}(\varepsilon q_y(x,H(t)) + \psi_{xx}(x,H)) - c\psi(x,H), \tag{6.45}$$

$$p_2(t) = \psi(0,H(t)), \tag{6.46}$$

$$p_3(t) = \psi(H(t),H(t)) - \varepsilon, \tag{6.47}$$

$$p_4(t) = c - \beta(\varepsilon q(H(t),H(t)) - \psi_x(H(t),H(t))), \tag{6.48}$$

and the function $f(x,H(t))$ must satisfy

$$f(x,H) + \varepsilon q(x,H) + \psi_H(x,H) = \int_x^H q(x,y) f(y,H) dy. \tag{6.49}$$

The solutions to (6.42)–(6.44) are uniquely given by

$$q(x,y) = -\bar{\lambda} x \frac{I_1\left(\sqrt{\bar{\lambda}(y^2 - x^2)}\right)}{\sqrt{\bar{\lambda}(y^2 - x^2)}}, \tag{6.50}$$

$$\psi(x,H(t)) = -\frac{\lambda}{\beta} x \frac{I_1(z)}{z}, \tag{6.51}$$

where z is defined by (6.26). Then, using (6.50)–(6.51), the conditions (6.45)–(6.48) are led to the explicit formulations of the observer gains given as (6.22)–(6.25). In the similar manner, the

conditions for the gain kernel functions of the inverse transformation (6.30) are given by

$$r_{xx}(x,y) - r_{yy}(x,y) = \bar{\lambda} r(x,y), \tag{6.52}$$

$$\frac{d}{dx} r(x,x) = \frac{\bar{\lambda}}{2}, \quad r(0,y) = 0, \tag{6.53}$$

$$\beta \phi(x,H(t)) = D_{\mathrm{i}} r(x,H(t)), \tag{6.54}$$

and, the function $f(x,H(t))$ is obtained by

$$f(x,H(t)) = r(x,H(t)) p_3(H(t)) + \phi_H(x,H(t)). \tag{6.55}$$

The solutions to (6.52)–(6.54) are given by

$$r(x,y) = \bar{\lambda} x \frac{J_1\left(\sqrt{\bar{\lambda}(y^2 - x^2)}\right)}{\sqrt{\bar{\lambda}(y^2 - x^2)}}, \; \phi(x,H) = \frac{\lambda}{\beta} x \frac{J_1(z)}{z}, \tag{6.56}$$

where J_1 is Bessel function of the first kind. Using the solutions (6.56), the function $f(x,H(t))$ is obtained explicitly by (6.55), which also satisfies the condition (6.49). Hence, the transformation from $(\tilde{T},\tilde{H})$ to $(w,\tilde{H})$ is invertible.

Stability Analysis

We prove the exponential stability of the origin of the estimation error system (6.18)-(6.21) in the spatial L_2 norm. First, we show the exponential stability of the origin of the target system (6.31)-(6.34). We consider the following Lyapunov functional

$$V = \frac{1}{2}||w||^2 + \frac{\varepsilon}{2\beta}\tilde{H}(t)^2. \tag{6.57}$$

Taking the time derivative of (6.57) together with the solution of (6.31)-(6.34) yields

$$\begin{aligned}\dot{V} = &- D_{\mathrm{i}}||w_x||^2 - \lambda||w||^2 - \frac{\varepsilon c}{\beta}\tilde{H}(t)^2 + \frac{\dot{H}(t)}{2}\varepsilon^2\tilde{H}(t)^2 \\ &- \dot{H}(t)\tilde{H}(t)\int_0^{H(t)} w(x,t)f(x,H(t))dx. \end{aligned} \tag{6.58}$$

Applying Young's and Cauchy-Schwarz inequalities to the last term in (6.58) with the help of Assumption 13, and choosing the gain parameter c to satisfy

$$c > \frac{\beta M^2 \bar{f}}{\varepsilon\lambda} + \beta M\varepsilon, \tag{6.59}$$

one can obtain the following inequality:

$$\dot{V} \leq -\min\{\lambda, c\}V. \tag{6.60}$$

Applying comparison principle to the differential inequality (6.60), we get

$$V(t) \leq V(0)e^{-\min\{\lambda,c\}t}. \tag{6.61}$$

Hence, the target system (6.31)-(6.34) is exponentially stable at the origin. Due to the invertibility of the transformations (6.29) and (6.30), there exist positive constants $\underline{M} > 0$ and $\bar{M} > 0$ such that for the norm $\Phi(t)$ defined in (6.27) the inequalities hold $\underline{M}\Phi(t) \leq V(t) \leq \bar{M}\Phi(t)$. Hence, we obtain (6.28) by defining $\tilde{M} = \bar{M}/\underline{M}$, which completes the proof of Theorem 12. Note that the designed backstepping observer achieves faster convergence with a possibility of causing overshoot since the overshoot coefficient $\bar{M}/\underline{M}$ is a monotonically increasing function in the observer gains' parameters (λ, c).

While we have focused on the simplified PDE (6.11) to derive a rigorous proof of the proposed state estimation design (6.13)-(6.16) with observer gains given by (6.22)–(6.25),

simulation studies are performed by applying the estimation design to the original thermodynamic model (6.1)-(6.7) including salinity.

Initial conditions

The simulation results of temperature estimation $\hat{T}_{\mathrm{i}}$ computed by (6.13)-(6.16) along with the available measurements obtained by the online calculation of (6.1)-(6.7) are shown in Fig. 6.3. Here the initial temperature profiles are formulated as

$$T_{\mathrm{s}}(x,0) = \frac{k_0(T_{\mathrm{m1}} - T_0)}{k_s H_0} x + T_0, \tag{6.62}$$

$$T_{\mathrm{i}}(x,0) = \frac{T_{\mathrm{m1}} - T_0}{H_0} x + T_0 + a \sin\left(\frac{4\pi x}{H_0}\right), \tag{6.63}$$

where $T_0 = T_{\mathrm{i}}(0,0)$ which is obtained by solving fourth order algebraic equation from (6.1) and the input data, and a is set as $a = 1$ [C$^\circ$]. The estimated initial temperature is chosen as

$$\hat{T}_{\mathrm{i}}(x,0) = \frac{T_{\mathrm{m1}} - T_0}{H_0^2(1-2d)}(x^2 - 2dH_0 x) + T_0 \tag{6.64}$$

with setting $d = 1/4$. Hence, the initial temperature estimate is lower than the actual temperature. This initial condition satisfies the boundary conditions (6.14) and (6.15). The initial state of the estimated ice thickness $\hat{H}(0)$ is set as that of the true thickness, i.e., $\hat{H}(0) = H(0)$, which is feasible because the thickness is actually measured.

Tuning method for gain parameters

The design parameters $(\lambda, c, \varepsilon)$ are selected as follows:

(i) Choose $\varepsilon \approx \beta$ for the norm (6.57) to be similarly weighted.

(ii) Select λ to be the inverse of a desired time constant (i.e., the time at 63% decay of the estimation error is achieved): here we set as one day, leading to $\lambda \approx \frac{1}{24\times 3600} = 1.2 \cdot 10^{-5}$.

(iii) Select c sufficiently larger than λ so that the decay rate $\min\{\lambda, c\}$ is not reduced and (6.59) is satisfied.

Finally, these parameters are varied around these reference values until we observe a smooth and sufficiently fast convergence. Throughout the simulation, we see that the minimum value of the time step size in ode solver is more than 1 minute, while the computation time of each time update is less than 0.1 seconds, which shows its real-time implementability as addressed in Remark 4.

Simulation Results

Numerical Simulation of State Estimation

The contour plot of the simulation results of $T_{\mathrm{i}}(x,t)$ and $\hat{T}_{\mathrm{i}}(x,t)$ for open-loop estimation by setting all the observer gain to be zero is depicted in Fig. 6.3 (a), and those for the proposed estimation are depicted in Fig. 6.3 (b) and Fig. 6.4 (a)-(b) with observer gains (6.22)–(6.25), respectively, by using input data on January. For the proposed estimation, we fix the parameters of $c = 3.0 \times 10^{-5}$ and $\varepsilon = 1.0 \times 10^{-8}$, and use the parameter of $\lambda = 5.0 \times 10^{-6}$ in Fig. 6.3 (b), $\lambda = 1.0 \times 10^{-5}$ in Fig. 6.4 (a), and $\lambda = 5.0 \times 10^{-7}$ in Fig. 6.4 (b). The figures show that the backstepping observer gain makes the convergence speed of the estimation to the actual value approximately 5 to 10 times faster at every point in sea ice. As seen in Fig. 6.4, while the larger value of λ makes the convergence speed faster, it causes more overshoot beyond the actual temperature. Hence, the tradeoff between the convergence speed and overshoot can be handled by tuning the gain parameter λ appropriately, thereby the parameters used in (b) achieve the desired performance. The overshoot behavior is noted at the end of Section 6.4 from a theoretical perspective. Consequently, the stability properties stated in Theorem 12 for the simplified model can be observed in numerical results of the proposed estimation applied to the original model (6.1)-(6.7). To visualize the convergence of the estimated temperature profile used in 6.3 (b)

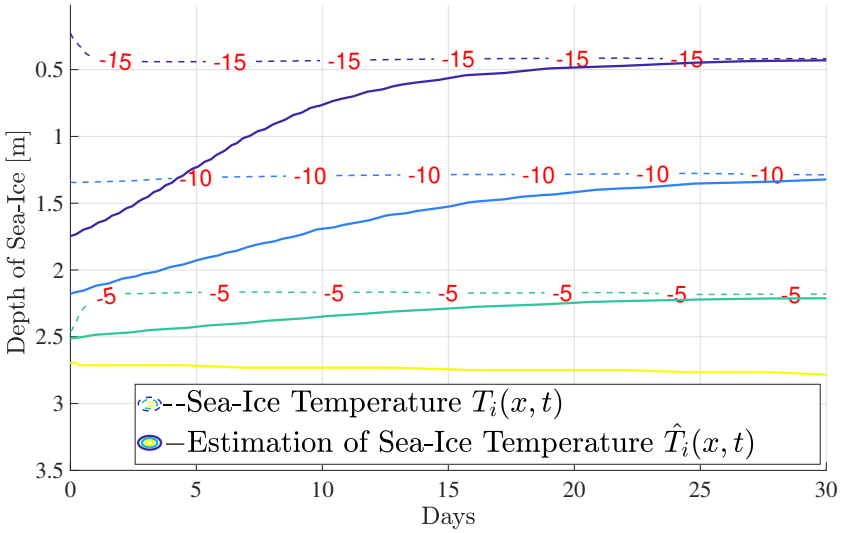

(a) Open-loop estimation, i.e., $p_1(x,t) = 0$ and $p_i(t) = 0$ for $i = 2,3,4$.

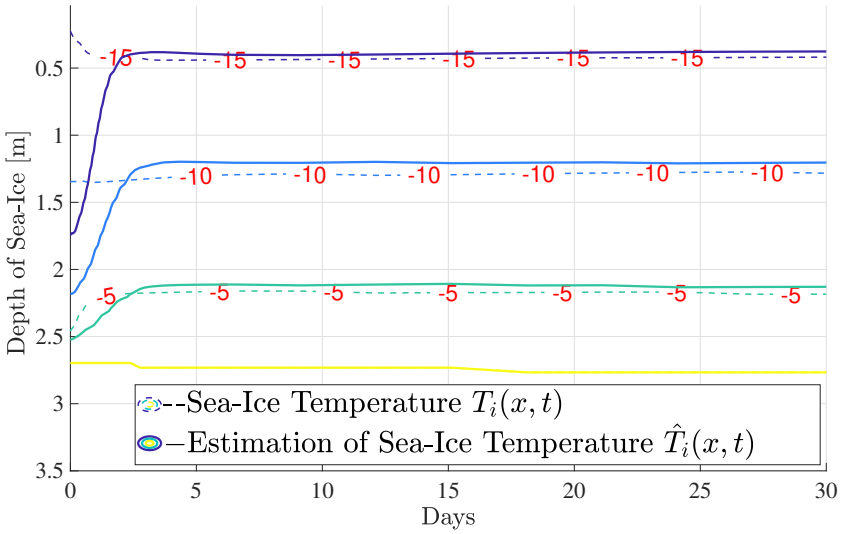

(b) The proposed estimation with the observer gains given in (6.22)–(6.25).

Figure 6.3: Simulation results of the plant (6.1)–(6.7) and the estimator (6.13)-(6.16) using parameters on January. The designed backstepping observer achieves faster convergence to the actual state than the straightforward open-loop estimation.

more clearly, Fig. 6.5 illustrates the profiles of both true temperature (black solid) and estimated temperature (red dash) on January 1st to 3rd in (a)–(c), respectively. We observe that the estimated temperature profile becomes almost the same as the true temperature profile on January 3rd,

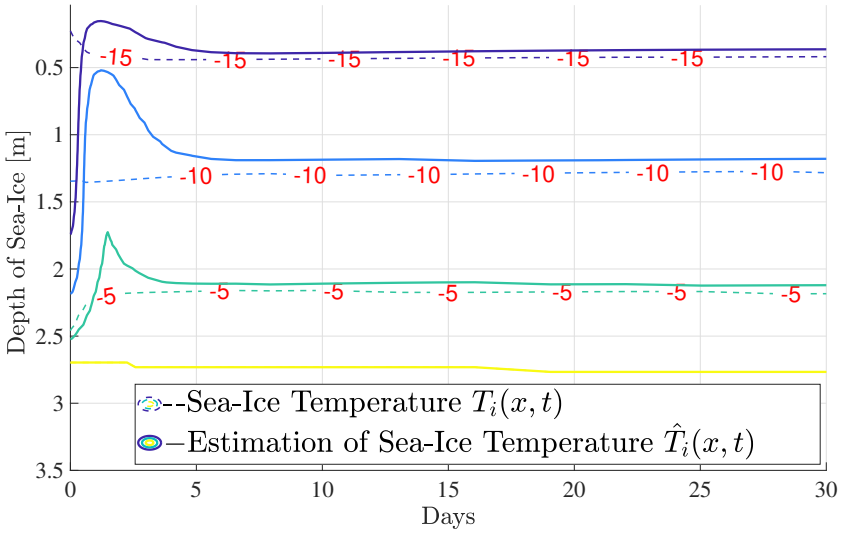

(a) The proposed estimation with larger value of λ than Fig. 6.3 (b). The overshoot beyond the true temperature is observed during the first two days.

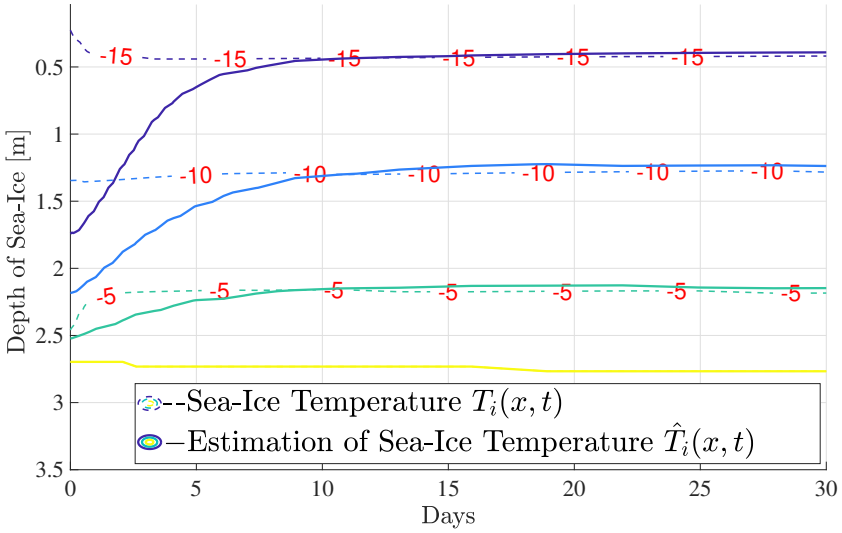

(b) The proposed estimation with smaller value of λ than Fig. 6.3 (b). The convergence speed gets slower than the result of Fig. 6.3 (b).

Figure 6.4: Simulation results of the plant (6.1)–(6.7) and the bacsktepping estimator (6.13)-(6.16) with some chosen free parameters.

which is two days after the estimation algorithm runs. Moreover, Fig. 6.5 (d) depicts the time evolution of $\tilde{H}(t)$, which is an estimation error of the ice's thickness. We observe that the error

is "enlarged" from $\tilde{H}(0) = 0$ due to the error of temperature profile, and returns to zero after the temperature profiles become almost indistinguishable on January 3rd, from which the necessity of the estimator of the ice's thickness is ensured while the thickness is actually measured.

Finally, we have studied the robustness of the proposed observer by varying the parameters D_{i}, β, and F_{w} in the observer (6.13)-(6.16) and the gains (6.22)–(6.25) to $D_{\mathrm{i}}(1+\delta_1)$, $\beta(1+\delta_2)$, and $F_{\mathrm{w}}(1+\delta_3)$ with setting $\delta_1 = 0.3$, $\delta_2 = -0.3$, and $\delta_3 = 0.4$. Fig. 6.6 (a) shows the contour plots of estimated and true temperature profiles and Fig. 6.6 (b) shows the evolution of $\tilde{H}(t)$. From both figures, we can see that the observer states converge and stay around the true states with a modest error after 5 days, which illustrates robust performance of the proposed observer under the parameters' uncertainties.

6.5 Conclusion and Future Work

In this chapter, we develop the estimation algorithm for temperature profile in the Arctic sea ice via backstepping observer design. The observer gains are derived so that the convergence of the state estimate to the actual state is guaranteed theoretically for a simplified model. Numerical simulation is employed to investigate the performance of the observer design with the original thermodynamic model, which illustrates ten times faster convergence of state estimation to the actual temperature than the straightforward open-loop estimation.

While we have assumed the *online* availability of the measurements, these data acquired by satellites typically accompany a time-delay due to the communication. Such a time-delay can be compensated by extending the method developed in [84] for control design under actuator delay to the estimator design under sensor delay following the procedure in [97]. In addition, the physical parameters used in this paper are uncertain variables in practice, where the uncertain parameters can be assumed to be constants at each month, and hence it is significant to design a simultaneous state and parameter estimation algorithm such as [118] using a reduced-order model

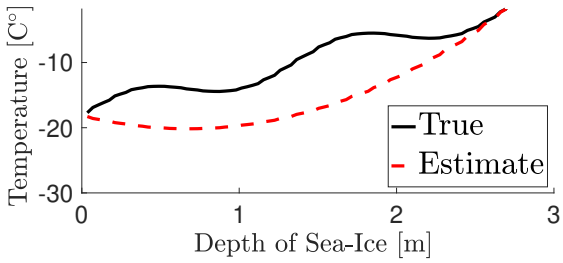

(a) Temperature profile of both true and estimate on January 1st.

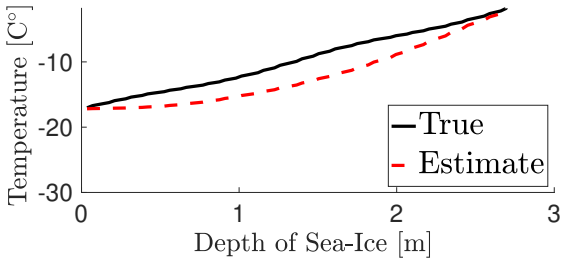

(b) Temperature profile of both true and estimate on January 2nd.

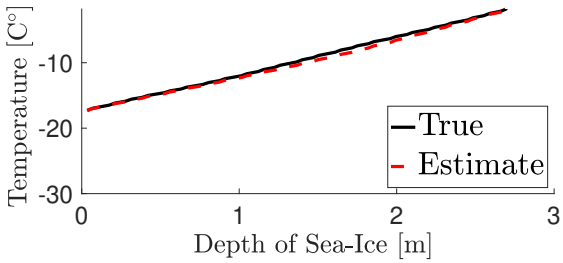

(c) Temperature profile of both true and estimate on January 3rd.

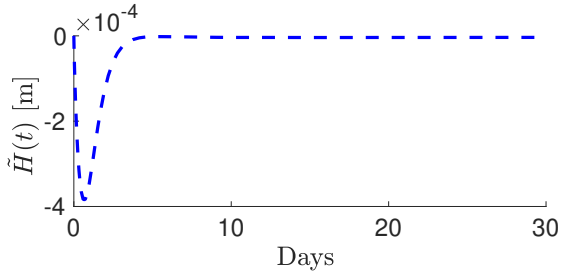

(d) The time evolution of thickness estimation error $\tilde{H}(t)$.

Figure 6.5: Simulation result of the plant (6.1)–(6.7) and the estimator (6.13)-(6.16) with parameters used in Fig. 6.3 (b).

via Pade-approximation and [12] using data-driven extremum seeking as an iterative learning method. Instead of adaptive estimation, interval observers for the state estimation of uncertain

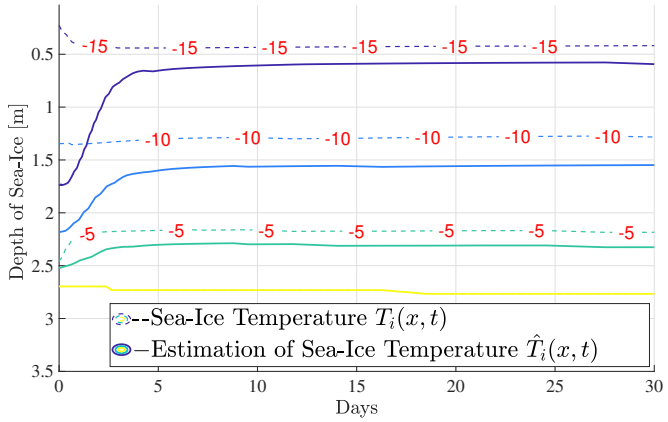

(a) Estimated temperature converges to the true temperature with a modest error.

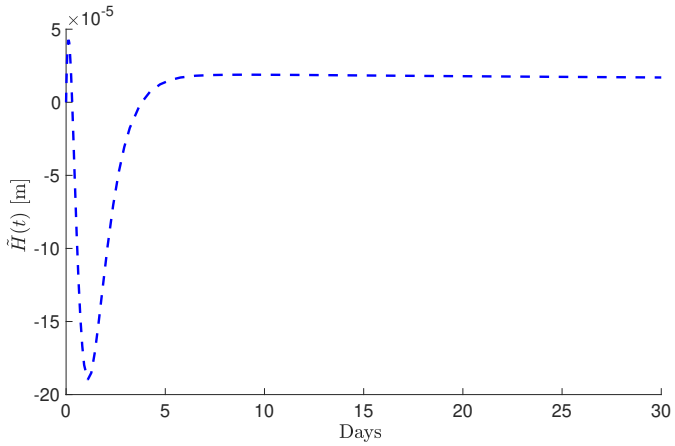

(b) $\tilde{H}(t)$ dynamically varies first and stays at a value near zero after 5 days.

Figure 6.6: Robustness of the proposed estimation with significant parametric errors: 30[%] in diffusion coefficient D_{i}, 30[%] in latent heat parameter β, and 30[%] in heat flux F_{w} from the ocean.

parabolic PDEs have been proposed in [79]. Moreover, applying the optimal control of the Stefan problem developed in [63, 13, 3] to the estimation of the sea ice model is also an interesting direction. These extensions will be considered as our future work.

6.6 Acknowledgement

Chapter 6, in part, is a reprint of the material as it appears in:

- S. Koga and M. Krstic, “Arctic Sea Ice Temperature Profile Estimation via Backstepping Observer Design”, *IEEE Conference on Control Technology and Applications*, 2017,
- S. Koga and M. Krstic, “Arctic Sea Ice State Estimation from Thermodynamic PDE Model”, *Automatica*, vol. 112, p. 108713, 2020.

The dissertation author was the primary investigators and author of this paper. The author would like to thank I. Eisenman for suggesting the sea ice model we considered throughout this paper and helpful discussions. The author would like to thank I. Fenty for enriching our knowledge on recent trend of sea ice state estimation developed in NASA Jet Propulsion Laboratory.

Chapter 7

Lithium-Ion Batteries

7.1 Battery Management Systems

Battery management is crucial for safe and efficient use of numerous kinds of electronics such as smartphones and laptops, and electric vehicles. Among several chemical materials used for electrodes of lithium-ion batteries, Lithium Iron Phosphate (LFP) has several attractive features as an active material in lithium-ion batteries such as thermal safety, high energy, and power density [120]. LFP and other common active materials show unique charge-discharge characteristics due to an underlying crystallographic solid-solid phase transition. Electrochemical models for lithium-ion batteries with single phase materials do not allow to capture these unique characteristics and thus a mathematical description of phase transitions needs to be added to these models. Electrochemical models are of interest for the design of accurate estimation algorithms in battery management systems. Estimation algorithms based on these models provide visibility into operating regimes that induce degradation enabling a larger domain of operation, therefore, increasing the performance of the battery in terms of energy capacity, power capacity, and fast charge rates [27, 124]. Electrochemical model-based estimation is challenging for several reasons. First, measurements of lithium concentrations outside specialized laboratory environments is

impractical. Second, the concentration dynamics are governed by coupled and nonlinear partial differential algebraic equations (PDAE) [158]. Finally, the only measurable quantities (voltage and current) are related to dynamic states through a nonlinear function.

Electrochemical models describe the relevant dynamic phenomena in lithium-ion cells: diffusion, intercalation and electrochemical kinematics (see Figure 7.1). These models predict accurately the internal states of the battery, however, their complexity renders a challenging problem for estimation algorithms. For this reason, most approaches develop estimation algorithms based on simplified models. Among the various simplified models, the single particle model (SPM) has been broadly used in the observer design problem, see [41, 118, 171, 36, 123, 117, 155]. The main characteristic of the SPM is the use of a single spherical particle to represent diffusion of lithium ions in the intercalation sites of the porous active materials in the electrodes.

LFP has been extensibility used in lithium ion cells due to its thermal stability, cost effectiveness, non-toxic nature, and long cycle life [120]. An electrochemical model for LFP batteries was proposed in [150] based on a *core-shell* model, where the concentration at the core is assumed constant and diffusion is allowed for the phase in the shell. The LFP model with phase transition electrode was revisited in [184] with a more complete *core-shell* model, allowing diffusion in both phases of an $LiCoO_2$ cathode.

The estimation problem for batteries with LFP electrodes has been relatively less studied; a particle filter was derived in [135] and a Sequential Monte Carlo filter was derived in [109]. The *core-shell* model proposed for phase transition electrodes is described by a parabolic PDE with a state-dependent moving boundary.

7.2 Electrochemical Model with Phase Change Electrode

The electrochemical model for lithium-ion cells with a phase transition material in the positive electrode follows [150]. We restrict the problem to particular initial conditions of the

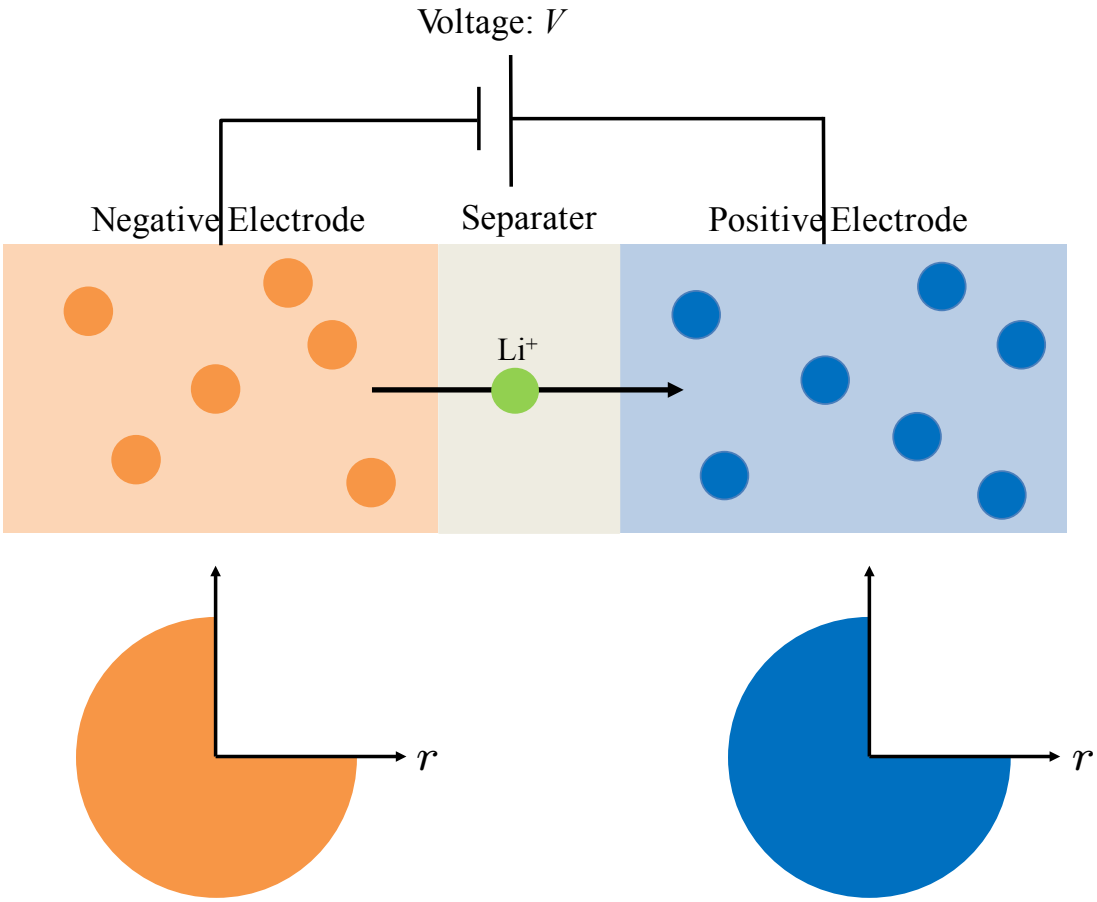

Figure 7.1: Schematic of lithium-ion battery and the description of particles in electrochemical models. The concentration dynamics of lithium-ion is governed on the geometry of each particle.

concentration of lithium ions in the particles (i.e. intercalation sites) of the positive electrode and consider only discharge processes. The initial concentration of lithium ions in the particles of the positive electrode follows a core-shell configuration where the core has a constant distribution of lithium ions in a low concentration phase (the α phase), and the shell has a constant distribution of lithium ions in a high concentration phase (the β phase). During discharge, the fluxes of lithium ions at the surface of the particles in the positive electrode are positive, thus, increasing the concentration of lithium ions in the shell and the phase boundary is moving to the center, i.e., a *shrinking core* process as depicted in Figure 7.2.

Single Particle Model

The single particle model is a simple electrochemical model that accounts for some phenomena in lithium-ion cells. The main simplification in this model comes from the assumption that a single diffusion equation in an spherical particle can be used to model the diffusion of lithium ions in all the intercalation sites of the active material of each electrode. In the SPM, the ionic molar fluxes $j_{\mathrm{n},\pm}(t)$ on both electrodes are proportional the current density $I(t)$ applied to the cell

$$j_{\mathrm{n},\pm}(t) = \mp \frac{I(t)}{a_{\mathrm{s},\pm} F L_{\pm}}, \tag{7.1}$$

where $a_{\mathrm{s},\pm} = 3\varepsilon_{\mathrm{s},\pm}/R_{\mathrm{p},\pm}$ is the interfacial area (per unit volume), $\varepsilon_{\mathrm{s},\pm}$ is the volume fraction of active material in each electrode, $R_{\mathrm{p},\pm}$ is the averaged radius of the intercalation sites (particles) in the electrodes, F is the Faraday constant, and $L_{\pm}$ is the thickness of each electrode. Throughout this paper, the subscripts $+$ and $-$ indicate that the variable corresponds to the positive or negative particle. The concentration dynamics of lithium ions in the negative electrode (single phase) follow the Fick's law for diffusion

$$\frac{\partial c_{\mathrm{s},-}}{\partial t}(r,t) = \frac{D_{\mathrm{s},-}}{r^2} \frac{\partial}{\partial r} \left[r^2 \frac{\partial c_{\mathrm{s},-}}{\partial r}(r,t) \right], \tag{7.2}$$

for $r \in (0, R_{\mathrm{p},-})$, $t > 0$ with boundary conditions

$$\frac{\partial c_{\mathrm{s},-}}{\partial r}(0,t) = 0, \tag{7.3}$$

$$D_{\mathrm{s},-}\frac{\partial c_{\mathrm{s},-}}{\partial r}(R_{\mathrm{p},-},t) = -j_{\mathrm{n},-}(t), \tag{7.4}$$

and initial condition $c_{0,-} \in \mathcal{C}(0, R_{\mathrm{p},-})$. Diffusion in the positive particle follows a core-shell model. In the core of the particle, i.e., for $r \in (0, r_{\mathrm{p}}(t))$, lithium ions are in the α-phase. The concentration in the core is assumed to be constant and equal to the equilibrium value of the α-phase, i.e., $c_{s,+}(r) = c_{\mathrm{s},\alpha}$ for all $r \in (0, r_{\mathrm{p}}(t))$. In the shell of the spherical particle, i.e. for $r \in (r_{\mathrm{p}}(t), R_{p,+})$, the concentration of lithium ions is in β-phase. The concentration dynamics of lithium-ions in the shell of the positive particle follows the Fick's law for diffusion

$$\frac{\partial c_{\mathrm{s},+}}{\partial t}(r,t) = \frac{D_{\mathrm{s},+}}{r^2}\frac{\partial}{\partial r}\left[r^2\frac{\partial c_{\mathrm{s},+}}{\partial r}(r,t)\right], \tag{7.5}$$

for $r \in (r_{\mathrm{p}}(t), R_{\mathrm{p},+})$ with boundary conditions

$$c_{\mathrm{s},+}(r_{\mathrm{p}}(t),t) = c_{\mathrm{s},\beta}, \tag{7.6}$$

$$D_{\mathrm{s},+}\frac{\partial c_{\mathrm{s},+}}{\partial r}(R_{\mathrm{p},+},t) = -j_{\mathrm{n},+}(t), \tag{7.7}$$

and initial conditions $c_{0,+} \in \mathcal{C}(r_{\mathrm{p}}(0), R_{\mathrm{p},+})$. The time-evolution of the moving interface $r_p(t)$ is not given explicitly. Instead, mass balance at the moving interface yields the following state-dependent dynamics:

$$(c_{\mathrm{s},\beta} - c_{\mathrm{s},\alpha})\frac{dr_{\mathrm{p}}(t)}{dt} = -D_{\mathrm{s},+}\frac{\partial c_{\mathrm{s},+}}{\partial r}(r_{\mathrm{p}}(t),t). \tag{7.8}$$

Overpotentials $\eta_{\pm}(t)$ are found by solving the nonlinear algebraic equation

$$j_{\mathrm{n},\pm}(t) = \frac{i_{0,\pm}(t)}{F}\left[e^{\frac{\alpha_{\mathrm{a}}F}{RT}\eta_{\pm}(t)} - e^{-\frac{\alpha_{\mathrm{c}}F}{RT}\eta_{\pm}(t)}\right], \tag{7.9}$$

$$i_{0,\pm}(t) = Fk_{\pm}\left[c_{\mathrm{ss},\pm}(t)\right]^{\alpha_{\mathrm{c}}}\left[c_{\mathrm{e},0}\left(c_{\mathrm{s,max},\pm} - c_{\mathrm{ss},\pm}(t)\right)\right]^{\alpha_{\mathrm{a}}}, \tag{7.10}$$

where $c_{\mathrm{ss},\pm}(t) := c_{\mathrm{s},\pm}(R_{\mathrm{p},\pm}, t)$. The electric potential in each electrode is given by

$$\phi_{\mathrm{s},\pm}(t) = \eta_{\pm}(t) + U_{\pm}(c_{\mathrm{ss},\pm}(t)) + R_{\mathrm{f},\pm}F\,j_{\mathrm{n},\pm}(t). \tag{7.11}$$

Finally, output voltage is computed as the difference between the electric potential in each electrode

$$V(t) = \phi_{\mathrm{s},+}(t) - \phi_{\mathrm{s},-}(t). \tag{7.12}$$

Equations (7.5) -(7.12) form a complete description of the single particle model with a phase transition electrode, and it provides the following property on the moving interface during the discharge process.

Remark 6 *During the single discharge process, the current density $I(t)$ maintains positive, i.e. $I(t) > 0$ for $\forall t > 0$. This current positivity ensures the moving interface being shrinking. Furthermore, the initial interface position is less than the cell radius. Hence,*

$$\frac{dr_{\mathrm{p}}(t)}{dt} < 0, \tag{7.13}$$

$$0 \leq r_{\mathrm{p}}(t) < R_{\mathrm{p},+}. \tag{7.14}$$

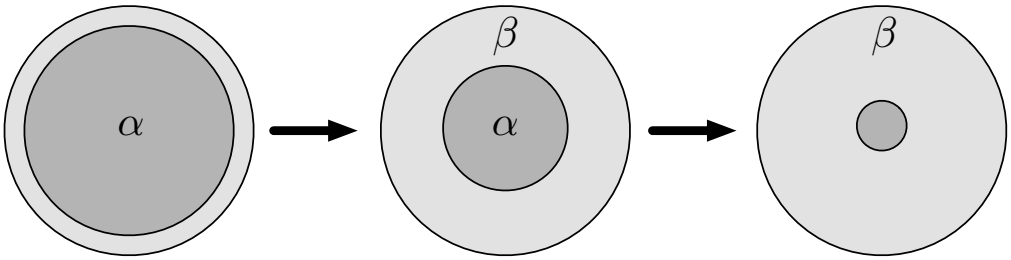

Figure 7.2: Phase transition in the positive particle during discharge. The particle starts with a large core of low concentration phase α and a small shell of high concentration phase β. During discharge there is a positive flux of lithium ion in the surface of the positive particle, increasing the concentration and increasing the size of the β-phase shell.

Mass Conservation

In this model, the total amount of lithium ions is conserved. The mathematical description of this property is given in the following lemma.

Lemma 11 *The total amount of lithium n_{Li} in solid phase (moles per unit area) defined as*

$$n_{\mathrm{Li}}(t) = \varepsilon_{\mathrm{s},-} L_- \overline{c}_{\mathrm{s},-}(t) + \varepsilon_{\mathrm{s},+} L_+ \overline{c}_{\mathrm{s},+}(t), \tag{7.15}$$

where $\overline{c}_{\mathrm{s},-}(t)$ and $\overline{c}_{\mathrm{s},+}(t)$ are the volumetric averages of the concentrations

$$\overline{c}_{\mathrm{s},-}(t) = \frac{3}{R_{\mathrm{p},-}^3} \int_0^{R_{\mathrm{p},-}} c_{\mathrm{s},-}(r,t) r^2 \mathrm{d}r, \tag{7.16}$$

$$\overline{c}_{\mathrm{s},+}(t) = \frac{3}{R_{\mathrm{p},+}^3} \int_0^{R_{\mathrm{p},+}} c_{\mathrm{s},+}(r,t) r^2 \mathrm{d}r, \tag{7.17}$$

is conserved, namely $dn_{\mathrm{Li}}(t)/dt = 0$.

Lemma 11 was derived in [81] for electrodes with a single phase, and we can show that this result extends to electrodes with phase transition materials.

Proof:

In our problem formulation there is a single phase in the negative particle and there are two

phases in the positive particle, i.e., α-phase in the core and β-phase in the shell. The concentration in α-phase at the core is assumed to be constant (at its equilibrium value $c_{s,\alpha}$). Under these assumptions, the time derivative of (7.15) is given by

$$\begin{aligned}\frac{dn_{\mathrm{Li}}}{dt}(t) =& -a_{s,-}L_{-}j_{n,-}(t) - a_{s,+}L_{+}j_{n,+}(t) - \frac{3\varepsilon_{s,+}L_{+}}{R_{p,+}^{3}}r_{p}^{2}(t) \\ &\times\left[\frac{dr_{p}}{dt}(t)\left[c_{s,\beta}-c_{s,\alpha}\right] + D_{s,+}\frac{\partial c_{s,+}}{\partial r}(r_{p}(t),t)\right]. \end{aligned} \tag{7.18}$$

Hence, the molar flux equations in (7.1) and the dynamics of the moving interface in (7.8) lead to $dn_{\mathrm{Li}}(t)/dt = 0$. In a more general formulation introduced in [78, 77], i.e. when both electrodes have multiple phase transitions not necessarily at the equilibrium, mass conservation of lithium ions is guaranteed with the following interface dynamics

$$\frac{dr_{i}^{[a,b]}}{dt}(t) = \frac{1}{c_{b}-c_{a}}\left[D_{a}\frac{\partial c}{\partial r}(r_{i}^{[a,b]}(t)^{-},t) - D_{b}\frac{\partial c}{\partial r}(r_{i}^{[a,b]}(t)^{+},t)\right], \tag{7.19}$$

where $r_{i}^{[a,b]}$ is the interface radius between any two phases (phase a and phase b) in any electrode. Each phase has a distinct equilibrium c_{a}, c_{b} and diffusion coefficient D_{a}, D_{b}.

7.3 State-of-Charge Estimation

Now, a state estimation algorithm for concentration of lithium ions, in both negative and positive electrodes, is provided in this section from the single particle model. The state observer for the positive electrode is derived via the backstepping method for moving boundary PDEs, and the observer for the negative electrode is derived from the mass conservation property.

Observer for Phase Transition Positive Electrode

The state observer is a copy of the diffusion system (7.5)-(7.7) in the positive electrode together with output error injection

$$\begin{aligned}\frac{\partial \widehat{c}_{\mathrm{s},+}}{\partial t}(r,t) =& \frac{D_{\mathrm{s},+}}{r^2}\frac{\partial}{\partial r}\left[r^2\frac{\partial \widehat{c}_{\mathrm{s},+}}{\partial r}(r,t)\right] \\ &+ P(\widehat{r}_{\mathrm{p}}(t),r)\left[c_{\mathrm{ss},+}(t)-\widehat{c}_{\mathrm{s},+}(R_{\mathrm{p},+},t)\right], \end{aligned} \tag{7.20}$$

for $r \in (\widehat{r}_{\mathrm{p}}(t), R_{\mathrm{p},+})$ with boundary conditions

$$\widehat{c}_{\mathrm{s},+}(\widehat{r}_{\mathrm{p}}(t),t) = c_{\beta}, \tag{7.21}$$

$$\begin{aligned} D_{\mathrm{s},+}\frac{\partial \widehat{c}_{\mathrm{s},+}}{\partial r}(R_{\mathrm{p},+},t) =& -j_{\mathrm{n},+}(t) \\ &+ Q(\widehat{r}_{\mathrm{p}}(t))\left[c_{\mathrm{ss},+}(t)-\widehat{c}_{\mathrm{s},+}(R_{\mathrm{p},+},t)\right], \end{aligned} \tag{7.22}$$

and initial conditions $\widehat{c}_{0,+} \in \mathcal{L}^2(\widehat{r}_{\mathrm{p}}(0), R_{\mathrm{p},+})$ and $\widehat{r}_{\mathrm{p}}(0) \in (0, R_{\mathrm{p},+})$. Observer gains are given by

$$P(\widehat{r}_{\mathrm{p}}(t),r) = D_{s,+}\overline{\lambda}^2\frac{R_{\mathrm{p},+}}{r}l(t)s(t)\frac{I_2(z(t))}{z(t)}, \tag{7.23}$$

$$Q(\widehat{r}_{\mathrm{p}}(t)) = \frac{D_{s,+}}{R_{\mathrm{p},+}}\left(\frac{\overline{\lambda}}{2}s(t)+1\right), \tag{7.24}$$

where $I_2(\cdot)$ is a modified Bessel function of the second kind and

$$\overline{\lambda} = \frac{\lambda}{D_{s,+}}, \tag{7.25}$$

$$s(t) = R_{\mathrm{p},+} - \widehat{r}_{\mathrm{p}}(t), \quad l(t) = r - \widehat{r}_{\mathrm{p}}(t), \tag{7.26}$$

$$z(t) = \sqrt{\overline{\lambda}[s(t)^2 - l(t)^2]}. \tag{7.27}$$

The parameter $\lambda > 0$ is designed to achieve faster convergence of the estimated concentration to true concentration. Moreover, the estimator for the moving interface position is given by the following dynamics:

$$(c_{\mathrm{s},\beta} - c_{\mathrm{s},\alpha})\frac{d\widehat{r}_{\mathrm{p}}(t)}{dt} = -\kappa\left[c_{\mathrm{ss},+}(t) - \widehat{c}_{\mathrm{s},+}(R_{\mathrm{p},+},t)\right] - D_{\mathrm{s},+}\frac{\partial \widehat{c}_{\mathrm{s},+}}{\partial r}(\hat{r}_{\mathrm{p}}(t),t), \tag{7.28}$$

where the parameter $\kappa > 0$ is designed to achieve fast convergence of the estimated interface position to the true value.

The stability of the estimation error system is theoretically proven for the PDE observer (7.20)–(7.22) with gains (7.23), (7.24) under the assumption $\widehat{r}_{\mathrm{p}}(t) \equiv r_{\mathrm{p}}(t)$ for all $t \geq 0$ in the next section. As the moving interface position $r_{\mathrm{p}}(t)$ is unknown in practice, we construct the estimator (7.28), and use the estimated interface position $\widehat{r}_{\mathrm{p}}(t)$ in the gains (7.23), (7.24) of PDE observer.

The sign of the observer gain in (7.28) (first term in the right hand side) is determined based on the monotonic relation, namely, as the surface concentration $c_{\mathrm{ss},+}(t)$ is increased the moving interface position $r_{\mathrm{p}}(t)$ is decreased. Physically, as the battery is discharged, the domain of the lithium rich β-phase in the positive electrode is expanded from the outer region. Hence, the observer (7.28) is designed so that if the measured surface concentration is larger than the estimated surface concentration, the battery is discharged more than estimated, and the domain of β-phase for the estimator is driven to be expanded.

Stability Analysis of the Estimation Error System with Known Interface Position

Let $\widetilde{c}_{\mathrm{s},+}(r,t)$ be an estimation error defined by $\widetilde{c}_{\mathrm{s},+}(r,t) := c_{\mathrm{s},+}(r,t) - \widehat{c}_{\mathrm{s},+}(r,t)$. The stability analysis of the estimation error system is presented in the following theorem.

Theorem 13 *Consider the plant PDE* (7.5)–(7.7) *and the PDE observer* (7.20)–(7.22) *with observer gains* (7.23) *and* (7.24) *under the properties of* (7.13)*,* (7.14)*, and the assumption* $\widehat{r}_{\mathrm{p}}(t) \equiv r_{\mathrm{p}}(t)$ *for all* $t \geq 0$*. Then, for any initial estimation error* $\widetilde{c_{\mathrm{s},+}}(r,0)$*, the estimation error is exponentially stable at the origin in the sense of the norm*

$$\int_{r_{\mathrm{p}}(t)}^{R_{\mathrm{p},+}} r^2 \widetilde{c}_{\mathrm{s},+}(r,t)^2 \mathrm{d}r. \tag{7.29}$$

Note that subtracting (7.20)-(7.22) from (7.5)-(7.7) under $\widehat{r}_{\mathrm{p}}(t) \equiv r_{\mathrm{p}}(t)$ yields the estimation error dynamics

$$\frac{\partial \widetilde{c}_{\mathrm{s},+}}{\partial t}(r,t) = \frac{D_{\mathrm{s},+}}{r^2}\frac{\partial}{\partial r}\left[r^2 \frac{\partial \widetilde{c}_{\mathrm{s},+}}{\partial r}(r,t)\right] - P(r_{\mathrm{p}}(t),r)\widetilde{c}_{\mathrm{s},+}(R_{\mathrm{p},+},t), \tag{7.30}$$

$$\widetilde{c}_{\mathrm{s},+}(r_{\mathrm{p}}(t),t) = 0, \tag{7.31}$$

$$D_{\mathrm{s},+}\frac{\partial \widetilde{c}_{\mathrm{s},+}}{\partial r}(R_{\mathrm{p},+},t) = -Q\left(r_{\mathrm{p}}(t)\right)\widetilde{c}_{\mathrm{s},+}(R_{\mathrm{p},+},t). \tag{7.32}$$

Change of coordinate

First, we introduce the following change of coordinate and state variable to simplify the structure of the estimation error dynamics in a cartesian coordinate:

$$x = R_{\mathrm{p},+} - r, \tag{7.33}$$

$$\widetilde{u}(x,t) = r\widetilde{c}_{\mathrm{s},+}(r,t), \tag{7.34}$$

$$s(t) = R_{\mathrm{p},+} - \widehat{r}_{\mathrm{p}}(t). \tag{7.35}$$

The estimation error dynamics (7.30)-(7.32) is rewritten by the new coordinate and state as

$$\frac{\partial \widetilde{u}}{\partial t}(x,t) = D_{\mathrm{s},+}\frac{\partial^2 \widetilde{u}}{\partial x^2}(x,t) - \overline{P}(s(t),x)\widetilde{u}(0,t), \tag{7.36}$$

$$\widetilde{u}(s(t),t) = 0, \tag{7.37}$$

$$\frac{\partial \widetilde{u}}{\partial x}(0,t) = -\overline{Q}(s(t))\widetilde{u}(0,t), \tag{7.38}$$

where

$$\overline{P}(s(t),x) = \frac{r}{R_{\mathrm{p},+}}P(r_{\mathrm{p}}(t),r), \tag{7.39}$$

$$\overline{Q}(s(t)) = \frac{1}{R_{\mathrm{p},+}} - \frac{1}{D_{\mathrm{s},+}}Q(r_{\mathrm{p}}(t)). \tag{7.40}$$

With respect to the variable (7.35), the properties (7.13) and (7.14) presented in Remark 6 are equivalent to

$$\dot{s}(t) > 0, \tag{7.41}$$

$$0 < s(t) \leq R_{\mathrm{p},+}. \tag{7.42}$$

Derivation of observer gains

Consider the following invertible transformation from the estimation error $\widetilde{u}(x,t)$ to the transformed state $\widetilde{w}(x,t)$:

$$\widetilde{w}(x,t) = \widetilde{u}(x,t) + \int_0^x q(\bar{x},\bar{y})\widetilde{u}(y,t)\mathrm{d}y, \tag{7.43}$$

$$\widetilde{u}(x,t) = \widetilde{w}(x,t) + \int_0^x p(\bar{x},\bar{y})\widetilde{w}(y,t)\mathrm{d}y, \tag{7.44}$$

where $\bar{x} = s(t) - x$, $\bar{y} = s(t) - y$. Similarly to observer design in Section 3.4, we can show that if the gain kernel functions and the observer gains satisfy the following conditions:

$$\frac{\partial^2 p}{\partial \bar{x}^2}(\bar{x},\bar{y}) - \frac{\partial^2 p}{\partial \bar{y}^2}(\bar{x},\bar{y}) = -\bar{\lambda} p(\bar{x},\bar{y}), \tag{7.45}$$

$$p(\bar{x},\bar{x}) = \frac{\bar{\lambda}}{2}\bar{x}, \tag{7.46}$$

$$p(0,\bar{y}) = 0, \tag{7.47}$$

$$\frac{\partial^2 q}{\partial \bar{x}^2}(\bar{x},\bar{y}) - \frac{\partial^2 q}{\partial \bar{y}^2}(\bar{x},\bar{y}) = \bar{\lambda} q(\bar{x},\bar{y}), \tag{7.48}$$

$$q(\bar{x},\bar{x}) = -\frac{\bar{\lambda}}{2}\bar{x}, \tag{7.49}$$

$$q(0,\bar{y}) = 0, \tag{7.50}$$

$$\overline{P}(s(t),x) = D_{\mathrm{s},+} p_{\bar{y}}(\bar{x},s(t)), \tag{7.51}$$

$$\overline{Q}(s(t)) = -p(s(t),s(t)), \tag{7.52}$$

then, the following target $\widetilde{w}$-system is obtained:

$$\begin{aligned}\frac{\partial \widetilde{w}}{\partial t}(x,t) = D_{\mathrm{s},+}\frac{\partial^2 \widetilde{w}}{\partial x^2}(x,t) - \lambda \widetilde{w}(x,t) + \dot{s}(t)\int_0^x q'(\bar{x},\bar{y}) \\ \times \left(\widetilde{w}(y,t) + \int_0^y p(\bar{y},\bar{z})\widetilde{w}(z,t)\mathrm{d}z\right) dy,\end{aligned} \tag{7.53}$$

$$\widetilde{w}(s(t),t) = 0, \tag{7.54}$$

$$\frac{\partial \widetilde{w}}{\partial x}(0,t) = 0, \tag{7.55}$$

where $q'(\bar{x},\bar{y}) = \frac{\partial q}{\partial \bar{x}}(\bar{x},\bar{y}) + \frac{\partial q}{\partial \bar{y}}(\bar{x},\bar{y})$. The equations (7.45)–(7.50) lead to the following explicit solutions:

$$p(\bar{x},\bar{y}) = \bar{\lambda}\bar{x}\frac{I_1\left(\sqrt{\bar{\lambda}\left[\bar{y}^2-\bar{x}^2\right]}\right)}{\sqrt{\bar{\lambda}\left[\bar{y}^2-\bar{x}^2\right]}}, \tag{7.56}$$

$$q(\bar{x},\bar{y}) = -\bar{\lambda}\bar{x}\frac{J_1\left(\sqrt{\bar{\lambda}\left[\bar{y}^2-\bar{x}^2\right]}\right)}{\sqrt{\bar{\lambda}\left[\bar{y}^2-\bar{x}^2\right]}}, \tag{7.57}$$

with a modified Bessel function $I_1(\cdot)$ and a Bessel function $J_1(\cdot)$ of the first kind, respectively. Substituting the solution (7.56) to the conditions (7.51), (7.52) (note that $\frac{dI_1(z)}{\mathrm{d}z} = \frac{I_2(z)}{z}$ for all z), and taking back to the original coordinate and variables, the observer gains are derived as (7.23) and (7.24).

Stability proof

As done in Section 3.4, we consider the time evolution of the following Lyapunov function:

$$W(t) = \frac{1}{2}\int_0^{s(t)} \widetilde{w}(x,t)^2 \mathrm{d}x. \tag{7.58}$$

Taking the time derivative of (7.58) along with (7.53)-(7.55) yields

$$\begin{aligned}\dot{W}(t) = &-D_{\mathrm{s},+}\int_0^{s(t)}\left(\frac{\partial \widetilde{w}}{\partial x}(x,t)\right)^2 \mathrm{d}x - \lambda\int_0^{s(t)}\widetilde{w}(x,t)^2\mathrm{d}x \\ &+\dot{s}(t)\int_0^{s(t)}\widetilde{w}(x,t)\left[\int_0^x q'(\bar{x},\bar{y})\right. \\ &\left.\left(\widetilde{w}(y,t)+\int_0^y P(\bar{y},\bar{z})\widetilde{w}(z,t)\mathrm{d}z\right)dy\right]\mathrm{d}x.\end{aligned} \tag{7.59}$$

Applying Young's, Cauchy Schwartz, and Poincare's inequalities with the help of the properties (7.41) and (7.42), one can show that there exists a constant $a > 0$ such that the following inequality

holds: (refer to Section 3.4 for the detailed steps)

$$\dot{W}(t) \leq -bW(t) + a\dot{s}(t)W(t), \tag{7.60}$$

where $b = \frac{D_{\mathrm{s},+}}{4R_{\mathrm{p},+}^2} + \lambda$. With the help of (7.41) and (7.42), it yields the exponential decay of $W(t)$ as

$$W(t) \leq e^{aR_{\mathrm{p},+}} W(0) e^{-bt}. \tag{7.61}$$

Hence, the origin of $\widetilde{w}$-system is shown to be exponentially stable, from which we conclude Theorem 13.

Observer for Negative Electrode

The observer design for lithium ion concentration in the negative electrode is constructed by the copy of the dynamics (7.2)-(7.4) together with the output injection of the *positive* electrode

$$\frac{\partial \widehat{c}_{\mathrm{s},-}}{\partial t}(r,t) = \frac{D_{\mathrm{s},-}}{r^2}\frac{\partial}{\partial r}\left[r^2 \frac{\partial \widehat{c}_{\mathrm{s},-}}{\partial r}(r,t)\right] + P_-(r_{\mathrm{p}}(t))\widetilde{c}_{\mathrm{s},+}(R_{\mathrm{p},+},t), \tag{7.62}$$

for $r \in (0, R_{\mathrm{p},-})$, $t > 0$ with boundary conditions

$$\frac{\partial \widehat{c}_{\mathrm{s},-}}{\partial r}(0,t) = 0, \tag{7.63}$$

$$D_{\mathrm{s},-}\frac{\partial \widehat{c}_{\mathrm{s},-}}{\partial r}(R_{\mathrm{p},-},t) = -j_{\mathrm{n},-}(t) + Q_-\left(r_{\mathrm{p}}(t)\right)\widetilde{c}_{\mathrm{s},+}(R_{\mathrm{p},+},t). \tag{7.64}$$

Observer gains in the negative electrode are computed to conserve the total amount of lithium ions in the state observer defined as

$$\widehat{n}_{\mathrm{Li}}(t) = \frac{3\varepsilon_{\mathrm{s},+}L_+}{R_{\mathrm{p},+}^3}\int_0^{R_{\mathrm{p},+}} \widehat{c}_{\mathrm{s},+}(r,t)r^2\mathrm{d}r + \frac{3\varepsilon_{\mathrm{s},-}L_-}{R_{\mathrm{p},-}^3}\int_0^{R_{\mathrm{p},-}} \widehat{c}_{\mathrm{s},-}(r,t)r^2\mathrm{d}r. \tag{7.65}$$

Taking the time derivative of (7.65) along with the dynamics (7.20)–(7.28) and (7.62)–(7.64) leads to

$$\frac{d\widehat{n}_{\mathrm{Li},+}}{dt} = -a_{\mathrm{s},+}L_+ j_{\mathrm{n},+}(t) - a_{\mathrm{s},-}L_- j_{\mathrm{n},-}(t) + F\widetilde{c}_{\mathrm{s},+}(R_{\mathrm{p},+},t), \tag{7.66}$$

where F is defined by

$$\begin{aligned} F = {} & a_{\mathrm{s},+}L_+\left(\frac{\kappa}{R_{\mathrm{p},+}^2}\widehat{r}_{\mathrm{p}}(t)^2 + Q(\widehat{r}_{\mathrm{p}}(t))\right) + a_{\mathrm{s},-}L_-Q_-(\widehat{r}_{\mathrm{p}}(t)) \\ & + \frac{3\varepsilon_{\mathrm{s},+}L_+}{R_{\mathrm{p},+}^3}\int_{\widehat{r}_{\mathrm{p}}(t)}^{R_{\mathrm{p},+}} r^2 P(\widehat{r}_{\mathrm{p}}(t),r)dr + \varepsilon_{\mathrm{s},-}L_-P_-(\widehat{r}_{\mathrm{p}}(t)). \end{aligned} \tag{7.67}$$

By the balance of the ionic molar fluxes given in (7.1), the first line in the right hand side of (7.66) is canceled. Therefore, by designing the observer gains as

$$Q_-(r_{\mathrm{p}}(t)) = -\frac{a_{s,+}L_+}{a_{s,-}L_-}\left(Q(r_{\mathrm{p}}(t)) + \frac{\kappa}{R_{\mathrm{p},+}^2}\widehat{r}_{\mathrm{p}}(t)^2\right), \tag{7.68}$$

$$P_-(r_{\mathrm{p}}(t)) = -\frac{\varepsilon_{\mathrm{s},+}L_+}{\varepsilon_{\mathrm{s},-}L_-}\frac{3}{R_{\mathrm{p},+}^3}\left[\int_{\widehat{r}_{\mathrm{p}}(t)}^{R_{\mathrm{p},+}} P(r_{\mathrm{p}}(t))r^2dr\right], \tag{7.69}$$

one can show that $\frac{d\widehat{n}_{\mathrm{Li},+}}{dt} = 0$ from (7.66). Hence, the observer error in the negative electrode approaches to zero uniformly in space with the help of Theorem 13.

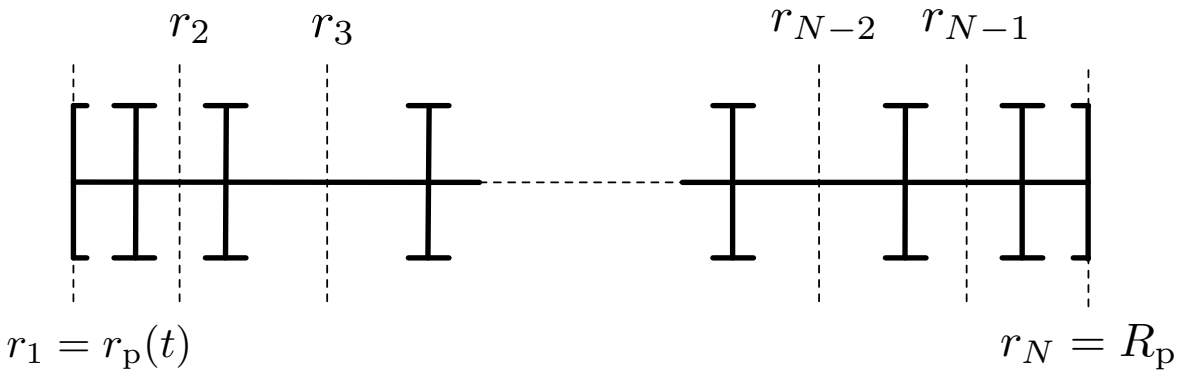

Figure 7.3: Non-uniform grid for spatial discretization.

7.4 Numerical Simulation

Description of the proposed algorithm

For the spatial discretization of the diffusion equations in the single particle model and the observer, we use a finite volume method with non-uniform grid [181]. The reason to use a finite volume method is to guarantee the mass conservation property after discretization. The grid, is a set of N points $r(t) = [r_1(t), r_2(t), \ldots, r_{N-1}(t), r_N(t)]$, that divide the domain $(r_{\mathrm{p}}(t), R_{\mathrm{p}})$ (or $(0, R_{\mathrm{p}})$ for the negative electrode) in a finite set of non-uniform intervals, as depicted in Figure 7.3, and allow us to define a fine discretization near the boundaries of the domain without increasing the size of the finite-dimensional state significantly. Briefly speaking, in the finite volume method, one defines a finite-dimensional state $c_{\mathrm{s}}(t) = [c_{\mathrm{s},2}, \ldots, c_{\mathrm{s},N-1}, c_{\mathrm{s},N}]$, where each element corresponds to the concentration at one of the spatial discretization points. Then, solving the diffusion equation within each of the intervals $\left[\frac{r_{i-1}+r_i}{2}, \frac{r_i+r_{i+1}}{2}\right]$ and using a linear interpolation, a set of ordinary differential equations is obtained; that define the dynamics of the finite-dimensional state. For example, in the positive electrode, the dynamic equation for the finite-dimensional approximation

in β-phase is

$$M(t)\frac{dc_{\mathrm{s}}}{dt}(t) = A(t)c_{\mathrm{s}}(t) + B(t)u(t), \tag{7.70}$$

$$c_{\mathrm{ss},+} = Cc_{\mathrm{s}}(t), \tag{7.71}$$

with

$$u(t) = \left[j_n(t), c_{\mathrm{s},\beta}\right], \tag{7.72}$$

and continuous matrices $M(t), A(t) \in \mathrm{R}^{N-1\times N-1}$, $B_1(t) \in \mathbb{R}^{N-1\times 2}$, $C \in \mathbb{R}^{1\times N-1}$ defined as

$$M(t) = \begin{bmatrix} \frac{3}{4}v_2(t) & \frac{1}{8}v_3(t) & 0 & \cdots & 0 \\ \frac{1}{4}v_2(t) & \frac{3}{4}v_3(t) & \frac{1}{8}v_4(t) & \cdots & 0 \\ 0 & \frac{1}{8}v_3(t) & \frac{3}{4}v_4(t) & \cdots & 0 \\ \vdots & \vdots & \vdots & & \vdots \\ 0 & 0 & 0 & \cdots & \frac{1}{4}v_N(t) \\ 0 & 0 & 0 & \cdots & \frac{3}{4}v_N(t) \end{bmatrix}, \tag{7.73}$$

$$A(t) = \begin{bmatrix} a_{2,2}(t) & a_{2,3}(t) & 0 & \cdots & 0 & 0 \\ a_{3,2}(t) & a_{3,3}(t) & a_{3,4}(t) & \cdots & 0 & 0 \\ 0 & a_{4,3}(t) & a_{4,4}(t) & \cdots & 0 & 0 \\ \vdots & \vdots & \vdots & & \vdots & \vdots \\ 0 & 0 & 0 & \cdots & a_{N-1,N-1}(t) & a_{N-1,N}(t) \\ 0 & 0 & 0 & \cdots & a_{N,N-1}(t) & a_{N,N}(t) \end{bmatrix}, \tag{7.74}$$

$$B(t) = \begin{bmatrix} 0 & b_{1,2}(t) \\ 0 & 0 \\ \vdots & \vdots \\ 0 & 0 \\ b_{N,1} & 0 \end{bmatrix}. \tag{7.75}$$

In (7.73), the volumes $v_i(t)$ are computed based on the geometry of the grid, that is

$$v_i(t) = \left(\left(\frac{r_i(t) + r_{i+1}(t)}{2} \right)^3 - \left(\frac{r_i(t) + r_{i-1}(t)}{2} \right)^3 \right), \tag{7.76}$$

for $i \in \{2,3,\ldots,N-1\}$, and

$$v_{N,N}(t) = \left(R_{\mathrm{p}}^3(t) - \left(\frac{R_{\mathrm{p}}(t) + r_{N-1}(t)}{2} \right)^3 \right). \tag{7.77}$$

The diagonal entries of the matrix $A(t)$ in 7.74 are

$$a_{ii}(t) = -\frac{D_{\mathrm{s}}}{4} \frac{(r_{i+1}(t) + r_i(t))^2}{r_{i+1}(t) - r_1(t)} - \frac{D_{\mathrm{s}}}{4} \frac{(r_i(t) + r_{i-1}(t))^2}{r_i(t) - r_{i-1}(t)}, \tag{7.78}$$

for $i \in \{2,3,\ldots,N-1\}$, and

$$a_{N,N}(t) = \frac{D_{\mathrm{s}}}{4} \frac{(R_{\mathrm{p}}(t) + r_{N-1}(t))^2}{R_{\mathrm{p}}(t) - r_{N-1}(t)}. \tag{7.79}$$

The entries in the line above the diagonal are

$$a_{i,i+1}(t) = \frac{D_{\mathrm{s}}}{4} \frac{(r_{i+1}(t) + r_i(t))^2}{r_{i+1}(t) - r_i(t)}, \tag{7.80}$$

for $i \in \{3,4,\ldots,N\}$, and the entries in the line below the diagonal are

$$a_{i,i-1}(t) = \frac{D_{\mathrm{s}}}{4} \frac{(r_i(t) + r_{i-1}(t))^2}{r_i(t) - r_{i-1}(t)}, \tag{7.81}$$

for $i \in \{2,3,4,\ldots,N-1\}$. The non-zero elements of the matrix $B(t)$ in (7.75) are

$$b_{1,2}(t) = \frac{D_{\mathrm{s}}}{4} \frac{(r_2(t) + r_{\mathrm{p}}(t))^2}{r_2 - r_{\mathrm{p}}(t)}, \tag{7.82}$$

$$b_{N,1} = -R_{\mathrm{p}}^2. \tag{7.83}$$

The initial conditions for (7.70)-(7.71) are the evaluation of the initial concentration profile at each point of the grid r. For the discretization of the continuous-time finite-dimensional system

we use the Euler backward method, which leads to

$$M_{[k+1]}\frac{c_{\mathrm{s},[k+1]}-c_{\mathrm{s},[k+1]}}{t_{[k+1]}-t_{[k]}}=A_{[k+1]}c_{\mathrm{s},[k+1]}+B_{[k+1]}j_{k+1}, \tag{7.84}$$

$$c_{\mathrm{ss},k+1}=Cc_{\mathrm{s},k+1}, \tag{7.85}$$

where the quantities with subscript $[k]\in\{0,1,\ldots,K\}$, correspond the quantities at the discrete times $\{t_0,t_1,\ldots,t_{N_T}\}$. The discretization of the boundary dynamics follows a discrete version of (7.8), derived properly to guarantee mass conservation, that is

$$\left(c_{\mathrm{s},\beta}-c_{\mathrm{s},\alpha}\right)\frac{r_{\mathrm{p},[k+1]}^3-r_{\mathrm{p},[k]}^3}{1}=-\left(t_{[k+1]}-t_{[k]}\right)D_{\mathrm{s}}\left(\frac{r_{2,[k]}-r_{1,[k]}}{2}\right)^2\frac{c_{\mathrm{s},1,[k+1]}-c_{\mathrm{s},\beta}}{r_{2,[k]}-r_{1,[k]}}. \tag{7.86}$$

The time update of the spatial grid, corresponding to the increase of domain in time is performed carefully to ensure mass conversation while keeping the size of the grid constant over time. For this reason a new point in the discretization grid at every time step according to the dynamics of the moving boundary is introduced, if a threshold in surpass. If the threshold is not exceed, the corresponding mass change is added to a mass memory variable for consideration in the next time step. To the new point in the grid we associate a new state equal to c_β. Then, to avoid an increase of the number of states at every time step, an interpolation is performed from the grid with the additional point, that is, with size $N+1$, to a new grid defined in the larger domain but with N point. The interpolation is linear and is corrected for mass conservation (see the description in Algorithm 5).

Test with Constant Discharge Input

To test the observer we run a numerical example with a constant discharge current of 5 [C-rate]. We are assuming $c_{\mathrm{ss},+}$ is available directly from measurements to be used as output error

Algorithm 5: Time Update for Increasing Domain (*Shrinking Core*)

Data: Priovided some spatial grid $r_{[k]} = [r_{1,[k]}, r_{2,[k]}, \ldots, r_{N,[k]}]$, state value $c_{\mathrm{s},[k]} = \left[c_{\mathrm{s},1,[k]}, c_{\mathrm{s},2,[k]}, \ldots, c_{\mathrm{s},N,[k]}\right]$, at time $t_{[k]}$, and memory of mass difference $\triangle m_{[k-1]}$ (the right hand side of (7.86))

compute the mass change $\triangle m_{[k]}$ due to non-zero flux at the interface, i.e., the right hand side of (7.86) and add it to the mass change memory

$$m_{[k]} \leftarrow m_{[k]} + m_{[k-1]},$$

if $m_{[k]} > m_{\text{threshold}}$ **then**

compute a new for the boundary from the interface dynamics (7.86):

$$r_{\mathrm{p},[k]} \leftarrow \left(r^3_{\mathrm{p},[k]} - \frac{m_{[k]}}{c_{\mathrm{s},\beta} - c_{\mathrm{s},\alpha}}\right)^{1/3},$$

add this value as a new point to the grid:

$$r_{[k]} \leftarrow \left[r_{\mathrm{p},[k]}, r_{1,[k]}, r_{2,[k]}, \ldots, r_{N,[k]}\right]$$

add a new entry to the state concentration with the value c_β:

$c_{\mathrm{s},[k]} \leftarrow [c_\beta, c_{\mathrm{s},1,[k]}, c_{\mathrm{s},2,[k]}, \ldots, c_{\mathrm{s},N,[k]}]$,

define a new non-uniform grid $r'_{[k]} = [r'_{1,[k]}, r'_{2,[k]}, \ldots, r'_{N,[k]}]$ such that $r'_{1,[k]} = r_{\mathrm{p},[k]}$ and $r'_{N,[k]} = R_\mathrm{p}$

interpolate (linearly) the concentration state to the new grid:

$$c'_s \leftarrow \texttt{interp}(r', r, c_\mathrm{s})$$

compute average concentrations $\overline{c'_\mathrm{s}}$ and $\overline{c_\mathrm{s}}$ over the spherical volumen

correct for mass conservation with the scaling factor $\overline{c_\mathrm{s}}/\overline{c'_\mathrm{s}}$:

$$c'_\mathrm{s} \leftarrow \frac{\overline{c_\mathrm{s}}}{\overline{c'_\mathrm{s}}} c'_\mathrm{s}$$

return updated grid $r'_{[k]}$, updated state value $c'_{\mathrm{s},[k]}$, and set memory $m_{[k]} = 0$.

else

return unchanged spatial grid $r_{[k]}$, unchanged state value $c_{\mathrm{s},[k]}$, and updated mass memory $m_{[k]}$.

end

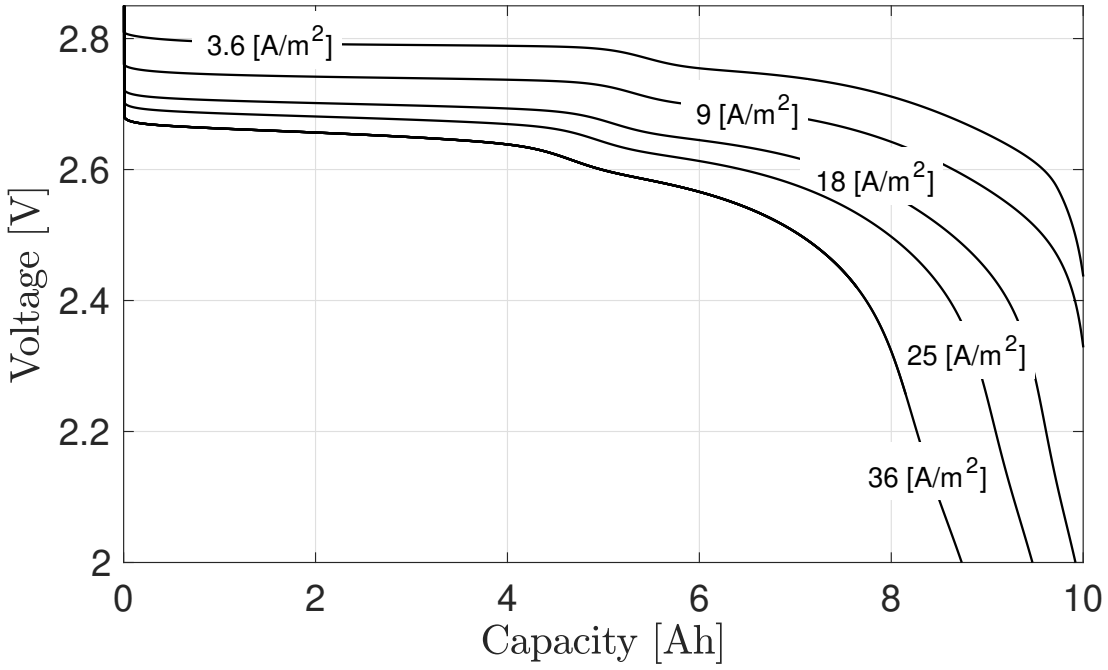

Figure 7.4: Voltage plot for different (constant) current discharge inputs, which shows the analogous behavior to [150].

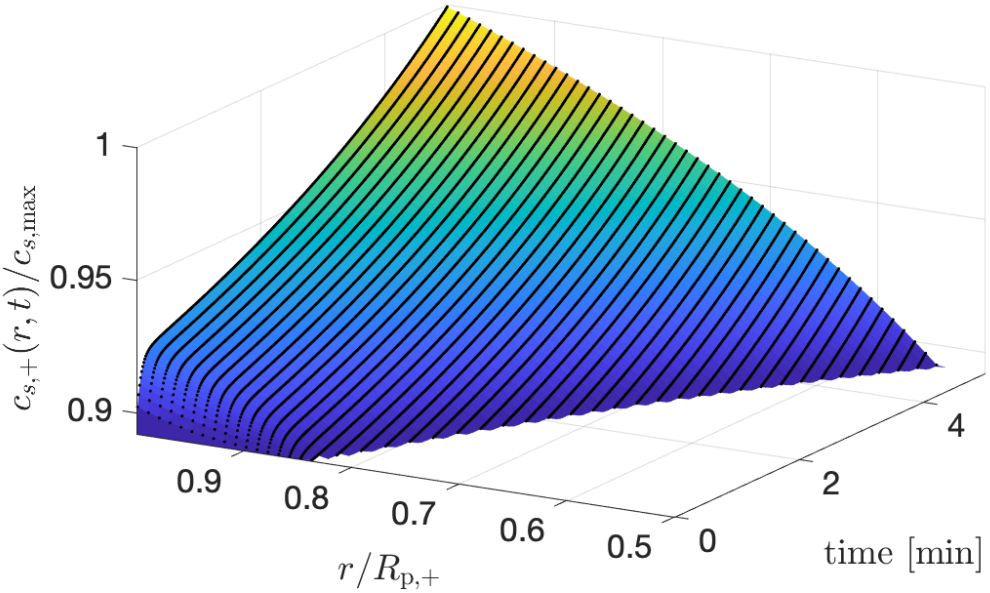

Figure 7.5: Normalized concentration of lithium ions in a growing β-phase region. The plot corresponds to a 5[min] simulation of constant 5[C − rate] discharge. The plot does not show the α-phase portion of the concentration since it is assumed to be constant.

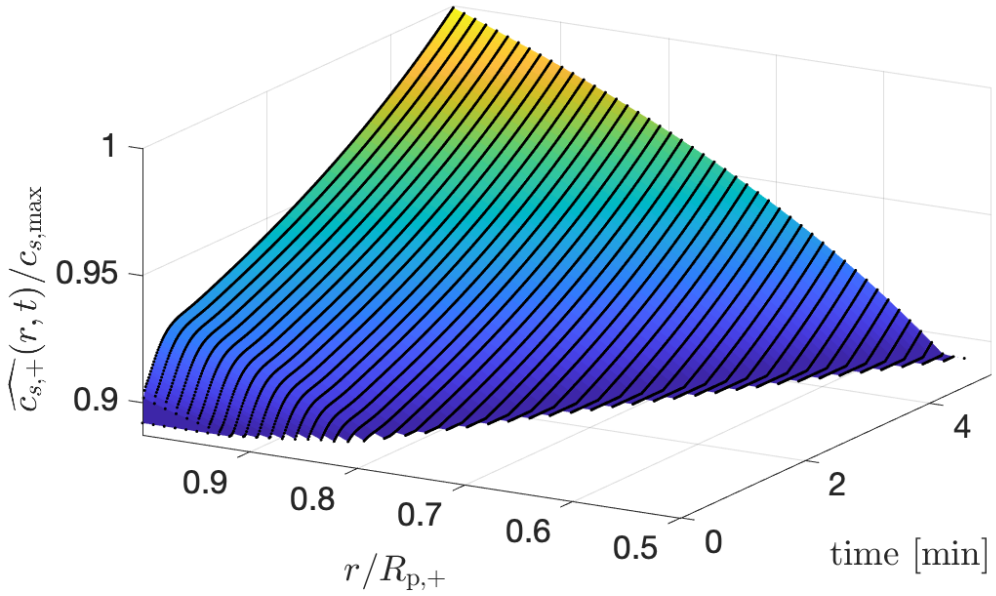

Figure 7.6: Estimate of the concentration of lithium ions in the positive particle. Starting from the initial error, the estimated profile converges to the true profile in Fig. 7.5.

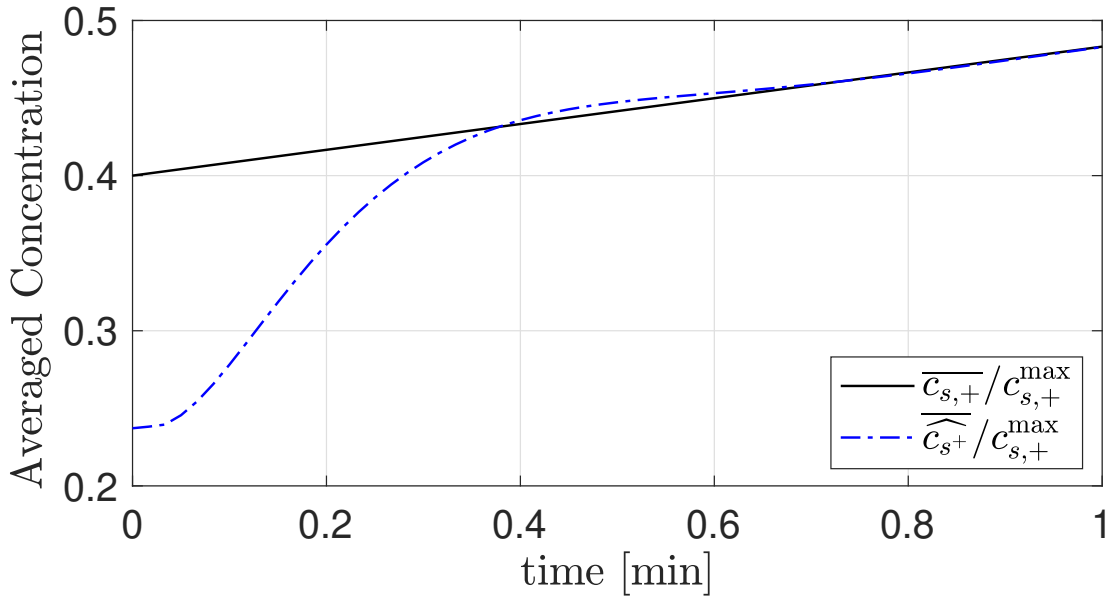

Figure 7.7: Averaged concentration of true value (black solid) and estimated averaged concentration (blue dashed) in the positive particle normalized by the maximum concentration.

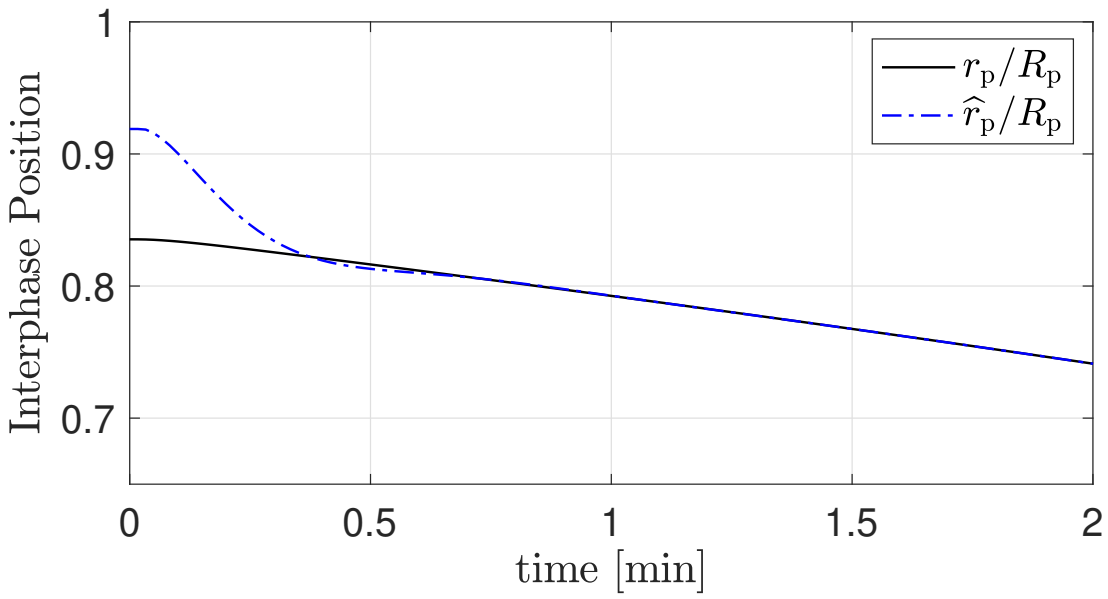

Figure 7.8: The estimated interface position becomes the same value as the true interface position after 0.5 [min].

injection in the observer. In practice, this quantity could be estimated from measurements. Figure 7.6 shows the estimated concentration of lithium ions in β-phase in the positive particle; one can compare this to the true concentration in Figure 7.5. Figure 7.7 shows the averaged concentration in the positive particle, both true value (black) and estimated value (blue). Convergence of the estimate to the true value is achieved within 0.8 [min], a relatively short time. Furthermore, Fig. 7.8 shows the time evolution of the moving interface of the both true value (black) and estimated value (blue), which also illustrates the convergence of the estimate to the true value. Note that SoC is directly proportional to the averaged concentrations; then the importance to evaluate the estimation of this quantity.

7.5 Conclusions and Future Work

This chapter develops the estimation algorithm for SoC via electrochemical-model based moving boundary PDE observer, and provides the numerical study illustrating the desired perfor-

mance of the proposed method. Towards a complete SoC estimation algorithm for lithium ion batteries with phase transition materials, an extension the existing SoC estimation algorithms from SPM to complex electrode settings will be considered, as was already achieved for electrodes with multiple active material [24]. It was noted in [151] that two different particles sizes are needed to correctly model LFP electrodes, this correction can be added to our results following [24]. One of the main assumptions for the model in this paper is the restriction to only two coexisting phases in a single particle reduced further to a single phase problem by assuming a constant core phase. The relaxation of this assumption could be achieved through designing the state observer of concentration of lithium-ions in *two phases* together with the estimation of the interface position, by extending the method for control design in Chapter 5 to the observer design. Furthermore, the robustness of the estimator's performance under some additive measurement noise can be studied in terms of input-to-state stability (ISS) following [23]. These further investigation will be addressed in our future work.

7.6 Acknowledgement

Chapter 7, in part, is a reprint of the material as it appears in:

- S. Koga, L. Camacho-Solorio, and M. Krstic, "State Estimation for Lithium Ion Batteries with Phase Transition Materials", *ASME Dynamic Systems and Control Conference*, 2017,
- S. Koga, L. Camacho-Solorio, and M. Krstic, "State Estimation for Lithium Ion Batteries with Phase Transition Materials via Boundary Observers", *ASME Journal of Dynamic Systems, Measurement, and Control*, under review.

The dissertation author was the primary investigators and author of this paper.

Table 7.1: Parameters of LFP used in the simulation.

Parameters			
	Negative	Separator	Positive
L[m][a]	50×10^{-6}	25×10^{-6}	74×10^{-6}
$c_{\mathrm{s}}^{\max}$[mol/m^3][a]	27760		20950
$c_{\mathrm{s},\alpha}$[mol/m^3][b]			$0.0480 \times c_{\mathrm{s},+}^{\max}$
$c_{\mathrm{s},\beta}$[mol/m^3][b]			$0.8920 \times c_{\mathrm{s},+}^{\max}$
R_{p} [m][a]	11×10^{-6}		52×10^{-9}
D_{s} [m^2/s][a]	9×10^{-14}		8×10^{-18}
ε_{s} [$-$][a]	0.33		0.27
R_{f} [Ωm^2][b]	1×10^{-5}		0
R_{c} [Ωm^2][b]	0		6.5×10^{-3}
k [m$^{2.5}$/mol$^{0.5}$s][a]	3×10^{-5}		3×10^{-17}

Other Parameters and Physical Constants	
A [m][b]	1
F [As/mol]	96487
R [J/Kmol]	8.314472
T [K][b]	298
c_{e} [mol/m^3][a]	1×10^3
$\alpha_{\mathrm{a}}, \alpha_{\mathrm{c}}$ [$-$][a]	0.5

[a] borrowed from [151]
[b] assumed

Chapter 8

Polymer 3D-Printing via Screw Extrusion

8.1 Emergence of 3D-Printing

On the verge of new manufacturing techniques, additive manufacturing stands out as a versatile tool for high flexibility and fast adaptability in production. It is applicable in a variety of producing industries, ranging from tissue engineering [114], thermoplastics [162], metal [106] and ceramic [137] fabrication. One of the most popular types of 3D printing is Fused Deposition Modeling (FDM) [115], which uses filaments as raw material, that have to be precisely manufactured to achieve a good final product quality [21].

8.2 Screw Extrusion Process

From the polymer processing and extrusion cooking industry, screw extruders are well-known devices. Results stated in [116, 154, 101, 108] give an in-depth description of screw geometrics, extruder setups and describe the dynamics of extrusion process consisting of a conveying zone, a melting zone, and a mixing zone. A mathematical description of such a model is derived by mass, momentum, and energy balances and appears as coupled transport equations

coupled through a moving interface. This model is used in [108] to describe an extrusion cooking process. The boundary control of a similar model is achieved in [38, 39] under the assumption of constant viscosity.

More recent contributions considered screw extrusion as a useful technology for 3D printing applications [162, 40, 37], allowing to manufacture a wider variety of materials than FDM, while using polymer granules as raw material [162]. In [37], a time-delay control was developed on a model consisting of two phases, similarly to [108]. In both cases, stabilization of the moving interface separating a conveying and a melting zone is achieved with a fast convergence rate. Another approach which enables to control screw extruders in 3D printing is proposed in [40], where an energy-based model is established, simplifying the implementation of the control law and circumventing difficulties with state measurement. In other words, the control of the outflow rate at the nozzle only relies on the measurement of the heater current and the screw speed.

In the screw extrusion process, the solid material is convected from the feed to the nozzle located at the end of a heating chamber. The solid raw material is melted and mixed before being expelled through the nozzle as a thin filament. For this process, the thermal behavior is an important factor which characterizes final product quality. Indeed, heat is supplied into the system by the heaters surrounding the extruder's barrel on the one hand and by the viscous heat generation due to a shearing effect [108] on the other hand. The process of the phase transition from the solid to the liquid polymer can be described as the Stefan problem. In this context, the dynamics of the solid-liquid phase interface is derived from the energy conservation in which the latent heat required for melting is driven by the internal heat of the liquid phase, resulting in the interface velocity to be proportional to the temperature gradients of the adjacent phase. For instance, in [44], the Stefan problem for a polymer crystallization process is described, and the analytical crystallization time is derived.

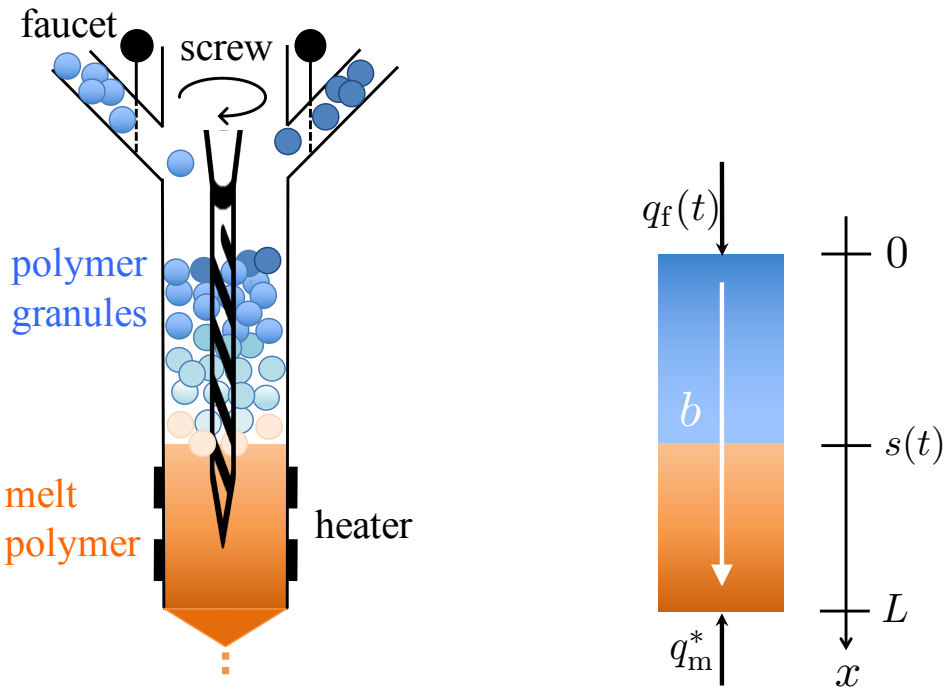

Figure 8.1: Schematic of screw extruder for original description (left) and model description (right).

8.3 Thermodynamic Modelling

We focus on the thermodynamic model of the screw extrusion process in one-dimensional coordinate along the vertical axis, motivated by [154] which developed a thermodynamic phase change model for polymer processing. The model provides the time evolution of the temperature profile of the extruded material and the interface position between the fed polymer granules and the molten polymer. The granular pellets are conveyed by the screw rotation at a given speed b along the vertical axis while the barrel temperature is uniformly maintained at T_{b}. Defining $T_{\mathrm{s}}(x,t)$ and $T_{\mathrm{l}}(x,t)$ as the temperature profiles of solid phase (polymer granules) over the spatial domain $x \in (0, s(t))$ and liquid phase (molten polymer) over the spatial domain $x \in (s(t), L)$,

respectively, the following thermodynamical model

$$\frac{\partial T_{\mathrm{s}}}{\partial t}(x,t) = \alpha_{\mathrm{s}} \frac{\partial^2 T_{\mathrm{s}}}{\partial x^2}(x,t) - b\frac{\partial T_{\mathrm{s}}}{\partial x}(x,t) + h_{\mathrm{s}}\left(T_{\mathrm{b}} - T_{\mathrm{s}}(x,t)\right), \quad 0 < x < s(t), \tag{8.1}$$

$$\frac{\partial T_{\mathrm{l}}}{\partial t}(x,t) = \alpha_{\mathrm{l}} \frac{\partial^2 T_{\mathrm{l}}}{\partial x^2}(x,t) - b\frac{\partial T_{\mathrm{l}}}{\partial x}(x,t) + h_{\mathrm{l}}\left(T_{\mathrm{b}} - T_{\mathrm{l}}(x,t)\right), \quad s(t) < x < L \tag{8.2}$$

is derived from the energy conservation and heat conduction laws. In this paper, we consider the temperature distribution in the liquid to be static as stated in (8.11) and in Assumption 14 (see Section 8.4). Here, $\alpha_i = \frac{k_i}{\rho_i c_i}$ and $h_i = \frac{\bar{h}_i}{\rho_i c_i}$, where ρ_i, c_i, k_i, and $\bar{h}_i$ for $i \in \{s,l\}$ are the density, the heat capacity, the thermal conductivity, and the heat transfer coefficient, respectively and the subscripts s and l are associated to the solid or liquid phase, respectively. Referring to [163] which introduces a model of spatially averaged temperature for screw extrusion, we incorporate the convective heat transfer through the barrel temperature in (8.1) (8.2). The boundary conditions at $x = 0$ and $x = L$ follow the heat conduction law, and the temperature at the interface $x = s(t)$ is maintained at the melting point T_{m}, described as

$$\frac{\partial T_{\mathrm{s}}}{\partial x}(0,t) = -\frac{q_{\mathrm{f}}(t)}{k_{\mathrm{s}}}, \quad T_{\mathrm{s}}(s(t),t) = T_{\mathrm{m}}, \tag{8.3}$$

$$\frac{\partial T_{\mathrm{l}}}{\partial x}(L,t) = \frac{q^*_{\mathrm{m}}}{k_{\mathrm{l}}}, \quad T_{\mathrm{l}}(s(t),t) = T_{\mathrm{m}}, \tag{8.4}$$

where $q_{\mathrm{f}}(t) < 0$ is a freezing controller at the inlet and $q^*_{\mathrm{m}} > 0$ is a heat flux at the nozzle which is assumed to be constant in time. The interface dynamics is derived by the energy balance at the interface as

$$\rho_s \Delta H \dot{s}(t) = k_{\mathrm{s}} \frac{\partial T_{\mathrm{s}}}{\partial x}(s(t),t) - k_{\mathrm{l}} \frac{\partial T_{\mathrm{l}}}{\partial x}(s(t),t). \tag{8.5}$$

The equations (8.1)-(8.5) are the solid-liquid phase change model known as the "two-phase" Stefan problem. Such a phase change model was developed for polymer processing. Here, we

give the following remark to emphasize the conditions for the model (8.1)-(8.5) to be physically validated.

Remark 7 *In this paper, we assume the pressure in the chamber to be static, and the melting temperature is constant to avoid supercooling. Then, to keep the physical state of each phase, the following conditions must hold:*

$$T_{\mathrm{s}}(x,t) \leq T_{\mathrm{m}}, \quad \forall x \in (0, s(t)), \quad \forall t > 0, \tag{8.6}$$

$$T_{\mathrm{l}}(x,t) \geq T_{\mathrm{m}}, \quad \forall x \in (s(t), L), \quad \forall t > 0, \tag{8.7}$$

which represent the model validity conditions.

Remark 8 *We assume the existence of a heating/cooling system that maintains the pellets at a controlled temperature, as stated in* (8.3)*, which describes the heat flux control at the inlet. Extruders can be equipped with raw material preconditioners as intermediate unit operators, which for instance help to pre-heat ingredients before they enter the extruder chamber by adding steam. The preconditioners are usually located between the inlet and the extruder chamber, and a continuous flow of material from the feeder to the preconditioner is maintained [131, 48].*

8.4 Ink Production Control Based on Screw Speed

To ensure a continuous extrusion process, the control of the quantity of molten polymer that remains in the extruder chamber at any given time is crucial. By definition, the volume of fully melted material contained in the chamber is directly related to the position of the solid-liquid interface that needs to be controlled, consequently. Physically, any given position of the interface along the spatial domain corresponds to a melt temperature profile along the extruder.

Steady-state solution

An analytical solution of the steady-state temperature profile denoted as $\left(T_{\mathrm{s,eq}}(x), T_{\mathrm{l,eq}}(x)\right)$ for any given setpoint value of the interface position defined as s_{r}, can be computed by setting the time derivative of the system (8.1)-(8.5) to zero. Hence, from (8.1) and (8.2) the following set of ordinary differential equations in space are obtained

$$\begin{cases} 0 = & \alpha_{\mathrm{s}} T''_{\mathrm{s,eq}}(x) - b T'_{\mathrm{s,eq}}(x) + h_{\mathrm{s}} \left(T_{\mathrm{b}} - T_{\mathrm{s,eq}}(x)\right), \\ 0 = & \alpha_{\mathrm{l}} T''_{\mathrm{l,eq}}(x) - b T'_{\mathrm{l,eq}}(x) + h_{\mathrm{l}} \left(T_{\mathrm{b}} - T_{\mathrm{l,eq}}(x)\right), \end{cases} \tag{8.8}$$

and the boundary values are given as

$$\begin{cases} T'_{\mathrm{s,eq}}(0) = & -\frac{q^*_{\mathrm{f}}}{k_{\mathrm{s}}}, \quad T_{\mathrm{s,eq}}(s_{\mathrm{r}}) = T_{\mathrm{m}}, \\ T'_{\mathrm{l,eq}}(L) = & \frac{q^*_{\mathrm{m}}}{k_{\mathrm{l}}}, \quad T_{\mathrm{l,eq}}(s_{\mathrm{r}}) = T_{\mathrm{m}}. \end{cases} \tag{8.9}$$

At equilibrium, the interface equation (8.5) satisfies the following equality:

$$0 = k_{\mathrm{s}} T'_{\mathrm{s,eq}}(s_{\mathrm{r}}) - k_{\mathrm{l}} T'_{\mathrm{l,eq}}(s_{\mathrm{r}}). \tag{8.10}$$

The solution to the set of differential equations (8.8) has the following form

$$\begin{cases} T_{\mathrm{l,eq}}(x) = & p_1 e^{q_1 (x - s_{\mathrm{r}})} + p_2 e^{q_2 (x - s_{\mathrm{r}})} + T_{\mathrm{b}}, \\ T_{\mathrm{s,eq}}(x) = & p_3 e^{q_3 (x - s_{\mathrm{r}})} + p_4 e^{q_4 (x - s_{\mathrm{r}})} + T_{\mathrm{b}}, \end{cases} \tag{8.11}$$

where

$$q_1 = \frac{b + \sqrt{b^2 + 4\alpha_{\mathrm{l}} h_{\mathrm{l}}}}{2\alpha_{\mathrm{l}}}, \quad q_2 = \frac{b - \sqrt{b^2 + 4\alpha_{\mathrm{l}} h_{\mathrm{l}}}}{2\alpha_{\mathrm{l}}}, \tag{8.12}$$

$$q_3 = \frac{b + \sqrt{b^2 + 4\alpha_{\mathrm{s}} h_{\mathrm{s}}}}{2\alpha_{\mathrm{s}}}, \quad q_4 = \frac{b - \sqrt{b^2 + 4\alpha_{\mathrm{s}} h_{\mathrm{s}}}}{2\alpha_{\mathrm{s}}}. \tag{8.13}$$

Let $r = T_{\mathrm{b}} - T_{\mathrm{m}}$. Substituting (8.11) into the boundary conditions (8.9) and (8.10), we obtain

$$p_1 = \frac{rq_2 e^{q_2(L-s_{\mathrm{r}})} + q_{\mathrm{m}}^*/k_{\mathrm{l}}}{q_1 e^{q_1(L-s_{\mathrm{r}})} - q_2 e^{q_2(L-s_{\mathrm{r}})}}, \tag{8.14}$$

$$p_2 = -\frac{rq_1 e^{q_1(L-s_{\mathrm{r}})} + q_{\mathrm{m}}^*/k_{\mathrm{l}}}{q_1 e^{q_1(L-s_{\mathrm{r}})} - q_2 e^{q_2(L-s_{\mathrm{r}})}}, \tag{8.15}$$

$$p_3 = \frac{rq_4 + K/k_{\mathrm{s}}}{q_3 - q_4}, \tag{8.16}$$

$$p_4 = \frac{-rq_3 - K/k_{\mathrm{s}}}{q_3 - q_4}, \tag{8.17}$$

$$K = \frac{k_{\mathrm{l}} r(-q_1 q_2)\left(e^{q_1(L-s_{\mathrm{r}})} - e^{q_2(L-s_{\mathrm{r}})}\right) + (q_1 - q_2)q_{\mathrm{m}}^*}{q_1 e^{q_1(L-s_{\mathrm{r}})} - q_2 e^{q_2(L-s_{\mathrm{r}})}}, \tag{8.18}$$

and the steady-state input is given by

$$q_{\mathrm{f}}^* = p_3 q_3 e^{-q_3 s_{\mathrm{r}}} + p_4 q_4 e^{-q_4 s_{\mathrm{r}}}. \tag{8.19}$$

Hence, once the parameters $(s_{\mathrm{r}}, T_{\mathrm{b}}, q_{\mathrm{m}}^*)$ are prescribed, the steady-state input is uniquely obtained.

Barrel temperature condition for a valid steady-state

For the model validity, the steady-state must satisfy (8.6) and (8.7), which restricts the barrel temperature to some physically admissible values.

Lemma 12 *If the barrel temperature satisfies*

$$-\underline{q} \le T_{\mathrm{b}} - T_{\mathrm{m}} \le \bar{q}, \tag{8.20}$$

where

$$\underline{q} = \frac{(q_1 - q_2) q_{\mathrm{m}}^*}{q_{den}}, \quad \bar{q} = -\frac{q_{\mathrm{m}}^*}{k_{\mathrm{l}} q_2 e^{q_2 (L - s_{\mathrm{r}})}}, \tag{8.21}$$

$$q_{den} = -k_{\mathrm{l}} q_1 q_2 \left(e^{q_1 (L - s_{\mathrm{r}})} - e^{q_2 (L - s_{\mathrm{r}})} \right) + k_{\mathrm{s}} q_3 \left(q_1 e^{q_1 (L - s_{\mathrm{r}})} - q_2 e^{q_2 (L - s_{\mathrm{r}})} \right), \tag{8.22}$$

then the steady-state solution satisfies (8.6) *and* (8.7).

Proof:

Since $T_{\mathrm{l,eq}}(s_{\mathrm{r}}) = T_{\mathrm{m}}$, it is necessary to have $T'_{\mathrm{l,eq}}(s_{\mathrm{r}}) \geq 0$ which yields

$$p_1 q_1 + p_2 q_2 \geq 0. \tag{8.23}$$

Substituting (8.14) and (8.15) into (8.23), we get

$$T_{\mathrm{b}} - T_{\mathrm{m}} \geq \frac{(q_1 - q_2)\, q_{\mathrm{m}}^*}{k_{\mathrm{l}} q_1 q_2 \left(e^{q_1 (L - s_{\mathrm{r}})} - e^{q_2 (L - s_{\mathrm{r}})} \right)}, \tag{8.24}$$

knowing that $q_1 q_2 < 0$. With the help of (8.23) and from (8.11) the derivative of $T_{\mathrm{l,eq}}(x)$ satisfies

$$T'_{\mathrm{l,eq}}(x) \geq p_1 q_1 \left(e^{q_1 (x - s_{\mathrm{r}})} - e^{q_2 (x - s_{\mathrm{r}})} \right). \tag{8.25}$$

Thus, the sufficient condition of $T'_{\mathrm{l,eq}}(x) \geq 0$ for all $x \in (s_{\mathrm{r}}, L)$ is $p_1 q_1 \geq 0$ which yields

$$T_{\mathrm{b}} - T_{\mathrm{m}} \leq -\frac{q_{\mathrm{m}}^*}{k_{\mathrm{l}} q_2 e^{q_2 (L - s_{\mathrm{r}})}}. \tag{8.26}$$

Next, the solid steady-state satisfies $T_{\mathrm{s,eq}}(s_{\mathrm{r}}) = T_{\mathrm{m}}$, so it is necessary to have $T'_{\mathrm{s,eq}}(s_{\mathrm{r}}) \geq 0$ leading to $p_3 q_3 + p_4 q_4 \geq 0$ which trivially holds under condition of (8.23). Hence, from (8.11), the

derivative of $T_{\mathrm{s,eq}}(x)$ satisfies

$$T'_{\mathrm{s,eq}}(x) \geq p_4 q_4 \left(-e^{q_3(x-s_{\mathrm{r}})} + e^{q_4(x-s_{\mathrm{r}})} \right). \tag{8.27}$$

Then, the sufficient condition for $T'_{\mathrm{s,eq}}(x) \geq 0$ is $p_4 q_4 \geq 0$, which yields

$$T_{\mathrm{b}} - T_{\mathrm{m}} \geq -\frac{(q_1 - q_2) q^*_{\mathrm{m}}}{q_{den}}. \tag{8.28}$$

One can notice that condition (8.28) is less conservative than condition (8.24). Hence, combining (8.26) and (8.28), we conclude Lemma 12.

Estimator Design of the Temperature Profile

Generally, the full-state feedback control law is designed by assuming that the spatially distributed temperature profile can be measured. Some imaging-based thermal sensors, such as the IR camera, enable to capture the entire profile of temperature. However, these sensors include high noise and detect the temperature of the chamber, which contains a nominal error from the temperature of the polymer inside. Instead, single point thermal sensors such as thermocouples enable to accurately measure the surface temperature at the inlet of the extruder. Moreover, the interface position between the polymer granules and the melt polymer can be detected by cameras via image signal processing. Thus, we build an observer to estimate the temperature profile by utilizing these two available measurements.

Let $\hat{T}_{\mathrm{s}}(x,t)$ be the estimated temperature profile. The observer design for $\hat{T}_{\mathrm{s}}(x,t)$ is stated in the following theorem.

Theorem 14 *Consider the plant model* (8.1)*,* (8.3) *with the two available measurements of*

$$Y_1(t) = s(t), \quad Y_2(t) = T_s(0,t), \tag{8.29}$$

and the following PDE observer

$$\begin{aligned}
\frac{\partial \hat{T}_{\mathrm{s}}}{\partial t}(x,t) =& \alpha_{\mathrm{s}} \frac{\partial^2 \hat{T}_{\mathrm{s}}}{\partial x^2}(x,t) - b \frac{\partial \hat{T}_{\mathrm{s}}}{\partial x}(x,t) \\
&+ h_{\mathrm{s}} \left(T_{\mathrm{b}} - \hat{T}_{\mathrm{s}}(x,t) \right), \quad 0 < x < Y_1(t), && (8.30) \\
\frac{\partial \hat{T}_{\mathrm{s}}}{\partial x}(0,t) =& - \frac{q_{\mathrm{f}}(t)}{k_{\mathrm{s}}} - \gamma \left(Y_2(t) - \hat{T}_{\mathrm{s}}(0,t) \right), && (8.31) \\
\hat{T}_{\mathrm{s}}(s(t),t) =& T_{\mathrm{m}}, && (8.32)
\end{aligned}$$

where $\gamma = \frac{b}{2\alpha_{\mathrm{s}}}$*. Assume that* $s(t) \in (0,L)$ *and* $\dot{s}(t) \geq 0$ *for all* $t \geq 0$*. Then, the observer error system is exponentially stable at the origin in the sense of the norm*

$$\tilde{\Phi}(t) := ||T_{\mathrm{s}}(x,t) - \hat{T}_{\mathrm{s}}(x,t)||_{\mathcal{H}_1}. \tag{8.33}$$

More precisely, there exists a positive constant $\tilde{M} > 0$ *such that the following inequality holds:*

$$\tilde{\Phi}(t) \leq \tilde{M} \tilde{\Phi}(0) e^{-2\left(h_s + \frac{b^2}{4\alpha_{\mathrm{s}}} + \frac{\alpha_s}{4L^2}\right)t}. \tag{8.34}$$

Remark 9 *As stated in Lemma 14 (Section 8.4), the assumption* $\dot{s}(t) \geq 0$ *for all* $t \geq 0$ *holds under the closed-loop control law proposed in Section 8.4.*

Proof:

Let $\tilde{u}$ be the estimation error state defined by

$$\tilde{u} := T_{\rm s} - \hat{T}_{\rm s}. \tag{8.35}$$

Subtraction of the observer system (8.30)–(8.32) from the plant (8.1) and (8.3) yields the following estimation error system:

$$\frac{\partial \tilde{u}}{\partial t}(x,t) = \alpha_{\rm s}\frac{\partial^2 \tilde{u}}{\partial x^2}(x,t) - b\frac{\partial \tilde{u}}{\partial x}(x,t) - h_{\rm s}\tilde{u}(x,t), \tag{8.36}$$

$$\frac{\partial \tilde{u}}{\partial x}(0,t) = \gamma\tilde{u}(0,t), \tag{8.37}$$

$$\tilde{u}(s(t),t) = 0. \tag{8.38}$$

Let us introduce the following change of variable

$$\tilde{z}(x,t) = \tilde{u}(x,t)e^{-\gamma x}. \tag{8.39}$$

Then, $\tilde{u}$-system in (8.36)–(8.38) is converted into the following $\tilde{z}$-system:

$$\frac{\partial \tilde{z}}{\partial t} = \alpha\frac{\partial^2 \tilde{z}}{\partial x^2} - \lambda\tilde{z}, \tag{8.40}$$

$$\frac{\partial \tilde{z}}{\partial x}(0,t) = 0, \tag{8.41}$$

$$\tilde{z}(s(t),t) = 0. \tag{8.42}$$

where $\lambda = h_s + \frac{b^2}{4\alpha_{\rm s}}$. To study the stability of the estimation error state at the origin, we consider the Lyapunov functional

$$\tilde{V} = \frac{1}{2}\int_0^{s(t)} \tilde{z}(x,t)^2 dx + \frac{1}{2}\int_0^{s(t)} \frac{\partial \tilde{z}}{\partial x}(x,t)^2 dx. \tag{8.43}$$

Taking the time derivative of (8.43) along the solution of (8.36)–(8.38) leads to

$$\dot{\tilde{V}} = -\alpha_s \left|\left| \frac{\partial^2 \tilde{z}}{\partial x^2} \right|\right|_{L_2}^2 - (\alpha_s + \lambda) \left|\left| \frac{\partial \tilde{z}}{\partial x} \right|\right|_{L_2}^2 - \lambda ||\tilde{z}||_{L_2}^2 - \frac{\dot{s}(t)}{2} \frac{\partial \tilde{z}}{\partial x}(s(t),t)^2. \tag{8.44}$$

Note that we used $\frac{\partial \tilde{z}}{\partial t}(s(t),t) = -\dot{s}(t)\frac{\partial \tilde{z}}{\partial x}(s(t),t)$ derived from the time derivative of the boundary condition (8.42). With the help of $s(t) \in (0,L)$, Poincare's inequality gives $||\tilde{z}||_{L_2}^2 \leq 4L^2 ||\frac{\partial \tilde{z}}{\partial x}||_{L_2}^2$ and $||\frac{\partial \tilde{z}}{\partial x}||_{L_2}^2 \leq 4L^2 ||\frac{\partial^2 \tilde{z}}{\partial x^2}||_{L_2}^2$. Applying these inequalities and $\dot{s}(t) \geq 0$ to (8.44) leads to the following differential inequality

$$\dot{\tilde{V}} \leq -2\left(\lambda + \frac{\alpha_s}{4L^2}\right)\tilde{V}. \tag{8.45}$$

Applying the comparison principle to (8.45) yields

$$\tilde{V}(t) \leq \tilde{V}(0) e^{-2\left(\lambda + \frac{\alpha_s}{4L^2}\right)t}. \tag{8.46}$$

By the definition of $\tilde{z}$ given in (8.39), for the norm of $\tilde{u}$-system, the following upper and lower bounds hold $||\tilde{z}||_{L_2}^2 \leq ||\tilde{u}||_{L_2}^2 \leq e^{2\gamma L}||\tilde{z}||_{L_2}^2$, $\left|\left|\frac{\partial \tilde{z}}{\partial x}\right|\right|_{L_2}^2 \leq 2\left|\left|\frac{\partial \tilde{u}}{\partial x}\right|\right|_{L_2}^2 + 2\gamma^2 ||\tilde{u}||_{L_2}^2$, $\left|\left|\frac{\partial \tilde{u}}{\partial x}\right|\right|_{L_2}^2 \leq 2e^{2\gamma L}\left(\left|\left|\frac{\partial \tilde{z}}{\partial x}\right|\right|_{L_2}^2 + \gamma^2 ||\tilde{z}||_{L_2}^2\right)$. Hence, by defining $\tilde{\Phi}(t) = ||\tilde{u}||_{\mathcal{H}_1}^2$, the following inequalities hold

$$\tilde{M}_1 \tilde{V} \leq \tilde{\Phi} \leq \tilde{M}_2 \tilde{V} \tag{8.47}$$

where $\tilde{M}_1 = 1/\max\{3, 2\gamma^2\}$, and $\tilde{M}_2 = e^{2\gamma L}\max\{3, 2\gamma^2\}$. Applying (8.46) to (8.47) with defining $\tilde{M} = \tilde{M}_2/\tilde{M}_1$ leads to the conclusion in Theorem 14.

In addition, the estimated temperature can maintain not greater value than the true temperature in the plant, as stated in the following lemma.

Lemma 13 *If $\tilde{u}(x,0) \geq 0$, $\forall x \in (0,s_0)$, then*

$$\tilde{u}(x,t) \geq 0, \quad \forall x \in (0,s(t)), \quad \forall t \geq 0, \tag{8.48}$$

$$\frac{\partial \tilde{u}}{\partial x}(s(t),t) \leq 0, \quad \forall t \geq 0 \tag{8.49}$$

Proof:

Applying Maximum principle to $\tilde{z}$-system governed by (8.40)–(8.42) leads to the statement that if $\tilde{z}(0,t) \geq 0$, $\forall x \in (0,s_0)$ then $\tilde{z}(x,t) \geq 0$, $\forall x \in (0,s(t)), \forall t \geq 0$. By the relation between $\tilde{z}$ and $\tilde{u}$ given in (8.39), we prove Lemma 13, with the help of Hopf's lemma.

The properties in Lemma 13 are required to guarantee the positivity of the boundary heat input under the output feedback control design which is given in the later sections.

Remark 10 *The convergence speed of the designed observer is characterized by $h_s + \frac{b^2}{4\alpha_s} + \frac{\alpha_s}{4L^2}$ as seen in the estimate of the norm* (8.34)*, which cannot be chosen arbitrary fast for given physical constants and the manufacturing speed. The performance improvement to fasten the observer's convergence can be achieved by adding the measurement error injection to the observer PDE formulated by*

$$\begin{aligned}\frac{\partial \hat{T}_{\mathrm{s}}}{\partial t}(x,t) =& \alpha_{\mathrm{s}} \frac{\partial^2 \hat{T}_{\mathrm{s}}}{\partial x^2}(x,t) - b\frac{\partial \hat{T}_{\mathrm{s}}}{\partial x}(x,t) + h_{\mathrm{s}}\left(T_{\mathrm{b}} - \hat{T}_{\mathrm{s}}(x,t)\right) \\ &+ p(x,t)(Y_2(t) - \hat{T}_{\mathrm{s}}(0,t)), \ \ 0 < x < Y_1(t),\end{aligned} \tag{8.50}$$

where the distributed observer gain $p(x,t)$ can be designed using backstepping method as developed in Chapter 3. However, with the PDE observer (8.50)*, it is challenging to ensure the positivity of the output feedback control law. Since this paper's primary focus is on control design, we use the PDE observer given in* (8.30)–(8.32)*.*

Control Design of Boundary Heat

When the solid pellets are injected and heated into the extruder chamber, the amount of the molten polymer expands, reducing the quantity of solid material into the chamber. Thus a cooling effect arising from the continuous feeding of cooler pellets enables to maintain the interface at the desired setpoint. The setpoint open-loop boundary heat control $q_{\mathrm{f}}(t) = q_{\mathrm{f}}^*$ (see (8.9)) is not sufficient to drive the solid-liquid interface position to the desired setpoint. In this section, we develop the control design of the boundary heat at the inlet to drive the interface to the setpoint while stabilizing the temperature profile at the steady-state.

Reference error system for a dynamics reduced to a single phase

First, we impose the following assumption on the liquid temperature.

Assumption 14 *The liquid temperature is at steady-state profile, i.e.* $T_{\mathrm{l}}(x,t) = T_{\mathrm{l,eq}}(x)$.

Assumption 14 reasonably describes the case where the entire extruder chamber is filed with molten polymer at equilibrium temperature at the initial time. Thus, under the setup introduced later in Section 8.4, the L^2-norm of the reference error temperature $\|v(x,t) = T_{\mathrm{l}}(x,t) - T_{\mathrm{l,eq}}(x)\|_{L^2}$ converges to zero according to a straightforward Lyapunov analysis. Under Assumption 14, the two-phase dynamics governed by (8.1)–(8.5) is reduced to a single-phase model. Let $(u(x,t), \hat{u}(x,t), X(t))$ be the reference error variables defined by

$$u(x,t) = -k_{\mathrm{s}}(T_{\mathrm{s}}(x,t) - T_{\mathrm{s,eq}}(x)), \tag{8.51}$$

$$\hat{u}(x,t) = -k_{\mathrm{s}}(\hat{T}_{\mathrm{s}}(x,t) - T_{\mathrm{s,eq}}(x)), \tag{8.52}$$

$$X(t) = s(t) - s_{\mathrm{r}}. \tag{8.53}$$

Note that the negative signs are included in (8.51) and (8.52) to make the states $(u, \hat{u})$ have positivity properties for the model validity conditions to hold. Then, the estimation error state

$\tilde{u}$ defined by (8.35) yields $\tilde{u}(x,t) = \hat{u}(x,t) - u(x,t)$. We rewrite the original system (8.1)–(8.5) using the reference and estimation error states $(\hat{u}, X, \tilde{u})$. Substituting $x = s(t)$ into (8.52) with the help of (8.32), we get

$$\hat{u}(s(t),t) = k_{\mathrm{s}}(T_{\mathrm{s,eq}}(s(t)) - T_{\mathrm{m}}). \tag{8.54}$$

In addition, rewriting (8.5) in term of $\hat{u}(x,t)$ with $\tilde{u}(x,t)$ leads to the following equation of interface dynamics

$$\dot{X}(t) = -\bar{\beta}\left(\frac{\partial \hat{u}}{\partial x}(s(t),t) - \frac{\partial \tilde{u}}{\partial x}(s(t),t)\right) + \bar{\beta}\left(k_{\mathrm{s}}T'_{\mathrm{s,eq}}(s(t)) - k_{\mathrm{l}}T'_{\mathrm{l,eq}}(s(t))\right), \tag{8.55}$$

where $\bar{\beta} = (\rho_s \Delta H)^{-1}$. Taking a linearization of the right hand side of (8.54) and (8.55) with respect to $s(t)$ around the setpoint s_{r} and by the steady-state solutions in (8.11), the dynamics of the reference error system is obtained by

$$\frac{\partial \hat{u}}{\partial t}(x,t) = \alpha_{\mathrm{s}}\frac{\partial^2 \hat{u}}{\partial x^2}(x,t) - b\frac{\partial \hat{u}}{\partial x}(x,t) - h_{\mathrm{s}}\hat{u}(x,t), \tag{8.56}$$

$$\frac{\partial \hat{u}}{\partial x}(0,t) = -U(t) + \gamma\tilde{u}(0,t), \tag{8.57}$$

$$\hat{u}(s(t),t) = CX(t), \tag{8.58}$$

$$\dot{X}(t) = AX(t) - \bar{\beta}\frac{\partial \hat{u}}{\partial x}(s(t),t) + \bar{\beta}\frac{\partial \tilde{u}}{\partial x}(s(t),t), \tag{8.59}$$

where

$$U(t) = -(q_{\mathrm{f}}(t) - q_{\mathrm{f}}^*), \tag{8.60}$$

$$C = k_{\mathrm{s}}\left(p_3 q_3 + p_4 q_4\right), \tag{8.61}$$

$$A = \bar{\beta}\left(k_{\mathrm{s}}(p_3 q_3^2 + p_4 q_4^2) - k_{\mathrm{l}}(p_1 q_1^2 + p_2 q_2^2)\right). \tag{8.62}$$

Backstepping transformation

A well-known design method of the output feedback control for PDEs is achieved by introducing the backstepping transformation which maps the observer PDE with using the gain kernel function derived for the full-state feedback control. Therefore, we consider the following transformation:

$$\hat{w}(x,t) = \hat{u}(x,t) - \frac{\bar{\beta}}{\alpha_{\mathrm{s}}} \int_x^{s(t)} \phi(x-y)\hat{u}(y,t)dy - \phi(x-s(t))X(t), \tag{8.63}$$

where ϕ is the gain kernel function derived in Section 4.1, which satisfies the following differential equation with the initial condition:

$$\alpha_{\mathrm{s}}\phi''(x) - (b+\bar{\beta}C)\phi'(x) - \left(A - \frac{\bar{\beta}b}{\alpha_{\mathrm{s}}}C + h_{\mathrm{s}}\right)\phi(x) = 0, \tag{8.64}$$

$$\phi(0) = 0, \quad \phi'(0) = \frac{c}{\bar{\beta}}, \tag{8.65}$$

where $c > 0$ is a control gain. The solution to (8.64) with (8.65) is uniquely given by

$$\phi(x) = \frac{c}{\bar{\beta}(d_1 - d_2)}\left(e^{d_1 x} - e^{d_2 x}\right), \tag{8.66}$$

where d_1, d_2 are defined by

$$d_1 = \frac{\bar{b} + \sqrt{D}}{2\alpha_{\mathrm{s}}}, \quad d_2 = \frac{\bar{b} - \sqrt{D}}{2\alpha_{\mathrm{s}}}, \tag{8.67}$$

$$\bar{b} = b + \bar{\beta}C, \quad D = \bar{b}^2 + 4\alpha_{\mathrm{s}}\left(A - \frac{\bar{\beta}b}{\alpha_{\mathrm{s}}}C + h_{\mathrm{s}}\right). \tag{8.68}$$

The full-state feedback control law is designed by

$$U_{\mathrm{full}}(t) = -\gamma u(0,t) - \frac{\bar{\beta}}{\alpha_{\mathrm{s}}} \int_0^{s(t)} f(x)u(x,t)dx - f(s(t))X(t), \tag{8.69}$$

where $\gamma = \frac{b}{2\alpha_s}$, and

$$f(x) = \phi'(-x) - \gamma\phi(-x), \tag{8.70}$$

$$= \frac{c}{\bar{\beta}(d_1 - d_2)} \left((d_1 - \gamma)e^{-d_1 x} - (d_2 - \gamma)e^{-d_2 x} \right). \tag{8.71}$$

The associated output feedback control law is generally designed by replacing the plant state in the full-state feedback control law with the observer state. Since $X(t)$ in (8.69) can be directly measured and its observer state is not constructed, we keep the term $X(t)$. Moreover, for the sake of proving the positivity of the designed control law later, we also hold the boundary value term $u(0,t)$ in (8.69), which can also be directly measured. Hence, the resulting observer-based output feedback control law is designed by

$$U(t) = -\gamma u(0,t) - \frac{\bar{\beta}}{\alpha_s} \int_0^{s(t)} f(x)\hat{u}(x,t)dx - f(s(t))X(t), \tag{8.72}$$

Then, taking the derivatives of (8.63) in x and t along the solution of (8.56)-(8.59) with the gain kernel function (8.66), the transformed $(\hat{w}, X)$-system (so-called "target system") is described by the following dynamics

$$\begin{aligned} \frac{\partial \hat{w}}{\partial t}(x,t) =& \alpha_s \frac{\partial^2 \hat{w}}{\partial x^2}(x,t) - b\frac{\partial \hat{w}}{\partial x}(x,t) - h_s \hat{w}(x,t) + \dot{s}(t)g(x - s(t))X(t) \\ & - \bar{\beta}\phi(x - s(t))\frac{\partial \tilde{u}}{\partial x}(s(t),t), \quad 0 < x < s(t) \end{aligned} \tag{8.73}$$

$$\frac{\partial \hat{w}}{\partial x}(0,t) = \gamma \hat{w}(0,t), \tag{8.74}$$

$$\hat{w}(s(t),t) = CX(t), \tag{8.75}$$

$$\dot{X}(t) = (A - c)X(t) - \bar{\beta}\frac{\partial \hat{w}}{\partial x}(s(t),t) + \bar{\beta}\frac{\partial \tilde{u}}{\partial x}(s(t),t), \tag{8.76}$$

where $g(x) = \phi'(x) - \frac{\bar{\beta}}{\alpha_s} C\phi(x)$. Rewriting the control law (8.72) with respect to the boundary heat control $q_f(t)$, the estimated temperature $\hat{T}_s$, the reference steady-state $T_{s,eq}$, and the measured

variables $Y_1(t)$ and $Y_2(t)$, the resulting output feedback control is described by

$$\begin{aligned} q_{\mathrm{f}}(t) =& q_{\mathrm{f}}^* - \gamma k_{\mathrm{s}}(Y_2(t) - T_{\mathrm{s,eq}}(0)) - \frac{\bar{\beta} k_{\mathrm{s}}}{\alpha_{\mathrm{s}}} \int_0^{Y_1(t)} f(x)(\hat{T}_{\mathrm{s}}(x,t) - T_{\mathrm{s,eq}}(x))\mathrm{d}x \\ &+ f(Y_1(t))(Y_1(t) - s_r). \end{aligned} \tag{8.77}$$

Theoretical Analysis for a Specific Setup

While the controller is designed through the backstepping method, the stability of the target system is not proven theoretically. Moreover, the condition of model validity needs to be satisfied under the control law. To achieve a theoretical result, in this section, we impose the following assumptions.

Assumption 15 *The initial condition of the estimated temperature profile is not higher than that of the true temperature profile, i.e.,* $\hat{T}_{\mathrm{s}}(x,0) \leq T_{\mathrm{s}}(x,0)$*, for all* $x \in (0, s_0)$*, where* $s_0 := s(0)$.

Assumption 16 *The barrel temperature is set as melting temperature and the external heat input is zero, i.e.,* $T_{\mathrm{b}} = T_{\mathrm{m}}$, $q_{\mathrm{m}}^* = 0$.

Corollary 3 *Under Assumption 15, it holds* $\tilde{u}(x,t) \geq 0$ *and* $\frac{\partial \tilde{u}}{\partial x}(s(t),t) \leq 0$*, for all* $x \in (0, s(t))$ *and for all* $t \geq 0$*, as proven in Lemma 13.*

Corollary 4 *Under Assumption 16, the steady-state profiles* (8.11)*, and steady-state input* (8.19) *becomes* $T_{\mathrm{l,eq}}(x) = T_{\mathrm{m}}$, $T_{\mathrm{s,eq}}(x) = T_{\mathrm{m}}$*, and* $q_{\mathrm{f}}^* = 0$*. Also,* $C = 0$ *and* $A = 0$.

In addition, the following setpoint restriction is given.

Assumption 17 *The setpoint is chosen to satisfy*

$$s_r > s_0 + \frac{\bar{\beta} k_{\mathrm{s}}}{\alpha_{\mathrm{s}}} \int_0^{s_0} \frac{f(x)}{f(s_0)} (T_{\mathrm{m}} - \hat{T}_{\mathrm{s}}(x,0))\mathrm{d}x. \tag{8.78}$$

The physical meaning of Assumption 4 is that the user needs to choose the setpoint position s_{r} sufficiently closer to the outlet of the extruder than the initial interface position s_0 depending on the initial temperature profile of the solid polymer granules. Such a choice of the setpoint position becomes more restrictive as the initial temperature profile in the solid polymer decreases.

The main theorem is stated as follows.

Theorem 15 *Let Assumptions 14–17 hold. Then, the closed-loop system consisting of the plant* (8.1)–(8.5)*, the measurements* (8.29)*, the observer* (8.30)–(8.32)*, and the control law* (8.77) *satisfies the conditions for model validity* (8.6)*,* (8.7)*, and is exponentially stable at the origin in the norm*

$$\hat{\Phi}(t) := ||T_{\mathrm{s}}(x,t) - T_{\mathrm{s,eq}}(x)||_{\mathcal{H}_1} + ||T_{\mathrm{s}}(x,t) - \hat{T}_{\mathrm{s}}(x,t)||_{\mathcal{H}_1} + |s(t) - s_{\mathrm{r}}|, \tag{8.79}$$

namely, there exists a positive constant $\hat{M} > 0$ *such that* $\hat{\Phi}(t) \leq \hat{M}\hat{\Phi}(0)e^{-dt}$ *holds, where* $d = \min\left\{\frac{\alpha_{\mathrm{s}}}{16 s_{\mathrm{r}}} + \frac{b^2}{4\alpha_{\mathrm{s}}} + h_{\mathrm{s}}, c\right\}$.

The proof of Theorem 15 is established by showing that (8.6) and (8.7) are satisfied and employing a Lyapunov analysis through the remaining of this section.

Model validity condition

Let $Z(t)$ be defined as

$$\begin{aligned} Z(t) =& U(t) + \gamma u(0,t) \\ =& -\frac{\bar{\beta}}{\alpha_{\mathrm{s}}} \int_0^{s(t)} f(x)\hat{u}(x,t)\mathrm{d}x - f(s(t))X(t). \end{aligned} \tag{8.80}$$

The following lemma is stated.

Lemma 14 *The following properties hold:*

$$Z(t) > 0, \quad \forall t \geq 0, \tag{8.81}$$

$$u(x,t) > 0, \quad \dot{s}(t) > 0 \quad \forall x \in (0, s(t)), \quad \forall t \geq 0, \tag{8.82}$$

$$s(0) < s(t) < s_{\mathrm{r}}, \quad \forall t \geq 0. \tag{8.83}$$

Proof:

Taking into account $A = C = 0$, the differential equation for ϕ in (8.64) is given by $\alpha_{\mathrm{s}}\phi''(x) - b\phi'(x) - h_{\mathrm{s}}\phi(x) = 0$. Thus, recalling $f(x) = \phi'(-x) - \gamma\phi(-x)$, we have

$$\alpha_{\mathrm{s}} f''(x) + b f'(x) - h_{\mathrm{s}} f(x) = 0, \tag{8.84}$$

$$\alpha_{\mathrm{s}} f'(0) + (b - \alpha_{\mathrm{s}}\gamma) f(0) = 0. \tag{8.85}$$

Taking the time derivative of (8.80) along with the solution of (8.56)–(8.59), and substituting (8.84), (8.85), we obtain

$$\dot{Z}(t) \geq -cZ(t) - \dot{s}(t) f'(s(t)) X(t), \quad \forall t \geq 0, \tag{8.86}$$

where we used Corollary 3 and $f(x) > 0$. We prove (8.81) by contradiction approach. Assume that (8.81) is not valid, which implies $\exists t^* > 0$ such that

$$Z(t) > 0, \quad \forall t \in (0, t^*), \qquad Z(t^*) = 0. \tag{8.87}$$

Similarly to Lemma 13, by Maximum principle and Hopf's lemma, we get

$$u(x,t) > 0, \quad \dot{s}(t) > 0, \quad \forall x \in (0, s(t)), \quad \forall t \in (0, t^*), \tag{8.88}$$

which, with the help of Lemma 13, leads to

$$\hat{u}(x,t) > 0, \quad s(t) > 0, \quad \forall x \in (0, s(t)), \quad \forall t \in (0, t^*). \tag{8.89}$$

Applying (8.87) and (8.89) to (8.80) with $f(x) > 0$ leads to $X(t) < 0$, for all $t \in (0, t^*)$. Therefore, applying this inequality and (8.88) to (8.86) leads to

$$\dot{Z}(t) > -cZ(t), \quad \forall t \in (0, t^*). \tag{8.90}$$

Applying Gronwall's inequality to (8.90) leads to $Z(t) \geq Z(0)e^{-ct}, \quad \forall t \in (0, t^*]$. Thus, we have $Z(t^*) \geq Z(0)e^{-ct^*} > 0$, which contradicts with the assumption (8.87). Hence, (8.81) is proved. Then, by Maximum principle, (8.82) holds. Imposing (8.81) and (8.82) on (8.80), we obtain $X(t) < 0$ which leads to (8.83).

Stability analysis

Taking into account $A = C = 0$, we study the stability of the target (w, X)-system governed by (8.73)–(8.76). Let $\hat{z}$ be a variable defined by

$$\hat{z}(x,t) = \hat{w}(x,t)e^{-\gamma x}. \tag{8.91}$$

Applying (8.91) and $\tilde{z} := \tilde{u}e^{-\gamma x}$ in (8.39), the target (w,X)-system in (8.73)–(8.76) leads to the following $(\hat{z},X)$-system

$$\begin{aligned}
\frac{\partial \hat{z}}{\partial t}(x,t) =& \alpha_{\mathrm{s}} \frac{\partial^2 \hat{z}}{\partial x^2}(x,t) - \lambda \hat{z}(x,t) + \dot{s}(t) g(x-s(t)) X(t) e^{-\gamma x} \\
& - \bar{\beta} \phi(x-s(t)) \frac{\partial \tilde{z}}{\partial x}(s(t),t), \quad 0 < x < s(t) \qquad (8.92) \\
\frac{\partial \hat{z}}{\partial x}(0,t) =& 0, \qquad (8.93) \\
\hat{z}(s(t),t) =& 0, \qquad (8.94) \\
\dot{X}(t) =& -cX(t) - \bar{\beta} e^{\gamma s(t)} \left(\frac{\partial \hat{z}}{\partial x}(s(t),t) - \frac{\partial \tilde{z}}{\partial x}(s(t),t) \right), \qquad (8.95)
\end{aligned}$$

where $\lambda := h_{\mathrm{s}} + \frac{b^2}{4\alpha_{\mathrm{s}}}$. Consider the following functional

$$\hat{V} = \frac{1}{2} \int_0^{s(t)} \hat{z}(x,t)^2 \mathrm{d}x + \frac{1}{2} \int_0^{s(t)} \left(\frac{\partial \hat{z}}{\partial x}(x,t) \right)^2 \mathrm{d}x + \frac{p}{2} X(t)^2, \qquad (8.96)$$

where $p > 0$ is to be determined. Taking the time derivative of (8.96) along with the solution of (8.92)–(8.95), and applying Young's, Cauchy-Schwarz, and Agmon's inequalities, we get

$$\begin{aligned}
\dot{\hat{V}} \leq & - \left(\frac{\alpha_{\mathrm{s}}}{2} - \frac{4p\bar{\beta}^2 s_{\mathrm{r}} e^{2\gamma s_{\mathrm{r}}}}{c} \right) \left|\left| \frac{\partial^2 \hat{z}}{\partial x^2} \right|\right|^2 \\
& - (\alpha_{\mathrm{s}} + \lambda) \left|\left| \frac{\partial \hat{z}}{\partial x} \right|\right|^2 - \lambda ||\hat{z}||^2 - \frac{pc}{2} X(t)^2 \\
& + \left(\bar{\beta}^2 ||\phi||^2 \left(\frac{1}{2h_{\mathrm{s}}} + \frac{1}{\alpha_{\mathrm{s}}} \right) + \frac{p\bar{\beta}^2 e^{2\gamma s_{\mathrm{r}}}}{c} \right) \frac{\partial \tilde{z}}{\partial x}(s(t),t)^2 \\
& + \frac{\dot{s}(t)}{2} \left((1+\bar{g}) X(t)^2 + ||g||^2 ||\hat{z}||^2 + \left|\left| \frac{\partial \hat{z}}{\partial x} \right|\right|^2 \right). \qquad (8.97)
\end{aligned}$$

where $\bar{g} := \max_{s(t)\in(0,s_{\rm r})}(g(0)^2+g(-s(t))^2+||g'||^2)$. Choosing $p=\frac{c\alpha_{\rm s}e^{-2\gamma s_{\rm r}}}{16\bar{\beta}^2 s_{\rm r}}$, the inequality (8.97) is led to

$$\begin{aligned}\dot{\hat{V}} \leq & -\frac{\alpha_{\rm s}}{4}\left|\left|\frac{\partial^2\hat{z}}{\partial x^2}\right|\right|^2-(\alpha_{\rm s}+\lambda)\left|\left|\frac{\partial\hat{z}}{\partial x}\right|\right|^2-\lambda||\hat{z}||^2-\frac{pc}{2}X(t)^2\\ & +a\dot{s}(t)\hat{V}+M_1\left|\left|\frac{\partial^2\tilde{z}}{\partial x^2}\right|\right|^2,\end{aligned} \tag{8.98}$$

where $a=\max\{\frac{(1+\bar{g})}{p},||g||^2,1\}$, $M_1=4s_{\rm r}\left(\bar{\beta}^2||\phi||^2\left(\frac{1}{2h_{\rm s}}+\frac{1}{\alpha_{\rm s}}\right)+\frac{\alpha_{\rm s}}{16s_{\rm r}}\right)$. Thus, using the Lyapunov function $\tilde{V}$ in (8.43) for the estimation error $\tilde{z}$-system (8.40)–(8.42), we define the Lyapunov function for the total $(\hat{z},X,\tilde{z})$-system as

$$V=\hat{V}+\frac{2M_1}{\alpha_{\rm s}}\tilde{V}. \tag{8.99}$$

Combining the inequalities (8.44) and (8.98) leads to

$$\dot{V}\leq -dV+a\dot{s}(t)V, \tag{8.100}$$

where $d=\min\left\{\frac{\alpha_{\rm s}}{16s_{\rm r}}+\lambda,c\right\}$. Following the procedure in Chapter 2, the inequality (8.100) with (8.82) and (8.83) leads to the exponential norm estimate

$$V(t)\leq e^{a(s(t)-s_0)}V(0)e^{-dt}\leq e^{as_{\rm r}}V(0)e^{-dt}. \tag{8.101}$$

Let $\Psi(t)=||w||^2_{\mathcal{H}_1}+X(t)^2$. Then, we have $\underline{M}V\leq\Psi(t)\leq\bar{M}V$ where $\bar{M}=2\max\{e^{2\gamma s_{\rm r}}(1+\gamma^2),\frac{1}{p}\}$, $\underline{M}=\left(\max\{2(1+\gamma^2),\frac{p}{2}\}\right)^{-1}$. Therefore, $\Psi(t)\leq\frac{\bar{M}}{\underline{M}}e^{as_{\rm r}}\Psi(0)e^{-dt}$, which proves the exponential stability of the target w-system in $\mathcal{H}_1$-norm. Since the u-system in (8.56)-(8.59) and the target w-system in (8.73)-(8.76) have equivalent stability property due to the invertibility of the back-stepping transformation (8.63), the exponential estimate in $\mathcal{H}_1$-norm is also guaranteed for the u-system, which concludes the proof of Theorem 15.

Table 8.1: HDPE parameters obtained by [154].

melting point	T_{m}	$135\,^{\circ}\mathrm{C}$
specific heat solid	c_{s}	$1895\,\mathrm{Jkg}^{-1}\mathrm{K}^{-1}$
specific heat melt	c_{l}	$2640\,\mathrm{Jkg}^{-1}\mathrm{K}^{-1}$
therm. conduct. solid	k_{s}	$0.373\,\mathrm{Wm}^{-1}\mathrm{K}^{-1}$
therm. conduct. melt	k_{l}	$0.324\,\mathrm{Wm}^{-1}\mathrm{K}^{-1}$
solid density	ρ_{s}	$955\,\mathrm{kgm}^{-3}$
melt density	ρ_{l}	$780\,\mathrm{kgm}^{-3}$
heat of fusion	ΔH	$39000\,\mathrm{Jkg}^{-1}$

8.5 Simulation Results

Setup and method

For numerical study to investigate the controller's performance in different operating conditions, we have employed the simulation of the original "two-phase" model governed by (8.1)–(8.5) without assuming that the liquid phase is at stead-state, run the PDE observer given in (8.30)–(8.32), and implemented the associated output feedback controller (8.77). We used the boundary immobilization method to obtain a fixed boundary system and discretized the system with finite differences to construct a finite dimensional representation of the model and the estimate.

Using Matlab's ode23s solver, we simulated the setup with three different advection speeds b ranging from 2[mm/s] to 50[mm/s], to cover a wide spectrum of operating modes. The material parameters are chosen from [154], in which distinct values for high-density polyethylene in solid and liquid state were experimentally derived (see Table 8.1). The extruder length is given by a physical device, and here we used $L=10$[cm]. The initial conditions of the true temperature profile and the estimated temperature profiles are set as linear profiles with the boundary temperature $\underline{T}$ and $\hat{\underline{T}}$, namely, $T_{\mathrm{s}}(x,0)=(\underline{T}-T_{\mathrm{m}})(1-x/s_0)+T_{\mathrm{m}}$, $\hat{T}_{\mathrm{s}}(x,0)=(\hat{\underline{T}}-T_{\mathrm{m}})(1-x/s_0)+T_{\mathrm{m}}$. In the simulation, we set $\underline{T}=125[^{\circ}\mathrm{C}]$ and $\underline{T}=105[^{\circ}\mathrm{C}]$ to satisfy Assumption 15.

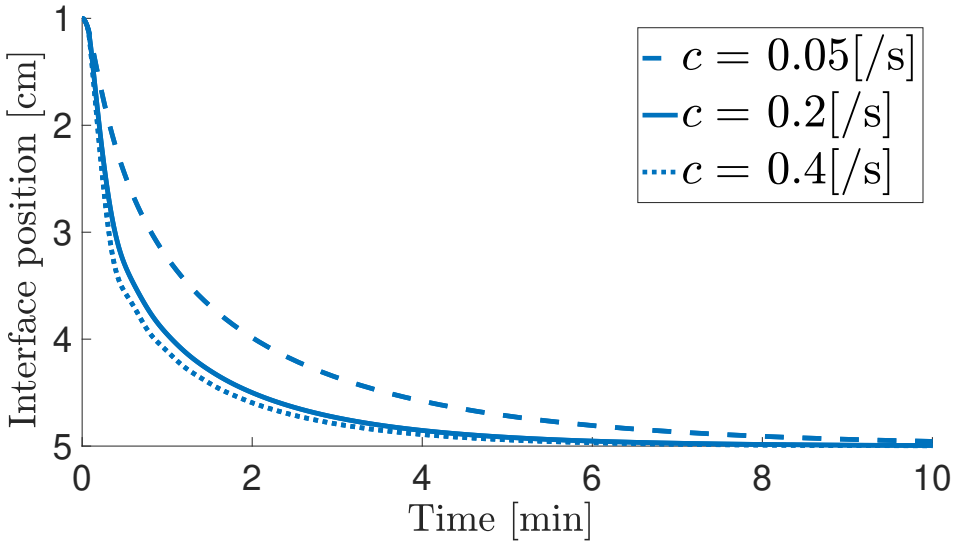

(a) The time evolution of the interface position.

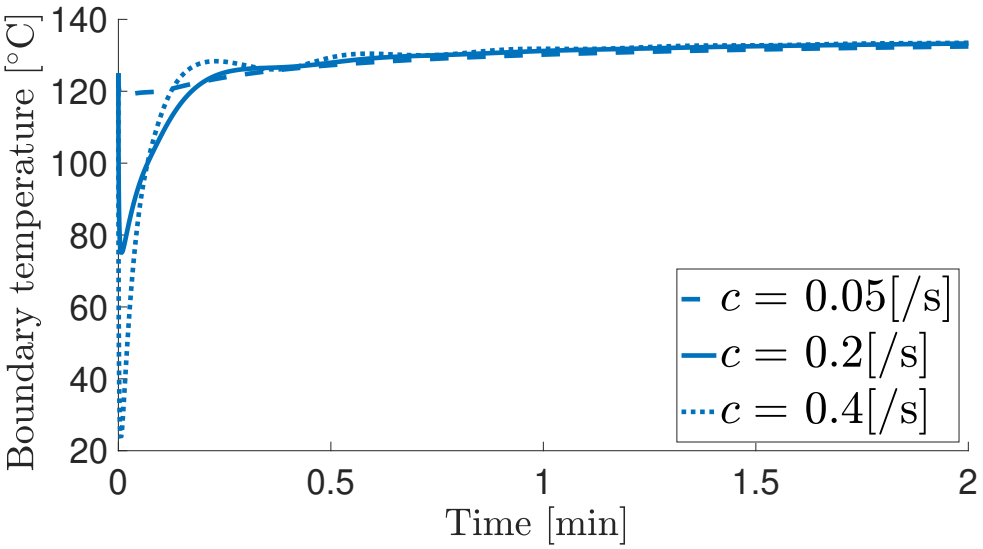

(b) The time evolution of the boundary temperature.

Figure 8.2: The closed-loop responses under the control gains c =0.05[/s] (dash), c =0.2[/s] (solid), and c =0.4[/s] (dotted). The convergence of the interface position is sufficiently fast and the boundary temperature remains a reasonable range for c =0.2[/s] (solid).

The free parameters are the constant barrel temperature T_{b}, the auxiliary heat input q^*_{m} at the outlet, and the control gain c. The barrel temperature and the auxiliary heat input are chosen so that they neutralize the cooling effect of the initial temperature in the solid phase within a

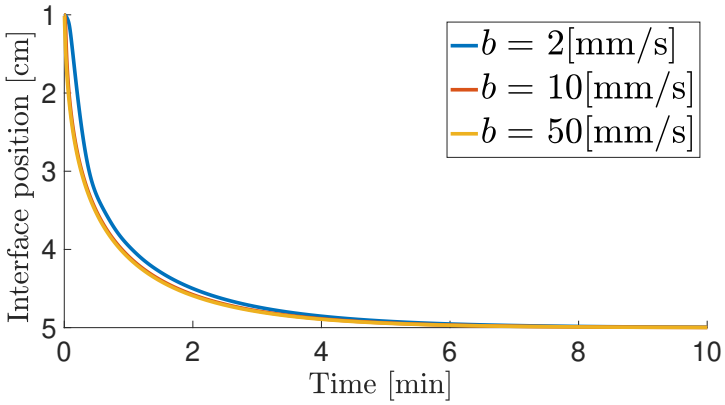

(a) For each operating speed, the interface position is stabilized after 6 minutes.

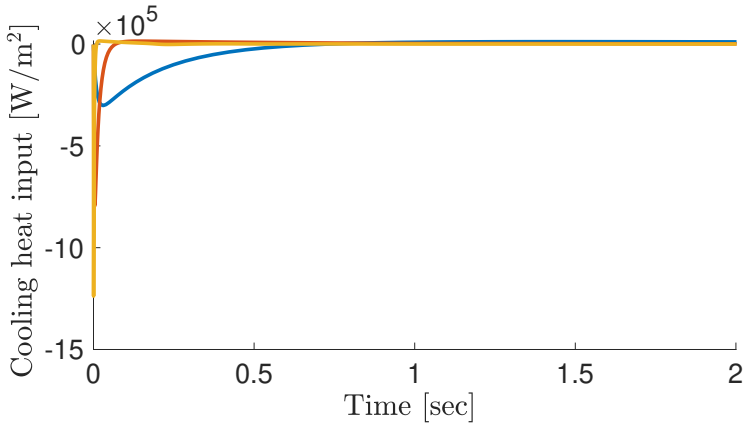

(b) The transient of the control input gets shorter as the operation gets faster.

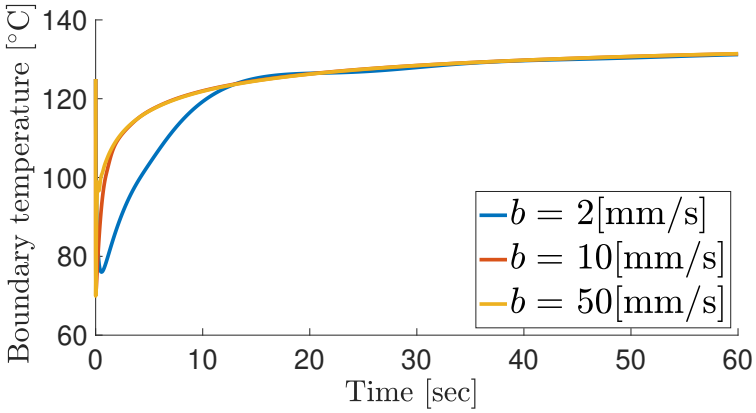

(c) The boundary temperature maintains reasonable value for the material and safe operation.

Figure 8.3: The closed-loop responses under the proposed output feedback control law for each operating speed.

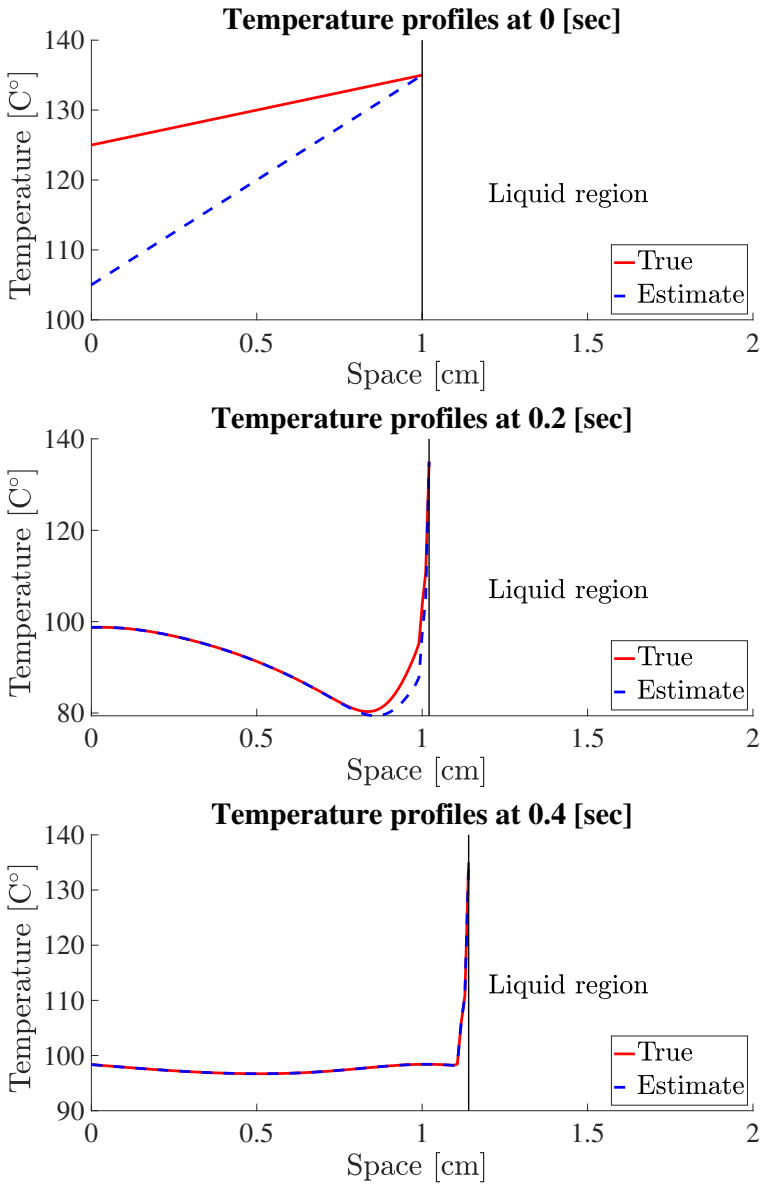

Figure 8.4: The comparison of the true and estimated temperature profiles at $t = 0$ [s], $t = 0.2$ [s], and $t = 0.4$ [s].

range close to the conditions imposed in Section 8.4, namely, the barrel temperature is chosen close to the melting temperature T_b and the auxiliary heat input is chosen as a positive value close to zero. Since the initial profile of the estimated temperature is slightly below the melting temperature, the cooling effect of the initial temperature is limited, and thereby we set the free

parameters sufficiently close to the specific setup, $T_{\mathrm{b}} = 145[^{\circ}\mathrm{C}]$ and $q^{*}_{\mathrm{m}} = 100\,\mathrm{W/m^2}$.

Gain tuning

For a given advection speed, the control gain c is adjusted so that the following two properties are observed:

- The convergence of the interface position to the setpoint position is achieved sufficiently fast.
- The temperature in the solid phase maintains a reasonable value during the process.

As the control gain gets larger, the convergence becomes faster, however, the temperature in the solid phase can reach an unreasonably low value due to the large amount of the cooling input. Hence, we aim to choose a suitable value of the control gain c. First, we test three simulations under the small advection speed b =2[mm/s] by setting the control gain as c =0.05[/s], c =0.2[/s], and c =0.4[/s], respectively. The closed-loop responses of the interface position $s(t)$ and the boundary temperature $T_{\mathrm{s}}(0,t)$ are depicted in Fig. 8.2 (a) and (b), respectively. From Fig. 8.2 (a), we can observe that the convergence of the interface position with c =0.05[/s] takes approximately 10[min], while those with c =0.2[/s] and c =0.4[/s] take 6[min]. Additionally, from Fig. 8.2 (b), the boundary temperature with c =0.4[/s] reaches a value around 20[°C] that is a relatively low temperature while the boundary temperatures with c =0.05[/s] and c =0.2[/s] remain the reasonable range 80[°C]–135[°C]. Therefore, the control gain c =0.2[/s] is a suitable value which satisfies the two desired properties.

Simulation results

Following the gain tuning, the simulation results for higher advection speed b =10[mm/s] and b =50[mm/s] are performed, and the control gain is adjusted as c =1.0[/s] and c =5.0[/s],

respectively. For these advection speeds and the adjusted control gains, the closed-loop responses of the interface position $s(t)$, the boundary control input $q_{\mathrm{f}}(t)$, and the boundary temperature $T_{\mathrm{s}}(0,t)$ are shown in Fig. 8.3 (a)–(c), respectively. The interface responses, depicted in Fig. 8.3 (a), have quite similar behaviors in all three setups. However, the control input, shown in Fig. 8.3 (b), appears to act faster for higher advection speeds but exhibits similar qualitative behavior. Similar properties were observed in the boundary temperature response in Fig.8.3 (c). Note that all three figures have different time ranges.

Moreover, for the fast operating condition b =50[mm/s], the comparison of the estimated temperature profile and the true temperature profile at t =0[sec], 0.2[sec], 0.4[sec] are shown in Fig. 8.4 (a)–(c), respectively. We can observe that the estimated temperature profile gets almost the same as the true temperature profile at 0.4[sec], associated with the expansion of the solid granules' region. Hence, the convergence of the designed observer to the true temperature profile is approximately 1000 times faster than the convergence of the interface position to the setpoint position, which is a sufficiently quick performance of the temperature estimation.

Comparison with PI control

For comparison, we also tested a closed-loop setup with PI control given by

$$q_{\mathrm{f}}(t) = q_{\mathrm{f}}^{*} + K_{\mathrm{P}}(s(t) - s_{\mathrm{r}}) + K_{\mathrm{I}} \int_{t_0}^{t} (s(\tau) - s_{\mathrm{r}}) d\tau, \tag{8.102}$$

where K_{P} and K_{I} are gain parameters to be tuned in order to achieve the desired performance. However, for any choice of the parameters we have tried, the closed-loop response of the interface position does not stabilize at the setpoint s_{r}. Fig. 8.5 depicts the responses under PI control with a relatively suitable choice of the gains. The plot in Fig. 8.5 (b) shows that the temperature at the inlet of the extruder gets above the melting temperature at approximately 2.9 [min], which violates the validity condition (8.7) of the solid polymer temperature, while our proposed output

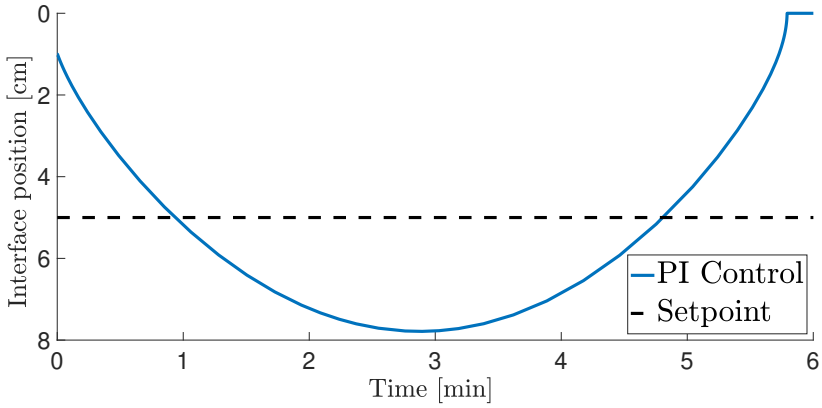

(a) The interface position causes a huge overshoot and is not stabilized.

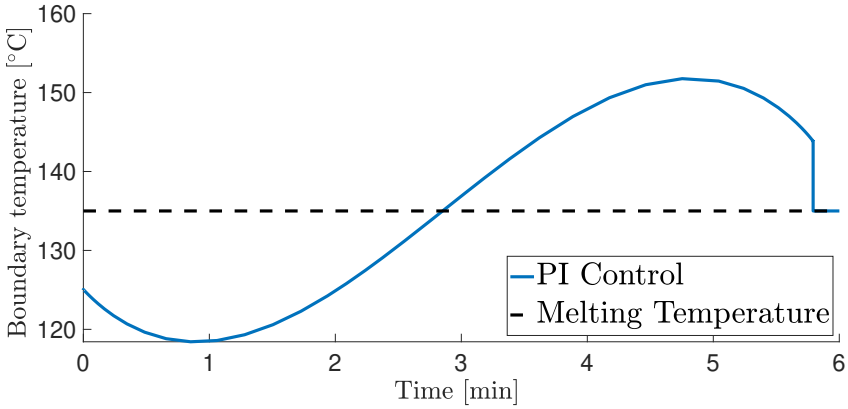

(b) The boundary temperature is heated up after 1 (min) and gets above the melting temperature after 2.9 (min), which violates the condition for the solid phase temperature.

Figure 8.5: The closed-loop response under PI control. The performance is bad due to the violation of the physical condition.

feedback control guarantees to satisfy the condition under the closed-loop system. Such an overshoot behavior beyond the melting temperature might be reduced by PID control; however, the velocity of the interface position is nearly impossible to measure online, and the differentiator generally causes high noise. Overall, the proposed output feedback control law illustrates superior performance to PI control in terms of both convergence to the setpoint and the validity condition.

From the simulations, we conclude that our control design achieves a stable interface position, even with very fast advection speeds 50 mm/s, with which a particle inserted in the inlet

will travel in two seconds through the extruder, when assuming a 10 cm extruder.

8.6 Conclusion and Future Work

In this chapter, we designed an observer and the associated output feedback control to stabilize a filament production process of the screw extrusion-based polymer 3D-printing. The steady-state analysis is provided by setting the setpoint as a given value, and the control design to stabilize the interface position is derived. The simulation results illustrate the effectiveness of the boundary feedback control law for some given screw speeds. While the theoretical analysis in this chapter is established under the assumptions on the liquid phase temperature maintaining the steady-state temperature and on the heat flux at the outlet being zero, it is expected to further developing the control law for the two-phase system following Chapter 5, and guaranteeing the robustness of the control with respect to the non-zero heat flux at the outlet following Chapter 4, which could relax the aforementioned two assumptions.

8.7 Acknowledgement

Chapter 8, in part, is a reprint of the material as it appears in:

- S. Koga, D. Straub, M. Diagne, and M. Krstic, "Thermodynamic Modeling and Control of Screw Extruder for 3D Printing", *American Control Conference*, 2018,

- S. Koga, D. Straub, M. Diagne, and M. Krstic, "Stabilization of Filament Production Rate for Screw Extrusion-Based Polymer 3D-Printing", *ASME Journal of Dynamic Systems, Measurement, and Control*, vol. 142, no. 3, p. 031005, 2020.

The dissertation author was the primary investigators and author of this paper. The author would like to thank David Straub and Mamadou Diagne for their collaboration.

Chapter 9

Metal 3D-Printing via Selective Laser Sintering

9.1 Selective Laser Sintering

Metal Additive Manufacturing (AM) is a state-of-the-art manufacturing technology which has emerged rapidly in the recent decade as observed from the growth in global market. AM's impact relies on products and supply chains in numerous industries such as automobiles, consumer electronics, aerospace, medical devices, etc [32]. While industrial AM systems for polymer materials can produce reasonable quality for customers, AM for metallic materials still has room for quality improvement.

Selective Laser Sintering (SLS) is the most common technique of the powder-bed fusion AM processes that fabricate structurally sound three-dimensional products from a computer-aided design (CAD) models [1]. Using a high powered laser, a thin layer of the metal powder at the surface of the bed is fused to produce a desired geometry. A melt pool created by the laser solidifies to a solid metal component. Such a layer-by-layer process to fabricate the entire object enables a relatively fast process speed together with complex geometry.

As the phase transformation of the metal powder occurs in a short time scale while operating a fast scanning speed of the laser, SLS yields an inhomogeneous temperature field which leads to a complex computational prediction of the geometry of the melt pool (see for example [91]). The large thermal gradient inside the metal can lead to brittle parts, and thus the temporal evolution of the temperature field has a significant role to guarantee the quality of the fabrication. Using a thermodynamic model for phase transformations, several research articles have studied the evolution of the melt pool in SLS by means of Stefan problem [60], and employed Finite Element (FE) methods to obtain computational models [132, 2, 29, 34]. The Stefan problem is governed by a parabolic Partial Differential Equation (PDE) for temperature field defined on the time-varying spatial domains of the melting front, whose evolution is given by the Neumann boundary value of the PDE state at the front position. A comprehensive review of the thermal modeling of melt pool dynamics in SLS can be found in [182].

Process control for SLS has been developed to guarantee sufficient mechanical properties of the fabricated three-dimensional object. For instance, in [183] a control system to eliminate thermal gradients in the post-sintering temperature is designed using an IR camera as a sensor and laser power density as an actuator. Repetitive control methods for SLS-based AM have been developed in [164, 165] by utilizing three-dimensional finite element simulation for the melt-pool evolution. As a powder deposition process, [26] proposed a control design for laser power and scanning speed to drive the solid-liquid interface position in the melt pool to some pre-determined setpoint geometry using an adjoint-based optimization for the Stefan problem developed in [63].

9.2 Physical Model

SLS is a common AM technique as layer-by-layer process to fabricate a 3D-object through repetitive phenomena of the melting and solidification. At each layer, firstly the solid object under the process of fabrication is covered by a thin granular metal powder layer at the surface.

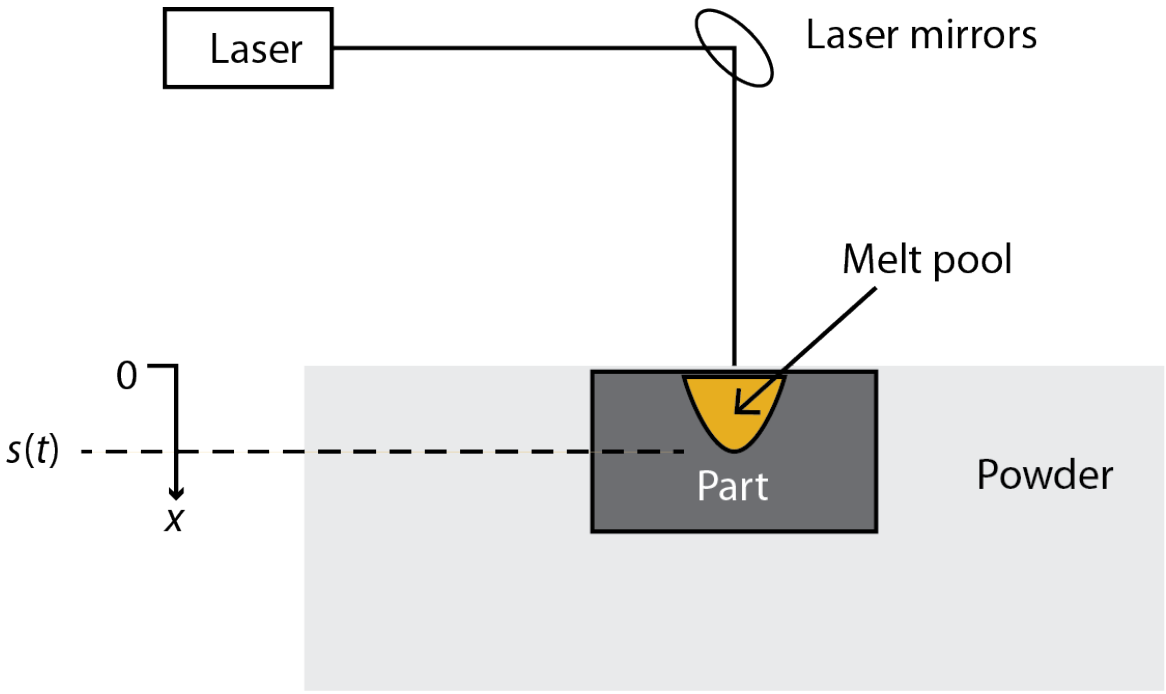

Figure 9.1: Schematic of the powder-bed metal AM via Selective Laser Sintering (SLS). The melt pool is generated due to the emission of the laser energy.

Next, a laser beam is injected through reflection by scanner mirrors to heat up and fuse the metal powder at selective areas of the surface. A local melt pool is developed by the laser power in the metal powder. Through a phase change phenomena, the domain of the melt pool is given by the position of the melting front that is varying in time. This configuration is depicted in Fig. 9.1. The physical modeling of the melt pool dynamics has been developed in literature by means of a Stefan problem. Following the work in [2] for one-dimensional approximation of the Stefan problem in the vertical direction, and incorporating the in-domain effect of the laser power to the

temperature dynamics, we consider the following governing equations:

$$\frac{\partial T}{\partial t}(x,t) = \alpha \frac{\partial^2 T}{\partial x^2}(x,t) + g(x) q_{\mathrm{c}}(t), \quad x \in (0, s(t)), \tag{9.1}$$

$$-k \frac{\partial T}{\partial x}(0,t) = q_{\mathrm{c}}(t), \tag{9.2}$$

$$T(s(t),t) = T_{\mathrm{m}}, \tag{9.3}$$

$$\dot{s}(t) = -\beta \frac{\partial T}{\partial x}(s(t),t), \tag{9.4}$$

where $T(x,t)$ denotes the temperature profile in the melt pool along the vertical coordinate $x \in (0, s(t))$, $\alpha := \frac{k}{\rho c_{\mathrm{p}}}$ is the diffusion coefficient, k is the thermal conductivity, ρ is the density, c_{p} is the specific heat capacity, T_{m} is the constant melting temperature, $\beta := \frac{k}{\rho H_{\mathrm{f}}}$ with the latent heat of fusion H_{f}, and $q_{\mathrm{c}}(t)$ is the controlled laser power. By Beer's law for optical penetration of the energy, in [132] the spatially varying function $g(x)$ is given by $g(x) = \frac{1}{\rho c_{\mathrm{p}} \delta} \exp\left(-\frac{x}{\delta}\right)$, where δ is called optical penetration rate. Here, we consider a broader class of the spatial function $g(x)$ satisfying the following assumption.

Assumption 18 *The spatially varying function $g(x)$ is positive, i.e., $g(x) \geq 0$, $\forall x \geq 0$.*

The condition to validate the physical model (9.1)–(9.4) is given in the following remark.

Remark 11 *The model* (9.1)–(9.4) *is physically valid if and only if*

$$T(x,t) \geq T_{\mathrm{m}}, \quad \forall x \in (0, s(t)), \quad \forall t \geq 0. \tag{9.5}$$

Based on the above condition, we impose the following assumption on the initial data.

Assumption 19 *$s_0 := s(0) > 0$, $T_0(x) := T(x,0) \geq T_{\mathrm{m}}$ for all $x \in [0, s_0]$, and $T_0(x)$ is continuously differentiable in $x \in [0, s_0]$.*

A sufficient condition to guarantee (9.5) is given by the following lemma.

Lemma 3 *If $q_c(t) > 0$ for all $t \in [0, t_1)$ for some $t_1 > 0$, then $T(x,t) > T_m$ for all $x \in (0, s(t))$ and for all $t \in [0, t_1)$. Moreover, if $q_c(t) > 0$ for all $t \geq 0$, then $T(x,t) > T_m$ for all $x \in (0, s(t))$ and for all $t \geq 0$.*

Lemma 3 is proven by applying the maximum principle and Hopf's lemma for parabolic PDEs as shown in [50] (p. 26, Corollary 2). Therefore, the condition $q_c(t) > 0$ for all $t \geq 0$ stands as a constraint of the laser power input, which needs to be ensured after the feedback control law is designed.

9.3 State Feedback Control

Problem statement and main result

The steady-state solution $(T_{eq}(x), s_{eq})$ of the system (9.1)-(9.4) with zero laser power $q_c(t) = 0$ yields a uniform melting temperature $T_{eq}(x) = T_m$ and a constant interface position given by the initial data. As proposed in [26], driving the depth of the melt pool to the setpoint is desired in AM, and thus we design $q_c(t) > 0$ such that the interface position $s(t)$ converges to the setpoint s_r. A restriction on the choice of the setpoint is given in the following assumption.

Assumption 20 *Given the initial conditions $T_0(x)$ and s_0, the setpoint s_r is chosen to satisfy the following inequality:*

$$s_r > s_0 + \frac{\beta}{\alpha} \int_0^{s_0} (T_0(x) - T_m) \mathrm{d}x. \tag{9.6}$$

The necessity of Assumption 20 can be derived by considering the energy conservation law described by

$$\frac{\mathrm{d}}{\mathrm{d}t} \left(\frac{k}{\alpha} \int_0^{s(t)} (T(x,t) - T_m) \mathrm{d}x + \frac{k}{\beta} s(t) \right) = \left(1 + \frac{k}{\alpha} \int_0^{s(t)} g(x) \mathrm{d}x \right) q_c(t). \tag{9.7}$$

Imposing the constraint $q_{\mathrm{c}}(t) > 0$ for all $t \geq 0$ and taking the time integration of (9.7) from the initial time to infinity, the condition given in Assumption (20) is obtained. Under these assumptions, we design the control law and state our main result as follows.

Theorem 6 *Under Assumptions 18–20, the closed-loop system consisting of the plant* (9.1)–(9.4) *and the control law*

$$q_{\mathrm{c}}(t) = -c\left(\frac{k}{\alpha}\int_0^{s(t)}(T(x,t)-T_{\mathrm{m}})\mathrm{d}x + \frac{k}{\beta}(s(t)-s_r)\right), \tag{9.8}$$

where $c > 0$ *is a control gain, satisfies the model validity condition* (9.5)*, and there exists a positive constant* $M > 0$ *such that the norm*

$$\Phi(t) := ||T(x,t)-T_{\mathrm{m}}||^2_{\mathcal{H}_{\mathrm{l}}} + (s(t)-s_r)^2, \tag{9.9}$$

satisfies the following exponential decay

$$\Phi(t) \leq M\Phi(0)e^{-bt}, \tag{9.10}$$

where $b = \min\left\{\frac{\alpha}{4s_r^2}, c\right\}$*, namely, the origin of the closed-loop system is exponentially stable in the spatial* $\mathcal{H}_{\mathrm{l}}$ *norm.*

Remark 12 *The control law* (9.8) *is equivalent to the design developed in Section 2.3 for the system without in-domain effect, as we can see that* (9.8) *is not dependent on the spatially varying function* $g(x)$*. Hence, the stability of the closed-loop system is* robust *with respect to the uncertainty of* $g(x)$ *as far as Assumption 18 holds.*

The proof of Theorem 6 is established through the remainder of this section by following the steps in Chapter 2.

Reference error and target system

We define the reference error states as follows

$$u(x,t) = T(x,t) - T_{\mathrm{m}}, \quad X(t) = s(t) - s_r. \tag{9.11}$$

Using these variables, the original system (9.1)–(9.4) is led to the following reference error system

$$u_t(x,t) = \alpha u_{xx}(x,t) + g(x) q_{\mathrm{c}}(t), \quad x \in (0, s(t)), \tag{9.12}$$

$$-k u_x(0,t) = q_{\mathrm{c}}(t), \tag{9.13}$$

$$u(s(t),t) = 0, \tag{9.14}$$

$$\dot{X}(t) = -\beta u_x(s(t),t). \tag{9.15}$$

Following the procedure in Chapter 2, we introduce the following backstepping transformation

$$w(x,t) = u(x,t) - \frac{c}{\alpha}\int_x^{s(t)} (x-y) u(y,t)\mathrm{d}y + \frac{c}{\beta}(s(t)-x)X(t). \tag{9.16}$$

Taking the time and spatial derivatives of (9.16) along the solution of (9.12)–(9.15) yields the following target system

$$w_t(x,t) = \alpha w_{xx}(x,t) + \frac{c}{\beta}\dot{s}(t)X(t) + \bar{g}(x, s(t)) q_{\mathrm{c}}(t), \tag{9.17}$$

$$w(s(t),t) = 0, \tag{9.18}$$

$$w_x(0,t) = 0, \tag{9.19}$$

$$\dot{X}(t) = -cX(t) - \beta w_x(s(t),t), \tag{9.20}$$

where

$$\bar{g}(x,s(t)) := g(x) - \frac{c}{\alpha}\int_x^{s(t)} (x-y)g(y)\mathrm{d}y. \tag{9.21}$$

The boundary condition (9.13) leads to the control design

$$q_{\mathrm{c}}(t) = -ck\left(\frac{1}{\alpha}\int_0^{s(t)} u(x,t)\mathrm{d}x + \frac{1}{\beta}X(t)\right), \tag{9.22}$$

which is equivalent to (9.8).

Model validity conditions

To guarantee the condition (9.5) for the model validity to hold under the closed-loop system, we provide the following lemma.

Lemma 4 *The closed-loop system of* (9.12)–(9.15) *under the control law* (9.22) *satisfies the following properties:*

$$q_{\mathrm{c}}(t) > 0, \quad \forall t \geq 0, \tag{9.23}$$

$$u(x,t) > 0, \quad \forall x \in (0,s(t)), \quad \forall t \geq 0, \tag{9.24}$$

$$\dot{s}(t) > 0, \quad \forall t \geq 0, \tag{9.25}$$

$$s_0 < s(t) < s_r, \quad \forall t > 0. \tag{9.26}$$

Proof:

First, we use contradiction approach to prove (9.23), namely, we assume that there exists a finite time $t^* > 0$ such that $q_{\mathrm{c}}(t) > 0$, $\forall t \in [0,t^*)$ and $q_c(t^*) = 0$. Then, by Lemma 3, we have $u(x,t) > 0$, $\forall x \in (0,s(t))$, $\forall t \in [0,t^*)$, and $\dot{s}(t) > 0$, $\forall t \in [0,t^*)$. Then, by the control law (9.22), we deduce $0 < s_0 < s(t) < s_r$, $\forall t \in (0,t^*)$. Taking the time derivative of the control law (9.22)

leads to

$$\dot{q}_c(t) = -c\left(1+\frac{k}{\alpha}\int_0^{s(t)} g(x)\mathrm{d}x\right) q_{\mathrm{c}}(t). \tag{9.27}$$

Applying $s(t) < s_r \; \forall t \in (0,t^*)$ with the help of $g(x) \geq 0$ yields the following inequality

$$\dot{q}(t) > -c\left(1+\frac{k}{\alpha}\int_0^{s_r} g(x)\mathrm{d}x\right) q_{\mathrm{c}}(t), \quad \forall t \in (0,t^*). \tag{9.28}$$

Applying comparison principle to (9.28), we get the following inequality

$$q_{\mathrm{c}}(t) > q_{\mathrm{c}}(0) e^{\left(-c\left(1+\frac{k}{\alpha}\int_0^{s_r} g(x)\mathrm{d}x\right)t\right)}, \quad \forall t \in (0,t^*). \tag{9.29}$$

Hence, $q_c(t^*) \geq q_{\mathrm{c}}(0)\exp\left(-c\left(1+\frac{k}{\alpha}\int_0^{s_r} g(x)\mathrm{d}x\right)t^*\right)$. However, Assumption 20 for setpoint restriction ensures $q_c(0) > 0$, and hence $q_c(t^*) > 0$, which contradicts with the imposed assumption $q_c(t^*) = 0$. Thus, the positivity (9.23) is proven. Moreover, the properties (9.24)–(9.26) are shown by applying Lemma 3 for infinite time domain, and extending the manner we presented at the beginning of this proof for finite time domain to the infinite time domain.

Moreover, we have the following lemma.

Lemma 5 *The control law* (9.22) *under the closed-loop system satisfies the following inequalities*

$$q_c(0) e^{\left(-c\left(1+\frac{k}{\alpha}\int_0^{s_r} g(x)\mathrm{d}x\right)t\right)} < q_{\mathrm{c}}(t) < q_{\mathrm{c}}(0) e^{-ct}, \quad \forall t \geq 0. \tag{9.30}$$

Applying the conditions (9.23) and (9.26) to (9.27) with the use of comparison principle directly leads to (9.30).

Stability proof

In this section, we prove the exponential stability of the closed-loop system by Lyapunov method with the help of the properties shown in Lemmas 4 and 5. First, we prove the stability of the target (w,X)-system given in (9.17)–(9.20). Note that for this target system, Poincare's and Agmon's inequalities are given by

$$||w||^2 \leq 4s_r^2||w_x||^2, \quad ||w_x||^2 \leq 4s_r^2||w_{xx}||^2, \tag{9.31}$$

$$w_x(s(t),t)^2 \leq 4s_r||w_{xx}||^2. \tag{9.32}$$

Let V be the Lyapunov function defined by

$$V(t) = \frac{1}{2s_r^2}||w||^2 + \frac{1}{2}||w_x||^2 + \frac{p}{2}X(t)^2. \tag{9.33}$$

Taking the time derivative of (9.33) along the solution of (9.17)–(9.20) leads to

$$\begin{aligned}\dot{V}(t) = &-\frac{\alpha}{s_r^2}||w_x||^2 + \frac{c}{\beta s_r^2}\dot{s}(t)X(t)\int_0^{s(t)} w(x,t)\mathrm{d}x + \frac{1}{s_r^2}\int_0^{s(t)} \bar{g}(x,s(t))w(x,t)\mathrm{d}x q_\mathrm{c}(t)\\ &-\alpha||w_{xx}||^2 - \frac{c}{\beta}\dot{s}(t)X(t)w_x(s(t),t) - \frac{1}{2}\dot{s}(t)w_x(s(t),t)^2\\ &-\int_0^{s(t)} \bar{g}(x,s(t))w_{xx}(x,t)\mathrm{d}x q_\mathrm{c}(t) - pcX(t)^2 - p\beta X(t)w_x(s(t),t)\end{aligned} \tag{9.34}$$

Applying Cauchy Schwarz, Young's, and Poincare's inequalities to the term on the second line in (9.34), for a positive constant $\gamma_1 > 0$, we get

$$\int_0^{s(t)} \bar{g}(x,s(t))w(x,t)\mathrm{d}x q_\mathrm{c}(t) \leq 2\gamma_1 s_r^2||w_x||^2 + \frac{1}{2\gamma_1}||\bar{g}||^2 q_\mathrm{c}(t)^2. \tag{9.35}$$

Applying Young's and Cauchy Schwarz inequalities to the term on the fifth line in (9.34), for a positive constant $\gamma_2 > 0$, we get

$$-\int_0^{s(t)} \bar{g}(x,s(t))w_{xx}(x,t)\mathrm{d}x q_{\mathrm{c}}(t) \leq \frac{||\bar{g}||^2}{2\gamma_2}||w_{xx}||^2 + \frac{\gamma_2}{2}q_{\mathrm{c}}(t)^2. \tag{9.36}$$

Applying Young's and Agmon's inequalities, we get

$$-p\beta X(t)w_x(s(t),t) \leq \frac{pc}{2}X(t)^2 + \frac{2p\beta^2 s_r}{c}||w_{xx}||^2. \tag{9.37}$$

Therefore, by applying (9.35)–(9.37) to (9.34) with setting

$$\gamma_1 = \frac{\alpha}{4s_r^2}, \quad \gamma_2 = \frac{2||\bar{g}||^2}{\alpha}, \quad p = \frac{c\alpha}{4\beta^2 s_r}, \tag{9.38}$$

we arrive at

$$\begin{aligned}\dot{V}(t) \leq & -\frac{\alpha}{8s_r^2}\left(||w_x||^2 + \frac{1}{s_r^2}||w||^2\right) - \frac{pc}{2}X(t)^2 \\ & + \frac{3}{\alpha}||\bar{g}||^2 q_{\mathrm{c}}(t)^2 + \dot{s}(t)\left(\frac{1}{2s_r^3}||w||^2 + \frac{8s_r c}{\alpha}\frac{p}{2}X(t)^2\right) \\ \leq & -bV + a\dot{s}(t)V + \frac{3}{\alpha}||\bar{g}||^2 q_{\mathrm{c}}(t)^2,\end{aligned} \tag{9.39}$$

where

$$a = \max\left\{\frac{1}{s_r}, \frac{8s_r c}{\alpha}\right\}, \quad b = \min\left\{\frac{\alpha}{4s_r^2}, c\right\}. \tag{9.40}$$

Let W be the functional defined by

$$W(t) = V(t)e^{-as(t)}. \tag{9.41}$$

With the use of (9.39), the time derivative of (9.41) is shown to satisfy

$$\dot{W}(t) \leq -bW(t) + \frac{3}{\alpha}||\bar{g}||^2 q_c(t)^2 e^{-as(t)}. \tag{9.42}$$

Recalling the definition of $\bar{g}$ in (9.21) and applying Young's and Cauchy Schwarz inequalities, the spatial L_2 norm is bounded by

$$\begin{aligned}
||\bar{g}||^2 \leq & 2\int_0^{s(t)} \left(g(x)^2 + \left(\frac{c}{\alpha} \int_x^{s(t)} (x-y) g(y) dy \right)^2 \right) \mathrm{d}x \\
\leq & 2||g||^2 + 2\frac{c^2}{\alpha^2} \int_0^{s(t)} \left(\int_x^{s(t)} (x-y) g(y) dy \right)^2 \mathrm{d}x \\
\leq & 2\left(1 + \frac{c^2 s_r^4}{12\alpha^2} \right) ||g||^2_{L_2(0,s_r)},
\end{aligned} \tag{9.43}$$

which is time-independent. By Lemma 5, the square of the controller is bounded by

$$q_c(t)^2 \leq q_c(0)^2 e^{-2ct}. \tag{9.44}$$

Applying (9.43) and (9.44) to (9.42), we get

$$\dot{W}(t) \leq -bW(t) + Nq_c(0)^2 e^{-2ct}, \tag{9.45}$$

where N is a positive constant defined by

$$N = \frac{6}{\alpha} \left(1 + \frac{c^2 s_r^4}{12\alpha^2} \right) ||g||^2_{L_2(0,s_r)}. \tag{9.46}$$

Applying comparison principle to (9.45) leads to

$$W(t) \leq W_0 e^{-bt} + Nq_c(0)^2 e^{-bt} \int_0^t e^{-(2c-b)\tau} d\tau \tag{9.47}$$

Noting $b = \min\left\{\frac{\alpha}{4s_r^2}, c\right\}$ given in (9.40), it is easy to see that $2c > b$. Thus, through the calculation of the integration, the inequality (9.47) is led to

$$W \leq \left(W_0 + \frac{Nq_c(0)^2}{2c-b}\right) e^{-bt}. \tag{9.48}$$

By $V = We^{as(t)}$, (9.48) leads to the inequality of V as

$$\begin{aligned} V \leq & e^{as(t)} \left(W_0 + \frac{Nq_c(0)^2}{2c-b}\right) e^{-bt}, \\ \leq & e^{as_r} \left(V_0 + \frac{Nq_c(0)^2}{2c-b}\right) e^{-bt}. \end{aligned} \tag{9.49}$$

By the invertibility of the transformation, there exist positive constants $\bar{M} > 0$ and $\underline{M} > 0$ such that for the norm of the original (u,X)-system and the norm of the target (w,X)-system, it holds

$$\underline{M}\Phi(t) \leq V(t) \leq \bar{M}\Phi(t), \tag{9.50}$$

where

$$\Phi(t) := ||u||^2_{\mathcal{H}_1} + X(t)^2. \tag{9.51}$$

Moreover, since the control law is $q_c(t) = -ck\left(\frac{1}{\alpha}\int_0^{s(t)} u(x,t)\mathrm{d}x + \frac{1}{\beta}X(t)\right)$, taking the square of the control law and applying Young's and Cauchy-Schwarz inequalities lead to the following inequality

$$q_c(0)^2 \leq L\Phi(0), \tag{9.52}$$

where $L = 2c^2k^2 \max\{\frac{s_r}{\alpha^2}, \frac{1}{\beta^2}\}$. Combining these, we arrive at

$$\Phi(t) \leq \frac{e^{as_r}}{\underline{M}} \left(\bar{M} + \frac{NL}{2c-b} \right) \Phi_0 e^{-bt}, \tag{9.53}$$

from which the origin of the closed-loop system of (u, X) is shown to be exponentially stable.

9.4 Observer and Output Feedback Control Design

Here, we construct a state observer to estimate the temperature profile with measuring only the position of the melting front $s(t)$, and design an output-feedback control law for the actuated laser power by utilizing the estimated temperature profile. Therefore, the measured output $y(t)$ is given by

$$y(t) = s(t). \tag{9.54}$$

Throughout this section, we assume that the output (9.54) does not include a disturbance for the purpose of proving the stability of the closed-loop system. In later section, we study the numerical simulation with including the disturbance in the measurement (9.54).

Observer for the temperature profile

Let $\hat{u}(x,t)$ be the estimate of the reference error of the temperature $u(x,t) = T(x,t) - T_{\mathrm{m}}$. We design the PDE observer for $\hat{u}$ as a copy of the plant (9.12)–(9.14) with utilizing the

measurement $y(t)$ as the domain of the PDE estimator as follows:

$$\hat{u}_t(x,t) = \alpha \hat{u}_{xx}(x,t) + \hat{g}(x) q_{\mathrm{c}}(t), \quad x \in (0, y(t)), \tag{9.55}$$

$$-k\hat{u}_x(0,t) = q_{\mathrm{c}}(t), \tag{9.56}$$

$$\hat{u}(y(t),t) = 0, \tag{9.57}$$

where $\hat{g}(x)$ is the guess of the spatial function $g(x)$ in the plant, which is essentially uncertain. Let $\tilde{u}$ be the estimation error state defined by $\tilde{u} := u - \hat{u}$. Then, the dynamics of ODE (9.15) can be rewritten with respect to $\hat{u}$ and $\tilde{u}$ as follows:

$$\dot{X}(t) = -\beta \hat{u}_x(s(t),t) - \beta \tilde{u}_x(s(t),t). \tag{9.58}$$

Subtracting the observer PDE (9.55)–(9.57) from the plant PDE (9.12)–(9.14), we get the dynamics of the estimation error as follows:

$$\tilde{u}_t(x,t) = \alpha \tilde{u}_{xx}(x,t) + \tilde{g}(x) q_c(t), \quad x \in (0, s(t)), \tag{9.59}$$

$$\tilde{u}_x(0,t) = 0, \tag{9.60}$$

$$\tilde{u}(s(t),t) = 0, \tag{9.61}$$

where $\tilde{g}(x) := g(x) - \hat{g}(x)$.

Output feedback control design and stability proof

The output feedback control law is designed by replacing the plant state u in the full-state feedback control law (9.22) with the observer state $\hat{u}$, resulting in the following description

$$q_{\mathrm{c}}(t) = -c \left(\frac{k}{\alpha} \int_0^{y(t)} \hat{u}(x,t) \mathrm{d}x + \frac{k}{\beta} (y(t) - s_r) \right). \tag{9.62}$$

To prove the stability of the closed-loop system, we require the following assumptions.

Assumption 21 $\hat{u}(x,0) \geq u(x,0) \geq 0$ *for all* $x \in (0, s_0)$.

Assumption 22 $\hat{g}(x) \geq g(x) \geq 0$ *for all* $x \in (0, s_r)$.

Assumption 23 *The setpoint* s_r *is chosen to satisfy*

$$s_r > y(0) + \frac{\beta}{\alpha} \int_0^{y(0)} \hat{u}(x,0)dx. \tag{9.63}$$

Remark 13 $\hat{g}(x)$ *can be chosen so that Assumption 22 holds. In laser sintering,* $g(x)$ *is given by* $g(x) = \frac{1}{\rho c_p \delta} e^{-\frac{x}{\delta}}$*, and the penetration rate coefficient* δ *is highly uncertain. However, it is possible to know the upper bound* $\overline{\delta}$ *and lower bound* $\underline{\delta}$*, i.e.,* $0 < \underline{\delta} \leq \delta \leq \overline{\delta} < \infty$*. Thus, a conservative choice of* $\hat{g}(x)$ *to satisfy Assumption 22 is*

$$\hat{g}(x) = \frac{1}{\rho c_p \underline{\delta}} \exp\left(-\frac{x}{\overline{\delta}}\right). \tag{9.64}$$

The theorem for the observer-based output feedback control is given below.

Theorem 7 *Under Assumptions 21–23, consider the closed-loop system consisting of the plant* (9.12)–(9.15)*, the measurement* (9.54)*, the observer* (9.55)–(9.57)*, and the output feedback control* (9.62)*. Then, for any* $\hat{g}(x)$ *satisfying*

$$\int_0^{s_r} (g(x) - \hat{g}(x))^2 dx \leq \frac{\alpha}{80k^2 s_r}, \tag{9.65}$$

the closed-loop system satisfies the model validity condition (9.5)*, and there exists a positive constant* $M > 0$ *such that the norm*

$$\Phi(t) := ||u||^2_{\mathcal{H}_1} + (s(t) - s_r)^2 + ||\tilde{u}||^2_{\mathcal{H}_1}, \tag{9.66}$$

satisfies the following exponential decay

$$\Phi(t) \leq M\Phi(0)e^{-bt}, \tag{9.67}$$

where $b = \frac{1}{4}\min\left\{\frac{\alpha}{4s_r^2}, c\right\}$*, namely, the origin of the closed-loop system is exponentially stable in the spatial* $\mathcal{H}_1$ *norm.*

The proof of Theorem 7 is provided in the remainder of this section.

Model validity conditions

First, we prove the following lemma that is analogous to Lemma 4.

Lemma 6 *The closed-loop system satisfies the following properties:*

$$q_{\rm c}(t) > 0, \quad \forall t \geq 0, \tag{9.68}$$

$$\tilde{u}(x,t) < 0, \quad \forall x \in (0, s(t)), \quad \forall t \geq 0, \tag{9.69}$$

$$\tilde{u}_x(s(t),t) > 0, \quad \forall t \geq 0, \tag{9.70}$$

$$u(x,t) > 0, \quad \forall x \in (0, s(t)), \quad \forall t \geq 0, \tag{9.71}$$

$$s_0 < s(t) < s_r, \quad \forall t > 0. \tag{9.72}$$

Proof:

We use the contradiction approach. Assume that there exists a finite time $t_1 > 0$ such that (9.68) is violated, namely, $q_{\rm c}(t) > 0$ for all $t \in (0, t_1)$ and $q_{\rm c}(t_1) = 0$. Then, owing to $\tilde{g}(x) < 0$ given by Assumption 22, the estimation error PDE (9.59) satisfies $\tilde{u}_t(x,t) < \alpha\tilde{u}_{xx}$, and thereby applying maximum principle to $\tilde{u}$-system leads to the negativity of the solution, i.e., $\tilde{u}(x,t) < 0$, for all

$x \in (0, s(t))$, for all $t \in (0, t_1)$, and

$$\tilde{u}_x(s(t), t) \geq 0, \quad \forall t \in (0, t_1). \tag{9.73}$$

Taking the time derivative of the control law (9.62) along the solution of (9.55)–(9.58) leads to the following differential equation

$$\dot{q}_{\mathrm{c}}(t) = -c\left(1 + \frac{k}{\alpha}\int_0^{s(t)} \hat{g}(x)\mathrm{d}x\right) q_{\mathrm{c}}(t) + ck\tilde{u}_x(s(t), t). \tag{9.74}$$

Applying (9.73) to (9.74) leads to

$$\dot{q}_{\mathrm{c}}(t) > -c\left(1 + \frac{k}{\alpha}\int_0^{s(t)} \hat{g}(x)\mathrm{d}x\right) q_{\mathrm{c}}(t), \quad \forall t \in (0, t_1). \tag{9.75}$$

Using the same procedure as the derivation in Lemma 4, the differential inequality (9.75) leads to the following inequality of the solution

$$q_{\mathrm{c}}(t) > q_{\mathrm{c}}(0) e^{\left(-c\left(1+\frac{k}{\alpha}\int_0^{sr} \hat{g}(x)\mathrm{d}x\right)t\right)}, \quad \forall t \in (0, t_1). \tag{9.76}$$

Thus, we have $q_{\mathrm{c}}(t_1) > 0$, which contradicts with the assumption $q_{\mathrm{c}}(t_1) = 0$. Hence, we deduce (9.68), and again applying the maximum principle to (9.59)–(9.61) leads to the properties (9.69) and (9.70) for all $t \geq 0$. The conditions (9.71) and (9.72) are derived by same procedure as in Lemma 4.

Stability analysis

To study the stability of the plant states (u, X) under the output feedback design (9.62), we prove the stability of coupled $\tilde{u}$-system (9.59)–(9.61) and $(\hat{u}, X)$-system (9.55)–(9.58). As in full-state feedback design, we introduce the following backstepping transformation from

$(\hat{u},X)$-system to $(\hat{w},X)$-system:

$$\hat{w}(x,t) = \hat{u}(x,t) - \frac{c}{\alpha}\int_x^{s(t)} (x-y)\hat{u}(y,t)\mathrm{d}y + \frac{c}{\beta}(s(t)-x)X(t). \tag{9.77}$$

Taking the time and spatial derivatives of (9.77) together with (9.55)–(9.58) yields the following target system:

$$\begin{aligned}
\hat{w}_t(x,t) =& \alpha\hat{w}_{xx}(x,t) + \frac{c}{\beta}\dot{s}(t)X(t) + \bar{g}(x,s(t))q_c(t) \\
&- c(s(t)-x)\tilde{u}_x(s(t),t), && (9.78)\\
\hat{w}(s(t),t) =& 0, && (9.79)\\
\hat{w}_x(0,t) =& 0, && (9.80)\\
\dot{X}(t) =& -cX(t) - \beta\hat{w}_x(s(t),t) - \beta\tilde{u}_x(s(t),t). && (9.81)
\end{aligned}$$

First, we prove the stability of the coupled $\tilde{u}$-system (9.59)–(9.61) and $(\hat{w},X)$-system (9.78)–(9.81). Consider the functional $\tilde{V}$ defined by

$$\tilde{V} = \frac{1}{2s_r^2}||\tilde{u}||^2 + \frac{1}{2}||\tilde{u}_x||^2. \tag{9.82}$$

Taking the time derivative of (9.82) along the solution of (9.59)–(9.61), we get

$$\begin{aligned}
\dot{\tilde{V}} =& -\frac{\alpha}{s_r^2}||\tilde{u}_x||^2 + \int_0^{s(t)} \tilde{u}(x,t)\tilde{g}(x)\mathrm{d}x q_c(t) - \frac{\dot{s}(t)}{2}\tilde{u}_x(s(t),t)^2 - \alpha||\tilde{u}_{xx}||^2 \\
&- \int_0^{s(t)} \tilde{u}_{xx}(x,t)\tilde{g}(x)\mathrm{d}x q_c(t). && (9.83)
\end{aligned}$$

Applying Young's and Cauchy-Schwarz inequalities to (9.83) leads to

$$\dot{\tilde{V}} \leq -\frac{\alpha}{2}||\tilde{u}_{xx}||^2 - \frac{\alpha}{2s_r^2}||\tilde{u}_x||^2 + \frac{5}{2\alpha}||\tilde{g}||^2|q_c(t)|^2. \tag{9.84}$$

In the stability proof of the full-state feedback system, the square norm of the control law was shown to be bounded by an exponential function in time *prior to* Lyapunov analysis with the help of the closed-form of the differential equation of the controller. However, under the output feedback control design, as observed from the differential equation (9.74) including the extra term of $\tilde{u}_x(s(t),t)$, it is hard to apply the same approach. To deal with the problem, we additionally consider the functional $Q(t)$ defined by

$$Q(t) = \frac{1}{2} q_{\mathrm{c}}(t)^2. \tag{9.85}$$

The time derivative of (9.85) with the help of (9.74) yields the following

$$\begin{aligned} \dot{Q}(t) =& -c\left(1+\frac{k}{\alpha}\int_0^{s(t)} g(x)\mathrm{d}x\right) q_{\mathrm{c}}(t)^2 + ck\tilde{u}_x(s(t),t) q_{\mathrm{c}}(t) \\ \leq& -\frac{c}{2} q_{\mathrm{c}}(t)^2 + 2ck^2 s_r ||\tilde{u}_{xx}||^2, \end{aligned} \tag{9.86}$$

where we used Young's, Cauchy-Schwarz, and Agmon's inequalities for the derivation from the first line to the second line. We consider the following functional

$$\Theta(t) = \tilde{V} + \frac{\alpha}{8ck^2 s_r} Q. \tag{9.87}$$

Taking time derivative of (9.87) and applying the inequalities (9.84) and (9.86) with the help of (9.65) yields

$$\dot{\Theta}(t) \leq -\frac{\alpha}{4}||\tilde{u}_{xx}||^2 - \frac{\alpha}{2s_r^2}||\tilde{u}_x||^2 - \frac{\alpha}{32k^2 s_r}|q_c(t)|^2. \tag{9.88}$$

Additionally, as defined by (9.33), we consider the following functional

$$\hat{V}(t) = \frac{1}{2s_r^2}||\hat{w}||^2 + \frac{1}{2}||\hat{w}_x||^2 + \frac{p}{2}X(t)^2, \tag{9.89}$$

where $p = \frac{c\alpha}{4\beta^2 s_r}$. Referring to the derivation of (9.39) with additional terms involving $\tilde{u}_x(s(t),t)$ in (9.78) and (9.81), one can deduce that the time derivative of (9.89) is bounded by

$$\begin{aligned}\dot{\hat{V}}(t) \leq & -\frac{\alpha}{16s_r^2}\left(||w_x||^2+\frac{1}{s_r^2}||w||^2\right)-\frac{pc}{4}X(t)^2+\left(\frac{18s_r^3c^2}{3\alpha}+\frac{\alpha}{4s_r}\right)\tilde{u}_x(s(t),t)^2 \\ & +\frac{3}{\alpha}||\bar{g}||^2 q_{\mathrm{c}}(t)^2+\dot{s}(t)\left(\frac{1}{2s_r^3}||w||^2+\frac{8s_r c}{\alpha}\frac{p}{2}X(t)^2\right) \\ \leq & -\frac{b}{2}\hat{V}+a\dot{s}(t)\hat{V}+\frac{3}{\alpha}||\bar{g}||^2 q_{\mathrm{c}}(t)^2+\left(\frac{72s_r^4c^2}{3\alpha}+\alpha\right)||\tilde{u}_{xx}||^2. \end{aligned} \tag{9.90}$$

Finally, by defining

$$V(t) = \hat{V}(t) + r\Theta(t), \tag{9.91}$$

for sufficiently large $r > 0$, taking the time derivative of (9.91) and applying (9.90) and (9.88) leads to

$$\begin{aligned}\dot{V} \leq & -\frac{b}{2}\hat{V}+a\dot{s}(t)\hat{V}-\frac{r\alpha}{16s_r^2}\tilde{V}-\frac{r\alpha}{32k^2 s_r}Q(t), \\ \leq & -\bar{b}V+a\dot{s}(t)V, \end{aligned} \tag{9.92}$$

where

$$\bar{b} = \frac{1}{4}\min\left\{\frac{\alpha}{4s_r^2}, c\right\}. \tag{9.93}$$

Applying comparison principle to (9.92) with the help of $\dot{s}(t) > 0$ and $s_0 < s(t) < s_r$ leads to the exponential decay of the norm as

$$V(t) \leq e^{as_r}V(0)e^{-\bar{b}t}. \tag{9.94}$$

Table 9.1: Physical properties of Ti6Al4V alloy given by [113].

Description	**Symbol**	**Value**
Density (liquid)	ρ_{l}	$3920\ \mathrm{kg}\cdot\mathrm{m}^{-3}$
Density (solid)	ρ_{s}	$4200\ \mathrm{kg}\cdot\mathrm{m}^{-3}$
Latent heat of fusion	H_{f}	$2.86\times10^{5}\ \mathrm{J}\cdot\mathrm{kg}^{-1}$
Heat capacity (liquid)	$c_{\mathrm{p,l}}$	$830\ \mathrm{J}\cdot\mathrm{kg}^{-1}\cdot\mathrm{K}^{-1}$
Heat capacity (solid)	$c_{\mathrm{p,s}}$	$730\ \mathrm{J}\cdot\mathrm{kg}^{-1}\cdot\mathrm{K}^{-1}$
Thermal conductivity (liquid)	k_{l}	$32.5\ \mathrm{W}\cdot\mathrm{m}^{-1}$
Thermal conductivity (solid)	k_{s}	$26.0\ \mathrm{W}\cdot\mathrm{m}^{-1}$
Melting temperature	T_{m}	$1650\ ^{\circ}\mathrm{C}$

Let $\Psi(t) = ||\hat{u}||^2_{\mathcal{H}_{\mathrm{l}}} + X(t)^2 + ||\tilde{u}||^2_{\mathcal{H}_{\mathrm{l}}}$ and $\bar{\Psi}(t) = ||\hat{u}||^2_{\mathcal{H}_{\mathrm{l}}} + X(t)^2 + ||\tilde{u}||^2_{\mathcal{H}_{\mathrm{l}}} + q_{\mathrm{c}}(t)^2$. Due to the invertibility of the transformation from $(\hat{u},X)$ and $(\hat{w},X)$, the norm equivalence between V and $\bar{\Psi}$ holds, i.e., there exist positive constants $\overline{M} > 0$ and $\underline{M} > 0$ such that $\underline{M}\bar{\Psi}(t) \leq V(t) \leq \overline{M}\bar{\Psi}(t)$ holds. Furthermore, using the bound of $q_{\mathrm{c}}(t)^2$ derived in (9.52) ($q_{\mathrm{c}}(t)^2 \leq L\Psi(t)$ for some $L > 0$), we obtain $\Psi(t) \leq \bar{\Psi}(t) \leq (1+L)\Psi(t)$. Therefore, we get

$$\Psi(t) \leq e^{as_r}\frac{\overline{M}}{\underline{M}}(1+L)\Psi(0)e^{-bt}. \tag{9.95}$$

Finally, the norm equivalence between $(u,X,\tilde{u})$-system and $(\hat{u},X,\tilde{u})$-system holds due to the relation $u = \hat{u} + \tilde{u}$, and therefore the exponential decay of the norm holds for the functional $\Phi(t) = ||u||^2_{\mathcal{H}_{\mathrm{l}}} + X(t)^2 + ||\tilde{u}||^2_{\mathcal{H}_{\mathrm{l}}}$, from which we conclude Theorem 7.

9.5 Numerical Simulation

In this section we provide two illustrations. First, we show that the controller is effective even when applied to a considerably more complex and realistic model than the one for which the design was conducted and the theorems proven. Second, we push the model mismatch to the point of the controller failing, identifying the size of the modeling error which is intolerable for

the controller.

Incorporating the freezing effect from the solid phase

The dynamics of the moving interface (9.4) is given under the assumption that the freezing effect from the solid metal part is negligible, however, we incorporate the freezing effect in the numerical simulation by modifying the dynamics as

$$\dot{s}(t) = -\beta_{\mathrm{l}} \frac{\partial T_{\mathrm{l}}}{\partial x}(s(t),t) + \beta_{\mathrm{s}} \frac{\partial T_{\mathrm{s}}}{\partial x}(s(t),t), \tag{9.96}$$

where the variables with subscript l and s denote those of the liquid phase (melt pool) and the solid phase (metal part), respectively. Similarly to PDE for the liquid phase, the governing equation of the solid phase is given by

$$\frac{\partial T_{\mathrm{s}}}{\partial t}(x,t) = \alpha_{\mathrm{s}} \frac{\partial^2 T_{\mathrm{s}}}{\partial x^2}(x,t), \quad x \in (s(t),L), \tag{9.97}$$

$$\frac{\partial T_{\mathrm{s}}}{\partial x}(L,t) = 0, \tag{9.98}$$

$$T_{\mathrm{s}}(s(t),t) = T_{\mathrm{m}}, \tag{9.99}$$

where L is the thickness of the metal part. For computation of the Stefan problem (9.1)–(9.3), (9.96)–(9.99), we use boundary immobilization method combined with finite difference semi-discretization [102] for both the liquid and solid PDEs. The resulting approximated ODEs are calculated by using MATLAB ode15 solver.

Input parameters

We use the physical parameters of Ti6Al4V which is a popular composite material for metal AM, as given in Table 9.1. The initial values are set as $s_0 = 50$ [μm], and

$$T_{\mathrm{l}}(x,0) = \overline{T}\frac{1+\cos\left(\frac{\pi x}{s_0}\right)}{2} + T_{\mathrm{m}}, \quad \forall x \in [0, s_0], \tag{9.100}$$

$$\hat{T}_{\mathrm{l}}(x,0) = \hat{\overline{T}}\left(1 - \frac{x}{s_0}\right) + T_{\mathrm{m}}, \quad \forall x \in [0, s_0], \tag{9.101}$$

$$\hat{T}_{\mathrm{s}}(x,0) = \underline{T}\left(1 - \frac{L-x}{L-s_0}\right) + T_{\mathrm{m}}, \quad \forall x \in [s_0, L], \tag{9.102}$$

where $\overline{T} = 10$ [$^\circ$C], $\hat{\overline{T}} = 50$ [$^\circ$C], and $\underline{T} = -100$ [$^\circ$C]. Note that the profiles have boundary values $T_{\mathrm{l}}(0,0) = \overline{T} + T_{\mathrm{m}}$, $\hat{T}_{\mathrm{l}}(x,0) = \hat{\overline{T}} + T_{\mathrm{m}}$, and $\hat{T}_{\mathrm{s}}(x,0) = \underline{T} + T_{\mathrm{m}}$. The setpoint is chosen as $s_r = 200$ [μm], which is a reasonable value for layer thickness of the SLS-based AM. Then, the setpoint restriction (9.6) is satisfied. The control gain c is set to have a reasonable value for the laser power at initial time, and here we choose $c = 10000$ [1/sec]. The spatially varying function is set as $g(x) = \frac{1}{\rho c_{\mathrm{p}} \delta} e^{-\frac{x}{\delta}}$ following [132], where $\delta = 10$ [μm]. The thickness L of the metal part is set as $L = 2$ [cm].

Practical setup for the observer design

As presented in Remark 22, the spatially varying function $\hat{g}(x)$ in the observer (9.55)–(9.57) is chosen as (9.64), where the upper bound and the lower bound of the penetration rate are chosen as $\underline{\delta} = 8$ [μm] and $\overline{\delta} = 12$ [μm]. Moreover, we incorporate the measurement uncertainty as the constant bias d, namely, the measured value $y(t)$ for the interface position $s(t)$ is given by

$$y(t) = s(t) + d. \tag{9.103}$$

In the simulation study, we investigate the results with noise-free $d = 0$, the positive bias $d > 0$, and the negative bias $d < 0$.

Simulation results

Robustness of the performance under the small perturbations

The simulation results of the interface position, the laser power controller, and the surface temperature are given in Fig. 9.2 (a)–(c), respectively, for the cases of the measurements under noise-free $d = 0$ [μm] (red), the positive bias $d = 5$ [μm] (blue), and the negative bias $d = -5$ [μm] (green). Fig. 9.2 (a) shows that under the noise-free measurement (red) the interface position $s(t)$ converges to the setpoint s_r without overshooting in a short time scale 10 [msec], which illustrates sufficiently fast process of the melting each layer. On the other hand, in the presence of the measurement bias, a modest error of the converging position of the interface from the setpoint position is observed in both positive and negative bias. From Fig. 9.2 (b) we observe that the implemented output feedback control maintains positive value under noise-free measurement and even in the presence of the measurement bias, which satisfies the constraint for the input laser power. Owing to the positive valued input, Fig. 9.2 (c) shows that the temperature at the surface position remains above the melting temperature T_{m}, which ensures the condition (9.5) for the validity of the model addressed in Remark 11 under both noise-free measurement and the biased measurement. Therefore, the numerical results illustrate that the proposed observer-based output feedback control law performs robustly even in the presence of the measurement uncertainty.

Fig. 9.3 depicts the snapshots of the true temperature profile (solid line) and the estimated temperature profile (dash line) at t =0, 1, 5 [msec] in the presence of the positive bias. From Fig. 9.3, we observe that the estimated temperature profile gradually converges to the true temperature profile, albeit the convergence speed is not fast. Nevertheless, the control objective and the model validity conditions are well satisfied as observed in Fig. 9.2, which shows the sufficient

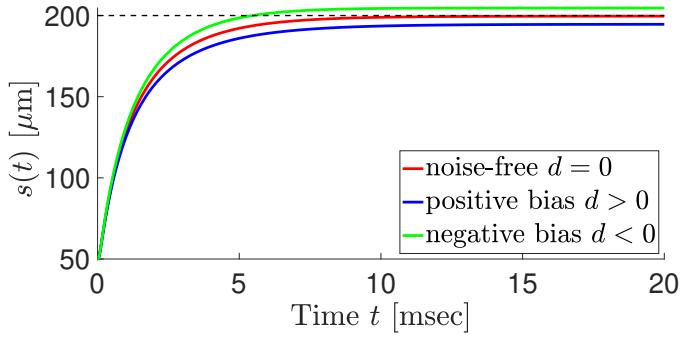

(a) In spite of the interface measurement bias d in (9.103), the regulation near the interface setpoint is achieved.

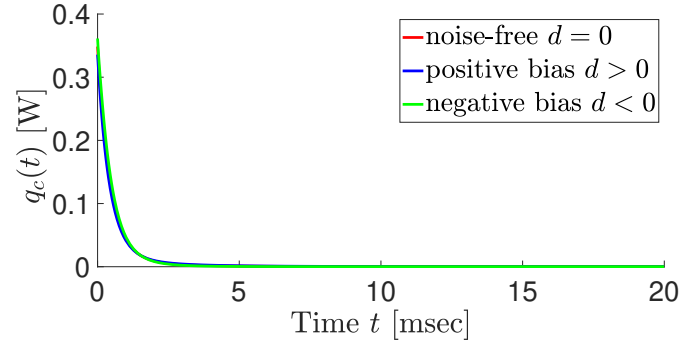

(b) Positivity of the laser power control is maintained.

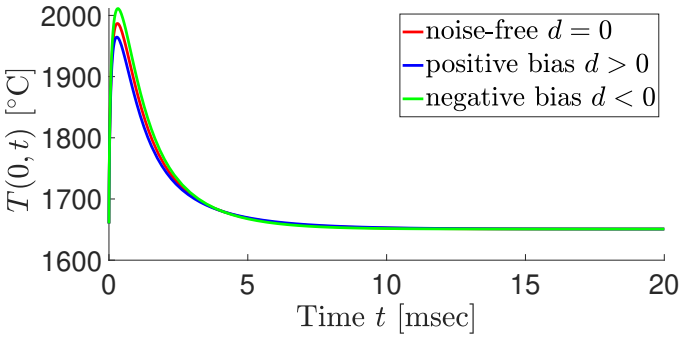

(c) The model validity of the boundary liquid temperature is maintained, i.e., $T(0,t) \geq T_{\mathrm{m}}$, in spite of the presence of the solid phase and of the interface measurement bias.

Figure 9.2: The responses of the system (9.1)–(9.3) and (9.96)–(9.99), under the output feedback control law (9.62) associated with the observer (9.55)–(9.57). The proposed method is successful: the convergence of the interface, the positivity of input, and the required condition for the liquid temperature are all achieved for both positive and negative measurement biases, namely, for $d = 0, 5, -5$ [μm], and in the presence of the solid phase.

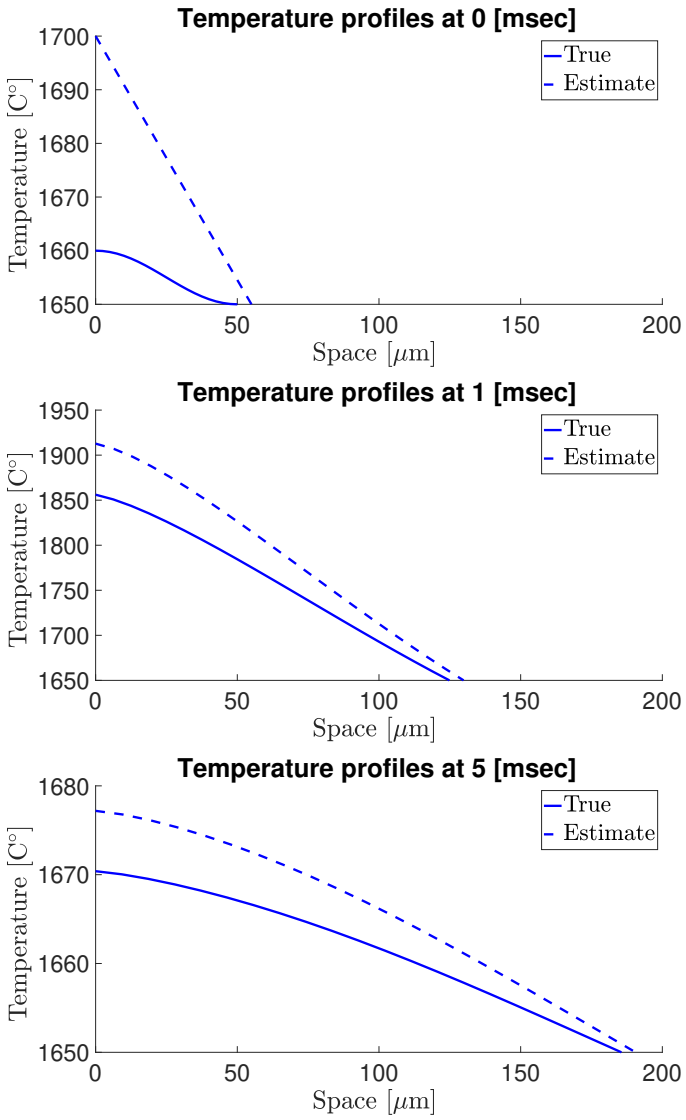

Figure 9.3: The snapshots of the true temperature profile (solid line) and the estimated temperature profile (dash line) at $t = 0$, 1, and 5 [msec] under the positive bias.

performance of the observer for the purpose of stabilization of the melt pool in SLS.

Limitation of the performance under large perturbations

However, under large uncertainty in model caused by the cold (the negative heat) in the solid metal, or by the measurement uncertainties, the proposed method is shown to, expectedly, violate the required conditions for the physical model. Fig. 9.4 depicts the interface response

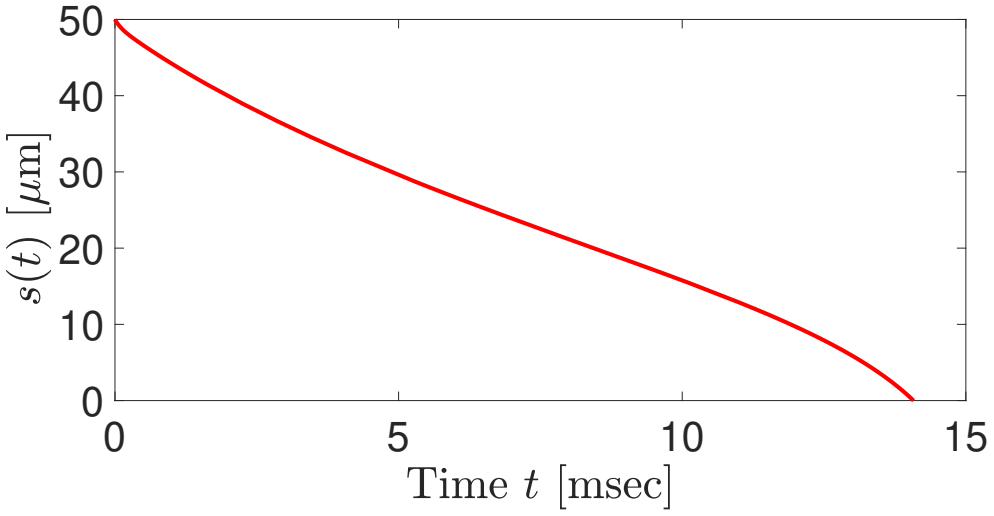

Figure 9.4: The interface response of the closed-loop system under very cold initial temperature of the solid phase. The proposed method fails, in this caricatured scenario, and the melt pool gets entirely frozen, as observed from the disappearance of the interface position around $t = 14$ [msec].

under an initial very low temperature in the solid phase (9.102), namely, $\underline{T} = -1630$ [°C] that results in the boundary value $T_{\rm s}(L,0) = \underline{T} + T_{\rm m} = 20$ [°C], which is still physically possible. As we observe from Fig. 9.4, the interface disappears and with it the molten metal phase, at around 14 [msec] due to the complete solidification of the melt pool. This is caused by an insufficient amount of the laser power input for the given "deeply" frozen solid metal initial state. The limitation of the proposed control law can be relaxed by designing a "two-phase"-based control law proposed in the absence of radiation in Chapter 5, which will be considered with radiation in future work.

Next, we investigate the closed-loop response under $d = -30$ [μm], namely, a large negative bias in the measurement. Fig. 9.5 shows the response of the control input and the boundary temperature. Fig. 9.5 (a) illustrates that the controlled laser power reaches negative value after $t = 2$ [msec], which violates the input constraint. Due to the negative input, Fig. 9.5 (b) illustrates that the boundary temperature of the melt pool reaches below the melting temperature, which physically causes the solidification of the melt pool from the controlled boundary and

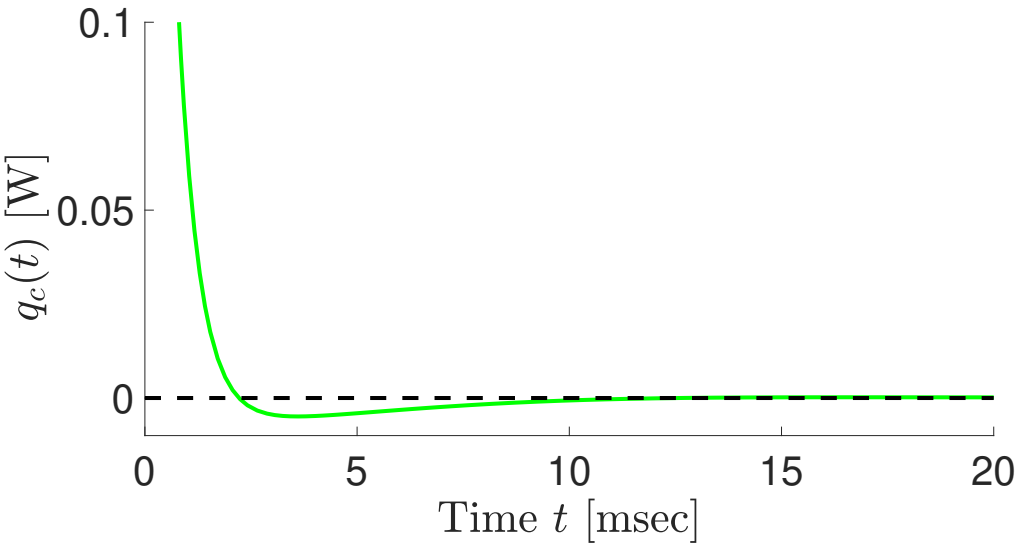

(a) The input of the laser power reaches negative value, which cannot be implemented in practice.

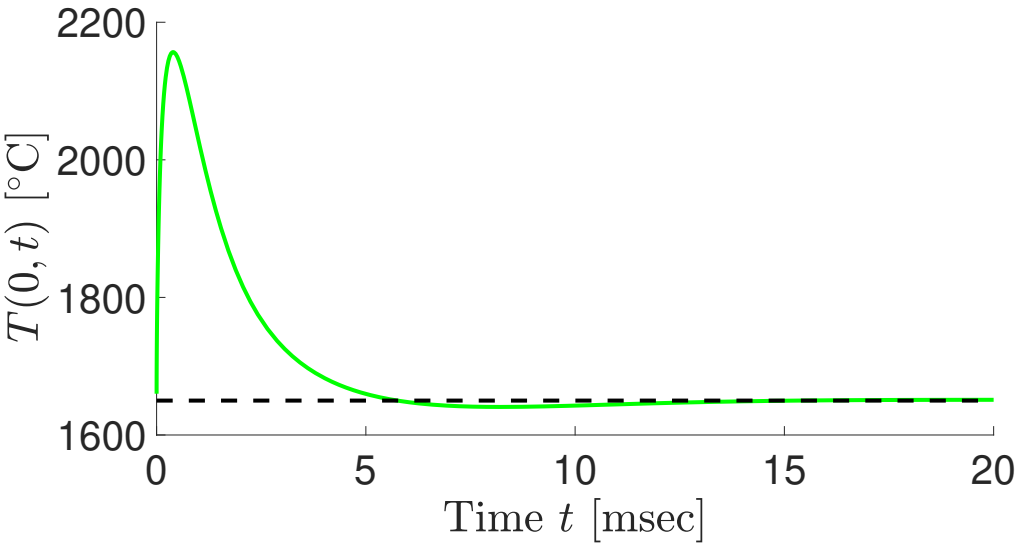

(b) The liquid temperature can be below the melting temperature, which causes the solidification of the melt pool from the controlled boundary.

Figure 9.5: The response of the closed-loop system under a large negative bias $d = -30$ [μm]. The proposed method fails due to the violation of the positivity of the input and of the condition of the liquid temperature.

therefore the condition of the model is violated. Hence, there is a limitation of the performance of the proposed control law with respect to the level of the measurement uncertainty in the case

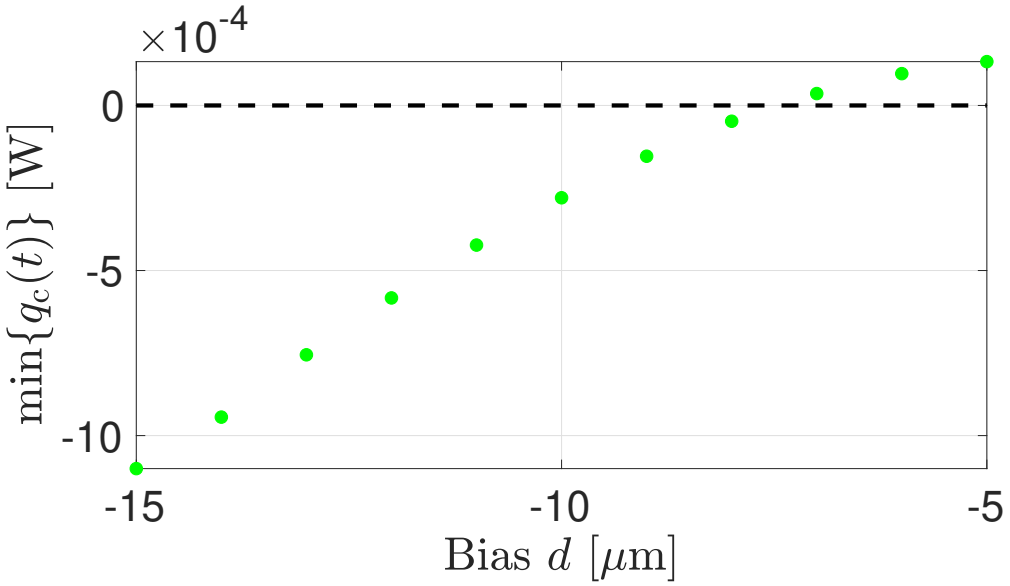

Figure 9.6: Plot of the minimum value of the control input over time through varying the bias d from -5 [μm] to -15 [μm]. Positivity of the input is violated under the bias $d \leq -8$ [μm].

of negative bias. Fig. 9.6 shows the plot of minimum value of the control input $q_{\rm c}(t)$ over the time interval $t \in [0, t_{\rm f}]$ where $t_{\rm f} = 20$ [msec] under the bias d ranging from -5 [μm] to -15 [μm]. From Fig. 9.6, we observe that the critical value of the bias violating the positivity of the input is between -7 and -8 [μm], which is approximately 15 % of the initial interface position $s_0 = 50$ [μm]. On the other hand, under the positive bias, as long as Assumption 23 holds, we observe that the performance of the control law is robust as we have seen in Fig. 9.2.

9.6 Conclusion and Future Work

In this chapter we have developed the control design of laser power in SLS for metal AM by using the PDE backstepping method in a form of both full-state and output feedback design. The governing equation is given by the one-phase Stefan problem with in-domain effect of the controlled laser power to the PDE dynamics. The closed-loop system is shown to satisfy some required conditions for the physical model to be valid, and the exponential stability at the origin

is proven. Numerical simulation is performed by computing the full "two-phase" Stefan model incorporating the cooing from the solid metal part and adding the measurement uncertainty. The simulation results illustrate that the proposed output feedback control design enables sufficiently fast process of the laser melting to drive the depth of the melt pool to the desired setpoint, and the performance is robust under perturbations of the model and the measurements. We push the proposed control law to its failure limit by exhibiting the closed-loop responses that violate the required conditions of the physical states under the large perturbations of the model and the measurement.

The limitation of the controller's robustness might be exploited analytically in the sense of Input-to-State Stability (ISS), by using the Lyapunov method for the perturbed system including the model and measurement uncertainties, similarly to ISS analysis in Chapter 4. One challenge lies in the fact that the model and the estimator are defined on a distinct range of the spatial domains, $(0, s(t))$ and $(0, s(t)+d(t))$, under the measurement uncertainty of the moving interface. Such a discrepancy of the domains makes the analysis of the estimation error system much harder. Moreover, while we have focused only on the stabilization of the melt pool's depth in this chapter, the stabilization of the surface area of the melt pool is also a significant task for the scanning process. This motivates us to exploit the control design for the Stefan problem along the surface geometry of the powder bed in metal AM process, which is also challenging due to the movement of the scanner mirror. We will consider these problems as future work.

9.7 Acknowledgement

Chapter 9, in part, is a reprint of the material as it appears in:

- S. Koga, M. Krstic, and J. Beaman, "Laser Sintering Control for Metal Additive Manufacturing by PDE Backstepping", *IEEE Conference on Decision and Control*, 2019,

- S. Koga, M. Krstic, and J. Beaman, "Laser Sintering Control for Metal Additive Manufac-

turing by PDE Backstepping", *IEEE Transactions on Control Systems Technology*, under review.

The dissertation author was the primary investigators and author of this paper. The author would like to thank Joseph Beaman for the collaboration.

Chapter 10

Experimental Study using PCM

There are a few results on the experimental application of the backstepping design for boundary control and observer of PDEs. In [122], the tracking control for flexible articulated wings on a robotic aircraft is designed by combining PDE backstepping for feedback stabilization and feedforward trajectory planning, and the performance of the designed boundary controller is demonstrated by conducting the experiment of bending a long thin beam. The validation of the backstepping boundary observer design using experimental data have been studied in [80] for microfluidic systems, in [62] for oil drilling, and in [178] for congested freeway traffic following their design in [179, 176]. However, there has not been any experimental results on the boundary control and observer for the Stefan system which is governed by a parabolic PDE with state-dependent moving boundaries "(a nonlinear system)".

The fidelity of the Stefan model has been validated in several experimental studies. Among the various materials in the aforementioned applications, phase change materials (PCMs) in latent heat thermal energy storage systems for numerous applications (e.g. heat pumps, solar engineering, and spacecraft thermal controls) have been intensively used to investigate the correspondence of the experimental data with the numerical model of the Stefan problem (see [42] for detailed review on simulations of PCMs). While there are several materials of PCMs,

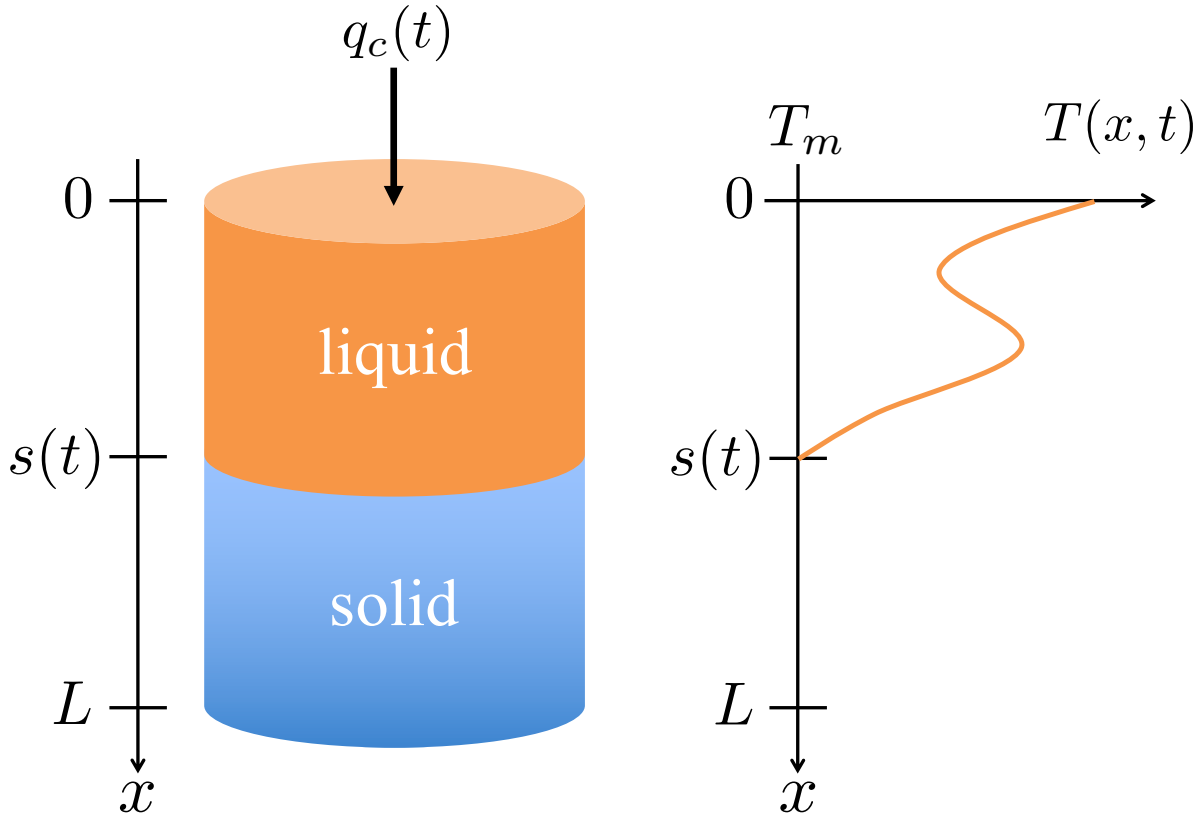

Figure 10.1: Schematic of one-dimensional model of paraffin as a Phase Change Material (PCM) in vertical coordinate.

paraffins have been utilized owing to the attractive features on safe temperature range for melting, low cost, non-corrosive, and predictable thermal and chemical behavior [139].

10.1 Modelling of PCM

We consider a cylindrical paraffin with the diameter R and the total length L, which is enclosed with an acrylic container serving as a thermal insulation. Hence, the geometry of the model is represented by a cylindrical coordinate (r, θ, x) which denotes the radial distance from the center, the angular degree from a base, and a displacement from the upper side of the container, respectively (see Fig. 10.1). In the phase change material, the liquid-solid phase

boundary exists as a domain inside the coordinate. We establish the physical model under the following assumptions.

Assumption 24 *The temperature profile of the paraffin is uniformly distributed along the circle-shaped cross section of the cylinder. Mathematically, we can describe the property as*

$$T(r,\theta,x,t) \equiv T(x,t), \quad \forall r \in [0,R], \forall \theta \in [0,2\pi) \tag{10.1}$$

Moreover, the domain of the phase boundary is uniform along the cross section of the cylinder, which enables to describe the location as $x = s(t)$.

Assumption 25 *There is no convection in the liquid phase.*

Owing to the cylindrical geometry and the thermal insulation along the side, if Assumption 24 holds at the initial time $t = t_0$ then it holds for all time $t > t_0$. By Assumption 24, the geometry of the physical model can be described by one dimensional coordinate in x. In addition, by Assumption 25, the governing equation is only given by the energy conservation without imposing a mass and momentum balance. Combining the local energy conservation law inside the liquid phase domain $x \in (0, s(t))$ and the Fourier's thermal conduction law, the time evolution of the temperature profile is given by the following parabolic PDE

$$\frac{\partial T}{\partial t}(x,t) = \alpha \frac{\partial^2 T}{\partial x^2}(x,t), \quad 0 < x < s(t), \tag{10.2}$$

where $\alpha := \frac{k}{\rho C_\mathrm{p}}$ with a density ρ, heat capacity C_p, and the thermal conductivity k for liquid phase, respectively. At the surface $x = 0$, there is a heat loss due to the convective heat transfer through the surrounding air, which yields the following energy balance

$$-k\frac{\partial T}{\partial x}(0,t) = q_\mathrm{c}(t) - h(T(0,t) - T_a), \tag{10.3}$$

where $q_{\mathrm{c}}(t)$ is a manipulated heat flux per unit area, h denotes the heat transfer coefficient, and T_a denotes the ambient temperature (room temperature). As a fundamental physical condition of the thermal phase change, the temperature at the liquid-solid phase boundary $x = s(t)$ maintains the constant melting temperature T_{m}, which renders the boundary condition as

$$T(s(t),t) = T_{\mathrm{m}}. \tag{10.4}$$

Moreover, the local energy balance at the position of the liquid-solid phase boundary $x = s(t)$ leads to the Stefan condition defined as the following nonlinear ODE

$$\rho \Delta H^* \dot{s}(t) = -k \frac{\partial T}{\partial x}(s(t),t) - q_{\mathrm{los}}, \tag{10.5}$$

where ΔH^* and q_{los} denote the latent heat of fusion and heat loss at the interface, respectively.

Remark 14 *To maintain the model* (10.2)-(10.5) *to be physically validated, the following conditions must hold:*

$$T(x,t) \geq T_{\mathrm{m}}, \quad \forall x \in (0, s(t)), \quad \forall t > 0, \tag{10.6}$$

$$0 < s(t) < L, \quad \forall t > 0. \tag{10.7}$$

The conditions (10.6) and (10.7) are proven to hold after the design of the heat input $q_{\mathrm{c}}(t)$.

10.2 Nominal Feedback Control Design

Control objective and steady-state solution

The objective is to drive the phase boundary location $s(t)$ to a desired setpoint s_{r} by controlling the heat flux $q_c(t)$. As a desired state, the stead-state solution of the temperature

profile $T_r(x)$ at $s(t) = s_\mathrm{r}$ needs to be considered. By setting the time derivative of the physical model to be zero, the steady-state of the temperature is obtained by

$$T_r(x) = \frac{q_\mathrm{los}}{k}(s_\mathrm{r} - x) + T_\mathrm{m}. \tag{10.8}$$

Then, at the steady-state, the heat flux input must have a balance with the heat loss at the surface and the interface, which is described as

$$q_c^* = \left(1 + \frac{hs_\mathrm{r}}{k}\right) q_\mathrm{los} + h\left(T_\mathrm{m} - T_a\right). \tag{10.9}$$

Continuous-time full-state feedback control design

While the governing equations (10.2)–(10.5) are given by the local energy balance law at each location in the domain $x \in [0, s(t)]$, in order to prescribe the growth of the internal energy through the heat input and heat loss, the macroscopic energy conservation should be considered. The internal energy of the system is composed of the specific heat and the latent heat given by

$$E(t) = \frac{k}{\alpha}\int_0^{s(t)} (T(x,t) - T_\mathrm{m})\mathrm{d}x + \frac{k}{\beta}s(t), \tag{10.10}$$

where $\beta := \frac{k}{\rho \Delta H^*}$. Taking the time derivative of (10.10), we obtain the macroscopic energy conservation law as

$$\dot{E}(t) = q_c(t) - h(T(0,t) - T_a) - q_\mathrm{los}. \tag{10.11}$$

The setpoint energy is given by substituting the steady-state solution $(T_\mathrm{r}(x), s_\mathrm{r})$ into (10.10), which yields

$$E_r = \frac{k}{\alpha}\int_0^{s_\mathrm{r}} (T_r(x) - T_\mathrm{m})\mathrm{d}x + \frac{k}{\beta}s_\mathrm{r} = \frac{q_\mathrm{los}s_\mathrm{r}^2}{2\alpha} + \frac{k}{\beta}s_\mathrm{r} \tag{10.12}$$

To achieve the control objective driving the system states (T, s) to the reference setpoint $(T_{\mathrm{r}}, s_{\mathrm{r}})$, it is necessary that the internal energy $E(t)$ grows to the setpoint internal energy E_r. The idea of our control design originates from parabolic PDE-ODE backstepping in [95] but in this section we provide a simplified exposition based on energy shaping. Namely, we define the reference error of the internal energy as

$$\tilde{E}(t) = E(t) - E_r, \tag{10.13}$$

and design the control law as follows:

$$\begin{aligned} q_c(t) =& -c\tilde{E}(t) + h(T(0,t) - T_a) + q_{\mathrm{los}} && (10.14)\\ =& -c\left(\frac{k}{\alpha}\int_0^{s(t)} (T(x,t) - T_{\mathrm{m}})\mathrm{d}x + \frac{k}{\beta}(s(t) - s_{\mathrm{r}})\right) \\ &+ \frac{cq_{\mathrm{los}}s_{\mathrm{r}}^2}{2\alpha} + h(T(0,t) - T_a) + q_{\mathrm{los}}. && (10.15) \end{aligned}$$

Here, we impose the following restriction on the setpoint position s_{r}.

Assumption 26 *The setpoint s_{r} is chosen to satisfy*

$$s_0 + \frac{\beta}{\alpha}\int_0^{s_0} (T_0(x) - T_{\mathrm{m}})\mathrm{d}x < s_{\mathrm{r}} + \frac{\beta q_{\mathrm{los}}}{2k\alpha}s_{\mathrm{r}}^2 < L. \tag{10.16}$$

Then, the control (10.15) ensures the conditions (10.6) and (10.7), and we state the following theorem.

Theorem 16 *Consider the closed-loop system consisting of the plant* (10.2)–(10.5) *with the control law* (10.15)*. Then, the conditions* (10.6) *and* (10.7) *for the model validity hold, and there exists a positive constant $q_{\mathrm{los}}^* > 0$ such that for all $q_{\mathrm{los}} \in (0, q_{\mathrm{los}}^*)$ the closed-loop system is*

exponentially stable in the sense of the norm

$$\int_0^{s(t)} (T(x,t) - T_{\rm r}(x))^2 {\rm d}x + (s(t) - s_{\rm r})^2. \tag{10.17}$$

The proof of Theorem 16 is given at the end of this chapter. For accelerated convergence, the backstepping PDE-ODE control design in Theorem 2 in [95] would have to be pursued.

10.3 Implementable Control Algorithm Using Sensors and Software

This section presents the feedback control algorithm that we actually implement in the experiment. Note that the full-state feedback control design developed in Section 10.2 requires the following three assumptions:

- the spatial *profile* of the temperature is available,
- the spatial *integration* of the temperature profile is computed,
- and the measurements are obtained and the controller is manipulated *continuously in time*.

The first assumption is relaxed by introducing a state observer governed by a PDE to estimate the entire temperature profile under measured temperature only at the surface and the measured position of the phase interface, and re-designing the controller by associated output feedback control law. The block diagram is depicted in Fig. 10.2. Next, the PDE observer is approximated by an ODE observer through the truncation of the observer state and then the spatial integration in the output feedback control law is approximated by the trapezoidal rule, which removes the second assumption. Finally, the third assumption is relaxed by further improving the observer and the output feedback control by sampled-data design implemented under the measurements obtained at each discrete sampling time by following the idea of the sampled-data observer [69].

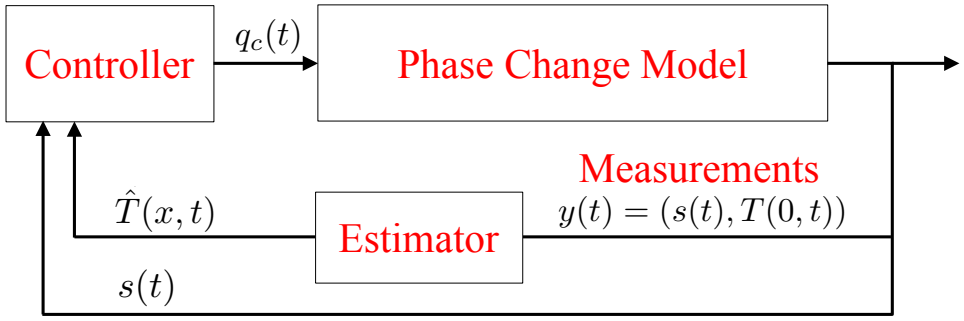

Figure 10.2: Block diagram of the observer-based output feedback control. The interface position $s(t)$ and the surface temperature $T(0,t)$ are available as two measurements.

PDE observer and output feedback design

Suppose that we have the following two measurements:

$$y^{(1)}(t) = s(t), \tag{10.18}$$

$$y^{(2)}(t) = T(0,t), \tag{10.19}$$

for all $t \geq 0$. The state observer for the PDE system (10.2)–(10.4) is designed by

$$\frac{\partial \hat{T}}{\partial t}(x,t) = \alpha \frac{\partial^2 \hat{T}}{\partial x^2}(x,t), \quad 0 < x < y^{(1)}(t), \tag{10.20}$$

$$-k\frac{\partial \hat{T}}{\partial x}(0,t) = q_c(t) - h(y^{(2)}(t) - T_a) + \kappa_1 (y^{(2)}(t) - \hat{T}(0,t)), \tag{10.21}$$

$$\hat{T}(y^{(1)}(t),t) = T_{\mathrm{m}}, \tag{10.22}$$

for all $t \geq 0$, where $\kappa_1 > 0$ is the observer gain tuned by the user. To study the performance of the observer, we introduce the estimation error variable $\tilde{T}(x,t)$ defined by

$$\tilde{T}(x,t) := T(x,t) - \hat{T}(x,t). \tag{10.23}$$

Subtracting the observer system (10.20)–(10.22) from the plant (10.2)–(10.5) leads to the estimation error system as follows:

$$\frac{\partial \tilde{T}}{\partial t}(x,t) = \alpha \frac{\partial^2 \tilde{T}}{\partial x^2}(x,t), \quad 0 < x < s(t), \tag{10.24}$$

$$\frac{\partial \tilde{T}}{\partial x}(0,t) = \frac{\kappa_1}{k}\tilde{T}(0,t), \tag{10.25}$$

$$\tilde{T}(s(t),t) = 0. \tag{10.26}$$

Then, the performance of the PDE observer (10.20)–(10.22) is guaranteed by the following lemma.

Lemma 15 *The estimation error system* (10.24)–(10.26) *is exponentially stable in the spatial* L_2*-norm* $||\tilde{T}|| = \sqrt{\int_0^{s(t)} \tilde{T}(x,t)^2 \mathrm{d}x}$.

In addition to the PDE observer given in (10.20)–(10.22) to estimate the temperature profile, we introduce the following observer reconstructing the interface position as a copy of (10.5) plus the measurement injection of the interface position:

$$\dot{\hat{s}}(t) = -\beta \frac{\partial \hat{T}}{\partial x}(s(t),t) - \frac{\beta}{k} q_{\mathrm{los}} + \kappa_2 (s(t) - \hat{s}(t)), \tag{10.27}$$

where $\kappa_2 > 0$ is an observer gain. The observer (10.27) is not essential to estimate the interface position since we suppose that we can accurately measure the interface position in continuous time. However, in the next section we propose the re-design of the observer under the sampled-data measurements, and the observer (10.27) is required to reconstruct the unmeasured interface position during the sampling time period. By defining $\tilde{s}(t) := s(t) - \hat{s}(t)$, the dynamics of $\tilde{s}(t)$ is given by

$$\dot{\tilde{s}}(t) = -\beta \frac{\partial \tilde{T}}{\partial x}(s(t),t) - \kappa_2 \tilde{s}(t). \tag{10.28}$$

The stability of $(\tilde{T},\tilde{s})$-system in (10.24)–(10.26), (10.28) is addressed in the following lemma.

Lemma 16 *Assume that there exists* $\bar{s}>0$ *such that* $0<s(t)<\bar{s}$ *for all* $t\geq 0$*, and* $0\leq q_{\rm los}<\frac{\alpha}{2\beta\bar{s}}$ *holds. The estimation error system* (10.24)–(10.26)*,* (10.28) *is exponentially stable in the norm* $\tilde{\Phi}(t):=||\tilde{T}||^2+||\frac{\partial\tilde{T}}{\partial x}||^2+\tilde{s}(t)^2$.

The proof of Lemma 16 can be done by analyzing the time derivative of $\tilde{\Phi}(t)$ and applying Lyapunov's method, of which the detail is omitted here. The associated output-feedback control is given by replacing the true temperature profile in the full-state feedback control law (10.15) with the estimated temperature $\hat{T}(x,t)$ calculated by the observer (10.20)–(10.22), resulting in the following form:

$$\begin{aligned} q_{\rm c}(t) =& -c\left(\frac{k}{\alpha}\int_0^{s(t)}(\hat{T}(x,t)-T_{\rm m})\mathrm{d}x+\frac{k}{\beta}(s(t)-s_{\rm r})\right)\\ &+\frac{cq_{\rm los}s_{\rm r}^2}{2\alpha}+h(T(0,t)-T_a)+q_{\rm los}. \end{aligned} \tag{10.29}$$

Then, owing to the separation principle, it is shown that the output feedback control law stabilize the plant states $(T(x,t),s(t))$ at the desired reference $(T_{\rm r}(x),s_{\rm r})$.

Theorem 17 *Assume that* $\hat{T}(x,0)\geq T(x,0)$ *for all* $x\in[0,s_0]$*. Consider the closed-loop system consisting of the plant* (10.2)–(10.5)*, the observer* (10.20)–(10.22)*, and the output feedback control law* (10.29)*. Then, the conditions* (10.6) *and* (10.7) *for the model validity and* $\tilde{T}(x,t)\leq 0$ *hold for all* $x\in(0,s(t))$ *and for all* $t\geq 0$*, and there exists a positive constant* $q_{\rm los}^*>0$ *such that for all* $q_{\rm los}\in(0,q_{\rm los}^*)$ *the closed-loop system is exponentially stable in the sense of the norm* $||T-T_{\rm r}||^2+(s(t)-s_{\rm r})^2+||\tilde{T}||^2$.

The proof of Theorem 17 is also presented at the end of this chapter.

ODE observer derived from discretized PDE

To implement the designed observer via numerical computation, we derive the spatially discretized model of (10.2)–(10.5). Let $N \in \mathcal{N}$ be the number of grids for the spatial discretization, Δx be the width defined by $\Delta x = \frac{1}{N}$, and $\phi^{(i)}(t)$ be defined by

$$\phi^{(i)}(t) = T\left(i\Delta x s(t), t\right) - T_{\mathrm{m}}, \quad i = 0, 1, 2, \cdots, N, \tag{10.30}$$

$$\phi(t) = [\phi^{(1)}(t), \phi^{(2)}(t), \phi^{(3)}(t), \cdots, \phi^{(N)}(t)]^T. \tag{10.31}$$

Note that taking the total time derivative of (10.30) yields

$$\dot{\phi}^{(i)}(t) = \left(\frac{\partial T}{\partial t} + i\Delta x \dot{s}(t) \frac{\partial T}{\partial x} \right) \Bigg|_{x = i\Delta x s(t)} \tag{10.32}$$

Then, the spatially discretized model of (10.2)–(10.5) is governed by the following coupled nonlinear ODEs of the states $\phi(t)$ and $s(t)$:

$$\dot{\phi}^{(0)}(t) = a(s(t))\phi^{(0)}(t) + p(s(t))\phi(t) + b(s(t))\bar{q}_{\mathrm{c}}(t), \tag{10.33}$$

$$\dot{\phi}(t) = q(s(t))\phi^{(0)}(t) + R(s(t))\phi(t) + f(\phi(t), s(t)), \tag{10.34}$$

$$\dot{s}(t) = g(s(t))\phi(t) - \frac{\beta}{k} q_{\mathrm{los}}, \tag{10.35}$$

where $\bar{q}_{\mathrm{c}}(t) := q_{\mathrm{c}}(t) - h(\phi^{(0)}(t) + T_{\mathrm{m}} - T_{\mathrm{a}})$, and

$$a(s(t)) = -\frac{2\alpha}{(s(t)\Delta x)^2}, \tag{10.36}$$

$$b(s(t)) = \frac{4\alpha}{ks(t)\Delta x}, \tag{10.37}$$

$$p(s(t)) = \frac{2\alpha}{(s(t)\Delta x)^2}\begin{bmatrix} 1 & 0_{1,N-1} \end{bmatrix}, \tag{10.38}$$

$$q(s(t)) = \frac{\alpha}{(s(t)\Delta x)^2}\begin{bmatrix} 1 & 0_{1,N-1} \end{bmatrix}, \tag{10.39}$$

$$g(s(t)) = -\frac{\beta}{2s(t)\Delta x}\begin{bmatrix} 0_{1,N-3} & 1 & -4 \end{bmatrix}, \tag{10.40}$$

$0_{i,j} \in \mathbb{R}^{i\times j}$ denotes a matrix in which all the elements are zero, and $R(s(t)) \in \mathbb{R}^{N-1\times N-1}$ has its elements $r_{i,j}$ at i-th row and j-th column given by

$$r_{i,i} = -\frac{2\alpha}{(s(t)\Delta x)^2}, \quad \forall i = 1,2,\cdots,N-1 \tag{10.41}$$

$$r_{i+1,i} = r_{i,i+1} = \frac{\alpha}{(s(t)\Delta x)^2}, \quad \forall i = 1,2,\cdots,N-1, \tag{10.42}$$

and all other elements are zero. The function $f(\phi(t), s(t))$ is a nonlinear function of the dynamics derived from the last term in (10.32), which has its i-th element

$$f_i = i\Delta x\left(g(s(t))\phi(t) - \frac{\beta}{k}q_{\mathrm{los}}\right)\frac{\phi^{(i+1)} - \phi^{(i-1)}}{2\Delta x s(t)}. \tag{10.43}$$

Hence, by defining the state vector $\psi \in \mathbb{R}^{N+1}$

$$\psi = \begin{bmatrix} \phi^{(0)} & \phi & s \end{bmatrix}^T \tag{10.44}$$

the coupled dynamics (10.33)–(10.35) can be described by the following ODE on the state ψ:

$$\dot{\psi} = A(s)\psi + B(s)\bar{q}_{\mathrm{c}} + F(\psi) + \theta, \tag{10.45}$$

where

$$A(s) = \begin{bmatrix} a(s) & p(s) & 0 \\ q(s) & R(s) & 0 \\ 0 & g(s) & 0 \end{bmatrix}, \tag{10.46}$$

$$B(s) = \begin{bmatrix} b(s) & 0_{1,N-1} & 0 \end{bmatrix}^T, \tag{10.47}$$

$$F(\psi) = \begin{bmatrix} 0 & f(\phi, s) & 0 \end{bmatrix}^T, \tag{10.48}$$

$$\theta = \begin{bmatrix} 0 & 0_{1,N-1} & -\frac{\beta}{k} q_{\text{los}} \end{bmatrix}^T. \tag{10.49}$$

Let $y \in \mathbb{R}^2$ be the vector associated with the measurements (10.18) and (10.19) defined by

$$y = \begin{bmatrix} y^{(1)} & y^{(2)} \end{bmatrix}^T. \tag{10.50}$$

The measurement vector is described by

$$y = C\psi + d, \tag{10.51}$$

where

$$C = \begin{bmatrix} 0 & 0_{1,N-1} & 1 \\ 1 & 0_{1,N-1} & 0 \end{bmatrix}, \tag{10.52}$$

$$d = \begin{bmatrix} 0 & T_{\text{m}} \end{bmatrix}^T. \tag{10.53}$$

Following the same procedure, the continuous-time PDE observer designed in (10.24)–(10.26) is implemented by the following ODE observer:

$$\dot{\hat{\psi}} = A(y^{(1)})\hat{\psi} + B(y^{(1)})\bar{q}_c + F(\hat{\psi}) + \theta + K(y - \hat{y}) \tag{10.54}$$

where $\hat{y} = C\hat{\psi} + d$, and $K \in \mathbb{R}^{N+2,2}$ is defined by

$$K = \begin{bmatrix} 0 & b(s)\kappa_1 \\ 0_{N-1,1} & 0_{N-1,1} \\ \kappa_2 & 0 \end{bmatrix}. \tag{10.55}$$

Sampled-data design of ODE observer and output feedback

The measured data are obtained not continuously in time but at each sampling time $\{t_j : j = 0, 1, 2, \cdots\}$. Here, we consider the sampling scheduling as periodic sampling with period τ, which leads to the sequence of the sampling time as

$$t_j = t_0 + j\tau, \quad j = 1, 2, \cdots \tag{10.56}$$

Hence, the sampled-data measurements are obtained by

$$y^{(1)}(t_j) = s(t_j), \tag{10.57}$$

$$y^{(2)}(t_j) = T(0, t_j). \tag{10.58}$$

We employ the methods proposed in [69], namely, we introduce the so-called "Inter-Sample-Predictor" (ISP) which serves as an estimate of the measured variables during the sampling periods given the measurements at each sampling time as an initial state, and compute the continuous-time observer coupled with ISP as an estimate of the state variables.

Let $w^{(1)}(t)$ and $w^{(2)}(t)$ be the ISP states reconstructing $y^{(1)}(t) = s(t)$ and $y^{(2)}(t) = T(0,t)$, respectively. At every sampling time $t = t_j$, we set

$$w^{(1)}(t_j) = y^{(1)}(t_j), \quad w^{(2)}(t_j) = y^{(2)}(t_j), \tag{10.59}$$

For $t \in [t_j, t_{j+1})$, by referring to (10.33) and (10.35), the dynamics of ISP is given by

$$\dot{w}^{(1)}(t) = g(\hat{s}(t))\hat{\phi}(t) - \frac{\beta}{k} q_{\mathrm{los}}, \tag{10.60}$$

$$\dot{w}^{(2)}(t) = a(\hat{s}(t))\hat{\phi}^{(0)}(t) + p(\hat{s}(t))\hat{\phi}(t) + b(\hat{s}(t))\bar{q}_{\mathrm{c}}(t). \tag{10.61}$$

The dynamics of the continuous-time observer state $\hat{\psi}$ is given by the copy of the observer (10.54) with replacing the measurement states by ISP states as follows:

$$\dot{\hat{\psi}} = A(w^{(1)})\hat{\psi} + B(w^{(1)})\bar{q}_{\mathrm{c}} + F(\hat{\psi}) + \theta + K(w - \hat{y}) \tag{10.62}$$

where $w = \begin{bmatrix} w^{(1)} & w^{(2)} \end{bmatrix}^T$. Furthermore, the states $w^{(1)}, w^{(2)}, \hat{\psi}$ are discretized in time with the time step Δt, and ODEs (10.60)–(10.62) are computed numerically by forward Euler method, which leads to Algorithm 1 providing ISP-based sampled-data observer at each sampling time. Using the sampled-data observer states, the associated output feedback control law given in (10.29) under the availability of the continuous-time PDE observer is re-designed by

$$\begin{aligned} q_{\mathrm{c}}(t_j) = &- c\frac{k y^{(1)}(t_j)}{\alpha N}\left(\frac{1}{2}(y^{(2)}(t_j) - T_{\mathrm{m}}) + \sum_{i=2}^{N}\hat{\phi}^{(i)}(t_j)\right) + c\frac{k\varepsilon s_{\mathrm{r}}^2}{2\alpha} - c\frac{k}{\beta}(y^{(1)}(t_j) - s_{\mathrm{r}}) \\ &+ h(y^{(2)}(t_j) - T_a) + q_{\mathrm{los}}, \end{aligned} \tag{10.63}$$

where we use trapezoidal rule for approximating the spatial integration.

Algorithm 6: ISP-based sampled-data observer at sampling time t_j for $j \in \{0,1,\cdots\}$

Input : $y^{(1)}(t_j), y^{(2)}(t_j), \hat{\psi}_{j\tau}$;
$w_{j\tau}^{(1)} \leftarrow y^{(1)}(t_j)$; $w_{j\tau}^{(2)} \leftarrow y^{(2)}(t_j)$;
for $l = 0,1,\cdots,I$, **do**
$i \leftarrow j\tau + l$;
$\hat{y}_i \leftarrow C\hat{\psi}_i + d$;
$w_{i+1}^{(1)} \leftarrow w_i^{(1)} + \Delta t \left(g(\hat{s}_i)\hat{\phi}_i - \frac{\beta}{k} q_{\mathrm{los}} \right)$;
$w_{i+1}^{(2)} \leftarrow w_i^{(2)} + \Delta t \left(a(\hat{s}_i)\hat{\phi}_i^{(0)} + p(\hat{s}_i)\hat{\phi}_i + b(\hat{s}_i)\bar{q}_{\mathrm{c},i} \right)$;
$\hat{\psi}_{i+1} \leftarrow \hat{\psi}_i + \Delta t (A(w_i^{(1)})\hat{\psi}_i + B(w_i^{(1)})\bar{q}_{\mathrm{c},i} + F(\hat{\psi}_i) + \theta + K(w_i - \hat{y}_i))$;
end for
Output : $\hat{\psi}_{(j+1)\tau}$

10.4 Experimental Setup and Calibration of Unknown Parameters

This section presents the experimental setup and the results under a constant heat input to validate the sampled-data observer in Algorithm 1.

Sample preparation and heating chamber

PCM-37 (Microtek laboratories, inc. Dayton, OH, USA) is chosen as the phase change material for our experiment. Its melting temperature is 37 [°C]. Thermal properties of PCM-37 are summarized in Table.1. Cylindrical rod is prepared by casting of molten PCM-37 with an acrylic container with 63.5[mm] diameter and a flat bottom. Molten PCM-37 is poured through a paper filter to remove particles and casting can be done by keeping container in a room temperature for 12 hours. The rod of PCM-37 is pushed out from the mold once it becomes solid, then inserted into another acrylic chamber for a heating experiment.

Fig. 10.3 illustrates a structure of the chamber to heat the cast rod from top side. Our experiments show this configuration has least influence of convection. A removable lid on top

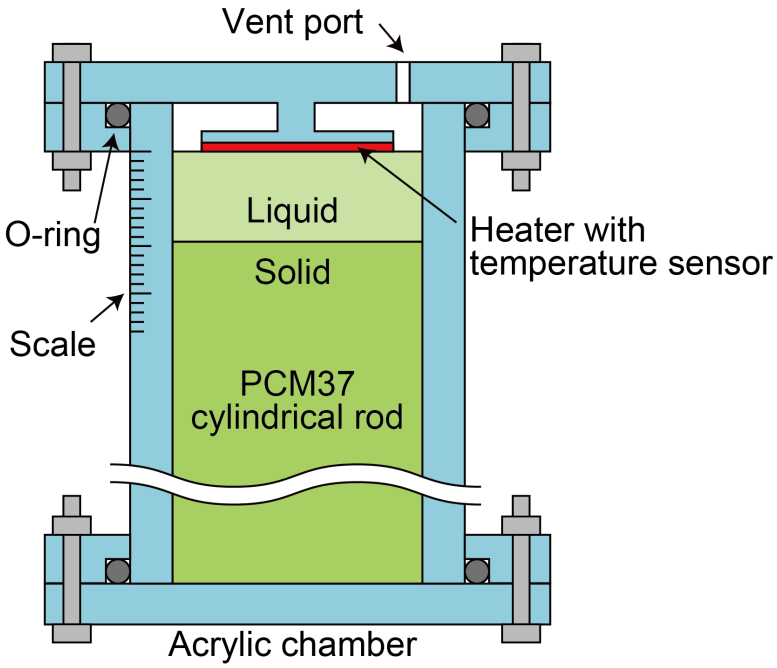

(a) Schematic of the apparatus for melting paraffin.

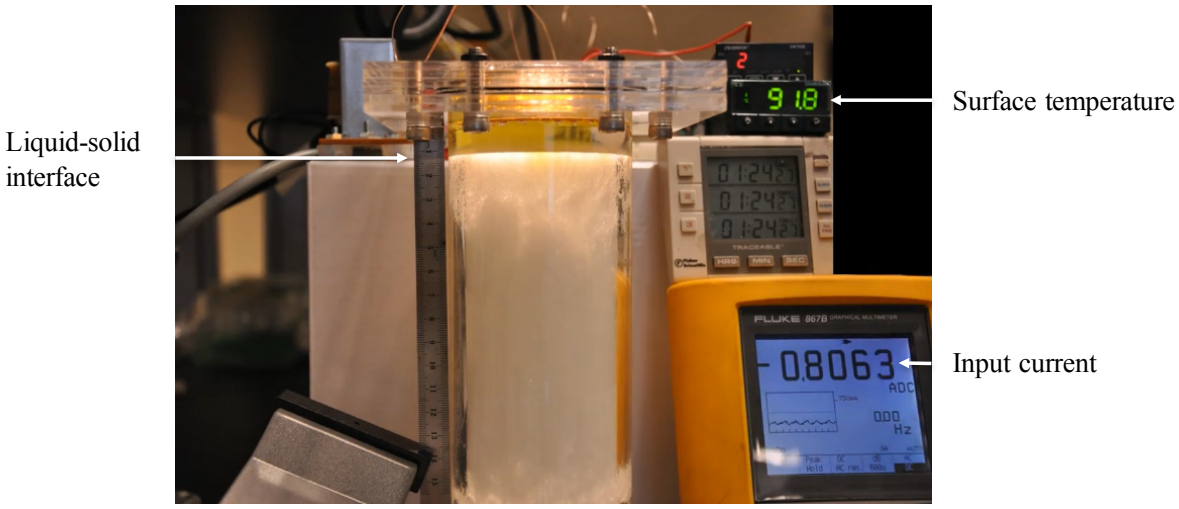

(b) The real experiment of melting paraffin with sensors and an actuator.

Figure 10.3: The images of the experimental apparatus and setup using PCM-37.

of chamber has a heater and thermocouple sensor and the PCM-37 rods are inserted so that it contacts with the heater firmly. The space above the heater is prepared for thermal insulation

Table 10.1: Thermophysical parameters of PCM-37.

Description	**Symbol**	**Value**
Density	ρ	$790\ \mathrm{kg}\cdot\mathrm{m}^{-3}$
Latent heat of fusion	ΔH^*	$210\ \mathrm{J}\cdot\mathrm{g}^{-1}$
Heat capacity	c_p	$2.38\ \mathrm{J}\cdot\mathrm{g}^{-1}\cdot\mathrm{K}^{-1}$
Melting temperature	T_m	$37\ ^\circ\mathrm{C}$
Thermal conductivity	k	$0.22\ \mathrm{W}\cdot\mathrm{m}^{-1}$

and avoids an accumulation of small bubbles on the heater, which are generated when PCM-37 is melted. Due to the transparency change of PCM-37 upon a phase change, the position of the boundary is measured by using a digital camera with interval shuttering.

Experiment under a constant input

The boundary heat actuator $q_\mathrm{c}(t)$ is controlled by an electric current $i_\mathrm{c}(t)$ connected with the film heater under the following relation:

$$i_c(t) \sim \sqrt{\frac{q_c(t)\pi R^2}{R_{es}}}, \tag{10.64}$$

where R is the radius of the cylinder, and R_{es} is the resistance of the film heater at room temperature. In this experiment, we had $R = 3.175$ [cm] and $R_{es} = 13.9$ [Ω]. Due to the limitation of the equipment, the electric current is bounded by the constant i_max, i.e.,

$$0 \leq i_c(t) \leq i_\mathrm{max}. \tag{10.65}$$

We conducted an open-loop melting test by keeping the current input at the maximum value $i_\mathrm{max} = 0.79$ [A] for 2 hours after the phase interface reaches 0.5 [cm]. Then, we observed that the phase interface position was evolving *uniformly* along the vertical coordinate of the cylinder, which validates Assumption 24. The image of the experiment is shown in Fig. 10.3 (b).

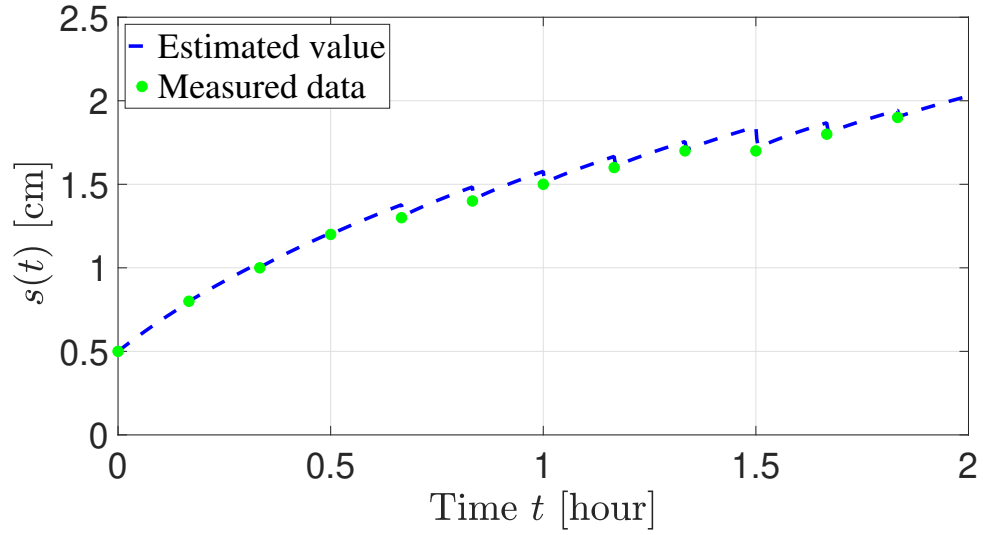

(a) The interface position.

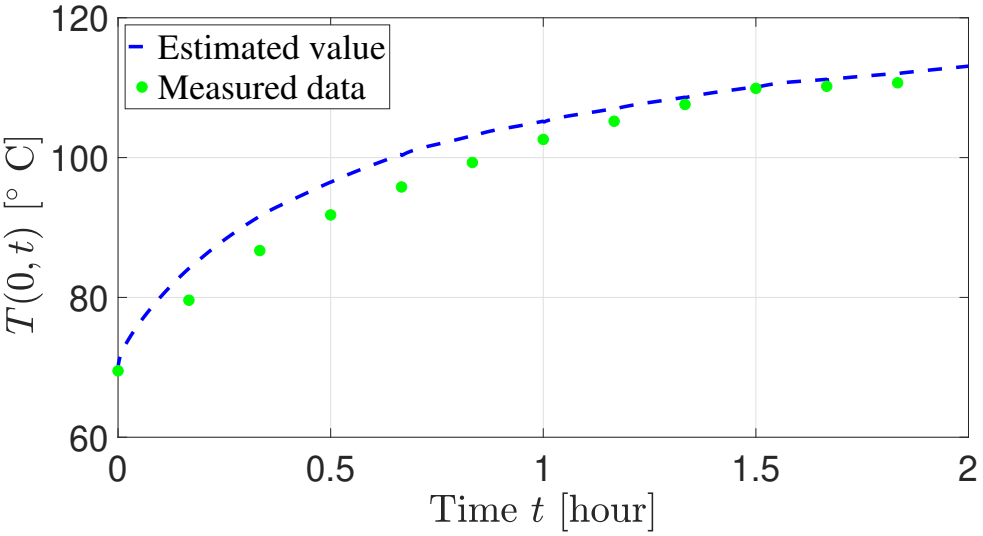

(b) The surface temperature.

Figure 10.4: The estimated values (blue dash) with h =20 [W/m^{2}K] and q_{los} =400 [W/m^2], which have good agreement with the measured data (green dots) and satisfy (10.68)

Calibration of unknown parameters

Let t_0 be the time we observe that $s(t_0) = 0.5$ [cm], and fix as $t_0 = 0$. Let t_f = 2 [hours] be the process time. We measured the phase boundary position and the surface temperature at every

10 [min] as a sampling time period, namely, the sampling scheduling is described as $t_j = t_0 + j\tau$ for $j = 1, 2, \cdots m$ with $\tau = 10$ [min] and $m = t_f/\tau = 12$. Let e be the normalized estimation error vector defined by

$$e = \left[e_0^{(1)}, e_1^{(1)}, \cdots, e_m^{(1)}, e_0^{(2)}, e_1^{(2)}, \cdots, e_m^{(2)} \right], \tag{10.66}$$

where

$$e_j^{(i)} = \frac{y^{(i)}(t_j) - \hat{y}^{(i)}(t_j)}{y^{(i)}(t_j)}, \quad i = 1, 2, \quad j = 0, 1, \cdots, m. \tag{10.67}$$

Using the measured data, the heat transfer coefficient h and the freezing heat from the solid phase q_{los} are calibrated to minimize the estimation error. However, for the sake of sustaining the robustness of the control algorithm, the estimated temperature profile should be higher than the true temperature profile, for the condition shown in Theorem 17 holds. Since both the measured surface temperature and the measured interface position are monotonically increasing as the temperature profile gets larger, both the estimated surface temperature and interface position should be higher than the measured values. Taking these into account, the unknown parameters are calibrated so that

$$\min_{h, q_{\text{los}}} e^T e, \quad \text{subject to } e \succeq 0, \tag{10.68}$$

where $\succeq$ denotes an element-wise inequality.

We varied the parameters in a range $0 \leq h \leq 30$ and $0 \leq q_{\text{los}} \leq 500$ with the step sizes $\Delta h = 1$ and $\Delta q_{\text{los}} = 20$, respectively. Then, we observed that the problem (10.68) is achieved with the parameters h =20 [W/m^{2}K] and q_{los} =400 [W/m^2]. Fig. 10.4 shows the comparison of the measured data with the estimated values of the interface position and the surface temperature under the obtained parameters. We can observe that the estimated values have good agreement

with the measured data and satisfy the constraint (10.68). A reference value of the convective heat transfer coefficient h for plastic is reported in [31] as $h = 21 \pm 2$[W/m^{2}K], which also shows a good agreement with the identified value.

10.5 Experiment of Closed-Loop Control

In this section, we present our main result on experimental validation of the proposed feedback control algorithm. The paraffin was completely solidified at the initial time of the experiment.

Gain tuning

The control gain $c > 0$ is an essential free parameter for the input current $i_{\rm c}(t)$ to satisfy the constraint (10.65). Here we provide how to tune the gain. First, the current input is kept as $i_{\max}$ while the paraffin starts to be molten from the top and the liquid-solid interface position is less than $s_0 := 0.5$ [cm] from the top. At the time when the interface position reaches to s_0, we measured the surface temperature $y^{(2)}(t_0)$, and compute

$$\tilde{E}_0 = \frac{k s_0}{2\alpha}(y^{(2)}(t_0) - T_{\rm m}) - \frac{q_{\rm los} s_{\rm r}^2}{2\alpha} + \frac{k}{\beta}(s_0 - s_{\rm r}), \tag{10.69}$$

$$c_{\max} = \frac{\frac{R_{es} i_{\max}^2}{\pi R^2} - h(y^{(2)}(t_0) - T_a) - q_{\rm los}}{-\tilde{E}_0}. \tag{10.70}$$

Then, at least we require $c < c_{\max}$, since the input becomes $i_{\rm c}(t_0) = i_{\max}$ when $c = c_{\max}$ by (10.63) and (10.64). Moreover, from the results in Section 4.4, for the sampled-data state feedback control of the Stefan problem, given a sampling time period $\tau > 0$, the control gain needs to be chosen to satisfy $c < \frac{1}{\tau}$ to ensure the conditions of model validity and the closed-loop stability. Considering

these two conditions, we take the gain tuning as

$$c = \delta \min \left\{ c_{\max}, \frac{1}{\tau} \right\}, \tag{10.71}$$

where $\delta \in (0,1)$ is a free parameter. In this experiment, we used δ =0.8.

Proposed control law

The control algorithm in the experiment is explained as follows.

1. The input current $i_{\mathrm{c}}(t)$ is injected at the maximum value $i_{\max}$ (0.79 [A]).
2. Once we observe that the liquid-solid interface arrives at 0.5 [cm], the surface temperature is measured and only the observer is computed by Algorithm 1 with keeping the maximum input current.
3. After that, at every sampling time 10 [min], both the surface temperature and the interface position are measured, and the observer is computed by Algorithm 1 and the heat controller is obtained by (10.63).
4. Given the value of the controller, the current input is given by (10.64). We repeat 3) and 4) for 5 hours.

Experimental results

We conducted the experiment of melting paraffin by implementing the control algorithm above. The setpoint position is chosen as $s_{\mathrm{r}} = 2$ [cm], and the time step size in the observer is $\Delta t = 0.05$ [sec]. Fig. 10.5 depicts the results of the experiment by showing measured data of the phase interface position, Fig. 10.6 shows the input current and the surface temperature,

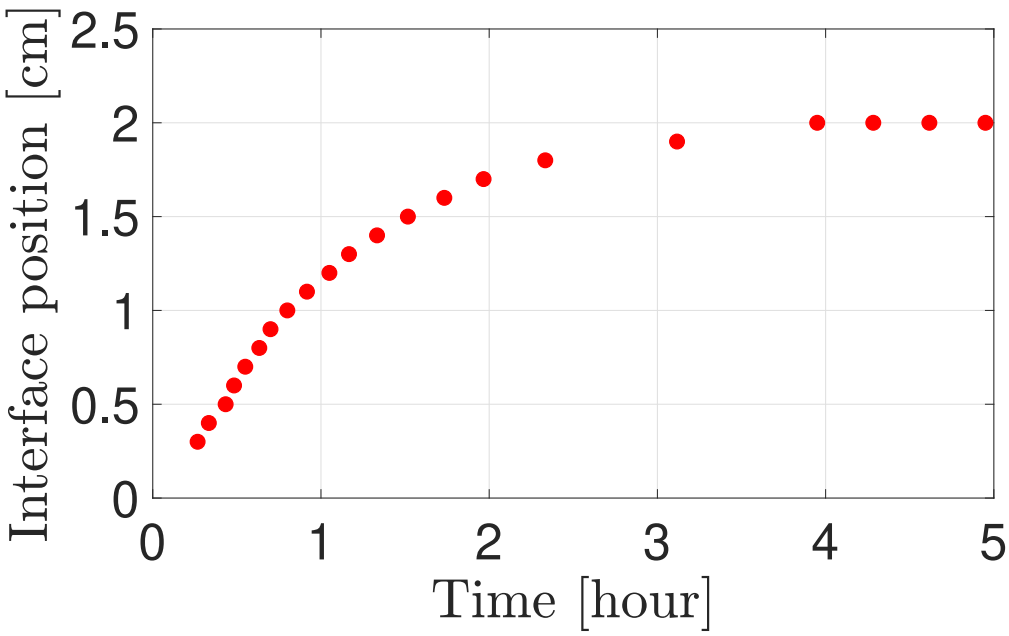

(a) The plot is depicted at every 0.1(cm) increase until the interface reaches 2(cm) and after that depicted at every 20(min).

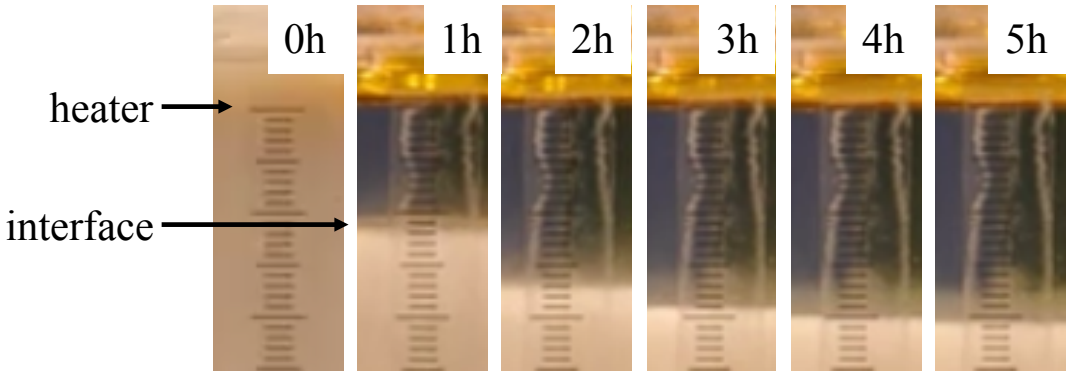

(b) The snapshots of the melting paraffin at every hour is given right, which shows the interface evolution by a ruler attached on the acrylic chamber.

Figure 10.5: The experimental result of the time evolution of the interface position under the proposed feedback control algorithm. The experiment was successful: the liquid-solid interface position converged to the setpoint position $s_r = 2$(cm).

and Fig. 10.7 depicts the estimated temperature profiles of the liquid paraffin and the measured temperature profile of the acrylic chamber obtained by IR camera, respectively.

From Fig. 10.5 (a), we can observe that the experiment was success: the phase interface position reached to the value $s_0 = 0.5$ [cm] at $t_0 = 25$ [min] and converged to the chosen setpoint

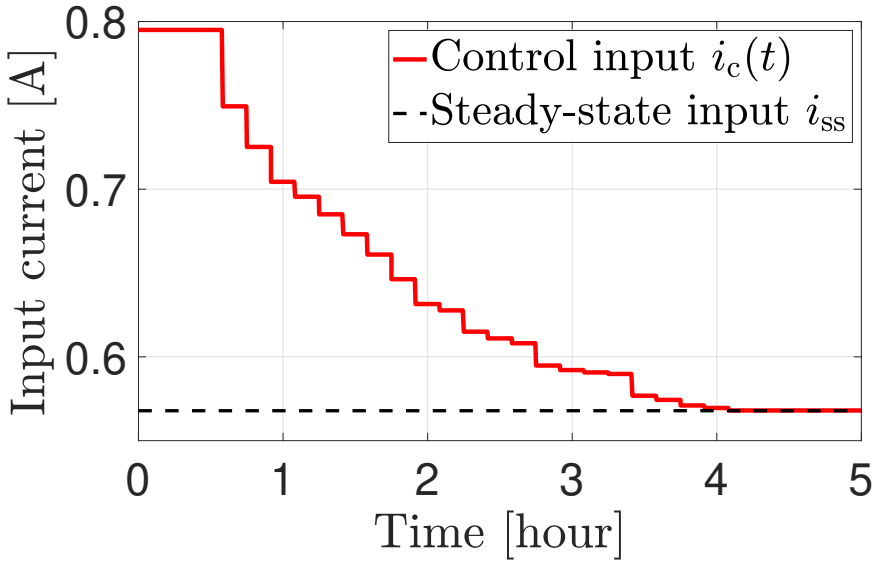

(a) The input current started from the maximum value i_{max} of the input constraint, and the feedback control was implemented from 35(min). After 4 hours, the current input stayed at the steady-state input calculated by (10.9).

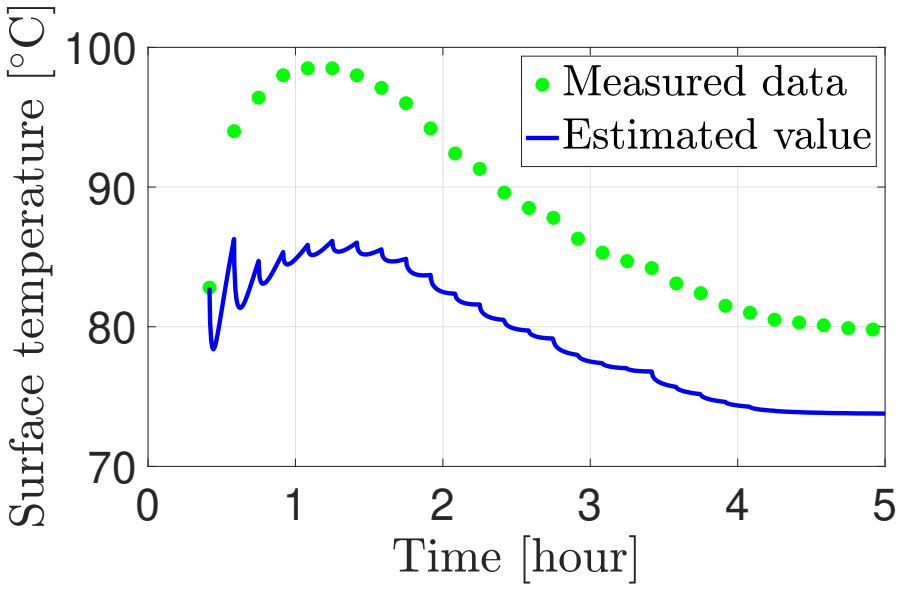

(b) The estimated surface temperature has a similar behavior to the measured surface temperature together with a nominal error around $5-10(^{\circ}\mathrm{C})$.

Figure 10.6: The experimental result of the proposed feedback control algorithm and the surface temperature.

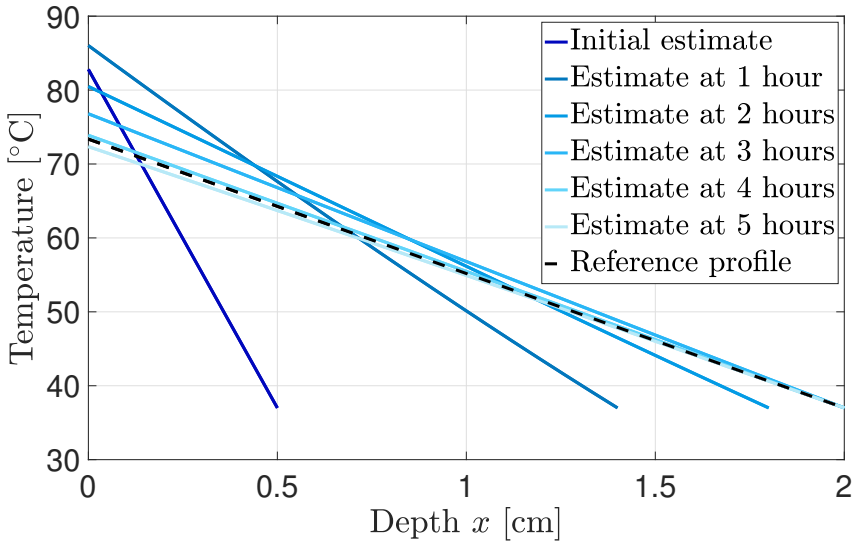

(a) The estimated temperature profile of the liquid paraffin at every hour. The profile gradually converged to the reference profile given by (10.8) and almost corresponded to the reference after 4 hours.

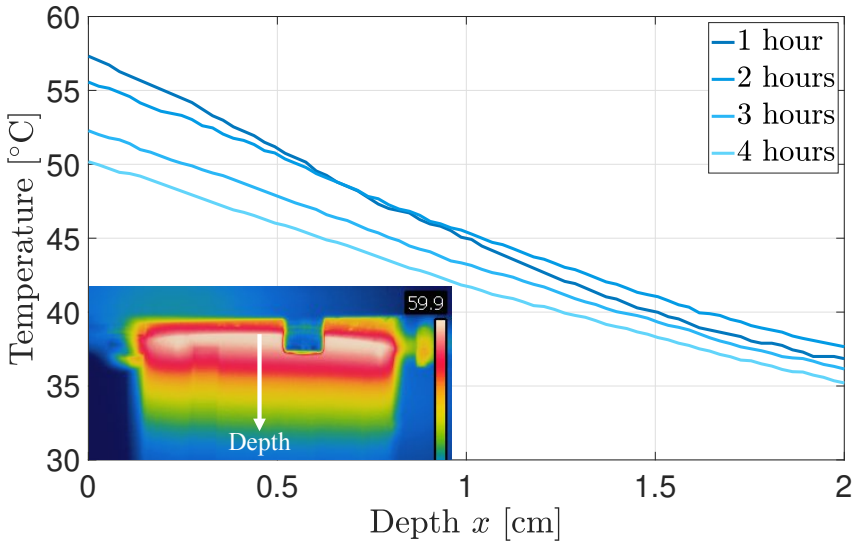

(b) The measured temperature profile of the acrylic chamber obtained by IR camera at every hour. The profile is given along the white arrow in the thermography.

Figure 10.7: The time evolution of the estimated temperature profile and the measured temperature profile of the cylinder by IR camera.

position $s_{\mathrm{r}} = 2$ [cm] asymptotically and stays at the setpoint after 4 hours. This result can be also visually seen in 10.5 (b) which are snapshots of the melting paraffin at every hour. A ruler

attached on the acrylic chamber shows the distance from the position of the heat actuator, which gives the measured value of the phase interface position depicted in the left plot, and hence the convergence of the interface position is visually observed. Fig. 10.6 (a) shows that the input current starts from the maximum value $i_{\max} = 0.79$[A] under the constraint and the feedback control is implemented at every sampling time 10 [min] from $t = 35$ [min] which is 10 [min] after $t_0 = 25$ [min]. After 4 hours, the current input stays at the steady-state input calculated by (10.9) and (10.64). From 10.6 (b), we can observe that the estimated surface temperature has similar behavior to the measured surface temperature together with a nominal error around $5-10$ [°C], of which the cause is discussed later. Fig. 10.7 (a) illustrates that the estimated temperature profile converges to the reference profile given by (10.8) and almost corresponds to the reference after 4 hours. The thermography included in Fig. 10.7 (b) is obtained by IR camera taken at $t = 2$ hours, which illustrates that the temperature is the highest (white color) at the position of the heat controller and is monotonically decreasing as the vertical position goes towards the bottom. The temperature profiles of the acrylic in the plot are given by referring to the temperature along the white arrow in the thermography. We observe that the profiles are almost linearly distributed in the space at every hour, of which the property is also observed in the estimated temperature profiles of the liquid paraffin shown in Fig. 10.7 (a), though the material of the focus is distinct and the temperature value is different. Moreover, the slope of the profiles are dropped from $t = 1$ hour to $t = 2$ hours in Fig. 10.7 (b), which is also similarly observed in Fig. 10.7 (a). Thus, while it is not accurate to refer to the thermography of the acrylic chamber as a temperature profile of the paraffin inside, we see some similar behavior of the evolution of the temperature profiles.

Discussion

While we observe that the control objective is successfully achieved in the experiment, the temperature estimation accompanies a nominal error from the measured value as illustrated in Fig. 10.6 (b). Since the estimated surface temperature is lower than the measured one, the

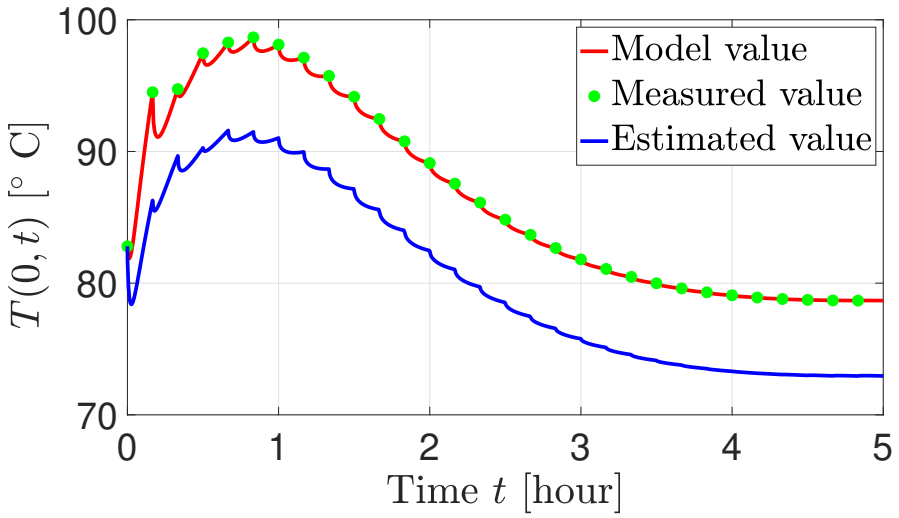

Figure 10.8: Simulation of the closed-loop system with setting h =16 [W/m^{2}K] in the model while h =20 [W/m^{2}K] in the observer. The plot is similar to Fig. 10.6 (b), by which we conjecture that the estimation error of the surface temperature in Fig. 10.6 (b) is caused by the parameter error of h.

incorporated heat loss in the observer is higher than the true heat loss in paraffin during the closed-loop experiment. This might be caused by over-estimating the calibrated heat transfer coefficient h. To investigate the validity, the numerical simulation of the closed-loop system of the model (10.45), the measurement (10.50), the observer in Algorithm 1, and the output feedback control law (10.63) is studied, where the heat transfer coefficient in the observer is set as h =20 [W/m^{2}K] while the one in the model is set as h =16 [W/m^{2}K]. Fig. 10.8 depicts the evolution of the measured surface temperature (green dots) at every sampling time and the estimated surface temperature (blue line), respectively. We observe that the plot in Fig. 10.8 is in good agreement with Fig. 10.6 (b), which leads us to conjecture that the cause of the estimation error lies in the parametric error of the calibrated heat loss h. Nevertheless, the control's performance was robust as we see in Fig. 10.5.

10.6 Proof of Theoretical Results

Hereafter we define

$$\varepsilon = \frac{q_{\rm los}}{k}. \tag{10.72}$$

Proof of Theorem 16

Guaranteeing conditions of model validity

First, we prove the following lemma to guarantee the conditions of model validity.

Lemma 17 *Under Assumption 26, consider the closed-loop system consisting of the plant* (10.2)–(10.5) *with the control law* (10.15)*. Then, the following properties hold for all* $t \geq 0$*:*

$$T(x,t) > T_{\rm m}, \quad \forall x \in (0, s(t)), \tag{10.73}$$

$$\frac{\partial T}{\partial x}(s(t),t) < 0, \tag{10.74}$$

$$q_c(t) > q_{\rm los}, \tag{10.75}$$

$$0 < s(t) < \bar{s} := s_{\rm r} + \frac{\beta\varepsilon s_{\rm r}^2}{2\alpha}. \tag{10.76}$$

Proof:

The proof of Lemma 17 is established by analysis of the energy and the use of maximum principle. Substituting the control law (10.15) to the conservation law (10.11) with respect to $\tilde{E}(t)$ defined by (10.13) leads to

$$\dot{\tilde{E}}(t) = -c\tilde{E}(t). \tag{10.77}$$

The explicit solution to (10.77) is given by $\tilde{E}(t) = \tilde{E}(0)e^{-ct}$. Since Assumption 26 leads to $\tilde{E}(0) < 0$, we have

$$\tilde{E}(t) < 0. \tag{10.78}$$

Then, clearly (10.14) leads to $q_c(t) - h(T(0,t) - T_a) > 0$ for all $t \geq 0$. With the help of this inequality, we can apply the theorem in [140] (page 3) to the governing equations (10.2)–(10.5), and thereby for any $\bar{t} \leq \sigma$ where $0 < \sigma \leq \infty$, there is a unique solution of the system (10.2)–(10.5) with satisfying the properties (10.73) and $0 < s(t) < L$ for all $t \in (0,\bar{t})$, and if $\sigma \neq \infty$ then $s(\sigma) = 0$ or $s(\sigma) = L$. However, by (10.11), (10.14), and (10.78) with the help of $E(0) > 0$, we obtain $E(t) > 0$, which at least ensures that $s(\sigma) \neq 0$. In addition, by (10.78), we have

$$\frac{\beta}{\alpha}\int_0^{s(t)} (T(x,t) - T_{\mathrm{m}})\mathrm{d}x < -s(t) + s_{\mathrm{r}} + \frac{\beta\varepsilon s_{\mathrm{r}}^2}{2\alpha}. \tag{10.79}$$

for all $t \in (0,\bar{t})$. Applying (10.73) to (10.79) with the help of Assumption 26 yields (10.76) for all $t \in (0,\bar{t})$. Thus, we also derive $s(\sigma) \neq L$. Therefore, $\sigma = \infty$, and the properties (10.73), (10.74), and (10.76) hold for all $t \geq 0$. Finally, applying (10.78) and (10.73) to (10.14) leads to (10.75), from which we additionally have the following property

$$|s(t) - s_{\mathrm{r}}| \leq M := \max\left\{\frac{\beta\varepsilon s_{\mathrm{r}}^2}{2\alpha}, s_{\mathrm{r}}\right\}. \tag{10.80}$$

Backstepping transformation

Next, we define the reference error states (u,X) as

$$u(x,t) = T(x,t) - T_r(x), \quad X(t) = s(t) - s_{\mathrm{r}}. \tag{10.81}$$

Then, rewriting the system's dynamics (10.2)–(10.5) with respect to (u,X) leads to the following reference error system:

$$\frac{\partial u}{\partial t}(x,t) = \alpha \frac{\partial^2 u}{\partial x^2}(x,t), \quad 0 < x < s(t), \tag{10.82}$$

$$\frac{\partial u}{\partial x}(0,t) = -\tilde{q}_c(t)/k, \tag{10.83}$$

$$u(s(t),t) = \varepsilon X(t), \tag{10.84}$$

$$\dot{X}(t) = -\beta \frac{\partial u}{\partial x}(s(t),t), \tag{10.85}$$

where

$$\tilde{q}_{\mathrm{c}}(t) := q_c(t) - h(T(0,t) - T_a) - q_{\mathrm{los}} = -c\tilde{E}(t). \tag{10.86}$$

Referring to the procedure in Chapter 2, we introduce the following backstepping transformation:

$$w(x,t) = u(x,t) - \frac{\beta}{\alpha}\int_x^{s(t)} \phi(x-y)u(y,t)dy - \phi(x-s(t))X(t), \tag{10.87}$$

where the gain kernel function ϕ is given by

$$\phi(x) = \frac{c}{\beta}x. \tag{10.88}$$

We derive the transformed (w,X)-system. Taking the time and spatial derivatives of (10.87) together with the solution of (10.82)–(10.85), and substituting he control law (10.15), the target

(w,X)-system is derived as follows:

$$\frac{\partial w}{\partial t}(x,t) = \alpha \frac{\partial^2 w}{\partial x^2}(x,t) - c\varepsilon X(t) - \dot{s}(t)\left(\frac{c}{\alpha}(x-s(t))\varepsilon - \frac{c}{\beta}\right)X(t), \tag{10.89}$$

$$\frac{\partial w}{\partial x}(0,t) = -\frac{c\varepsilon}{2\alpha}X(t)^2, \tag{10.90}$$

$$w(s(t),t) = \varepsilon X(t), \tag{10.91}$$

$$\dot{X}(t) = -cX(t) - \beta \frac{\partial w}{\partial x}(s(t),t). \tag{10.92}$$

Stability analysis

We prove the stability of (w,X)-system governed by (10.89)–(10.92) using Lyapunov's method. Let V be the Lyapunov function defined by

$$V = \frac{1}{2\alpha}||w||^2 + \frac{\varepsilon}{2\beta}X(t)^2. \tag{10.93}$$

Note that Poincare's and Agmon's inequalities for the system (10.89)–(10.92) with $0 < s(t) < \bar{s}$ lead to

$$||w||^2 \leq 2\bar{s}\varepsilon^2 X(t)^2 + 4\bar{s}^2\left|\left|\frac{\partial w}{\partial x}\right|\right|^2, \tag{10.94}$$

$$w(0,t)^2 \leq 2\varepsilon^2 X(t)^2 + 4\bar{s}\left|\left|\frac{\partial w}{\partial x}\right|\right|^2. \tag{10.95}$$

Taking the time derivative of (10.93) along the solution of (10.89)–(10.92) yields

$$\begin{aligned}\dot{V} =& \frac{\dot{s}(t)}{2\alpha}w(s(t),t)^2 - \left|\left|\frac{\partial w}{\partial x}\right|\right|^2 - \frac{c\varepsilon}{\alpha}\int_0^{s(t)} w(x,t)\mathrm{d}x X(t) + \frac{c\varepsilon}{2\alpha}w(0,t)X(t)^2 \\ & - \frac{c\dot{s}(t)}{\alpha}\int_0^{s(t)} f(x)w(x,t)\mathrm{d}x X(t) - \frac{c\varepsilon}{\beta}X(t)^2,\end{aligned} \tag{10.96}$$

where $f = \frac{1}{\alpha}(x - s(t))\varepsilon - \frac{1}{\beta}$. Applying Young's inequality to the two terms in the second line of (10.96), we get

$$-\frac{c\varepsilon}{\alpha}\int_0^{s(t)} w(x,t)\mathrm{d}xX(t) \leq \frac{c\varepsilon}{2\beta}X(t)^2 + \frac{\beta c\varepsilon\bar{s}}{2\alpha^2}||w||^2, \tag{10.97}$$

$$\frac{c\varepsilon}{2\alpha}w(0,t)X(t)^2 \leq \frac{1}{8\bar{s}}w(0,t)^2 + \frac{\bar{s}c^2\varepsilon^2}{2\alpha^2}X(t)^4. \tag{10.98}$$

In addition, applying Young's and Cauchy-Schwarz inequalities to the term in third line of (10.96), we get

$$-\frac{c\dot{s}(t)}{\alpha}\int_0^{s(t)} f(x)w(x,t)\mathrm{d}xX(t) \leq \frac{c|\dot{s}(t)|}{2\alpha}\left(\frac{1}{\sqrt{\varepsilon}}||f||^2||w||^2 + \sqrt{\varepsilon}|X(t)|^2\right). \tag{10.99}$$

Applying (10.97)–(10.99), and (10.94)–(10.95) to (10.96) with the help of $|X| \leq M$ derived in (10.80) leads to the following inequality:

$$\begin{aligned}\dot{V} \leq &-\left(\frac{1}{8\bar{s}^2} - \frac{\beta c\varepsilon\bar{s}}{2\alpha^2}\right)||w||^2 - \left(\frac{c\varepsilon}{2\beta} - \frac{\varepsilon^2}{2\bar{s}} - \frac{\bar{s}c^2\varepsilon^2M^2}{2\alpha^2}\right)X(t)^2 + \frac{|\dot{s}(t)|}{2\alpha}\varepsilon^2X(t)^2 \\ &\frac{c|\dot{s}(t)|}{2\alpha}\left(\frac{1}{\sqrt{\varepsilon}}||f||^2||w||^2 + \sqrt{\varepsilon}|X(t)|^2\right).\end{aligned} \tag{10.100}$$

Noting the property (10.74), the dynamics (10.5) yields the following bound:

$$|\dot{s}(t)| \leq -\beta\frac{\partial T}{\partial x}(s(t),t) + \beta\varepsilon. \tag{10.101}$$

Let $z(t)$ be a variable defined by

$$z(t) = s(t) + 2\beta\varepsilon t. \tag{10.102}$$

The time derivative of (10.102) is given by

$$\dot{z}(t) = -\beta \frac{\partial T}{\partial x}(s(t),t) + \beta\varepsilon > 0. \tag{10.103}$$

Therefore, $|\dot{s}(t)| \leq \dot{z}(t)$ holds. Applying this inequality to (10.100), and supposing that the following inequalities hold:

$$1 > \frac{8\beta c\varepsilon \bar{s}^3}{\alpha^2}, \tag{10.104}$$

$$\frac{c}{\beta} > \frac{2\varepsilon}{\bar{s}} + \frac{2\bar{s}c^2\varepsilon M^2}{\alpha^2}, \tag{10.105}$$

we get

$$\dot{V} \leq -bV + a\dot{z}(t)V \tag{10.106}$$

where $a = \frac{c}{\alpha} \max\left\{ \frac{2\alpha}{\sqrt{\varepsilon}} \left(\frac{\varepsilon^2 \bar{s}^3}{3\alpha^2} + \frac{\bar{s}}{\beta^2} \right), \left(\frac{\beta}{\sqrt{\varepsilon}} + \frac{\beta\varepsilon}{\alpha} \right) \right\}$, $b = \min\left\{ \frac{\alpha}{8\bar{s}^2}, \frac{c}{2} \right\}$. Consider the functional W defined by

$$W = Ve^{-az(t)}. \tag{10.107}$$

Then, the time derivative is shown to satisfy

$$\dot{W} \leq (\dot{V} - a\dot{z}(t)V)e^{-az(t)} \leq -bW(t), \tag{10.108}$$

which leads to $W(t) \leq W(0)e^{-bt}$, and hence

$$\begin{aligned} V(t) \leq & e^{a(z(t)-z(0))}V(0)e^{-bt} = e^{a(s(t)-s(0))}e^{2a\beta\varepsilon t}V(0)e^{-bt} \\ \leq & e^{a\bar{s}}V(0)e^{-\frac{b}{2}t}, \end{aligned} \tag{10.109}$$

under the condition $2a\beta\varepsilon < \frac{b}{2}$, which is equivalent to

$$\frac{8\beta c}{\alpha}\max\left\{2\alpha\sqrt{\varepsilon}\left(\frac{\varepsilon^2\bar{s}^3}{3\alpha^2}+\frac{\bar{s}}{\beta^2}\right),\beta\sqrt{\varepsilon}+\frac{\beta\varepsilon^2}{\alpha}\right\} < \min\left\{\frac{\alpha}{4\bar{s}^2},c\right\}. \tag{10.110}$$

Finally, all the conditions (10.104), (10.105), (10.110) introduced in the stability proof hold for sufficiently small $\varepsilon > 0$, i.e., there exists a positive constant $\varepsilon^* > 0$ such that for all $\varepsilon \in (0,\varepsilon^*)$ the conditions hold and therefore the decay of the norm (10.109) is satisfied, from which we complete the proof of Theorem 1.

Proof of Theorem 17

Since the procedure of the proof of Theorem 17 is analogous to the proof of Theorem 16, we omit here. We show only the proof of the properties in Lemma 17. Here, the reference error of the energy (10.13) is redefined by

$$\tilde{E}(t) = \frac{k}{\alpha}\left(\int_0^{s(t)}\left(\hat{T}(x,t)-T_{\mathrm{m}}\right)\mathrm{d}x-\frac{\varepsilon s_{\mathrm{r}}^2}{2}\right)+\frac{k}{\beta}(s(t)-s_{\mathrm{r}}). \tag{10.111}$$

Taking the time derivative of (10.111) with the help of (10.20)–(10.22) and (10.29) leads to

$$\dot{\tilde{E}} = -c\tilde{E}(t)+\kappa\tilde{T}(0,t)-k\frac{\partial\tilde{T}}{\partial x}(s(t),t). \tag{10.112}$$

Applying the maximum principle and Hopf's lemma to (10.24)–(10.26) yields the following properties:

$$\tilde{T}(x,t) \leq 0, \quad \forall x \in [0,s(t)], \quad \forall t \geq 0, \tag{10.113}$$

$$\frac{\partial\tilde{T}}{\partial x}(s(t),t) \geq 0, \quad \forall t \geq 0. \tag{10.114}$$

Thus, (10.112) yields $\dot{\tilde{E}}(t) \leq -c\tilde{E}(t)$, and applying the comparison principle, one can obtain $\tilde{E}(t) \leq \tilde{E}(0)e^{-ct}$. Finally, applying the same steps from (10.78) to (10.80), we deduce that the all the properties in Lemma 17 hold under the output feedback control system. Then, using the same procedure as in the proof of Theorem 16 leads to Theorem 17.

10.7 Conclusion and Future Work

This chapter has shown the experimental validation of a boundary feedback control algorithm developed for the phase change process. The physical model is formulated by the Stefan problem governed by a parabolic PDE with a state-dependent moving boundary described by an ODE, with unknown heat losses at both the surface and the phase interface. The nominal continuous-time full-state feedback control has been presented by means of energy-shaping and the closed-loop stability is proven by applying the backstepping-based state transformation and Lyapunov method. Then, an implementable control algorithm is developed by further designing an observer-based output feedback with finite-dimensional approximation, under the sampled-data measurements of the surface temperature and the interface position. The experiment was conducted by melting the paraffin with a cylindrical shape. The unknown parameters of the heat losses are calibrated using the experimental data under a constant input. Finally, the proposed feedback control was implemented in the experiment, which provided a successful result of the convergence of the phase interface position to a priori chosen setpoint position.

This chapter has provided the first experimental result of the boundary feedback control for the phase change process modeled by the Stefan problem. Therefore, there are several potential future work of the experimental validation of the extended models such as the two-phase Stefan problem in Chapter 4, the Stefan problem under materials' convection modeled for the polymer 3D-printing in Chapter 8, and the delay-compensated control under the actuator delay in Chapter 4. Developing event-triggered control is also an interesting problem, which can be achieved

for PDE dynamics referring to [45, 46, 47] for both hyperbolic and parabolic systems using backstepping approach. Another direction is designing an adaptive control to simultaneously regulating the input and learning the unknown parameters following [146, 70].

10.8 Acknowledgement

Chapter 10, in part, is a reprint of the material as it appears in:

- S. Koga, M. Makihata, R. Chen, M. Krstic, and A.P. Pisano, "Energy Storage in Paraffin: a PDE Backstepping Experiment", *IEEE Transactions on Control Systems Technology*, under review. (Chapter 10)

The dissertation author was the primary investigators and author of this paper. The author would like to thank Mitsutoshi Makihata, Renkun Chen, and Albert P. Pisano for their collaboration.

Appendix A

Bessel Functions

Bessel function of the first kind is a solution to the following Bessel's differential equation:

$$x^2\frac{d^2y}{dx^2}+x\frac{dy}{dx}+(x^2-n^2)y=0, \tag{A.1}$$

where n is generally an arbitrary complex number but here we consider a positive integer $n\in\{1,2,\cdots\}$. A series representation of the solution $y=J_n(x)$ is described by

$$J_n(x)=\sum_{m=0}^{\infty}\frac{(-1)^m(x/2)^{n+2m}}{m!(m+n)!}. \tag{A.2}$$

Modified Bessel function of the first kind is a solution to the following modified Bessel's differential equation:

$$x^2\frac{d^2y}{dx^2}+x\frac{dy}{dx}+(x^2-n^2)y=0. \tag{A.3}$$

A series representation of the solution $y=I_n(x)$ is described by

$$I_n(x)=\sum_{m=0}^{\infty}\frac{(x/2)^{n+2m}}{m!(m+n)!}. \tag{A.4}$$

Some properties of the functions are given by

$$2nJ_n(x) = x(J_{n-1}(x) + J_{n+1}(x)), \tag{A.5}$$

$$J_n(-x) = (-1)^n J_n(x), \tag{A.6}$$

$$I_n(x) = i^{-n} J_n(ix), \quad I_n(ix) = i^n J_n(x), \tag{A.7}$$

$$2nI_n(x) = x(I_{n-1}(x) - I_{n+1}(x)), \tag{A.8}$$

$$I_n(-x) = (-1)^n I_n(x). \tag{A.9}$$

Derivatives are given by

$$\frac{d}{dx}J_n(x) = \frac{1}{2}(J_{n-1}(x) - J_{n+1}(x)) = \frac{n}{x}J_n(x) - J_{n+1}(x), \tag{A.10}$$

$$\frac{d}{dx}(x^n J_n(x)) = x^n J_{n-1}(x), \quad \frac{d}{dx}(x^{-n} J_n(x)) = -x^{-n} J_{n+1}(x), \tag{A.11}$$

$$\frac{d}{dx}I_n(x) = \frac{1}{2}(I_{n-1}(x) + I_{n+1}(x)) = \frac{n}{x}I_n(x) + I_{n+1}(x), \tag{A.12}$$

$$\frac{d}{dx}(x^n I_n(x)) = x^n I_{n-1}(x), \quad \frac{d}{dx}(x^{-n} I_n(x)) = x^{-n} I_{n+1}(x), \tag{A.13}$$

Appendix B

Some Inequalities

B.1 Cauchy-Schwarz Inequality

$$\int_0^D f(x)g(x)dx \leq \left(\int_0^D f(x)^2 dx\right)^{1/2} \cdot \left(\int_0^D g(x)^2 dx\right)^{1/2} \tag{B.1}$$

B.2 Poincare's Inequality

$$\int_0^D w(x)^2 dx \leq 2Dw(D)^2 + 4D^2 \int_0^D w_x(x)^2 dx \tag{B.2}$$

$$\int_0^D w(x)^2 dx \leq 2Dw(0)^2 + 4D^2 \int_0^D w_x(x)^2 dx \tag{B.3}$$

Proof:

$$\begin{aligned}\int_0^D w(x)^2 dx &= xw(x)^2|_0^D - 2\int_0^D xw(x)w_x(x)dx \\ &= Dw(D)^2 - 2\int_0^D xw(x)w_x(x)dx \\ &\leq Dw(D)^2 + \frac{1}{2}\int_0^D w(x)^2 dx + 2\int_0^D x^2 w_x(x)^2 dx\end{aligned}$$

Thus, we arrived at (B.2).

$$\begin{aligned}\int_0^D w(x)^2 dx &= (x-D)w(x)^2|_0^D - 2\int_0^D (x-D)w(x)w_x(x)dx \\ &= Dw(0)^2 - 2\int_0^D (x-D)w(x)w_x(x)dx \\ &\leq Dw(0)^2 + \frac{1}{2}\int_0^D w(x)^2 dx + 2\int_0^D (x-D)^2 w_x(x)^2 dx\end{aligned}$$

Thus, we arrived at (B.3).

B.3 Agmon's Inequality

Agmon's Inequality (Case 1)

$$||w||_\infty^2 \leq w(0)^2 + 2||w||_2||w_x||_2 \tag{B.4}$$

Proof:

$$\int_0^x w(x)w_x(x)dx = \frac{1}{2}(w(x)^2 - w(0)^2)$$

Taking absolute values and triangle inequality,

$$\begin{aligned} w(x)^2 &\leq w(0)^2 + 2\int_0^x |w(x)||w_x(x)|dx \\ &\leq w(0)^2 + 2\int_0^D |w(x)||w_x(x)|dx \end{aligned}$$

Because the left hand side doesn't depend on x, we arrive at (B.5).

Agmon's Inequality (Case 1:Extended)

$$||w||_\infty^2 \leq 2w(0)^2 + 4D||w_x||_2 \tag{B.5}$$

Proof:

By (B.5) and applying Young's inequality with γD, we have

$$\begin{aligned} ||w||_\infty^2 &\leq w(0)^2 + \frac{1}{\gamma D}||w||_2^2 + \gamma D||w_x||_2 \\ &\leq \left(1 + \frac{2}{\gamma}\right) w(0)^2 + \left(\frac{4}{\gamma} + \gamma\right) D||w_x||_2 \end{aligned} \tag{B.6}$$

Setting $\gamma = 2$ leads to the inequality.

Agmon's Inequality (Case 2)

$$w(0)^2 \leq \frac{D+1}{D}||w||^2 + ||w_x||^2 \tag{B.7}$$

Proof:

Taking integral, we have

$$-\int_0^x w(x)w_x(x)dx = \frac{1}{2}(w(0)^2 - w(x)^2)$$

In addition, by Young's inequality, we have

$$\begin{aligned} -\int_0^x w(x)w_x(x)dx &\leq \int_0^x \frac{1}{2}\left(w(y)^2 + w_y(y)^2\right)dy \\ &\leq \frac{1}{2}\left(||w||^2 + ||w_x||^2\right) \end{aligned} \tag{B.8}$$

Taking integration, we have

$$\int_0^D \frac{1}{2}(w(0)^2 - w(x)^2)dx \leq \int_0^D \frac{1}{2}\left(||w||^2 + ||w_x||^2\right)dx \tag{B.9}$$

For non-x-dependent terms, we obtain

$$Dw(0)^2 - ||w||^2 \leq D\left(||w||^2 + ||w_x||^2\right) \tag{B.10}$$

Therefore, we arrive at

$$w(0)^2 \leq \frac{D+1}{D}||w||^2 + ||w_x||^2 \tag{B.11}$$

In the same way, we have

$$\begin{aligned}\int_x^D w(x)w_x(x)dx =& \frac{1}{2}(w(D)^2 - w(x)^2)\\ \int_x^D w(x)w_x(x)dx \leq& \int_x^D \frac{1}{2}\left(w(y)^2 + w_y(y)^2\right)dy\\ \leq& \frac{1}{2}\left(||w||^2 + ||w_x||^2\right)\end{aligned} \tag{B.12}$$

Therefore, we arrive at

$$w(D)^2 \leq \frac{D+1}{D}||w||^2 + ||w_x||^2 \tag{B.13}$$

Appendix C

Stable Systems and Their Proofs

C.1 One-Phase Stefan Problem With Monotonic Interface

Consider the system

$$w_t(x,t) = \alpha w_{xx}(x,t) + \dot{s}(t)\phi'(x-s(t))X(t), \tag{C.1}$$

$$w_x(0,t) = 0, \tag{C.2}$$

$$w(s(t),t) = 0, \tag{C.3}$$

$$\dot{X}(t) = -cX(t) - \beta w_x(s(t),t). \tag{C.4}$$

Lemma 7 *With the conditions*

$$\dot{s}(t) > 0, \quad 0 < s(t) < \bar{s}, \tag{C.5}$$

for some positive constant $\bar{s} > 0$, (w,X)*-system in* (C.1)–(C.4) *is exponentially stable at the origin*

in the sense of the spatial $\mathcal{H}_1$-norm defined by

$$\Phi(t) := \int_0^{s(t)} w(x,t)^2 dx + \int_0^{s(t)} w_x(x,t)^2 dx + X(t)^2 \tag{C.6}$$

Proof:

$$V_1 = \frac{1}{2}\int_0^{s(t)} w(x,t)^2 dx. \tag{C.7}$$

Taking the time derivative of (C.7), we have

$$\begin{aligned}
\dot{V}_1 &= \int_0^{s(t)} w(x,t) w_t(x,t) dx + \frac{1}{2}\dot{s}(t) w(s(t),t)^2 \\
&= \alpha \int_0^{s(t)} w(x,t) w_{xx}(x,t) dx + \dot{s}(t) X(t) \int_0^{s(t)} \phi'(x - s(t)) w(x,t) dx \\
&= \alpha w(x,t) w_x(x,t)|_{y=0}^{y=s(t)} - \alpha \int_0^{s(t)} w_x(x,t)^2 dx + \dot{s}(t) X(t) \int_0^{s(t)} \phi'(x - s(t)) w(x,t) dx \\
&= -\alpha \int_0^{s(t)} w_x(x,t)^2 dx + \dot{s}(t) X(t) \int_0^{s(t)} \phi'(x - s(t)) w(x,t) dx.
\end{aligned} \tag{C.8}$$

Next, we consider V_2 defined by

$$V_2 = \frac{1}{2}\int_0^{s(t)} w_x(x,t)^2 dx. \tag{C.9}$$

Taking the time derivative of (C.9), we get

$$\begin{aligned}\dot{V}_2 =& \int_0^{s(t)} w_x(x,t)w_{xt}(x,t)dx + \frac{1}{2}\dot{s}(t)w_x(s(t),t)^2 \\ =& w_x(x,t)w_t(x,t)|_{x=0}^{x=s(t)} - \int_0^{s(t)} w_{xx}(x,t)w_t(x,t)dx + \frac{1}{2}\dot{s}(t)w_x(s(t),t)^2 \\ =& w_x(s(t),t)w_t(s(t),t) - \alpha\int_0^{s(t)} w_{xx}(x,t)^2dx \\ & - \dot{s}(t)X(t)\int_0^{s(t)} \phi'(x-s(t))w_{xx}(x,t)dx + \frac{1}{2}\dot{s}(t)w_x(s(t),t)^2 \end{aligned} \tag{C.10}$$

Taking the total time derivative of (C.2) on both sides, we obtain the following

$$\frac{d}{dt}w(s(t),t) = w_t(s(t),t) + \dot{s}(t)w_x(s(t),t) = 0, \tag{C.11}$$

which yields

$$w_t(s(t),t) = -\dot{s}(t)w_x(s(t),t). \tag{C.12}$$

Moreover, the integration by parts in first term in the last line in (C.10) with the help of (C.2) is given by

$$\int_0^{s(t)} \phi'(x-s(t))w_{xx}(x,t)dx = \phi'(0)w_x(s(t),t) - \int_0^{s(t)} \phi''(x-s(t))w_x(x,t)dx. \tag{C.13}$$

Therefore, plugging (C.12) and (C.13) into (C.10), we arrive at

$$\begin{aligned}\dot{V}_2 =& -\alpha\int_0^{s(t)} w_{xx}(x,t)^2dx - \frac{1}{2}\dot{s}(t)w_x(s(t),t)^2 \\ & - \dot{s}(t)X(t)\left(\phi'(0)w_x(s(t),t) - \int_0^{s(t)} \phi''(x-s(t))w_x(x,t)dx\right). \end{aligned} \tag{C.14}$$

Next, we consider V_3 defined by

$$V_3 = \frac{1}{2}X(t)^2. \tag{C.15}$$

Using (C.4), the time derivative of (C.15) is given by

$$\begin{aligned}\dot{V}_3 =& X(t)\dot{X}(t)\\ =& -cX(t)^2 - \beta X(t)w_x(s(t),t).\end{aligned} \tag{C.16}$$

Let V be the functional defined by

$$V = V_1 + V_2 + pV_3. \tag{C.17}$$

By (C.8), (C.14), and (C.16), the time derivative of (C.17) is given by

$$\begin{aligned}\dot{V} =& -\alpha\int_0^{s(t)} w_{xx}(x,t)^2dx - \alpha\int_0^{s(t)} w_x(x,t)^2dx - pcX(t)^2 - p\beta X(t)w_x(s(t),t)\\ &+\dot{s}(t)X(t)\int_0^{s(t)}\phi'(x-s(t))w(x,t)dx - \frac{\dot{s}(t)}{2}w_x(s(t),t)^2\\ &-\dot{s}(t)X(t)\left(\phi'(0)w_x(s(t),t) - \int_0^{s(t)}\phi''(x-s(t))w_x(x,t)dx\right).\end{aligned} \tag{C.18}$$

Using the fact that $\dot{s}(t) > 0$ and applying Young's inequality yields

$$-p\beta X(t)w_x(s(t),t) \leq \frac{p}{2}\left(cX(t)^2 + \frac{\beta^2}{c}w_x(s(t),t)^2\right), \tag{C.19}$$

$$\dot{s}(t)X(t)\int_0^{s(t)}\phi'(x-s(t))w(x,t)dx \leq \frac{\dot{s}(t)}{2}\left(\gamma_1 X(t)^2 + \frac{1}{\gamma_1}\left(\int_0^{s(t)}\phi'(x-s(t))w(x,t)dx\right)^2\right), \tag{C.20}$$

$$-\dot{s}(t)X(t)\phi'(0)w_x(s(t),t) \leq \frac{\dot{s}(t)}{2}\left(\gamma_2\phi'(0)^2X(t)^2 + \frac{1}{\gamma_2}w_x(s(t),t)^2\right), \tag{C.21}$$

for some positive constants $\gamma_1 > 0$ and $\gamma_2 > 0$. Here we choose

$$\gamma_1 = \phi'(0)^2, \quad \gamma_2 = 1. \tag{C.22}$$

Also, by Cauchy-Schwarz inequality, we have

$$\begin{aligned}\left(\int_0^{s(t)} \phi'(x-s(t))w(x,t)dx\right)^2 &\leq \left(\int_0^{s(t)} \phi'(x-s(t))^2 dx\right)\left(\int_0^{s(t)} w(x,t)^2 dx\right) \\ &\leq \bar{\phi}' \int_0^{s(t)} w(x,t)^2 dx. \end{aligned} \tag{C.23}$$

where $\bar{\phi}' = \int_0^{\bar{s}} \phi'(-x)^2 dx$. Applying (C.19)–(C.23) to (C.18), the following inequality on V is derived

$$\begin{aligned}\dot{V} \leq &-\alpha \int_0^{s(t)} w_{xx}(x,t)^2 dx - \alpha \int_0^{s(t)} w_x(x,t)^2 dx - \frac{pc}{2} X(t)^2 + \frac{p\beta^2}{2c} w_x(s(t),t)^2 \\ &+ \dot{s}(t)\left(\frac{\bar{\phi}'}{2\phi'(0)^2}\int_0^{s(t)} w(x,t)^2 dx + \phi'(0)^2 X(t)^2\right)\end{aligned} \tag{C.24}$$

Applying Poincare's and Agmon's inequalities which give $\int_0^{s(t)} w(x,t)^2 dx \leq 4\bar{s}^2 \int_0^{s(t)} w_x(x,t)^2 dx$ and $w_x(s(t),t)^2 \leq 4\bar{s}\int_0^{s(t)} w_{xx}(x,t)^2 dx$, the inequality (C.24) becomes

$$\begin{aligned}\dot{V} \leq &-\left(\alpha - \frac{2p\beta^2\bar{s}}{c}\right)\int_0^{s(t)} w_{xx}(x,t)^2 dx - \alpha \int_0^{s(t)} w_x(x,t)^2 dx - \frac{pc}{2} X(t)^2 \\ &+ \dot{s}(t)\left(\frac{\bar{\phi}'}{2\phi'(0)^2}\int_0^{s(t)} w(x,t)^2 dx + \phi'(0)^2 X(t)^2\right).\end{aligned} \tag{C.25}$$

Therefore, by choosing $p = \frac{c\alpha}{4\beta^2\bar{s}}$, we arrive at

$$\begin{aligned}\dot{V} \leq & -\frac{\alpha}{8\bar{s}^2}\int_0^{s(t)} w_x(x,t)^2 dx - \frac{\alpha}{4\bar{s}^2}\int_0^{s(t)} w(x,t)^2 dx - \frac{pc}{2}X(t)^2 \\ & + \dot{s}(t)\left(\frac{\bar{\phi}'}{2\phi'(0)^2}\int_0^{s(t)} w(x,t)^2 dx + \phi'(0)^2 X(t)^2\right) \\ \leq & -bV + a\dot{s}(t)V \end{aligned} \tag{C.26}$$

where $a = \max\left\{\frac{\bar{\phi}'}{\phi'(0)^2}, \frac{2\phi'(0)^2}{p}\right\}$, $b = \min\left\{\frac{\alpha}{4\bar{s}^2}, c\right\}$.

However, the second term of the right-hand side of (C.26) does not enable to directly conclude the exponential stability. To deal with it, we introduce a new Lyapunov function W defined by

$$W = Ve^{-as(t)}. \tag{C.27}$$

The time derivative of (C.27) is written as

$$\dot{W} = \left(\dot{V} - a\dot{s}(t)V\right)e^{-as(t)}, \tag{C.28}$$

and using (C.26) the following estimate can be deduced

$$\dot{W} \leq -bW. \tag{C.29}$$

Hence, $W(t) \leq W(0)e^{-bt}$, and using $0 < s(t) < \bar{s}$ and (C.27), we obtain

$$V(t) \leq e^{a\bar{s}}V(0)e^{-bt}. \tag{C.30}$$

C.2 One-Phase Stefan Problem With Convection and Heat Loss

Consider the system

$$\begin{aligned} w_t(x,t) =& \alpha w_{xx}(x,t) + b w_x(x,t) - h w(x,t) \\ &+ \dot{s}(t)\phi'(x-s(t))X(t), \quad 0 < x < s(t) \end{aligned} \tag{C.31}$$

$$w_x(0,t) = \gamma w(0,t), \tag{C.32}$$

$$w(s(t),t) = 0, \tag{C.33}$$

$$\dot{X}(t) = -cX(t) - \beta w_x(s(t),t), \tag{C.34}$$

where b is an arbitral parameter (can be positive or negative), $h \geq 0$, $c > 0$, and $\gamma > \max\left\{0, -\frac{b}{2\alpha}\right\}$.

Lemma 8 *With the conditions*

$$\dot{s}(t) > 0, \quad 0 < s(t) < s_{\mathrm{r}}, \tag{C.35}$$

for some positive constant $s_{\mathrm{r}} > 0$, (w,X)-system in (C.31)–(C.34) *is exponentially stable at the origin in the sense of the spatial $\mathcal{H}_1$-norm defined by*

$$\Phi(t) := \int_0^{s(t)} w(x,t)^2 dx + \int_0^{s(t)} w_x(x,t)^2 dx + X(t)^2 \tag{C.36}$$

Proof:

We consider a functional V_1 defined by

$$V_1 = \frac{1}{2}\int_0^{s(t)} w(x,t)^2 dx. \tag{C.37}$$

Taking the time derivative of (C.37) along with (C.31)–(C.34), we have

$$\begin{aligned}
\dot{V}_1 =& \int_0^{s(t)} w(x,t)w_t(x,t)dx + \frac{1}{2}\dot{s}(t)w(s(t),t)^2 \\
=& \alpha \int_0^{s(t)} w(x,t)w_{xx}(x,t)dx + b\int_0^{s(t)} w(x,t)w_x(x,t)dx - h\int_0^{s(t)} w(x,t)^2dx \\
&+ \dot{s}(t)X(t)\int_0^{s(t)} \phi'(x-s(t))w(x,t)dx \\
=& \alpha w(x,t)w_x(x,t)|_{x=0}^{x=s(t)} - \alpha\int_0^{s(t)} w_x(x,t)^2dx + \frac{b}{2}(w(s(t),t)^2 - w(0,t)^2) \\
&- h\int_0^{s(t)} w(x,t)^2dx + \dot{s}(t)X(t)\int_0^{s(t)} \phi'(x-s(t))w(x,t)dx \\
=& -\alpha||w_x||^2 - h||w||^2 - \left(\gamma\alpha + \frac{b}{2}\right)w(0,t)^2 \\
&+ \dot{s}(t)X(t)\int_0^{s(t)} \phi'(x-s(t))w(x,t)dx. \qquad \text{(C.38)}
\end{aligned}$$

Applying Young's inequality with the help of $\dot{s}(t) > 0$ and $0 < s(t) < s_{\mathrm{r}}$, we have

$$\dot{s}(t)X(t)\int_0^{s(t)} \phi'(x-s(t))w(x,t)dx \leq \frac{\dot{s}(t)}{2}\left(X(t)^2 + \overline{\phi'}^2||w||^2\right), \qquad \text{(C.39)}$$

where $\overline{\phi} := \sup_{s(t)\in(0,s_{\mathrm{r}})}\sqrt{\int_0^{s(t)}\phi'(x-s(t))^2dx}$. Thus, applying the above inequality to (C.38), we get

$$\dot{V}_1 \leq -\alpha||w_x||^2 - h||w||^2 - \left(\gamma\alpha + \frac{b}{2}\right)w(0,t)^2 + \frac{\dot{s}(t)}{2}\left(X(t)^2 + \overline{\phi'}^2||w||^2\right). \qquad \text{(C.40)}$$

Next, we consider V_2 defined by

$$V_2 = \frac{1}{2}\int_0^{s(t)} w_x(x,t)^2dx. \qquad \text{(C.41)}$$

Taking the time derivative of (C.41), we get

$$\begin{aligned}\dot{V}_2 =& \int_0^{s(t)} w_x(x,t)w_{xt}(x,t)dx + \frac{1}{2}\dot{s}(t)w_x(s(t),t)^2 \\ =& w_x(x,t)w_t(x,t)|_{x=0}^{x=s(t)} - \int_0^{s(t)} w_{xx}(x,t)w_t(x,t)dx + \frac{1}{2}\dot{s}(t)w_x(s(t),t)^2 \\ =& w_x(s(t),t)w_t(s(t),t) - \gamma w(0,t)w_t(0,t) - \alpha||w_{xx}||^2 - b\int_0^{s(t)} w_{xx}(x,t)w_x(x,t)dx \\ &+ h\int_0^{s(t)} w_{xx}(x,t)w(x,t)dx - \dot{s}(t)X(t)\int_0^{s(t)} \phi'(x-s(t))w_{xx}(x,t)dx \\ &+ \frac{1}{2}\dot{s}(t)w_x(s(t),t)^2 \end{aligned} \tag{C.42}$$

The boundary condition $w(s(t),t) = 0$ yields

$$w_t(s(t),t) = -\dot{s}(t)w_x(s(t),t). \tag{C.43}$$

Moreover, we have

$$\begin{aligned}&\int_0^{s(t)} \phi'(x-s(t))w_{xx}(x,t)dx \\ =& \phi'(0)w_x(s(t),t) - \gamma\phi'(-s(t))w(0,t) - \int_0^{s(t)} \phi''(x-s(t))w_x(x,t)dx. \end{aligned} \tag{C.44}$$

Therefore, plugging (C.43) and (C.44) into (C.42), we arrive at

$$\begin{aligned}\dot{V}_2 =& -\alpha||w_{xx}||^2 - b\int_0^{s(t)} w_{xx}(x,t)w_x(x,t)dx - \gamma h w(0,t)^2 - h||w_x||^2 - \gamma w(0,t)w_t(0,t) \\ &- \dot{s}(t)X(t)\left(\phi'(0)w_x(s(t),t) - \gamma\phi'(-s(t))w(0,t) - \int_0^{s(t)} \phi''(x-s(t))w_x(x,t)dx\right) \\ &- \frac{1}{2}\dot{s}(t)w_x(s(t),t)^2. \end{aligned} \tag{C.45}$$

Applying Young's and Cauchy-Schwarz inequalities, we get

$$-b\int_0^{s(t)} w_{xx}(x,t)w_x(x,t)dx \leq \frac{\alpha}{2}||w_{xx}||^2 + \frac{b^2}{2\alpha}||w_x||. \tag{C.46}$$

Moreover, applying Young's inequality with the help of $\dot{s}(t) \geq 0$, we get

$$-\dot{s}(t)X(t)\phi'(0)w_x(s(t),t) \leq \frac{\dot{s}(t)}{2}(w_x(s(t),t)^2 + \phi'(0)^2X(t)^2), \tag{C.47}$$

$$\begin{aligned}&\dot{s}(t)X(t)\left(\gamma\phi'(-s(t))w(0,t) + \int_0^{s(t)} \phi''(x-s(t))w_x(x,t)dx\right)\\ \leq&\frac{\dot{s}(t)}{2}\left((\overline{\phi'_s}^2+1)X(t)^2 + \gamma^2 w(0,t)^2 + \overline{\phi''}^2||w_x||^2\right)\end{aligned} \tag{C.48}$$

where $\overline{\phi'_s} := \sup_{s(t)\in(0,s_r)}|\phi'(-s(t))|$, and $\overline{\phi''} := \sup_{s(t)\in(0,s_r)}\sqrt{\int_0^{s(t)}\phi''(x-s(t))^2dx}$. Applying these inequalities to (C.45), we have

$$\begin{aligned}\dot{V}_2 \leq& -\frac{\alpha}{2}||w_{xx}||^2 + \left(\frac{b^2}{2\alpha} - h\right)||w_x||^2 - \gamma h w(0,t)^2 - \gamma w(0,t)w_t(0,t)\\ &+\frac{\dot{s}(t)}{2}\left((\phi'(0)^2 + \overline{\phi'_s}^2 + 1)X(t)^2 + \gamma^2 w(0,t)^2 + \overline{\phi''}^2||w_x||^2\right).\end{aligned} \tag{C.49}$$

Next, we consider V_3 defined by

$$V_3 = \frac{1}{2}X(t)^2. \tag{C.50}$$

The time derivative of (C.50) and applying Young's and Agmon's inequalities, we get

$$\begin{aligned}
\dot{V}_3 =& X(t)\dot{X}(t) \\
=& -cX(t)^2 - \beta X(t) w_x(s(t),t) \\
\leq& -\frac{c}{2}X(t)^2 + \frac{\beta^2}{2c} w_x(s(t),t)^2 \\
\leq& -\frac{c}{2}X(t)^2 + \frac{\beta^2}{2c}(2w_x(0,t)^2 + 4s_{\mathrm{r}}||w_{xx}||^2) \\
=& -\frac{c}{2}X(t)^2 + \frac{\beta^2\gamma^2}{c} w(0,t)^2 + \frac{2s_{\mathrm{r}}\beta^2}{c}||w_{xx}||^2 \\
\leq& -\frac{c}{2}X(t)^2 + \frac{4s_{\mathrm{r}}\beta^2\gamma^2}{c}||w_x||^2 + \frac{2s_{\mathrm{r}}\beta^2}{c}||w_{xx}||^2
\end{aligned} \tag{C.51}$$

Let V^* be the functional defined by

$$V^* = V_2 + \frac{\gamma}{2} w(0,t)^2 + pV_3, \tag{C.52}$$

where $p = \frac{c\alpha}{8\beta^2 s_r}$. By (C.49) and (C.51), the time derivative of (C.52) satisfies

$$\begin{aligned}
\dot{V}^* \leq& -\frac{\alpha}{4}||w_{xx}||^2 + \left(\frac{b^2}{2\alpha} + \frac{\gamma^2\alpha}{2} - h\right)||w_x||^2 - \gamma h w(0,t)^2 - \frac{pc}{2}X(t)^2 \\
&+ \frac{\dot{s}(t)}{2}\left((\phi'(0)^2 + \overline{\phi'_s}^2 + 1)X(t)^2 + \gamma^2 w(0,t)^2 + \overline{\phi''}^2||w_x||^2\right).
\end{aligned} \tag{C.53}$$

By Poincare's inequality, we have

$$||w_x||^2 \leq 2s_{\mathrm{r}} w_x(0,t)^2 + 4s_{\mathrm{r}}^2||w_{xx}||^2 = 2s_{\mathrm{r}}\gamma^2 w(0,t)^2 + 4s_{\mathrm{r}}^2||w_{xx}||^2 \tag{C.54}$$

Applying this to (C.53), we get

$$\dot{V}^* \leq -\frac{\alpha}{16s_{\mathrm{r}}^2}||w_x||^2 + \left(\frac{b^2}{2\alpha} + \frac{\gamma^2\alpha}{2} - h\right)||w_x||^2 + \left(\frac{\alpha\gamma^2}{8s_{\mathrm{r}}} - \gamma h\right)w(0,t)^2 - \frac{pc}{2}X(t)^2 + \frac{\dot{s}(t)}{2}\left((\phi'(0)^2 + \overline{\phi'_s}^2 + 1)X(t)^2 + \gamma^2 w(0,t)^2 + \overline{\phi''}^2||w_x||^2\right). \tag{C.55}$$

Finally, let V be defined by

$$V = V^* + qV_1, \tag{C.56}$$

where $q > 0$ is a positive parameter to be determined. Then, the time derivative of V satisfies

$$\dot{V} \leq -\left(\frac{\alpha}{16s_{\mathrm{r}}^2} + h + \frac{q\alpha}{2} - \left(\frac{b^2}{2\alpha} + \frac{\gamma^2\alpha}{2}\right)\right)||w_x||^2 - q\left(\frac{\alpha}{8s_{\mathrm{r}}^2} + h\right)||w||^2 - \left(q\left(\gamma\alpha + \frac{b}{2}\right) - \frac{\alpha\gamma^2}{8s_{\mathrm{r}}} + \gamma h\right)w(0,t)^2 - \frac{pc}{2}X(t)^2 + \frac{\dot{s}(t)}{2}\left((\phi'(0)^2 + \overline{\phi'_s}^2 + 1 + q)X(t)^2 + q\overline{\phi'}^2||w||^2 + \gamma^2 w(0,t)^2 + \overline{\phi''}^2||w_x||^2\right). \tag{C.57}$$

Therefore, by choosing

$$\gamma > \max\left\{0, -\frac{b}{2\alpha}\right\}, \tag{C.58}$$

$$q = \max\left\{\frac{b^2}{\alpha^2} + \gamma^2, \frac{\alpha\gamma(2\gamma s_{\mathrm{r}} + 1)}{16s_{\mathrm{r}}^2(\gamma\alpha + \frac{b}{2})}\right\}, \tag{C.59}$$

there exists a positive constant $a > 0$ such that

$$\dot{V} \leq -dV + a\dot{s}V, \tag{C.60}$$

holds, where $d = \min\left\{\frac{\alpha}{16s_{\mathrm{r}}^2} + h, c\right\}$. Using the same approach as Appendix C.1, we can deduce

that it holds

$$V(t) \leq e^{as_{\mathrm{r}}} V(0) e^{-dt}. \tag{C.61}$$

Recall the definition of $\Phi = ||w||^2 + ||w_x||^2 + X(t)^2$ given in (C.36). Then, with the help of Agmon's inequality, we can obtain the following bound:

$$\underline{M}\Phi \leq V \leq \overline{M}\Phi, \tag{C.62}$$

where

$$\underline{M} = \frac{1}{2}\min\{q, 1, p\}, \quad \overline{M} = \frac{1}{2}\max\{q, 1 + 4\gamma s_{\mathrm{r}}, p\}. \tag{C.63}$$

Finally, by combining (C.61) and (C.62), we obtain

$$\Phi(t) \leq \frac{\overline{M}}{\underline{M}} e^{as_{\mathrm{r}}} V(0) e^{-dt}, \tag{C.64}$$

by which we complete the proof of Lemma 8.

C.3 One-Phase Stefan Problem With Delay

Consider the system

$$z_t(x,t) = -z_x(x,t), \quad -D < x < 0 \tag{C.65}$$

$$z(-D,t) = 0, \tag{C.66}$$

$$w_x(0,t) = -z(0,t), \tag{C.67}$$

$$w_t(x,t) = \alpha w_{xx}(x,t) + \frac{c}{\beta}\dot{s}(t)X(t), \quad 0 < x < s(t) \tag{C.68}$$

$$w(s(t),t) = 0, \tag{C.69}$$

$$\dot{X}(t) = -cX(t) - \beta w_x(s(t),t). \tag{C.70}$$

Lemma 9 *With the conditions*

$$\dot{s}(t) > 0, \quad 0 < s(t) < s_{\mathrm{r}}, \tag{C.71}$$

for some positive constant $s_{\mathrm{r}} > 0$*,* (w,X)*-system in* (C.65)–(C.70) *is exponentially stable at the origin in the sense of the spatial* $\mathcal{H}_1$*-norm defined by*

$$\Pi(t) := \int_{-D}^{0} z_x(x,t)^2 dx + \int_0^{s(t)} w(x,t)^2 dx + \int_0^{s(t)} w_x(x,t)^2 dx + X(t)^2. \tag{C.72}$$

Proof:

Change of variable

Introduce a change of variable

$$\omega(x,t) = w(x,t) + (x - s(t))\, z(0,t). \tag{C.73}$$

Using (C.73), the target (z,w,X)-system (C.65)–(C.70) is described by (z,ω,X)-system as

$$z(-D,t) = 0, \tag{C.74}$$

$$z_t(x,t) = -z_x(x,t), \quad -D < x < 0 \tag{C.75}$$

$$\omega_x(0,t) = 0, \tag{C.76}$$

$$\omega_t(x,t) = \alpha\omega_{xx}(x,t) - (x-s(t))z_x(0,t) + \dot{s}(t)\left(\frac{c}{\beta}X(t) - z(0,t)\right), \quad 0 < x < s(t) \tag{C.77}$$

$$\omega(s(t),t) = 0, \tag{C.78}$$

$$\dot{X}(t) = -cX(t) - \beta(\omega_x(s(t),t) - z(0,t)). \tag{C.79}$$

Stability analysis of (z,ω,X)-system

Firstly, we prove the exponential stability of the (z,ω,X)-system. Let V_1 be the functional defined by

$$V_1 = \int_{-D}^{0} e^{-mx} z_x(x,t)^2 dx, \tag{C.80}$$

where $m > 0$ is a positive parameter. (C.80) satisfies

$$||z_x||^2_{L_2(-D,0)} \leq V_1 \leq e^{mD}||z_x||^2_{L_2(-D,0)}. \tag{C.81}$$

Note that (C.74) yields $z_x(-D,t) = 0$ through taking the time derivative and applying PDE (C.75). With the help of it, taking the time derivative of (C.80) together with (C.74)-(C.75) leads to

$$\begin{aligned}
\dot{V}_1 &= -2\int_{-D}^{0} e^{-mx} z_x(x,t) z_{xx}(x,t) dx \\
&= -e^{-mx} z_x(x,t)^2 |_{x=-D}^{x=0} + \int_{-D}^{0} \left(\frac{d}{dx} e^{-mx}\right) z_x(x,t)^2 dx \\
&= -z_x(0,t)^2 - m\int_{-D}^{0} e^{-mx} z_x(x,t)^2 dx.
\end{aligned} \tag{C.82}$$

Let V_2 be the functional defined by

$$\begin{aligned} V_2 =& \frac{1}{2}\left(\frac{1}{s_r^2}||\omega||^2_{L_2(0,s(t))} + ||\omega_x||^2_{L_2(0,s(t))}\right) \\ =& \frac{1}{2}\int_0^{s(t)}\left(\frac{1}{s_r^2}\omega(x,t)^2 + \omega_x(x,t)^2\right)dx. \end{aligned} \tag{C.83}$$

(C.83) satisfies $\max\{s_r^2,1\}||\omega||^2_{\mathcal{H}_1(0,s(t))} \leq 2V_2 \leq \max\{1/s_r^2,1\}||\omega||^2_{\mathcal{H}_1(0,s(t))}$ Note that taking the total time derivative of (C.78) yields $\omega_t(s(t),t) = -\dot{s}(t)\omega_x(s(t),t)$. Taking the time derivative of (C.83) together with (C.76)-(C.78), we obtain

$$\begin{aligned} \dot{V}_2 =& \frac{\dot{s}(t)}{2}\left(\frac{1}{s_r^2}\omega(s(t),t)^2 + \omega_x(s(t),t)^2\right) \\ &+ \int_0^{s(t)}\left(\frac{1}{s_r^2}\omega(x,t)\omega_t(x,t) + \omega_x(x,t)\omega_{xt}(x,t)\right)dx \\ =& \frac{\dot{s}(t)}{2}\omega_x(s(t),t)^2 \\ &+ \frac{1}{s_r^2}\int_0^{s(t)}\omega(x,t)\left(\alpha\omega_{xx}(x,t) - (x-s(t))\,z_x(0,t) + \dot{s}(t)\left(\frac{c}{\beta}X(t) - z(0,t)\right)\right)dx \\ &+ \omega_x(s(t),t)\omega_t(s(t),t) - \omega_x(0,t)\omega_t(0,t) - \int_0^{s(t)}\omega_{xx}(x,t)\omega_t(x,t)dx \\ =& -\frac{\alpha}{s_r^2}||\omega_x||^2_{L_2(0,s(t))} - \frac{1}{s_r^2}z_x(0,t)\int_0^{s(t)}(x-s(t))\,\omega(x,t)dx \\ &+ \frac{\dot{s}(t)}{s_r^2}\left(\frac{c}{\beta}X(t) - z(0,t)\right)\int_0^{s(t)}\omega(x,t)dx - \alpha||\omega_{xx}||^2_{L_2(0,s(t))} + z_x(0,t)\omega(0,t) \\ &- \frac{\dot{s}(t)}{2}\omega_x(s(t),t)^2 - \dot{s}(t)\left(\frac{c}{\beta}X(t) - z(0,t)\right)\omega_x(s(t),t). \end{aligned} \tag{C.84}$$

Applying Young's and Cauchy Schwarz inequalities to the second terms on the first and second line of the (C.84) with the help of $0 < s(t) < s_{\mathrm{r}}$ yields

$$\begin{aligned}
\left| z_x(0,t) \int_0^{s(t)} (x - s(t))\, \omega(x,t) dx \right| \leq & \frac{\gamma_1}{2} z_x(0,t)^2 + \frac{1}{2\gamma_1} \left(\int_0^{s(t)} (x - s(t))\, \omega(x,t) dx \right)^2, \\
\leq & \frac{\gamma_1}{2} z_x(0,t)^2 \\
& + \frac{1}{2\gamma_1} \left(\int_0^{s(t)} (x - s(t))^2 dx \right) \left(\int_0^{s(t)} \omega(x,t)^2 dx \right), \\
\leq & \frac{\gamma_1}{2} z_x(0,t)^2 + \frac{s_r^3}{6\gamma_1} ||\omega||^2_{L_2(0,s(t))}, \\
\leq & \frac{\gamma_1}{2} z_x(0,t)^2 + \frac{2 s_r^5}{3\gamma_1} ||\omega_x||^2_{L_2(0,s(t))}, \qquad \text{(C.85)}
\end{aligned}$$

$$\begin{aligned}
|z_x(0,t)\omega(0,t)| \leq & \frac{\gamma_2}{2} z_x(0,t)^2 + \frac{1}{2\gamma_2} \omega(0,t)^2, \\
\leq & \frac{\gamma_2}{2} z_x(0,t)^2 + \frac{2 s_r}{\gamma_2} ||\omega_x||^2_{L_2(0,s(t))}, \qquad \text{(C.86)}
\end{aligned}$$

where we utilized Poincare's inequality $||\omega||^2_{L_2(0,s(t))} \leq 4 s_r^2 ||\omega_x||^2_{L_2(0,s(t))}$ and Agmon's inequality $\omega(0,t)^2 \leq 4 s_r ||\omega_x||^2_{L_2(0,s(t))}$, and $\gamma_1 > 0$ and $\gamma_2 > 0$ are positive parameters to be determined. Hence, applying (C.85) and (C.86) to (C.84) with the choice of $\gamma_1 = \frac{8 s_r^5}{3\alpha}$ and $\gamma_2 = \frac{8 s_r^3}{\alpha}$, the following differential inequality is deduced

$$\begin{aligned}
\dot{V}_2 \leq & -\frac{\alpha}{2} ||\omega_{xx}||^2_{L_2(0,s(t))} - \frac{\alpha}{2 s_r^2} ||\omega_x||^2_{L_2(0,s(t))} + \frac{16 s_{\mathrm{r}}^3}{3\alpha} z_x(0,t)^2 \\
& + \dot{s}(t) \left(2 \frac{c^2}{\beta^2} X(t)^2 + 2 z(0,t)^2 + \frac{1}{2 s_r^3} ||\omega||^2_{L_2(0,s(t))} \right). \qquad \text{(C.87)}
\end{aligned}$$

Let V_3 be the functional defined by

$$V_3 = \frac{1}{2} X(t)^2. \qquad \text{(C.88)}$$

Taking the time derivative of (C.88) and applying Young's and Agmon's inequalities, we obtain

$$\begin{aligned}\dot{V}_3 =& -cX(t)^2 - \beta X(t)(\omega_x(s(t),t) - z(0,t)) \\ \leq& -\frac{c}{2}X(t)^2 + \frac{4\beta^2 s_{\mathrm{r}}}{c}||\omega_{xx}||^2_{L_2(0,s(t))} + \frac{4D\beta^2}{c}||z_x||^2_{L_2(-D,0)}. \end{aligned} \tag{C.89}$$

Let V be the functional defined by

$$V = qV_1 + V_2 + pV_3, \tag{C.90}$$

where $q > 0$ and $p > 0$ are positive parameters to be determined. Combining (C.82), (C.87), and (C.89), we get

$$\begin{aligned}\dot{V} \leq& -\frac{\alpha}{2}\left(1 - \frac{8p\beta^2 s_{\mathrm{r}}}{c\alpha}\right)||\omega_{xx}||^2_{L_2(0,s(t))} - \frac{\alpha}{2s_r^2}||\omega_x||^2_{L_2(0,s(t))} - \left(q - \frac{16s_{\mathrm{r}}^3}{3\alpha}\right)z_x(0,t)^2 \\ & - m\left(q - p\frac{4D\beta^2}{mc}\right)||z_x||^2_{L_2(-D,0)} - \frac{pc}{2}X(t)^2 \\ & + \dot{s}(t)\left(2\frac{c^2}{\beta^2}X(t)^2 + 2z(0,t)^2 + \frac{1}{2s_r^3}\int_0^{s(t)}\omega(x,t)^2 dx\right). \end{aligned} \tag{C.91}$$

Hence, by choosing the parameters as

$$p = \frac{c\alpha}{16\beta^2 s_{\mathrm{r}}}, \quad q = \max\left\{\frac{16s_{\mathrm{r}}^3}{3\alpha}, \frac{D\alpha}{2ms_r}\right\}, \tag{C.92}$$

the inequality (C.91) leads to

$$\begin{aligned}\dot{V} \leq& -\frac{\alpha}{4}||\omega_{xx}||^2_{L_2(0,s(t))} - \frac{\alpha}{2s_r^2}||\omega_x||^2_{L_2(0,s(t))} - m\left(q - p\frac{4D\beta}{mc}\right)||z_x||^2_{L_2(-D,0)} - \frac{pc}{2}X(t)^2 \\ & + \dot{s}(t)\left(2\frac{c^2}{\beta^2}X(t)^2 + 2z(0,t)^2 + \frac{1}{2s_r^3}\int_0^{s(t)}\omega(x,t)^2 dx\right), \\ \leq& -\frac{\alpha}{8s_r^2}V_2 - \frac{mq}{2}e^{-mD}V_1 - \frac{pc}{2}X(t)^2 + \dot{s}(t)\left(\frac{4c}{\beta^2}V_3 + 8DV_1 + \frac{1}{s_r}V_2\right), \end{aligned} \tag{C.93}$$

from which we obtain the form of

$$\dot{V} \leq -bV + a\dot{s}(t)V, \tag{C.94}$$

where

$$b = \min\left\{\frac{m}{2}e^{-mD}, \frac{\alpha}{8s_{\mathrm{r}}^2}, c\right\}, \quad a = \max\left\{\frac{8D}{q}, \frac{1}{s_{\mathrm{r}}}, \frac{4c^2}{p\beta^2}\right\}. \tag{C.95}$$

Hence, applying $0 < s(t) < s_{\mathrm{r}}$, the exponential stability of (z, ω, X)-system is shown as

$$V(t) \leq V(0)e^{as_{\mathrm{r}}}e^{-bt}. \tag{C.96}$$

Stability analysis of (z, w, X)-system

Taking the square of (C.73) and applying Young's and Cauchy Schwarz inequality, we obtain

$$||\omega||^2_{\mathcal{H}_1(0,s(t))} \leq 2||w||^2_{\mathcal{H}_1(0,s(t))} + K_1||z_x||^2_{L_2(-D,0)}, \tag{C.97}$$

$$||w||^2_{\mathcal{H}_1(0,s(t))} \leq 2||\omega||^2_{\mathcal{H}_1(0,s(t))} + K_1||z_x||^2_{L_2(-D,0)}, \tag{C.98}$$

where $K_1 = \frac{8Ds_{\mathrm{r}}^3}{3} + 8Ds_{\mathrm{r}}$. Consider the following norm

$$\Pi(t) = ||z_x||^2_{L_2(-D,0)} + ||w||^2_{\mathcal{H}_1(0,s(t))} + X(t)^2. \tag{C.99}$$

Then, recalling $||z_x||^2_{L_2(-D,0)} \leq V_1 \leq e^{mD}||z_x||^2_{L_2(-D,0)}$ and $K_2||\omega||^2_{\mathcal{H}_1(0,s(t))} \leq 2V_2 \leq K_3||\omega||^2_{\mathcal{H}_1(0,s(t))}$ where $K_2 = \max\{s_r^2, 1\}$ and $K_3 = \max\{1/s_r^2, 1\}$, applying (C.98) to (C.99) yields the following

bound:

$$\begin{aligned}\Pi \leq & (1+K_1)||z_x||^2_{L_2(-D,0)} + 2||\omega||^2_{\mathcal{H}_1(0,s(t))} + X(t)^2, \\ \leq & (1+K_1)V_1 + 4K_2V_2 + 2V_3. \end{aligned} \tag{C.100}$$

Moreover, recalling $V = qV_1 + V_2 + pV_3$ and applying the above inequalities, the following bound on V is derived:

$$\begin{aligned} V \leq & qe^{mD}||z_x||^2_{L_2(-D,0)} + \frac{K_3}{2}||\omega||^2_{\mathcal{H}_1(0,s(t))} + \frac{p}{2}X(t)^2, \\ \leq & \left(qe^{mD} + \frac{K_1K_3}{2}\right)||z_x||^2_{L_2(-D,0)} + \frac{K_3}{2}||w||^2_{\mathcal{H}_1(0,s(t))} + \frac{p}{2}X(t)^2. \end{aligned} \tag{C.101}$$

Therefore, (C.100) and (C.101) leads to the following equivalence of the norm V and Π:

$$\underline{\delta}V(t) \leq \Pi(t) \leq \bar{\delta}V(t), \tag{C.102}$$

where $\underline{\delta} = \frac{1}{\max\left\{qe^{mD} + \frac{K_1K_3}{2}, K_3, \frac{p}{2}\right\}}$ and $\bar{\delta} = \max\left\{\frac{1}{q}(K_1+1), 4K_2, \frac{2}{p}\right\}$. By (C.96) and (C.102), we have

$$\Pi(t) \leq \frac{\bar{\delta}}{\underline{\delta}}\Pi(0)e^{as_{\mathrm{r}}}e^{-bt}, \tag{C.103}$$

which yields the exponential stability of (z,w,X)-system, and we complete the proof of Lemma 9.

C.4 One-Phase Stefan Problem With Non-Monotonic Interface and Disturbances

Consider the system

$$w_t(x,t) = \alpha w_{xx}(x,t) + \frac{c}{\beta}\dot{s}(t)X(t) + \phi(x-s(t))d(t), \tag{C.104}$$

$$w_x(0,t) = f(t) - \frac{\beta}{\alpha}\varepsilon\left[w(0,t) - \frac{\beta}{\alpha}\int_0^{s(t)}\psi(-y)w(y,t)\mathrm{d}y - \psi(-s(t))X(t)\right], \tag{C.105}$$

$$w(s(t),t) = \varepsilon X(t), \tag{C.106}$$

$$\dot{X}(t) = -cX(t) - \beta w_x(s(t),t) - d(t), \tag{C.107}$$

where $\varepsilon > 0$, $c > 0$, and $\phi(x)$ and $\psi(x)$ are bounded continuous functions in x.

Lemma 10 *Suppose that there exists a positive constant $\bar{s} > 0$ such that*

$$0 < s(t) < \bar{s}. \tag{C.108}$$

Let $V(t)$ be a Lyapunov function defined by

$$V(t) = \frac{1}{2\alpha}||w||^2 + \frac{\varepsilon}{2\beta}X(t)^2. \tag{C.109}$$

Then, there exists a positive constant $\varepsilon^* > 0$ such that for all $\varepsilon \in (0,\varepsilon^*)$ the following inequality holds:

$$\dot{V}(t) \leq -bV(t) + \Gamma d(t)^2 + 2\bar{s}f(t)^2 + a|\dot{s}(t)|V(t), \tag{C.110}$$

where $a = \frac{2\beta\varepsilon}{\alpha}\max\left\{1, \frac{\alpha c^2\bar{s}}{2\beta^3\varepsilon^3}\right\}$, $b = \frac{1}{8}\min\left\{\frac{\alpha}{\bar{s}^2}, c\right\}$, and $\Gamma = \frac{\varepsilon}{\beta c} + \frac{2\bar{s}^3}{\alpha^2}\left(\frac{c\bar{s}}{\beta} + \varepsilon\right)^2$. Moreover, suppose

that there exists a time-varying function $z(t)$ which satisfies

$$\dot{z}(t) \geq |\dot{s}(t)|, \quad \underline{z} \leq z(t) \leq \bar{z}, \tag{C.111}$$

for some constants $\underline{z} \in \mathbb{R}$ and $\bar{z} \in \mathbb{R}$. Then, the system (C.104)–(C.107) *is exponentially ISS with respect to $f(t)$ and $d(t)$.*

Proof:

Note that Poincare's and Agmon's inequalities for the system (C.104)–(C.106) with $0 < s(t) < \bar{s}$ lead to

$$||w||^2 \leq 2\bar{s}\varepsilon^2 X(t)^2 + 4\bar{s}^2||w_x||^2, \tag{C.112}$$

$$w(0,t)^2 \leq 2\varepsilon^2 X(t)^2 + 4\bar{s}||w_x||^2. \tag{C.113}$$

Taking the time derivative of (C.109) along with the solution of (C.104)–(C.107), we have

$$\begin{aligned}
\dot{V}(t) = &- ||w_x||^2 - \frac{\varepsilon}{\beta} cX(t)^2 + \frac{\beta}{\alpha}\varepsilon w(0,t)^2 - w(0,t)f(t) \\
&- \frac{\beta}{\alpha}\varepsilon w(0,t)\left[\frac{\beta}{\alpha}\int_0^{s(t)} \psi(-y)w(y,t)\mathrm{d}y + \psi(-s(t))X(t)\right] \\
&- \frac{\varepsilon}{\beta}X(t)d(t) + \frac{1}{\alpha}\int_0^{s(t)} \phi(x-s(t))w(x,t)\mathrm{d}x d(t) \\
&+ \frac{\dot{s}(t)}{\alpha}\left(\frac{\varepsilon^2}{2}X(t)^2 + \frac{c}{\beta}\int_0^{s(t)} w(x,t)\mathrm{d}x X(t)\right).
\end{aligned} \tag{C.114}$$

Applying Young's inequality to the last term in the first line, the second, third, and fourth lines of (C.114), we obtain

$$-w(0,t)f(t) \leq \frac{1}{8\bar{s}}w(0,t)^2 + 2\bar{s}f(t)^2, \tag{C.115}$$

$$
\begin{aligned}
&-w(0,t)\left[\frac{\beta}{\alpha}\int_0^{s(t)}\psi(-y)w(y,t)dy+\psi(-s(t))X(t)\right]\\
\leq&\frac{1}{2}w(0,t)^2+\frac{\beta^2}{\alpha^2\gamma_1}\left(\int_0^{s(t)}\psi(-y)w(y,t)\mathrm{d}y\right)^2+\gamma_1\left(\psi(-s(t))X(t)\right)^2, \qquad \text{(C.116)}
\end{aligned}
$$

$$
\begin{aligned}
&-\frac{\varepsilon}{\beta}X(t)d(t)+\frac{1}{\alpha}\int_0^{s(t)}\phi(x-s(t))w(x,t)\mathrm{d}xd(t)\\
\leq&\frac{1}{2\gamma_2}\left(\frac{\varepsilon}{\beta}X(t)\right)^2+\frac{(\gamma_2+\gamma_3)}{2}d(t)^2+\frac{1}{2\alpha^2\gamma_3}\left(\int_0^{s(t)}\phi(x-s(t))w(x,t)\mathrm{d}x\right)^2, \qquad \text{(C.117)}
\end{aligned}
$$

where $\gamma_i>0$ for $i=\{1,2,3\}$. Applying (C.115)-(C.117) and Cauchy Schwarz, Poincare, and Agmon's inequalities to (C.114) with choosing $\gamma_1=\frac{1}{8}$, $\gamma_2=\frac{2\varepsilon}{\beta c}$, and $\gamma_3=\frac{4\bar{s}^3}{\alpha^2}\left(\frac{c\bar{s}}{\beta}+\varepsilon\right)^2$, we have

$$
\begin{aligned}
\dot{V}(t)\leq&-\left(\frac{1}{2}-\frac{2\beta\bar{s}}{\alpha}\left(\frac{64c\bar{s}^2}{\alpha}+3\right)\varepsilon\right)||w_x||^2\\
&-\varepsilon\left(\frac{c}{8\beta}+g(\varepsilon)\right)X(t)^2+\Gamma d(t)^2+2\bar{s}f(t)^2\\
&+\frac{|\dot{s}(t)|}{2\alpha}\left(\varepsilon^2X(t)^2+\frac{2c}{\beta}\left|\int_0^{s(t)}w(x,t)\mathrm{d}xX(t)\right|\right), \qquad \text{(C.118)}
\end{aligned}
$$

where $\Gamma=\frac{(\gamma_2+\gamma_3)}{2}$, and $g(\varepsilon)=\frac{c}{8\beta}-\frac{\varepsilon}{2\bar{s}}-\frac{\beta}{\alpha}\left(\frac{64c\bar{s}^2}{\alpha}+3\right)\varepsilon^2$. Since $g(0)=\frac{c}{8\beta}>0$ and $g'(\varepsilon)=-\frac{1}{2\bar{s}}-\frac{2\beta\varepsilon}{\alpha}\left(\frac{64c\bar{s}^2}{\alpha}+3\right)<0$ for all $\varepsilon>0$, there exists ε^* such that $g(\varepsilon)>0$ for all $\varepsilon\in(0,\varepsilon^*)$ and $g(\varepsilon^*)=0$. Thus, setting $\varepsilon<\min\left\{\varepsilon^*,\frac{\alpha}{8\beta\bar{s}\left(\frac{64c\bar{s}^2}{\alpha}+3\right)}\right\}$, the inequality (C.118) leads to

$$
\begin{aligned}
\dot{V}(t)\leq&-bV(t)+\Gamma d(t)^2+2\bar{s}f(t)^2\\
&+\frac{|\dot{s}(t)|}{2\alpha}\left(\varepsilon^2X(t)^2+\frac{2c}{\beta}\left|\int_0^{s(t)}w(x,t)\mathrm{d}xX(t)\right|\right), \qquad \text{(C.119)}
\end{aligned}
$$

where $b=\frac{1}{8}\min\left\{\frac{\alpha}{\bar{s}^2},c\right\}$. Applying Young's inequality to (C.119), the inequality (C.110) is derived.

Bibliography

[1] M. Agarwala, D. Bourell, J. Beaman, H. Marcus, and J. Barlow, "Direct selective laser sintering of metals," *Rapid Prototyping Journal*, vol. 1, no. 1, pp. 26-36, 1995.

[2] S. Ahn, J. Murphy, J. Ramos, and J. Beaman, "Physical modeling for dynamic control of melting process in direct-SLS," In *Proceedings of the 12th Annual Solid Freeform Fabrication Symposium, Austin, TX*, pp. 591-598, 2001.

[3] A. Alessandri, P. Bagnerini, and M. Gaggero, "Optimal control of propagating fronts by using level set methods and neural approximations," *IEEE Transactions on Neural Networks and Learning Systems*, vol. 30, no. 3, pp. 902–912, 2018.

[4] B. N. Am, and E. Fridman, "Network-based H_∞ filtering of parabolic systems," *Automatica*, vol. 50, no. 12, pp.3139-3146, 2014.

[5] H. Anfinsen, and O. M. Aamo, *Adaptive Control of Hyperbolic PDEs*. Springer, 2019.

[6] M. Arcak and P. Kokotovic, "Nonlinear observers: a circle criterion design and robustness analysis," *Automatica*, vol. 37, pp.1923-1930, 2001.

[7] A. Armaou and P.D. Christofides, "Robust control of parabolic PDE systems with time-dependent spatial domains," *Automatica*, vol. 37, pp. 61–69, 2001.

[8] A. Baccoli, A. Pisano, Y. Orlov, "Boundary control of coupled reaction-advection-diffusion systems with spatially-varying coefficients," *Automatica*, vol. 54, pp. 80–90, 2015.

[9] N. Bekiaris-Liberis and M. Krstic, "Compensation of state-dependent input delay for nonlinear systems," *IEEE Transactions on Automatic Control*, vol. 58, no. 2, pp. 275–289, Feb. 2013.

[10] N. Bekiaris-Liberis and M. Krstic, "Compensation of wave actuator dynamics for nonlinear systems," *IEEE Transactions on Automatic Control*, vol. 59(6), pp.1555-1570, 2014.

[11] N. Bekiaris-Liberis, and M. Krstic, *Nonlinear control under nonconstant delays*. SIAM, Vol. 25, 2014.

[12] M. Benosman, *Learning-Based Adaptive Control: An Extremum Seeking Approach–Theory and Applications*. Butterworth-Heinemann, 2016.

[13] M.K. Bernauer and R. Herzog, "Optimal control of the classical two-phase Stefan problem in level set formulation," *SIAM Journal on Scientific Computing*, vol. 33, no. 1, pp. 342–363, 2011.

[14] C.M. Bitz, M.M. Holland, A.J. Weaver, and M. Eby, "Simulating the ice-thickness distribution in a coupled climate model," *Journal of Geophysical Research: Oceans*, vol. 106, no. C2, pp.2441-2463, 2001.

[15] C.M. Bitz and W.H. Lipscomb, "An energy-conserving thermodynamic model of sea ice," *Journal of Geophysical Research*, vol. 104, no. C7, pp.15-669, 1999.

[16] N. Boonkumkrong and S. Kuntanapreeda, "Backstepping boundary control: An application to rod temperature control with Neumann boundary condition," *Proceedings of the Institution of Mechanical Engineers, Part I: Journal of Systems and Control Engineering*, vol. 228(5), pp.295-302, 2014.

[17] D. M. Boskovic, M. Krstic, and W. Liu, "Boundary control of an unstable heat equation via measurement of domain-averaged temperature," *IEEE Transactions on Automatic Control*, vol. 46(12), pp. 2022–2028, 2001.

[18] D. Bresch-Pietri and M. Krstic, "Adaptive trajectory tracking despite unknown input delay and plant parameters," *Automatica*, vol. 45(9), pp.2074–2081, 2009.

[19] D. Bresch-Pietri and M. Krstic, "Delay-Adaptive Predictor Feedback for Systems With Unknown Long Actuator Delay," *IEEE Transactions on Automatic Control*, vol. 55(9), pp.2106–2112, 2010.

[20] D. Bresch-Pietri and M. Krstic, "Delay-adaptive control for nonlinear systems," *IEEE Transactions on Automatic Control*, vol. 59(5), pp.1203–1218, 2014.

[21] S. Bukkapatnam and B. Clark, "Dynamic Modeling and Monitoring of Contour Crafting - An Extrusion-Based Layered Manufacturing Process," In *Journal of Manufacturing Science and Engineering, 129(1),* pages 135-142. ASME 2007.

[22] X. Cai and M. Krstic, "Nonlinear control under wave actuator dynamics with time- and state-dependent moving boundary," *International Journal of Robust and Nonlinear Control*, vol. 25(2), pp.222-251, 2015.

[23] L. Camacho-Solorio, S. Moura, and M. Krstic, "Robustness of boundary observers for radial diffusion equations to parameter uncertainty," *2018 American Control Conference (ACC)*, pages 3484-3489. IEEE, 2018.

[24] L. Camacho-Solorio, M. Krstic, R. Klein, A. Mirtabatabaei, and S. J. Moura, "State estimation for an electrochemical model of multiple-material lithium-ion batteries," In *ASME 2016 Dynamic Systems and Control Conference*. American Society of Mechanical Engineers Digital Collection, 2016.

[25] J. R. Cannon and M. Primicerio, "A two phase Stefan problem with flux boundary conditions," *Annali di Matematica Pura ed Applicata,* 88.1, 193-205, 1971.

[26] X. Cao, and B. Ayalew, "Partial Differential Equation-Based Multivariable Control Input Optimization for Laser-Aided Powder Deposition Processes," *Journal of Manufacturing Science and Engineering*, vol. 138, no. 3, pp. 031001, 2016.

[27] N.A. Chaturvedi, R. Klein, J. Christensen, J. Ahmed, and A. Kojic, "Algorithms for advanced battery-management systems," *IEEE Control systems magazine*, vol. 30, no. 3, pp. 49-68, 2010.

[28] P.D. Christofides, "Robust control of parabolic PDE systems," *Chemical Engineering Science*, vol. 53, pp. 2949–2965, 1998.

[29] H. Chung and S. Das, "Numerical modeling of scanning laser-induced melting, vaporization and resolidification in metals subjected to step heat flux input," *International journal of heat and mass transfer*, vol. 47(19), pp.4153-4164, 2004.

[30] F. Conrad, D. Hilhorst, and T.I. Seidman, "Well-posedness of a moving boundary problem arising in a dissolution-growth process," *Nonlinear Analysis*, vol. 31, pp. 795–803, 2007.

[31] R. Conti, A.A. Gallitto, and E. Fiordilino, "Measurement of the convective heat-transfer coefficient," *The Physics Teacher* vol. 52.2, pp. 109-111, 2014.

[32] M. Cotteleer, and J. Joyce, "3D opportunity: Additive manufacturing paths to performance, innovation, and growth," Deloitte Review 14 (2014): 5-19.

[33] J. Crepeau, "Josef Stefan: His life and legacy in the thermal sciences," *Experimental thermal and fluid science*, vol. 15, pp. 445–465, 1990.

[34] K. Dai, and L. Shaw, "Finite element analysis of the effect of volume shrinkage during laser densification," *Acta materialia,* vol. 53, no. 18, pp. 4743-4754, 2005.

[35] N. Daraoui, P. Dufour, H. Hammouri, and A. Hottot, "Model predictive control during the primary drying stage of lyophilisation," *Control Engineering Practice*, vol. 18, pp. 483–494, 2010.

[36] S. Dey, B. Ayalew, and P. Pisu, "Nonlinear robust observers for state-of-charge estimation of lithium-ion cells based on a reduced electrochemical model," *IEEE Transactions on Control Systems Technology*, vol. 23, no. 5, pp.1935-1942, 2015.

[37] M. Diagne, N. Bekiaris-Liberis, A. Otto, and M. Krstic, "Control of Transport PDE/Nonlinear ODE Cascades with State-Dependent Propagation Speed," *IEEE Transactions on Automatic Control*, vol. 62, no. 12, pp. 6278-6293, 2017.

[38] M. Diagne, P. Shang and Z. Wang, "Feedback Stabilization of a Food Extrusion Process Described by 1D PDEs Defined on Coupled Time-Varying Spatial Domains" In *Proceedings of the 13th IFAC Workshop on Time-Delay Systems*, vol. 48, no. 12, 2015, pages 51-56, IFAC, 2015.

[39] M. Diagne, P. Shang and Z. Wang, "Feedback Stabilization for the Mass Balance Equations of an Extrusion Process," In *IEEE Transactions on Automatic Control*, vol. 61, no. 3, pp. 760-765, 2016.

[40] D. Drotman, M. Diagne, R. Bitmead and M. Krstic, "Control-Oriented Energy-Based Modeling of a Screw Extruder Used for 3D Printing," In *2016 Dynamic Systems and Control Conference*, volume 1001, pages 48109. ASME, 2016.

[41] D. Di Domenico, A. Stefanopoulou, and G. Fiengo, "Lithium-ion battery state of charge and critical surface charge estimation using an electrochemical model-based extended Kalman filter," *Journal of dynamic systems, measurement, and control*, no. 132, no. 6, 2010.

[42] Y. Dutil, D. R. Rousse, N. B. Salah, S. Lassue, and L. Zalewski, "A review on phase-change materials: mathematical modeling and simulations," *Renewable and sustainable Energy reviews*, vol. 15, no. 1, pp. 112-130, 2011.

[43] J. Deutscher "Backstepping design of robust output feedback regulators for boundary controlled parabolic PDEs," *IEEE Transactions on Automatic Control*, vol. 61(8), pp. 2288-2294, 2016.

[44] R. Escobedo and L. Fernández, "Classical One-Phase Stefan Problems for Describing Polymer Crystallization Processes," In *SIAM Journal on Applied Mathematics*, pages 254-280. SIAM, 2013.

[45] N. Espitia, A. Girard, N. Marchand, and C. Prieur, "Event-based control of linear hyperbolic systems of conservation laws," *Automatica*, vol. 70, pp.275-287, 2016.

[46] N. Espitia, A. Girard, N. Marchand, and C. Prieur, "Event-Based Boundary Control of a Linear 2×2 Hyperbolic System via Backstepping Approach, *IEEE Transactions on Automatic Control*, vol, 63, no. 8, pp.2686-2693, 2017.

[47] N. Espitia, I. Karafyllis, and M. Krstic, "Event-triggered boundary control of constant-parameter reaction-diffusion PDEs: a small-gain approach," Preprint, available at https://arxiv.org/abs/1909.10472, 2019.

[48] Q. Fang, M. Hanna, and Y. Lan, "Extrusion System Components," In *In: Heldman D. R. Ed., Encyclopedia of Agricultural, Food, and Biological Engineering, CRC Press,* pages 301-305, 2003.

[49] I. Fantoni, R. Lozano, and M.W. Spong, "Energy based control of the pendubot," *IEEE Transactions on Automatic Control*, vol. 45, no. 4, pp. 725-729, 2000.

[50] A. Fasano, and M. Primicerio, "General free-boundary problems for the heat equation, I," *Journal of Mathematical analysis and applications*, vol.57, no.3, pp. 694-723, 1977.

[51] J. Feiling, S. Koga, M. Krstic, and T.R. Oliveira, "Gradient extremum seeking for static maps with actuation dynamics governed by diffusion PDEs," *Automatica*, vol. 95, pp. 197–206, 2018.

[52] I. Fenty and P. Heimbach, "Coupled sea ice ocean-state estimation in the Labrador Sea and Baffin Bay," *Journal of Physical Oceanography*, vol. 43, no. 5, pp.884-904, 2013.

[53] I. Fenty, D. Menemenlis, and H. Zhang, "Global coupled sea ice-ocean state estimation," *Climate Dynamics*, vol. 49, no. 3, 931-956. 2015.

[54] R. Freeman, and P.V. Kokotovic, *Robust nonlinear control design: state-space and Lyapunov techniques*. Springer Science & Business Media, 2008.

[55] A. Friedman "Free boundary problems for parabolic equations I. Melting of solids," Journal of Mathematics and Mechanics, vol. 8(4), pp.499-517, 1959.

[56] A. Friedman and F. Reitich, "Analysis of a mathematical model for the growth of tumors," *Journal of mathematical biology*, vol. 38(3), pp.262-284, 1999.

[57] E. Fridman, and A. Blighovsky, "Robust sampled-data control of a class of semilinear parabolic systems," *Automatica*, vol. 48, no.5, pp.826-836, 2012.

[58] E. Fridman, "Sampled-Data Distributed H_∞ Control of Transport Reaction Systems," *SIAM Journal on Control and Optimization*, vol.51, no.2, pp.1500-1527, 2013.

[59] P. Frihauf and M. Krstic, " Leader-Enabled Deployment Onto Planar Curves: A PDE-Based Approach," *IEEE Transactions on Automatic Control*, vol. 56(8), pp. 1791–1806, 2011.

[60] S. Gupta, *The Classical Stefan Problem. Basic Concepts, Modelling and Analysis*. North-Holland: Applied mathematics and Mechanics, 2003.

[61] D.K. Hall, J.R. Key, K.A. Casey, G.A. Riggs, and D.J. Cavalieri, "Sea ice surface temperature product from MODIS," *IEEE Transactions on Geoscience and Remote Sensing*, vol. 42, no. 5, pp.1076-1087, 2004.

[62] A. Hasan, O.M. Aamo, and M. Krstic, "Boundary observer design for hyperbolic PDE-ODE cascade systems," *Automatica*, vol. 68, pp.75-86, 2016.

[63] M. Hinze and S. Ziegenbalg, "Optimal control of the free boundary in a two-phase Stefan problem," *Journal of Computational Physics*, 223.2, 657-684, 2007.

[64] T. Hu, and Z. Lin, *Control systems with actuator saturation: analysis and design.*. Springer Science & Business Media, 2001.

[65] M. Izadi and S. Dubljevic, "Backstepping output feedback control of moving boundary parabolic PDEs," *European Journal of Control*, vol. 21, pp. 27 – 35, 2015.

[66] Z.P. Jiang, A.R. Teel, and L. Praly, "Small-gain theorem for ISS systems and applications," *Mathematics of Control, Signals and Systems*, vol. 7, no.2, pp.95-120, 1994.

[67] Z.P. Jiang, I.M. Mareels, and Y. Wang, "A Lyapunov formulation of the nonlinear small-gain theorem for interconnected ISS systems," *Automatica*, vol. 32, no. 8, pp.1211-1215, 1996.

[68] I. Karafyllis, and C. Kravaris, "Global stability results for systems under sampled-data control," *International Journal of Robust and Nonlinear Control: IFAC-Affiliated Journal*, vol. 19, no. 10, pp.1105-1128, 2009.

[69] I. Karafyllis, and C. Kravaris, "From continuous-time design to sampled-data design of observers," *IEEE Transactions on Automatic Control*, vol. 54, no. 9, pp.2169-2174, 2009.

[70] I. Karafyllis, and M. Krstic, "Adaptive certainty-equivalence control with regulation-triggered finite-time least-squares identification," *IEEE Transactions on Automatic Control*, vol. 63.10, pp. 3261-3275, 2018.

[71] I. Karafyllis, and M. Krstic, "Nonlinear stabilization under sampled and delayed measurements, and with inputs subject to delay and zero-order hold," *IEEE Transactions on Automatic Control*, vol. 57, no. 5, pp. 1141-1154, 2012.

[72] I. Karafyllis and M. Krstic, *Predictor feedback for delay systems: Implementations and approximations*. Springer, 2017.

[73] I. Karafyllis, and M. Krstic, "ISS with respect to boundary disturbances for 1-D parabolic PDEs" *IEEE Transactions on Automatic Control*, 61(12), pp.3712-3724, 2016.

[74] I. Karafyllis, and M. Krstic, "ISS in different norms for 1-D parabolic PDEs with boundary disturbances" *SIAM Journal on Control and Optimization*, 55(3), pp.1716-1751, 2017.

[75] I. Karafyllis, and M. Krstic, "Sampled-data boundary feedback control of 1-D parabolic PDEs," *Automatica*, vol. 87, pp. 226-237, 2018.

[76] I. Karafyllis, and M. Krstic, *Input-to-state stability for PDEs*. Springer-Verlag, London (Series: Communications and Control Engineering), 2019.

[77] A. Khandelwal, K. S. Hariharan, P. Gambhire, S. M. Kolake, T. Yeo, and S. Doo, "Thermally coupled moving boundary model for charge–discharge of LiFePO4/C cells," *Journal of Power Sources*, vol. 279, pp.180-196, 2015.

[78] A. Khandelwal, K. S. Hariharan, V. S. Kumar, P. Gambhire, S. M. Kolake, D. Oh, and S. Doo, "Generalized moving boundary model for charge–discharge of LiFePO4/C cells," *Journal of Power Sources*, vol. 248, pp.101-114, 2014.

[79] T. Kharkovskaia, D. Efimov, E. Fridman, A. Polyakov, and J.P. Richard, "On design of interval observers for parabolic PDEs," In *Proc. of 20th IFAC World Congress*, vol. 50(1), pp. 4045-4050, 2017.

[80] R. B. Khosroushahi, and H. J. Marquez, "PDE backstepping boundary observer design for microfluidic systems," *IEEE Transactions on Control Systems Technology*, vol. 23, no.1, pp.380-388, 2014.

[81] R. Klein, N. A. Chaturvedi, J. Christensen, J. Ahmed, R. Findeisen, and A. Kojic, "Electrochemical model based observer design for a lithium-ion battery," *IEEE Transactions on Control Systems Technology*, vol. 21, no. 2, pp.289-301, 2012.

[82] S. Koga, M. Diagne, S. Tang, and M. Krstic, "Backstepping control of the one-phase Stefan problem," In *2016 American Control Conference (ACC)*, pages 2548–2553. IEEE, 2016.

[83] S. Koga, M. Diagne, and M. Krstic, "Output feedback control of the one-phase Stefan problem," In *55th Conference on Decision and Control (CDC)*, pages 526–531. IEEE, 2016.

[84] S. Koga, D. Bresch-Pietri, and M. Krstic, "Delay compensated control of the Stefan problem and robustness to delay mismatch," *International Journal of Robust and Nonlinear Control*, vol. 30, no. 6, pp. 2304-2334, 2020.

[85] S. Koga, L. Camacho-Solorio, and M. Krstic, "State Estimation for Lithium Ion Batteries With Phase Transition Materials," In *ASME 2017 Dynamic Systems and Control Conference*, American Society of Mechanical Engineers, 2017.

[86] S. Koga, M. Diagne, and M. Krstic, "Control and state estimation of the one-phase Stefan problem via backstepping design," *IEEE Transactions on Automatic Control*, vol. 64, no. 2, pp. 510–525, 2019.

[87] S. Koga, I. Karafyllis, and M. Krstic, "Sampled-Data Control of the Stefan System," Preprint, available at https://arxiv.org/abs/1906.01434, 2019.

[88] S. Koga, and M. Krstic, "Arctic sea ice state estimation from thermodynamic PDE model," *Automatica*, vol. 112, p. 108713, 2020.

[89] S. Koga, and M. Krstic, "Single-Boundary Control of the Two-Phase Stefan System," *Systems & Control Letters*, vol. 135, p. 104573, 2020.

[90] S. Koga, D. Straub, M. Diagne, and M. Krstic, "Stabilization of Filament Production Rate for Screw Extrusion-Based Polymer 3D-Printing," *Journal of Dynamic Systems, Measurement, and Control*, vol. 142, no. 3, p. 031005, 2020.

[91] S. Kolossov, E. Boillat, R. Glardon, P. Fischer, and M. Locher, "3D FE simulation for temperature evolution in the selective laser sintering process," *International Journal of Machine Tools and Manufacture*, vol. 44, no. 2-3, pp. 117-123, 2004.

[92] M. Krstic, I. Kanellakopoulos, and P.V. Kokotovic, *Nonlinear and adaptive control design* Wiley, 1995.

[93] M. Krstic "Lyapunov tools for predictor feedbacks for delay systems: Inverse optimality and robustness to delay mismatch," *Automatica*, vol. 44(11), pp.2930–2935, 2008.

[94] M. Krstic and A. Smyshlyaev, "Backstepping boundary control for first-order hyperbolic PDEs and application to systems with actuator and sensor delays," *Systems & Control Letters*, vol. 57, pp. 750–758, 2008.

[95] M. Krstic, "Compensating actuator and sensor dynamics governed by diffusion PDEs," *Systems & Control Letters*, vol. 58, pp. 372–377, 2009.

[96] M. Krstic "Control of an unstable reaction diffusion PDE with long input delay," *Systems & Control Letters*, vol. 58(10), pp.773-782, 2009.

[97] M. Krstic, *Delay compensation for nonlinear, adaptive, and PDE systems*. Boston: Birkhauser, 2009

[98] M. Krstic, "Input delay compensation for forward complete and strict-feedforward nonlinear systems," *IEEE Transactions on Automatic Control*, vol. 55(2), pp.287-303, 2010.

[99] M. Krstic and A. Smyshlyaev, *Boundary Control of PDEs: A Course on Backstepping Designs*. Singapore: SIAM, 2008.

[100] M. Krstic and A. Smyshlyaev, " Adaptive boundary control for unstable parabolic PDEs–Part I: Lyapunov Design," *IEEE Transactions on Automatic Control*, vol. 53(7), pp. 1575–1591, 2008.

[101] M. Kulshreshtha, C. Zaror and D. Jukes, "An Unsteady State Model for Twin Screw Extruders," In *Tran IChemE, TartC, vol70,* pages 21-28, 1995.

[102] S. Kutluay, A. R. Bahadir, and A. Özdes, "The numerical solution of one-phase classical Stefan problem," *Journal of computational and applied mathematics*, 81.1, pp. 135-144, 1997.

[103] F. Kuznik, J. Virgone, and J. Noel, "Optimization of a phase change material wallboard for building use," *Applied Thermal Engineering*, vol. 28(11), pp.1291-1298, 2008.

[104] R. Kwok, and G. F. Cunningham, "Variability of Arctic sea ice thickness and volume from CryoSat-2", *Phil. Trans. R. Soc. A*, vol. 373, no. 2045, 2015.

[105] R. Kwok and D.A. Rothrock, "Decline in Arctic sea ice thickness from submarine and ICESat records: 1958-2008," *Geophysical Research Letters*, vol. 36, no. 15, 2009.

[106] C. Ladd, J. H. So, J. Muth, and M.D. Dickey, "3D Printing of Free Standing Liquid Metal Microstructures," In *Advanced Materials, 25(36)*, pages 5081-5085, 2013.

[107] C. Lei, Z. Lin, and H. Wang, "The free boundary problem describing information diffusion in online social networks," *Journal of Differential Equations*, vol. 254(3), pp.1326-1341, 2013.

[108] C.-H. Li, "Modelling Extrusion Cooking" In *Mathematical and Computer Modelling 33*, pages 553-563. PERGAMON, 2001

[109] J. Li, J. K. Barillas, C. Guenther, and M. A. Danzer, "Sequential Monte Carlo filter for state estimation of LiFePO4 batteries based on an online updated model," *Journal of Power Sources*, vol. 247, pp.156-162, 2014.

[110] A. Maidi and J.-P. Corriou, "Boundary geometric control of a linear stefan problem," *Journal of Process Control*, vol. 24, pp. 939–946, 2014.

[111] J. Marshall, A. Adcroft, C. Hill, L. Perelman, & C. Heisey, "A finite volume, incompressible Navier Stokes model for studies of the ocean on parallel computers", *Journal of Geophysical Research: Oceans*, vol. 102, no. C3, pp.5753-5766, 1997.

[112] G.A. Maykut and N. Untersteiner, "Some results from a time dependent thermodynamic model of sea ice," *Journal of Geophysical Research*, vol. 76, pp. 1550–1575, 1971.

[113] K.C. Mills, *Recommended values of thermophysical properties for selected commercial alloys*. Woodhead Publishing, 2002.

[114] V. Mironov, T. Boland, T. Trusk, G. Forgacs, and R.R. Markwald (2003). "Organ Printing: Computer-Aided Jet-Based 3D Tissue Engineering" In *TRENDS in Biotechnology, 21(4)*, pages 157-161. ELSEVIER 2003.

[115] O. A. Mohamed, S. H. Masood, and J. L. Bhowmik, "Optimization of Fused Deposition Modeling Process Parameters: A Review of Current Research and Future Prospects," In *Advances in Manufacturing, 3(1),* pages 42-53. Springer 2015.

[116] D.H. Morton-Jones, "Polymer Processing," Chapman and Hall London, 1989

[117] S. J. Moura, F. B. Argomedo, R. Klein, A. Mirtabatabaei, and M. Krstic, "Battery state estimation for a single particle model with electrolyte dynamics," *IEEE Transactions on Control Systems Technology*, vol. 25, no. 2, pp.453-468, 2016.

[118] S.J. Moura, N.A. Chaturvedi, and M. Krstic, "Adaptive partial differential equation observer for battery state-of-charge/state-of-health estimation via an electrochemical model," *Journal of Dynamic Systems, Measurement, and Control*, vol. 136, no. 1, pp. 011015-1?011015-11, 2014.

[119] T.R. Oliveira, M. Krstic, and D. Tsubakino, "Extremum seeking for static maps with delays," *IEEE Transactions on Automatic Control*, vol. 62(4), pp.1911-1926, 2017.

[120] A.K. Padhi, K.S. Nanjundaswamy, and J.B. Goodenough, "Phospho-olivines as positive-electrode materials for rechargeable lithium batteries," *Journal of the electrochemical society*, vol. 144, no. 4, pp. 1188–1194, 1997

[121] C.V. Pao, *Nonlinear Parabolic and Elliptic Equations*. Springer, 1992.

[122] A.A. Paranjape, J. Guan, S.J. Chung, and M. Krstic, "PDE boundary control for flexible articulated wings on a robotic aircraft," *IEEE Transactions on Robotics*, vol. 29, no. 3, pp. 625-640, 2013.

[123] H. E. Perez, and S. J. Moura, 2015, July. "Sensitivity-based interval PDE observer for battery SOC estimation,". *In 2015 American Control Conference (ACC)*, pp. 323-328. 2015.

[124] H. Perez, N. Shahmohammadhamedani, and S. Moura, "Enhanced performance of li-ion batteries via modified reference governors and electrochemical models," *IEEE/ASME Transactions on Mechatronics*, vol. 20, no. 4, pp.1511-1520, 2015.

[125] N. Petit, "Control problems for one-dimensional fluids and reactive fluids with moving interfaces," In *Advances in the theory of control, signals and systems with physical modeling*, volume 407 of *Lecture notes in control and information sciences*, pages 323–337, Lausanne, Dec 2010.

[126] B. Petrus, J. Bentsman, and B.G. Thomas, "Application of enthalpy-based feedback control methodology to the two-sided Stefan problem," In *2014 American Control Conference (ACC)*, pages 1015–1020, IEEE, 2014.

[127] B. Petrus, J. Bentsman, and B.G. Thomas, "Enthalpy-based feedback control algorithms for the Stefan problem," *Decision and Control (CDC), 2012 IEEE 51st Annual Conference on*, pp. 7037–7042, 2012.

[128] B. Petrus, J. Bentsman, and B.G. Thomas, "Feedback control of the two-phase Stefan problem, with an application to the continuous casting of steel," *Decision and Control (CDC), 2010 49th IEEE Conference on*, pp. 1731–1736, 2010.

[129] B. Petrus, Z. Chen, J. Bentsman, and B.G. Thomas, "Online recalibration of the state estimators for a system with moving boundaries using sparse discrete-in-time temperature measurements," *IEEE Transactions on Automatic Control*, vol. 63, no. 4, pp. 1090-1096, 2017.

[130] J. Qi, R. Vazquez and M. Krstic, "Multi-Agent Deployment in 3-D via PDE Control," *IEEE Transactions on Automatic Control*, vol. 60(4), pp. 891–906, 2015.

[131] M.N. Riaz, "Extruders in Food Applications," In *Boca Raton: CRC Press,* 240 pages, 2000.

[132] A.A. Rostami, and A. Raisi, "Temperature distribution and melt pool size in a semi-infinite body due to a moving laser heat source," *Numerical Heat Transfer, Part A Applications*, vol. 31, no. 7, pp.783-796, 1997.

[133] D.A. Rothrock, D.B. Percival, and M. Wensnahan, "The decline in arctic sea-ice thickness: Separating the spatial, annual, and interannual variability in a quarter century of submarine data," *Journal of Geophysical Research: Oceans*, vol. 113, no. C5, 2008.

[134] C. Sagert, F. Di Meglio, M. Krstic, and P. Rouchon, P., "Backstepping and flatness approaches for stabilization of the stick-slip phenomenon for drilling," *IFAC Proceedings Volumes*, vol. 46, no. 2, pp.779-784, 2013.

[135] S. Schwunk, N. Armbruster, S. Straub, J. Kehl, and M. Vetter, "Particle filter for state of charge and state of health estimation for lithium?iron phosphate batteries," *Journal of Power Sources*, vol. 239, pp.705-710, 2013.

[136] A. Selivanov, and E. Fridman, "Sampled-data relay control of diffusion PDEs," *Automatica*, vol. 82, pp.59-68, 2017.

[137] H. Seitz, W. Rieder, S. Irsen, B. Leukers, and C. Tille, "Three-Dimensional Printing of Porous Ceramic Scaffolds for Bone Tissue Engineering," In *Journal of Biomedical Materials Research Part B: Applied Biomaterials, 74(2),* pages 782-788, 2005.

[138] A.J. Semtner Jr, "A model for the thermodynamic growth of sea ice in numerical investigations of climate," *Journal of Physical Oceanography*, vol. 6, no. 3, pp.379-389, 1976.

[139] A. Sharma, V. V. Tyagi, C. R. Chen, and D. Buddhi, "Review on thermal energy storage with phase change materials and applications," *Renewable and Sustainable energy reviews*, vol. 13, no. 2, pp. 318-345, 2009.

[140] B. Sherman, "A free boundary problem for the heat equation with prescribed flux at both fixed face and melting interface", *Quarterly of Applied Mathematics*, 25(1), pp.53-63, 1967.

[141] A. Smyshlyaev and M. Krstic, "Closed-form boundary state feedbacks for a class of 1-D partial integro-differential equations," *IEEE Transactions on Automatic Control*, vol. 49(12), pp. 2185–2202, 2004.

[142] A. Smyshlyaev and M. Krstic, " Backstepping observers for a class of parabolic PDEs," *Systems & Control Letters*, vol. 54(7), pp. 613–625, 2005.

[143] A. Smyshlyaev and M. Krstic, "On control design for PDEs with space-dependent diffusivity or time-dependent reactivity," *Automatica*, vol. 41(9), pp. 1601–1608, 2005.

[144] A. Smyshlyaev and M. Krstic, "Adaptive boundary control for unstable parabolic PDEs–Part II: Estimation-based designs," *Automatica*, vol. 43(9), pp. 1543–1556, 2007.

[145] A. Smyshlyaev and M. Krstic, "Adaptive boundary control for unstable parabolic PDEs–Part III: Output feedback examples with swapping identifiers," *Automatica*, vol. 43(9), pp. 1557–1564, 2007.

[146] A. Smyshlyaev and M. Krstic, *Adaptive control of parabolic PDEs*, Princeton University Press, 2010.

[147] E.D. Sontag, and Y. Wang, "On characterizations of the input-to-state stability property," *Systems & Control Letters*, vol. 24, no. 5, pp.351-359, 1995.

[148] E.D. Sontag, and Y. Wang, "New characterizations of input-to-state stability," *IEEE Transactions on Automatic Control*, vol. 41, no.9, pp.1283-1294, 1996.

[149] E.D. Sontag, "Input to state stability: Basic concepts and results," In Nonlinear and optimal control theory (pp. 163-220). Springer Berlin Heidelberg, 2008.

[150] V. Srinivasan and J. Newman, "Discharge model for the lithium iron-phosphate electrode," *Journal of the Electrochemical Society*, vol. 151, pp. A1517–A1529, 2004.

[151] V. Srinivasan, and J. Newman, "Design and optimization of a natural graphite/iron phosphate lithium-ion cell," *Journal of the Electrochemical Society*, vol. 151, no. 10, pp.A1530-A1538, 2004.

[152] J. Stefan, "Uber die Theorie der Eisbildung, insbesondere uber die Eisbildung im Polarmeere," *Annalen der Physik*, vol. 278, pp. 269–286, 1891.

[153] G.A. Susto and M. Krstic, "Control of PDE–ODE cascades with Neumann interconnections," *Journal of the Franklin Institute*, vol. 347, pp. 284–314, 2010.

[154] Z. Tadmor and C. Gogos "Principles of Polymer Processing," John Wiley & Sons, 2006.

[155] S. X. Tang, L. Camacho-Solorio, Y. Wang, and M. Krstic, "State-of-charge estimation from a thermal-electrochemical model of lithium-ion batteries," *Automatica*, vol. 83, pp.206-219, 2017.

[156] S. Tang and C. Xie, "State and output feedback boundary control for a coupled PDE–ODE system," *Systems & Control Letters*, vol. 60, pp. 540–545, 2011.

[157] S. Tang, C. Xie, and Z. Zhou, "Stabilization for a class of delayed coupled PDE-ODE systems with boundary control," *Control and Decision Conference (CCDC), Chinese,* pp. 320-324, 2011.

[158] K.E. Thomas, J. Newman, and R.M. Darling, "Mathematical modeling of lithium batteries," *In Advances in lithium-ion batteries*, pp. 345-392, Springer, Boston, MA, 2002.

[159] N. Untersteiner, "On the mass and heat budget of Arctic sea ice," *Arch. Meteorol. Geophys. Bioklimatol., A*, 12(2), pp.151-182, 1961.

[160] R. Vazquez and M. Krstic, "Boundary control and estimation of reaction-diffusion equations on the sphere under revolution symmetry conditions," *International Journal of Control*, to appear.

[161] R. Vazquez and M. Krstic, "Boundary control of coupled reaction-advection-diffusion systems with spatially-varying coefficients," *IEEE Transactions on Automatic Control*, to appear.

[162] H. Valkenaers, F. Vogeler, E. Ferraris, A. Voet and J. Kruth "A Novel Approach to Additive Manufacturing: Screw Extrusion 3D-Printing," In *Proceedings of the 10th International Conference on Multi-Material Micro Manufacture*, pages 235-238. Research Publishing, 2013.

[163] B. Vergnes, G.D. Valle, and L. Delamare, "A Global Computer Software for Polymer Flows in Corotating Twin Screw Extruders," *Polymer Engineering & Science*, 38(11), pp.1781-1792, 1998.

[164] D. Wang, and X. Chen, "A multirate fractional-order repetitive control for laser-based additive manufacturing," *Control Engineering Practice*, vol. 77, pp.41-51, 2018.

[165] D. Wang, T. Jiang, and X. Chen, "Control-oriented modeling and repetitive control in In-layer and cross-layer thermal interactions in selective laser sintering," In *Dynamic Systems and Control Conference*, vol. 59155, p. V002T27A001. American Society of Mechanical Engineers, 2019.

[166] J. Wang, S. Koga, Y. Pi, and M. Krstic, "Axial vibration suppression in a partial differential equation model of ascending mining cable elevator," *Journal of Dynamic Systems, Measurement, and Control*, vol. 140, no. 11, 2018.

[167] J. Wang and M. Krstic, "Delay-Compensated Control of Sandwiched ODE-PDE-ODE Hyperbolic Systems for Oil Drilling and Disaster Relief," Preprint available at https://arxiv.org/abs/1910.05948, 2019.

[168] J. Wang, Y. Pi, and M. Krstic, "Balancing and suppression of oscillations of tension and cage in dual-cable mining elevators," *Automatica*, 98, pp.223-238, 2018.

[169] J. Wang, S.X. Tang, and M. Krstic, "Adaptive output-feedback control of torsional vibration in off-shore rotary oil drilling systems," *Automatica*, vol. 111, p.108640, 2020.

[170] J. Wang, S.X. Tang, Y. Pi, and M. Krstic, "Exponential regulation of the anti-collocatedly disturbed cage in a wave PDE-modeled ascending cable elevator," *Automatica*, vol. 95, pp.122-136, 2018.

[171] Y. Wang, H. Fang, Z. Sahinoglu, T. Wada, and S. Hara, "Adaptive estimation of the state of charge for lithium-ion batteries: Nonlinear geometric observer approach," *IEEE Transactions on Control Systems Technology*, vol. 23, no. 3, pp.948-962, 2014.

[172] J.S. Wettlaufer, "Heat flux at the ice-ocean interface," *Journal of Geophysical Research: Oceans*, vol. 96, pp. 7215–7236, 1991.

[173] M. Winton, "A reformulated three-layer sea ice model," *Journal of atmospheric and oceanic technology*, vol. 17, no. 4, pp.525-531, 2000.

[174] C. Wunsch, *The Ocean Circulation Inverse Problem*. Cambridge University Press, 1996.

[175] C. Wunsch, and P. Heimbach, "Practical global oceanic state estimation," *Physica D: Nonlinear Phenomena*, vol. 230, no. 1-2, pp. 197–208, 2007.

[176] H. Yu, A. M. Bayen, and M. Krstic, "Boundary Observer for Congested Freeway Traffic State Estimation via Aw-Rascle-Zhang model," Preprint, available at https://arxiv.org/abs/1904.12963, 2019.

[177] H. Yu, M. Diagne, L. Zhang, M. Krstic, "Bilateral Boundary Control of Moving Shockwave in LWR Model of Congested Traffic". Preprint, available at https://arxiv.org/abs/1904.04303, 2019.

[178] H. Yu, Q. Gan, A. M. Bayen, and M. Krstic, "PDE Traffic Observer Validated on Freeway Data," Preprint, available at https://arxiv.org/abs/1906.04012, 2019.

[179] H. Yu and M. Krstic, "Traffic congestion control for Aw-Rascle-Zhang model," *Automatica*, vol. 100, pp.38-51, 2019.

[180] B. Zalba, J.M. Marin, L.F. Cabeza, and H. Mehling, "Review on thermal energy storage with phase change: materials, heat transfer analysis and applications," *Applied thermal engineering*, vol. 23, pp. 251–283, 2003.

[181] Y. Zeng, P. Albertus, R. Klein, N. Chaturvedi, A. Kojic, M. Z. Bazant, and J. Christensen, "Efficient conservative numerical schemes for 1d nonlinear spherical diffusion equations with applications in battery modeling," *Journal of The Electrochemical Society*, 160(9), pp.A1565-A1571, 2013.

[182] K. Zeng, D. Pal, and B. Stucker, "A review of thermal analysis methods in laser sintering and selective laser melting," In *Proceedings of Solid Freeform Fabrication Symposium Austin, TX*, vol. 60, pp. 796-814, 2012.

[183] L. Zhang, T. Phillips, A. Mok, D. Moser, and J. Beaman, "Automatic Laser Control System for Selective Laser Sintering," *IEEE Transactions on Industrial Informatics*, (early access), 2018.

[184] Q. Zhang, and R. E. White, "Moving boundary model for the discharge of a LiCoO2 electrode," *Journal of The Electrochemical Society,* vol. 154, no. 6, pp.A587-A596, 2007.